ARNOLD MATHEMATICAL JOURNAL

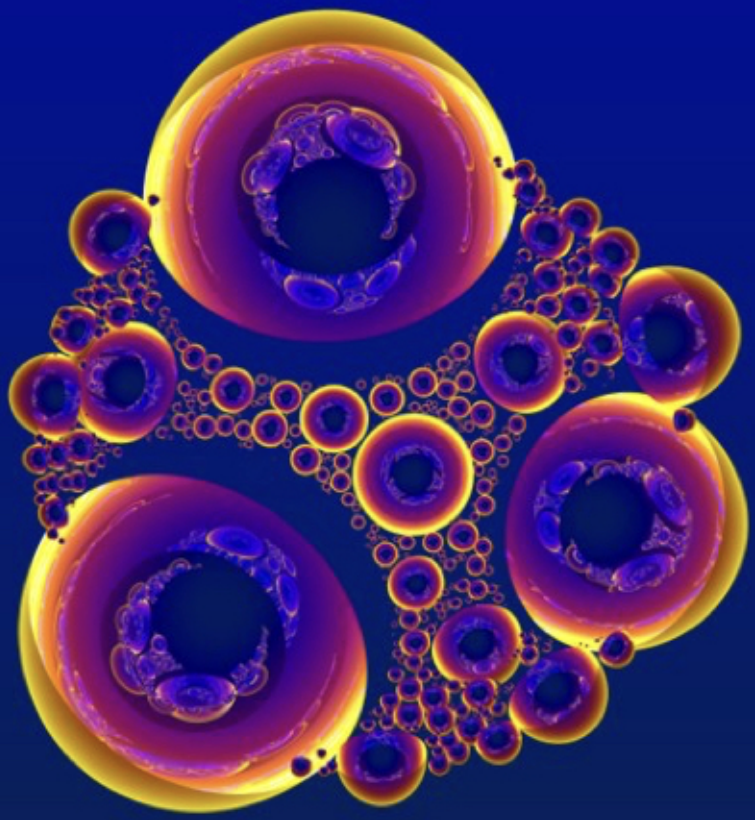

Special Issue

2025

Volume 11, Issue 4

Arnold Mathematical Journal

Journal of **Institute of Mathematical Sciences**, Stony Brook University, NY
Published by **Association for Mathematical Research**, Davis, CA; Jenkintown PA.

Foreword to the special issue

We are happy to present a special issue of Arnold Mathematical Journal; its topic is finite-dimensional completely integrable systems.

This special issue stemmed from the conference *"Finite Dimensional Integrable Systems" (FDIS23)* that took place in Antwerp, Belgium in summer of 2023. That was the 7th in a series of biennial conferences, preceded by the following editions:

- 2011 in Jena, Germany,
- 2013 in Luminy, France,
- 2015 in Bedlewo, Poland,
- 2017 in Barcelona, Spain,
- 2019 in Shanghai, China,
- 2022 in Tel Aviv, Israel
- 2023 in Antwerp, Belgium
- and the 8th took place in 2025 in Guanajuato, Mexico.

FDIS is a major international event in the field of finite dimensional integrable systems and their ramifications. It attracts main players in this area, along with junior researchers; its focus is on the theoretical development of the field and on its numerous applications in mathematics and adjacent disciplines.

It has been a tradition to publish special issues of research journals originated in this conference. These include *Journal of Geometry and Physics* January 2015, May 2017, and April 2019; *Philosophical Transactions of the Royal Society A*, October 2018; and *European Journal of Mathematics*, December 2022. The present issue continues this tradition.

The guest editors for this special issue are Misha Bialy (Tel Aviv University), Anton Izosimov (University of Glasgow), and Sonja Hohloch (University of Antwerp).

Contents

Arnold Mathematical Journal
Volume 11, Issue 4, 2025

Integrable geodesic flows with simultaneously diagonalisable quadratic integrals

Sergey I. Agafonov Vladimir S. Matveev

Received 09 Nov 2024; Accepted 27 Nov 2024

Abstract: We show that if n functionally independent commutative quadratic in momenta integrals for the geodesic flow of a Riemannian or pseudo-Riemannian metric on an n-dimensional manifold are simultaneously diagonalisable at the tangent space to every point, then they come from the Stäckel construction, so the metric admits orthogonal separation of variables.

AMS Classification: 37J35, 70H06

Key words and phrases: Quadratic in momenta integrals, orthogonal separation of variables, finite-dimensional integrable systems, Killing tensors, Stäckel matrix

DOI: 10.56994/ARMJ.011.004.001

1 Introduction

We work locally, on a smooth n-dimensional pseudo-Riemannian manifold (M, g) of any signature. By geodesic flow we understand the Hamiltonian system on T^*M generated by the Hamiltonian

$$H(x,p) = \tfrac{1}{2} g^{ij} p_i p_j.$$

We will study the situation when the geodesic flow admits n, including the Hamiltonian, integrals

$$\overset{1}{I}(x,p) = 2H\,,\ \overset{2}{I}(x,p)\,,\ \dots\,,\ \overset{n}{I}(x,p)$$

such that the following conditions are fulfilled:

1. The integrals are quadratic in momenta, that is, $\overset{\alpha}{I}(x,p) = \overset{\alpha}{K}{}^{ij} p_i p_j$. In particular, $g^{ij} = \overset{1}{K}{}^{ij}$. We assume without loss of generality that the (2,0)-tensor fields $\overset{\alpha}{K}{}^{ij}$ are symmetric in upper indexes.

2. At almost every point $x \in M$, there exists a basis in T_xM such that, for every $\alpha = 1, \dots, n$, the matrix $\left(\overset{\alpha}{K}{}^{ij}(x)\right)$ is diagonal.

3. The differentials of the integrals are linearly independent at least at one[1] point of T^*M.

In many publications on this topic, e.g. in [BCR02, Eis34, Kiy97], it is assumed that for almost every point $x \in M$ the restrictions of the tensor fields $\overset{\alpha}{K}{}^{ij}$, $\alpha = 1, \dots, n$, to T_xM are linearly independent. Our main result, Theorem 1 below, shows that this assumptions follows from conditions (1,2,3):

Theorem 1. *Under the assumptions above, for almost every point x the restrictions of the tensor fields $\overset{\alpha}{K}{}^{ij}$, $\alpha = 1, \dots, n$, to T_xM are linearly independent. In particular, for a*

[1] Using ideas of [KM16], is is easy to show that linear independence of the differentials of polynomial in momenta integrals at one point implies their linear independence at almost every point, provided the manifold is connected

generic linear combination $I = \sum_{\alpha=2}^{n} \lambda_\alpha \overset{\alpha}{I}$ *of the integrals, the corresponding (1,1)-tensor field* $K^i_j := K^{si} g_{sj}$, *where* $K^{ij} = \sum_{\alpha=2}^{n} \lambda_\alpha \overset{\alpha}{K}{}^{ij}$, *has* n *different eigenvalues.*

In dimension $n = 3$, Theorem 1 and Corollary 1.1 below were proven in [Aga24, Theorem 2] by other methods.

Corollary 1.1. *Assume the integrals* $\overset{\alpha}{I}$ *satisfy the conditions (1,2,3) above and in addition are in involution with respect to the standard Poisson bracket. Then, near almost every point, the metric* g *and the integrals come from the Stäckel construction.*

In view of Theorem 1, Corollary 1.1 follows from [KM80, Theorem 6], [Kiy97, Proposition 1.1.3], [BCR02, Theorem 8.6] or, possibly,[2] from A. Thimm 1976. In these references, it was shown that n quadratic functionally independent integrals in involution such that the corresponding Killing tensors are simultaneously diagonalisable at every tangent space and such that at least one of the Killing tensors with one index raised by the metric has n different eigenvalues, come from the Stäckel construction which we recall below.

As mentioned above, the difference between our conditions (1,2,3) and the assumptions used in [KM80, Theorem 6], [Kiy97, Proposition 1.1.3] or [BCR02, Theorem 8.6] is as follows: in [KM80, Theorem 6], [Kiy97, Proposition 1.1.3] or [BCR02, Theorem 8.6] it was assumed that one of the Killing tensors, with one index raised by the metric, has n different eigenvalues. We do not have this condition as an assumption and prove that it follows from other assumptions.

Let us recall the Stäckel[3] construction following [Eis34, St1]. Take a non-degenerate $n \times n$ matrix $S = (S_{ij})$ with S_{ij} being a function of the i-th variable x^i only . Next, consider the functions $\overset{\alpha}{I}$, $\alpha = 1, \dots, n$, given by the following system of linear equations

$$S\mathbb{I} = \mathbb{P}, \tag{1}$$

[2] By [Kli78, Note on page 185] the diploma thesis of A. Thimm 1976, which we were not able to find, contains this result

[3] The construction appeared already in [Lio49, §§13-14], see also discussion in [L̈0, pp. 703–705]

where $\mathbb{I} = \begin{pmatrix} 1 & 2 & & n \\ I, I, \dots, I \end{pmatrix}^\top$ and $\mathbb{P} = \left(p_1^2, p_2^2, \dots, p_n^2\right)^\top$. It is known that the functions $\overset{\alpha}{I}$ are in involution. Taking one of them (say, the first one, provided the inverse matrix to S has no zeros in the first raw) as twice the Hamiltonian of the metric, one obtains an integrable geodesic flow whose integrals satisfy the conditions (1,2,3). Corollary 1.1 says that locally, near almost every points, there exist no other examples of geodesic flows admitting n independend quadratic in momenta integrals in involution, such that the corresponding Killing tensors are simultaneously diagonalisable at almost every tangent space.

It is known that metrics coming from the Stäckel construction admit orthogonal separation of variables in the Hamilton-Jacobi equations, so the equation for their geodesics can be locally solved in quadratures [BKM25, KKM18]. Namely, J. Liouville [Lio49] and, independently, P. Stäckel [St1] has shown that the metrics are precisely those admitting othogonal separation of variables. L. P. Eisenhart, in his widely cited and very influential paper [Eis34], has shown that locally the metrics coming from the Stäckel construction are precisely those whose geodesic flows admit n functionally independent integrals in involution satisfying the following conditions: the integrals are quadratic in momenta, the corresponding matrices are simultaneously diagonalisable in a coordinate system, and at every point the corresponding matrices are linearly independent. In [BCR02, KM80, Kiy97] it was shown that the assumption that the integrals are simultaneously diagonalisable in a coordinate system may be replaced by a weaker assumption that the matrices of the integrals are diagonalisable in a frame. Our result further improves the result of Eisenhart and shows that the condition that the matrices of the integrals are linearly independent at each point is not necessary as this assumption follows from other conditions.

2 Proof of Theorem 1

Under the assumptions (1,2,3) from Section 1, near almost every point, there exist smooth vector fields $v_1(x), ..., v_n(x) \in T_xM$ such that they are linearly independent at every tangent

space and such that the metric g and the matrices $\overset{\alpha}{K}{}^{ij}$ are diagonal in the basis $(v_1, ..., v_n)$. After re-arranging and re-scaling the vectors v_i, there exists $m \in \mathbb{N}$, $m \leq n$, $k_1, ..., k_m \in \mathbb{N}$ with $k_1 + \cdots + k_m = n$ and smooth local functions $g_1, .., g_m, \overset{\alpha}{\rho}_1, \dots, \overset{\alpha}{\rho}_m$, $\alpha \in \{2, \dots, n\}$, on M such that the Hamiltonian and the integrals $\overset{\alpha}{I}$ with $\alpha = 2, \dots, n$ are given by the formulas

$$\begin{array}{rcl} 2H & = & V_1 + V_2 + \cdots + V_m \\ \overset{\alpha}{I} & = & \overset{\alpha}{\rho}_1 V_1 + \overset{\alpha}{\rho}_2 V_2 + \cdots + \overset{\alpha}{\rho}_m V_m \end{array} \tag{2}$$

In the formulas above, V_i are the functions on the cotangent bundle given by

$$\begin{array}{rcl} V_1 & = & (v_1)^2\varepsilon_1 + (v_2)^2\varepsilon_2 + \cdots + (v_{k_1})^2\varepsilon_{k_1}, \\ V_2 & = & (v_{k_1+1})^2\varepsilon_{k_1+1} + (v_{k_1+2})^2\varepsilon_{k_1+2} + \cdots + (v_{k_1+k_2})^2\varepsilon_{k_1+k_2}, \\ & \vdots & \\ V_m & = & (v_{k_1+\cdots+k_{m-1}+1})^2\varepsilon_{k_1+\cdots+k_{m-1}+1} + (v_{k_1+\cdots+k_{m-1}+2})^2\varepsilon_{k_1+\cdots+k_{m-1}+2} + \cdots + (v_n)^2\varepsilon_n, \end{array}$$

where v_i is the linear function on the T^*M generated by the vector field v_i via the canonical identification[4] $TM \equiv T^{**}M$, and $\varepsilon_i \in \{-1, 1\}$.

The Poisson bracket of H and $I = \overset{\alpha}{I}$ reads (we omit the index α since the equations hold for any $\overset{\alpha}{I}$):

$$0 = \{2H, I\} = \sum_{i,j=1}^{m} \left(\{V_i, \rho_j\} V_j + \rho_j \{V_i, V_j\} \right). \tag{3}$$

The right hand side of (3) is a cubic polynomial in momenta so all its coefficients are zero. For every point $x \in M$, this gives us a system of linear equations on the directional derivatives $v_s(\rho_j)$ with $s \in \{1, \dots, n\}$ and $j \in \{1, \dots, m\}$. The coefficients and free terms of this system depend on $\rho_j(x)$, on the entries of the vector fields v_s at x, and on the derivatives of the entries of the vector fields v_s at x. Let us show that all directional derivatives $v_s(\rho_i)$ can be reconstructed from this system. We will show this for the directional derivatives $v_1(\rho_2)$ and $v_1(\rho_1)$, since this will cover two principle cases $i = j$ and $i \neq j$; the proof for all other $v_i(\rho_j)$ is completely analogous.

[4] In naive terms, we consider the vector field $v = \sum_i v^i \partial_i$ as the linear function $p \longmapsto \sum_i v^i p_i$ on T^*M. This identification of vector fields on M and linear in momenta functions on the cotangent bundle is independent of a coordinate system

In order to extract $v_1(\rho_2)$, note that the cubic in momenta component $(v_{k_1+1})^2 v_1$ shows up only in the addends $\{V_1, \rho_2\}V_2$, $\rho_1\{V_2, V_1\}$ and $\rho_1\{V_1, V_2\}$. In these addends, the coefficient containing a derivative of one of the functions ρ_s is $v_1(\rho_2)$. Thus, equating the coefficient of $(v_{k_1+1})^2 v_1$ to zero gives us $v_1(\rho_2)$ as a function of ρ_1, ρ_2 and the entries of $\{V_1, V_2\}$.

Similarly, in order to extract $v_1(\rho_1)$, we note that the cubic in momenta component $(v_1)^3$ shows up only in the addends $\{V_1, \rho_1\}V_1$ and $\rho_1\{V_1, V_2\}$. Its coefficient containing the derivatives of ρ's is $v_1(\rho_1)$. Thus, equating the coefficient of $(v_1)^3$ to zero gives us $v_1(\rho_1)$ as a function of ρ_1.

Thus, all directional derivatives $v_s(\rho_j)$ can be obtained from the system (3). Let us now view the system (3) as a linear PDE-system on unknown functions ρ_i. The coefficients of this system come from the vector fields v_s and are given by certain nonlinear expressions in the components of v_s and their derivatives. Since the directional derivatives of all functions ρ_i are expressed in the terms of the functions ρ_i, the system can be solved with respect to all derivatives of the functions ρ_i. Therefore, the initial values of the functions ρ_i at one point x_0 determine the local solution of the system. This implies that the space of solutions is at most m-dimensional. Finally, the linear vector space of the integrals $\overset{\alpha}{I}$ is at most m-dimensional. Since n of them are functionally independent by our assumptions, $n = m$ and Theorem 1 is proved.

Remark 1. *The proof of Theorem 1 is motivated by [Ben92, proof of Lemma 1.2], [Kiy97, §1.1] and [KKM24, §2].*

Acknowledgments

V. M. thanks the DFG (projects 455806247 and 529233771) and ARC Discovery Programme (DP210100951) for the support. This research was partially supported by FAPESP (research fellowship 2018/20009-6), in particular the visit of V. M. to São José do Rio Preto, was supported by this grant. We thank C. Chanu and G. Rastelli for pointing out the references [BCR02, KM80] and for useful discussions. We are grateful to the anonymous referee for useful suggestions.

References

[Aga24] Sergey I. Agafonov. Integrable geodesic flow in 3D and webs of maximal rank. *Anal. Math. Phys.*, 14(6):Paper No. 128, 2024. 3

[BCR02] S. Benenti, C. Chanu, and G. Rastelli. Remarks on the connection between the additive separation of the Hamilton-Jacobi equation and the multiplicative separation of the Schrödinger equation. I. The completeness and Robertson conditions. *J. Math. Phys.*, 43(11):5183–5222, 2002. 2, 3, 4, 6

[Ben92] S. Benenti. Inertia tensors and Stäckel systems in the Euclidean spaces. volume 50, pages 315–341 (1993). 1992. Differential geometry (Turin, 1992). 6

[BKM25] A. V. Bolsinov, A. Yu. Konyaev, and V. S. Matveev. Orthogonal separation of variables for spaces of constant curvature. *Forum Mathematicum*, 37(1):13–41, 2025. 4

[Eis34] L. P. Eisenhart. Separable systems of Stackel. *Ann. of Math. (2)*, 35(2):284–305, 1934. 2, 3, 4

[Kiy97] Kazuyoshi Kiyohara. Two classes of Riemannian manifolds whose geodesic flows are integrable. *Mem. Amer. Math. Soc.*, 130(619):viii+143, 1997. 2, 3, 4, 6

[KKM18] E. G. Kalnins, J. M. Kress, and W. jun. Miller. *Separation of variables and superintegrability. The symmetry of solvable systems*. IOP Expand. Phys. Bristol: IOP Publishing, 2018. 4

[KKM24] A. Yu. Konyaev, J. M. Kress, and V. S. Matveev. When a (1,1)-tensor generates separation of variables of a certain metric. *Journal of Geometry and Physics*, 195:105031, 2024. 6

[Kli78] W. Klingenberg. *Lectures on closed geodesics*, volume 230 of *Grundlehren der Mathematischen Wissenschaften*. Springer-Verlag, Berlin-New York, 1978. 3

[KM80] E. G. Kalnins and W. jun. Miller. Killing tensors and variable separation for Hamilton-Jacobi and Helmholtz equations. *SIAM J. Math. Anal.*, 11(6):1011–1026, 1980. 3, 4, 6

[KM16] B. S. Kruglikov and V. S. Matveev. The geodesic flow of a generic metric does not admit nontrivial integrals polynomial in momenta. *Nonlinearity*, 29(6):1755–1768, 2016. 2

[Lö90] J. Lützen. *Joseph Liouville 1809–1882: master of pure and applied mathematics*, volume 15 of *Studies in the History of Mathematics and Physical Sciences*. Springer-Verlag, New York, 1990. 3

[Lio49] J. Liouville. Mémoire sur l'intégration des équations différentielles du mouvement d'un nombre quelconque de points matériels. *Journal de Mathématiques Pures et Appliquées*, 1e série, 14:257–299, 1849. 3, 4

[St1] P. Stäckel. Die integration der hamilton-jacobischen differentialgleichung mittelst separation der variablen. *Habilitationsschrift, Universität Halle*, 1891. 3, 4

AUTHORS

Sergey I. Agafonov,
Department of Mathematics,
São Paulo State University-UNESP,
São José do Rio Preto, Brazil
email: sergey.agafonov@gmail.com

Integrable geodesic flows with quadratic integrals

Vladimir S. Matveev
Institut für Mathematik,
Friedrich Schiller Universität Jena,
07737 Jena, Germany
email: vladimir.matveev@uni-jena.de

Arnold Mathematical Journal
Volume 11, Issue 4, 2025

The Flapping Birds in the Pentagram Zoo

Richard Evan Schwartz

Received 24 Dec 2024; Accepted 7 May 2025

Abstract: We study the $(k+1,k)$ diagonal map for $k = 2, 3, 4, \ldots$. We call this map Δ_k. The map Δ_1 is the pentagram map and Δ_k is a generalization. Δ_k does not preserve convexity, but we prove that Δ_k preserves a subset B_k of certain star-shaped polygons which we call *k-birds*. The action of Δ_k on B_k seems similar to the action of Δ_1 on the space of convex polygons. We show that some classic geometric results about Δ_1 generalize to this setting.

AMS Classification: 51A20

Key words and phrases: pentagram map, geometric dynamics, projective geometry, polygons

DOI: 10.56994/ARMJ.011.004.002

1 Introduction

1.1 Context

When you visit the pentagram zoo you should certainly make the pentagram map itself your first stop. This old and venerated animal has been around since the place opened up and it is very friendly towards children. When defined on convex pentagons, this map has a very long history. See e.g. [15]. In modern times [19], the pentagram is defined and studied much more generally. The easiest case to explain is the action on convex n-gons. One starts with a convex n-gon P, for $n \geq 5$, and then forms a new convex n-gon P' by intersecting the consecutive diagonals, as shown Figure 1.1 below.

The magic starts when you iterate the map. One of the first things I proved in [19] about the pentagram map is the successive iterates shrink to a point. Many years later, M. Glick [3] proved that this limit point is an algebraic function of the vertices, and indeed found a formula for it. See also [9] and [1].

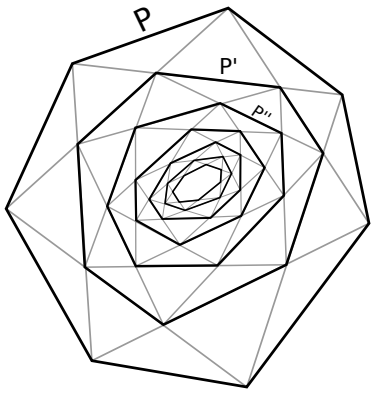

Figure 1.1: The pentagram map iterated on a convex 7-gon P.

Forgetting about convexity, the pentagram map is generically defined on polygons in the projective plane over any field except for $\boldsymbol{Z}/2$. In all cases, the pentagram map commutes with projective transformations and thereby defines a birational map on the space of n-gons modulo projective transformations. The action on this moduli space has a beautiful structure. As shown in [17] [18], and independently in [23], the pentagram

map is a discrete completely integrable system when the ground field is the reals. ([23] also treats the complex case.) Recently, M. Weinreich [24] generalized the integrability result, to a large extent, to fields of positive characteristic.

The pentagram map has many generalizations. See for example [2], [14], [16], [10], [11], [6]. The paper [2] has the first general complete integrability result. The authors prove the complete integrability of the $(k, 1)$ diagonal maps, i.e. the maps obtained by intersecting successive k-diagonals. Figure 1.3 below shows the $(3, 1)$ diagonal map. (Technically, [2] concentrates on what happens when these maps act on so-called *corregated polygons* in higher dimensional Euclidean spaces.) The paper [6] proves an integrability result for a very wide class of generalizations, including the ones we study below. (Technically, for the maps we consider here, the result in [6] does not establish the algebraic independence of invariants needed for complete integrability.) The pentagram map and its many generalizations are related to a number of topics: alternating sign matrices [20], dimers [5], cluster algebras [4], the KdV hierarchy [12], [13], spin networks [2], Poisson Lie groups [8], Lax pairs [23], [10], [11], [6], [8], and so forth. The zoo has many cages and sometimes you have to get up on a tall ladder to see inside them.

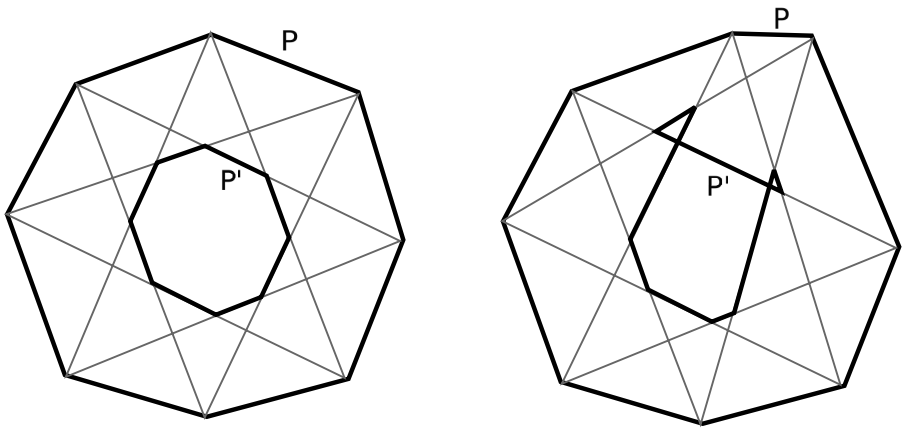

Figure 1.2: The $(3, 1)$-diagonal map acting on 8-gons.

The algebraic side of the pentagram zoo is extremely well developed, but the *geometric side* is hardly developed at all. In spite of all the algebraic results, we don't really know,

geometrically speaking, much about what the pentagram map and its relatives really do to polygons.

Geometrically speaking, there seems to be a dichotomy between convexity and non-convexity. The generic pentagram orbit of a projective equivalance class of a convex polygon lies on a smooth torus, and you can make very nice animations. What you will see, if you tune the power of the map and pick suitable representatives of the projective classes, is a convex polygon sloshing around as if it were moving through water waves. If you try the pentagram map on a non-convex polygon, you see a crazy erratic picture no matter how you try to normalize the images. The situation is even worse for the other maps in the pentagram zoo, because these generally do not preserve convexity. Figure 1.2 shows how the $(3,1)$-diagonal map does not necessarily preserve convexity, for instance. See [21], [22] for more details.

If you want to look at pentagram map generalizations, you have to abandon convexity. However, in this paper, I will show that sometimes there are geometrically appealing replacements. The context for these replacements is the $(k+1,k)$-diagonal map, which I call Δ_k, acting on what I call *k-birds*. Δ_k starts with the polygon P and intersects the $(k+1)$-diagonals which differ by k clicks. (We will give a more formal definition in the next section.) Δ_k is well (but not perfectly) understood algebraically [6]. Geometrically it is not well understood at all.

1.2 The Maps and the Birds

Definition of a Polygon: For us, a *polygon* is a choice of both vertices and the edges connecting them. Each polygon P we consider will all be *planar*, in the sense that there is some projective transformation that maps P, both vertices and edges, to the affine patch. Our classical example is a regular n-gon, with the obvious short edges chosen.

The Maps: Given a polygon P, let P_a denote the (a)th vertex of P. Let P_{ab} be the line

through P_a and P_b. The vertices of $\Delta_k(P)$ are

$$P_{j,j+k+1} \cap P_{j+1,j-k}. \tag{1}$$

Here the indices are taken mod n. Figure 1.3 shows this for $(k,n) = (2,7)$. The polygons in Figure 1.3 are examples of a concept we shall define shortly, that of a k-bird.

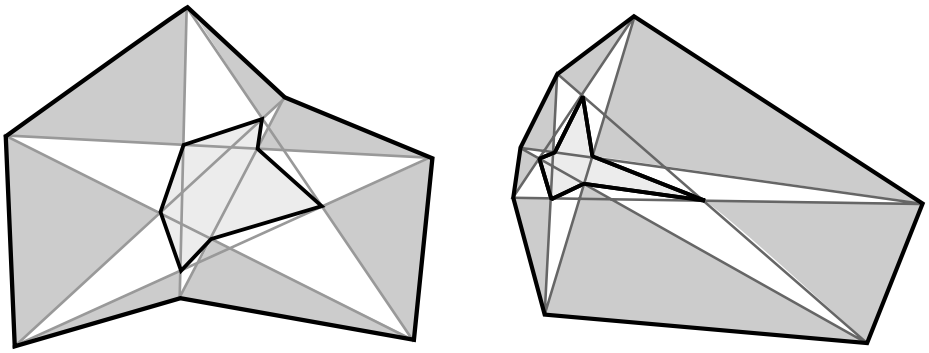

Figure 1.3: Δ_2 acting on 2-birds.

We should say a word about how the edges are defined. In the case for the regular n-gon we make the obvious choice, discussed above. In general, we define the class of polygons we consider in terms of a homotopy from the regular n-gon. So, in general, we make the edge choices so that the edges vary continuously.

The Birds: Given an n-gon P, we let $P_{a,b}$ denote the line containing the vertices P_a and P_b. We call P *k-nice* if $n > 3k$, and P is planar, and the 4 lines

$$P_{i,i-k-1}, \quad P_{i,i-k}, \quad P_{i,i+k}, \quad P_{i,i+k+1} \tag{2}$$

are distinct for all i. It is not true that the generic n-gon is k-nice, because there are open sets of non-planar polygons. (Consider a neighborhood of P, where P the regular 100-gon with the opposite choice of edges.) However, the generic perturbation of a planar n-gon is also k-nice.

We call P a *k-bird* if P is the endpoint of a path of k-nice n-gons that starts with the regular n-gon. We let $B_{k,n}$ be the subspace of n-gons which are k-birds. Note that $B_{k,n}$

contains the set of convex n-gons, and the containment is strict when $k > 1$. As Figure 1.3 illustrates, a k-bird need not be convex for $k \geq 2$. We will show that k-birds are always star-shaped, and in particular embedded. As we mentioned above, we use the homotopic definition of a k-bird, to define the edges of $\Delta_k(P)$ when P is a k-bird.

Example: The homotopy part of our definition looks a bit strange, but it is necessary. To illustrate this, we consider the picture further for the case $k = 1$. In this case, a 1-bird must be convex, though the 1-niceness condition just means planar and locally convex. Figure 1.4 shows how we might attempt a homoropy from the regular octagon to a locally convex octagon which essentially wraps twice around a quadrilateral. The little grey arrows give hints about how the points are moved. At some times, the homotopy must break the 1-niceness condition. The two grey polygons indicate failures and the highlighted vertices indicate the sites of the failures. There might be other failures as well; we are taking some jumps in our depiction.

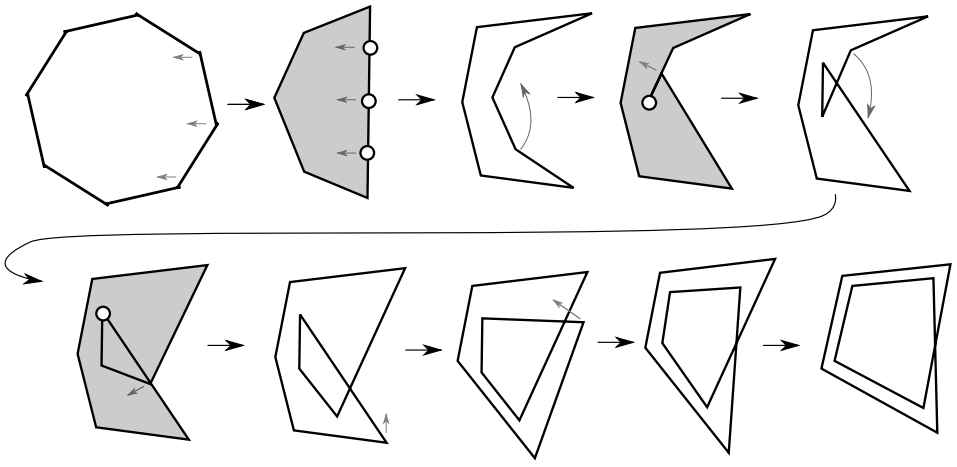

Figure 1.4: A homotopy that cannot stay 1-nice.

One could make similar pictures when $k \geq 1$, but the pictures might be harder to understand.

1.3 The Main Result

Given an embedded planar polygon P, let P^I denote the interior of region bounded by P. We say that P is *strictly star shaped* with respect to $x \in P^I$ if each ray emanating from x intersects P exactly once. More simply, we say that P is *strictly star shaped* if it is strictly star shaped with respect to some point $x \in P^I$. Here is the main result.

Theorem 1.1. *Let $k \geq 2$ and $n > 3k$ and $P \in B_{k,n}$. Then*

1. *P is strictly star-shaped, and in particular embedded.*
2. $\Delta_k(P) \subset P^I$.
3. $\Delta_k(B_{k,n}) = B_{k,n}$.

Remark: The statement that $n > 3k$ is present just for emphasis. $B_{n,k}$ is by definition empty when $n \leq 3k$. The restriction $n > 3k$ is necessary. Figure 1.5 illustrates what would be a counter-example to Theorem 1.1 for the pair $(k, n) = (3, 9)$. The issue is that a certain triple of 4-diagonals has a common intersection point. This does not happen for $n > 3k$. See Lemma 3.6.

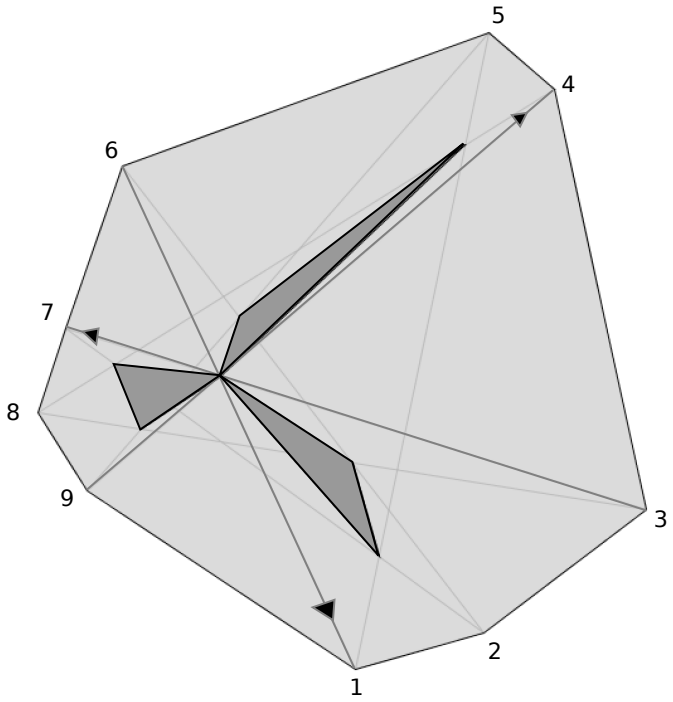

Figure 1.5: Δ_3 acting on a certain convex 9-gon.

1.4 The Energy

We will deduce Statements 1 and 2 of Theorem 1.1 in a geometric way. The key to proving Statement 3 is a natural quantity associated to a k-bird. We let $\sigma_{a,b}$ be the slope of the line $P_{a,b}$ and we define the *cross ratio*

$$\chi(a,b,c,d) = \frac{(a-b)(c-d)}{(a-c)(b-d)}. \tag{3}$$

We define

$$\chi_k(P) = \prod_{i=1}^{n} \chi(i,k,P), \qquad \chi(i,k,P) = \chi(\sigma_{i,i-k}, \sigma_{i,i-k-1}, \sigma_{i,i+k+1}, \sigma_{i,i+k}) \tag{4}$$

Here we are taking the cross ratio the slopes the lines involved in our definition of k-nice. When $k = 1$ this is the familiar invariant $\chi_1 = OE$ for the pentagram map Δ_1. See [19], [20], [17], [18]. When $n = 3k+1$, a suitable star-relabeling of our polygons converts Δ_k to Δ_1 and χ_k to $1/\chi_1$. So, in this case $\chi_k \circ \Delta_k = \chi_k$. Figure 1.5 illustrates this for $(k,n) = (3,10)$. Note that the polygons suggested by the dots in Figure 1.5 are not convex. Were we to add in the edges we would get a highly non-convex pattern.

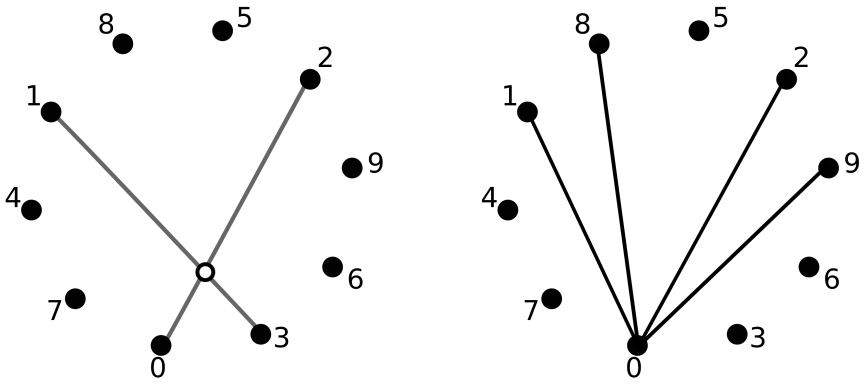

Figure 1.6: A star-relabeling converts Δ_1 to Δ_3 and $1/\chi_1$ to χ_3.

In general, χ_k is not as clearly related to χ_1. Nonetheless, we will prove

Theorem 1.2. $\chi_k \circ \Delta_k = \chi_k$.

Theorem 1.2 is meant to hold for all n-gons, as long as all quantities are defined. There is no need to restrict to birds.

1.5 The Collapse Point

When it is understood that $P \in B_{k,n}$ it is convenient to write

$$P^\ell = \Delta_k^\ell(P) \tag{5}$$

We also let $\widehat{P}$ denote the closed planar region bounded by P. Figure 1.7 below shows $\widehat{P} = \widehat{P}^0, \widehat{P}^1, \widehat{P}^2, \widehat{P}^3, \widehat{P}^4$ for some $P \in B_{4,13}$.

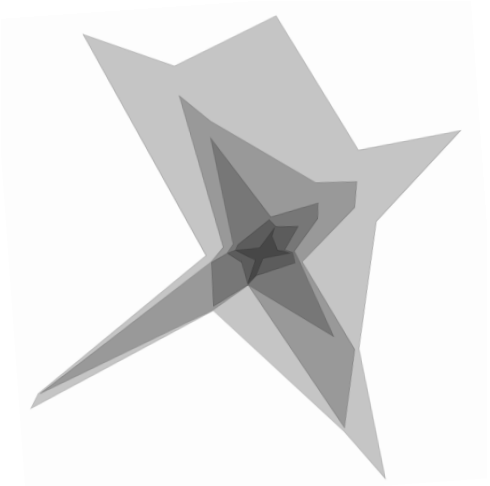

Figure 1.7: Δ_4 and its iterates acting on a member of $B_{4,13}$.

Define

$$\widehat{P}_\infty = \bigcap_{\ell \in \mathbf{Z}} \widehat{P}^\ell, \qquad \widehat{P}_{-\infty} = \bigcup_{\ell \in \mathbf{Z}} \widehat{P}^\ell. \tag{6}$$

Theorem 1.3. *If $P \in B_{k,n}$ then $\widehat{P}_\infty$ is a point and $\widehat{P}_{-\infty}$ is an affine plane.*

Our argument will show that $P \in B_{k,n}$ is strictly star-shaped with respect to all points in $\widehat{P}^n$. In particular, all polygons in the orbit are strictly star-shaped with respect to the collapse point $\widehat{P}_\infty$. See Corollary 7.3.

One might wonder if some version of Glick's formula works for the $\widehat{P}_\infty$ in general. I discovered experimentally that this is indeed the case for $n = 3k+1$ and $n = 3k+2$. See §9.2 for a discussion of this and related matters.

Here is a corollary of our results that is just about convex polygons.

Corollary 1.4. *Suppose that $n > 3k$ and P is a convex n-gon. Then the sequence $\{\Delta_k^\ell(P)\}$ shrinks to a point as $\ell \to \infty$, and each member of this sequence if strictly star-shaped with respect to the collapse point.*

1.6 The Triangulations

In §7.1 we associate to each k-bird P a triangulation $\tau_P \subset \boldsymbol{P}$, the projective plane. Here τ_P is an embedded degree 6 triangulation of $P_{-\infty} - P_\infty$. The edges are made from the segments in the δ-diagonals of P and its iterates for $\delta = 1, k, k+1$.

Figure 1.8 shows this tiling associated to a member of $B_{5,16}$. In this figure, the interface between the big black triangles and the big white triangles is some $\Delta_5^\ell(P)$ for some smallish value of ℓ. (I zoomed into the picture a bit to remove the boundary of the initial P.) The picture is normalized so that the line $P_{-\infty}$ is the line at infinity. When I make these kinds of pictures (and animations), I normalize so that the ellipse of inertia of P is the unit disk.

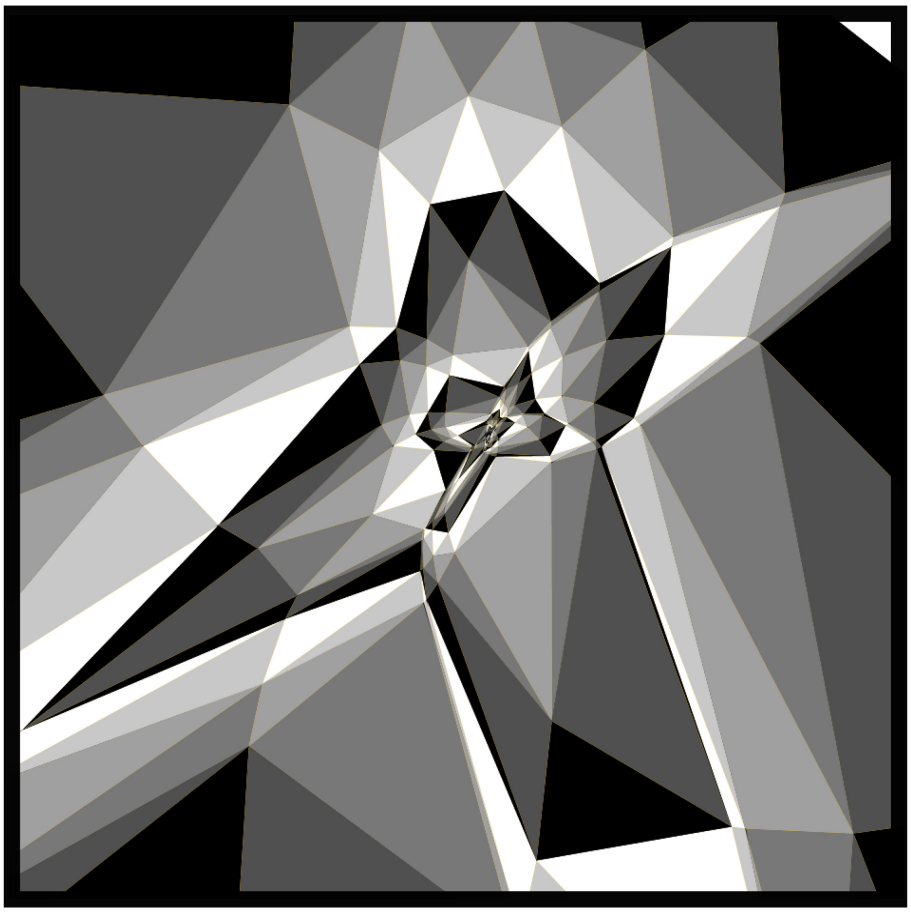

Figure 1.8: The triangulation associated to a member of $B_{5,16}$.

1.7 Paper Organization

This paper is organized as follows.

- In §2 we prove Theorem 1.2.
- In §3 we prove Statement 1 of Theorem 1.1.
- In §4 we prove Statement 2 of Theorem 1.1.
- In §5 we prove a technical result called the Degeneration Lemma, which will help with Statement 3 of Theorem 1.1.

- In §6 we prove Statement 3 of Theorem 1.1.
- In §7 we introduce the triangulations discussed above. Our Theorem 7.2 will help with the proof of Theorem 1.3.
- In §8 we prove Theorem 1.3.
- In §9, an appendix, we sketch an alternate proof of Theorem 1.2 which Anton Izosimov kindly explained. We also discuss Glick's collapse formula and star relabelings of polygons.

1.8 Visit the Flapping Bird Exhibit

Our results inject some more geometry into the pentagram zoo. Our results even have geometric implications for the pentagram map itself. See §9.3. There are different ways to visit the flapping bird exhibit in the zoo. You could read the proofs here, or you might just want to to look at some images:
http://www.math.brown.edu/~reschwar/BirdGallery
You can also download and play with the software I wrote:
http://www.math.brown.edu/~reschwar/Java/Bird.TAR
The software has detailed instructions. You can view this paper as a justification for why the nice images actually exist.

2 The Energy

The purpose of this chapter is to prove Theorem 1.2. The proof, which is similar to what I do in [19], is more of a verification than a conceptual explanation. My computer program allows the reader to understand the technical details of the proof better. The reader might want to just skim this chapter on the first reading. In §9 I will sketch an alternate proof, which I learned from Anton Izosimov. Izosimov's proof also uses the first two sections of this chapter.

2.1 Projective Geometry

Let $\boldsymbol{P}$ denote the real projective plane. This is the space of 1-dimensional subspaces of $\boldsymbol{R}^3$. The projective plane $\boldsymbol{P}$ contains $\boldsymbol{R}^2$ as the *affine patch*. Here $\boldsymbol{R}^2$ corresponds to vectors of the form $(x, y, 1)$, which in turn define elements of $\boldsymbol{P}$.

Let $\boldsymbol{P}^*$ denote the dual projective plane, namely the space of lines in $\boldsymbol{P}$. The elements in $\boldsymbol{P}^*$ are naturally equivalent to 2-dimensional subspaces of $\boldsymbol{R}^3$. The line in $\boldsymbol{P}$ such a subspace Π defines is equal to the union of all 1-dimensional subspaces of Π.

Any invertible linear transformation of $\boldsymbol{R}^3$ induces a *projective transformation* of $\boldsymbol{P}$, and also of $\boldsymbol{P}^*$. These form the *projective group* $PSL_3(\boldsymbol{R})$. Such maps preserve collinear points and coincident lines.

A *duality* from $\boldsymbol{P}$ to $\boldsymbol{P}^*$ is an analytic diffeomorphism $\boldsymbol{P} \to \boldsymbol{P}^*$ which maps collinear points to coincidence lines. The classic example is the map which sends each linear subspace of $\boldsymbol{R}^3$ to its orthogonal complement.

A *PolyPoint* is a cyclically ordered list of points of $\boldsymbol{P}$. When there are n such points, we call this an *n-Point*. A *PolyLine* is a cyclically ordered list of lines in $\boldsymbol{P}$, which is the same as a cyclically ordered list of points in $\boldsymbol{P}^*$. A projective duality maps PolyLines to PolyPoints, and *vice versa*.

Each n-Point determines 2^n polygons in $\boldsymbol{P}$ because, for each pair of consecutive points, we may choose one of two line segments to join them. As we mentioned in the introduction, we have a canonical choice for k-birds. Theorem 1.2 only involves PolyPoints, and our proof uses PolyPoints and PolyLines.

Given a n-Point P, we let P_j be its jth point. We make a similar definition for n-Lines. We always take indices mod n.

2.2 Factoring the Map

Like the pentagram map, the map Δ_k is the product of 2 involutions. This factorization will be useful here and in later chapters.

Given a PolyPoint P, consisting of points $P_1, ..., P_n$, we define $Q = D_m(P)$ to be the

PolyLine whose successive lines are $P_{0,m}$, $P_{1,m+1}$, etc. Here $P_{0,m}$ denotes the line through P_0 and P_m, etc. We labed the vertices so that

$$Q_{-m-i} = P_{i,i+m}. \tag{7}$$

This is a convenient choice. We define the action of D_m on PolyLines in the same way, switching the roles of points and lines. For PolyLines, $P_{0,m}$ is the intersection of the line P_0 with the line P_m. The map D_m is an involution which swaps PolyPoints with PolyLines. We have the compositions

$$\Delta_k = D_k \circ D_{k+1}, \qquad \Delta_k^{-1} = D_{k+1} \circ D_k. \tag{8}$$

The *energy* χ_k makes sense for n-Lines as well as for n-Points. The quantities $\chi_k \circ D_k(P)$ and $\chi_k \circ D_{k+1}(P)$ can be computed directly from the PolyPoint P. Figure 2.1 shows schematically the 4-tuples associated to $\chi(0, k, Q)$ for $Q = P$ and $D_k(P)$ and $D_{k+1}(P)$. In each case, $\chi_k(Q)$ is a product of n cross ratios like these. If we want to compute the factor of $\chi_k(D_k(P))$ associated to index i we subtract (rather than add) i from the indices shown in the middle figure. A similar rule goes for $D_{k+1}(P)$.

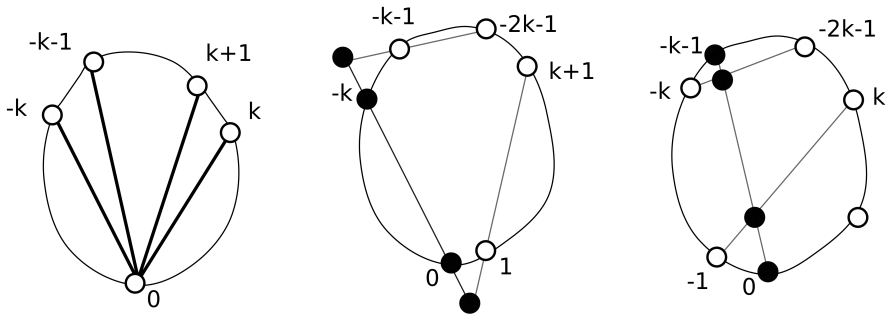

Figure 2.1: Computing the k-energy.

Theorem 1.2 follows from the next two results.

Lemma 2.1. $\chi_k \circ D_k = \chi_k$.

Lemma 2.2. $\chi_k \circ D_{k+1} = \chi_k$.

These results have almost identical proofs. We consider Lemma 2.1 in detail and then explain the small changes needed for Lemma 2.2.

2.3 Proof of the First Result

We study the ratio

$$R(P) = \frac{\chi_k \circ D_k(P)}{\chi_k(P)}. \tag{9}$$

We want to show that $R(P)$ equals 1 wherever it is defined. We certainly have $R(P) = 1$ when P is the regular n-Point.

Given a PolyPoint P we choose a pair of vertices a, b with $|a - b| = k$. We define $P(t)$ to be the PolyPoint obtained by replacing P_a with

$$(1 - t)P_a + tP_b. \tag{10}$$

Figure 2.2 shows what we are talking about, in case $k = 3$. We have rotated the picture so that P_a and P_b both lie on the X-axis.

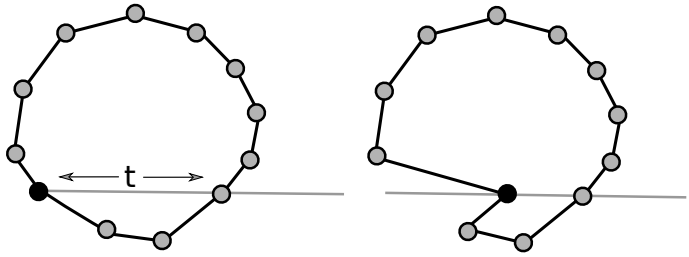

Figure 2.2: Connecting one PolyPoint to another by sliding a point.

The two functions

$$f(t) = \chi_k(P(t)), \qquad g(t) = \chi_k \circ D_k(P(t)) \tag{11}$$

are each rational functions of t. Our notation does not reflect that f and g depend on P, a, b.

A *linear fractional transformation* is a map of the form

$$t \to \frac{\alpha t + \beta}{\gamma t + \delta}, \qquad \alpha, \beta, \gamma, \delta \in \boldsymbol{R}, \qquad \alpha\delta - \beta\gamma \neq 0.$$

Lemma 2.3 (Factor I). *If $n \geq 4k + 2$ and P is a generically chosen n-Point, then $f(t)$ and $g(t)$ are each products of 4 linear fractional transformations. The zeros of f and g occur at the same points and the poles of f and g occur at the same points. Hence f/g is constant.*

The only reason we choose $n \geq 4k+2$ in the Factor Lemma is so that the various diagonals involved in the proof do not have common endpoints. The Factor Lemma I works the same way for all k and for all choices of (large) n. We write $P \leftrightarrow Q$ if we can choose indices a, b and some $t \in \boldsymbol{R}$ such that $Q = P(t)$. The Factor Lemma implies that when P, Q are generic and $P \leftrightarrow Q$ we have $R(P) = R(Q)$. The result for non-generic choices of P follows from continuity. Any n-Point Q can be included in a finite chain

$$P_0 \leftrightarrow P_1 \leftrightarrow \cdots \leftrightarrow P_{2n} = Q,$$

where P_0 is the regular n-Point. Hence $R(Q) = R(P_0) = 1$. This shows that Lemma 2.1 holds for (k, n) where $k \geq 2$ and $n \geq 4k+2$. (The case $k = 1$ is a main result of [19], and by now has many proofs.)

Lemma 2.4. *If Lemma 2.1 is true for all large values of n, then it is true for all values of n.*

Proof: If we are interested in the result for small values of n, we can replace a given PolyPoint P with its m-fold cyclic cover mP. We have $\chi_k(mP) = \chi_k(P)^m$ and $\chi_k(D_k(mP)) = \chi_k(D_k(p))^m$. Thus, the result for large n implies the result for small n. ♠

In view of Equation 4 we have

$$f(t) = f_1(t)...f_n(t), \qquad f_j(t) = \chi(j, k, P(t)). \tag{12}$$

Thus $f(t)$ is the product of n "local" cross ratios. We call an index j *asleep* if none of the lines involved in the cross ratio $f_j(t)$ depend on t. In other words, the lines do not vary at all with t. Otherwise we call j *awake*.

As we vary t, only the diagonals $P_{0,h}$ change for $h = -k, -k-1, k+1, k$. From this fact, it is not surprising that there are precisely 4 awake indices. These indices are

$$j_0 = 0, \quad j_1 = k+1, \quad j_2 = -k-1, \quad j_3 = -k. \tag{13}$$

The index k is not awake because the diagonal $P_{0,k}(t)$ does not move with t.

We define a *chord* of $P(t)$ to be a line defined by a pair of vertices of $P(t)$. The point $P_0(t)$ moves at linear speed, and the 4 lines involved in the calculation of $f_{c_j}(t)$ are distinct unless $P_0(t)$ lies in one of the chords of $P(t)$. Thus $f_{c_j}(t)$ only has zeros and poles at the corresponding values of t. It turns out that only the following chords are involved.

$$\begin{array}{cccccccc} -k & -k & -k & -k & -k-1 & -k-1 & k+1 & k+1 \\ -k-1 & k+1 & 1 & -2k-1 & -1 & -2k-1 & 1 & 2k+1 \end{array} \tag{14}$$

We call these $c_0, ..., c_7$. For instance, c_0 is the line through P_{-k} and P_{-k-1}. Let t_j denote the value of t such that $P(t_j) \in c_j$.

The PolyPoint $Q(t) = D_k(P(t))$ has the same structure as $P(t)$. Up to projective transformations $Q(t)$ is also obtained from the regular PolyPoint by moving a single vertex along one of the k-diagonals. The pattern of zeros and poles is not precisely the same because the chords of $Q(t)$ do not correspond to the chords of $P(t)$ in a completely straightforward way. The k-diagonals of $Q(t)$ correspond to the vertices of $P(t)$ and *vice versa*. The $(k+1)$ diagonals of $Q(t)$ correspond to the vertices of $\Delta_k^{-1}(P(t))$. This is what gives us our quadruples of points in the middle picture in Figure 2.1.

We now list the pattern of zeros and poles. We explain our notation by way of example. The quadruple $(f, 2, 4, 5)$ indicates that f_{c_2} has a simple zero at f_4 and a simple pole at t_5.

$$(f,0,0,1), \quad (f,1,6,7), \quad (f,2,4,5), \quad (f,3,2,3). \tag{15}$$

$$(g,0,6,5), \quad (g,1,0,3), \quad (g,2,2,1), \quad (g,3,4,7). \tag{16}$$

Since these functions have holomorphic extensions to $\boldsymbol{C}$ with no other zeros and poles, these functions are linear fractional transformations. This pattern establishes the Factor Lemma I.

Checking that the pattern is correct is just a matter of inspection. We give two example checks.

- To see why f_{c_2} has a simple zero at t_4 we consider the quintuple

$$(-k-1, -2k-1, -2k-2, 0, -1).$$

At t_4 the two diagonals $P_{-k-1,0}$ and $P_{-k-1,-1}$ coincide. In terms of the cross ratios of the slopes we are computing $\chi(a,b,c,d)$ with $a=b$. The point $P_0(t)$ is moving with linear speed and so the zero is simple.

- To see why g_{c_2} has a simple pole at t_1 we consider the 4 points

$$P_{2k+2,k+2} \cap P_{1,k+1}, \quad P_{k+1}, \quad P_1, \quad P_{1,k+1} \cap P_{-k,0}. \tag{17}$$

These are all contained in the k-diagonal $P_{1,k+1}$, which corresponds to the vertex $(-k-1)$ of $D_k(P)$. At $t=t_1$ the three points $P_0(t)$ and P_{-k} and P_{k+1} are collinear. This makes the 2nd and 4th listed point coincided. In terms of our cross ratio $\chi(a,b,c,d)$ we have $b=d$. This gives us a pole. The pole is simple because the points come together at linear speed.

The other explanations are similar. The reader can see graphical illustrations of these zeros and poles using our program.

2.4 Proof of the Second Result

The proof of Lemma 2.2 is essentially identical to the proof of Lemma 2.1. Here are the changes. The Factor Lemma II has precisely the same statement as the Factor Lemma I, except that

- When defining $P(t)$ we use points P_a and P_b with $|a-b|=k+1$.
- We are comparing $P(t)$ with $D_{k+1}(P(t))$.

This changes the definition of the functions f and g. With these changes made, the Factor Lemma I is replaced by the Factor Lemma II, which has an identical statement. This time the chords involved are as follows.

$$\begin{array}{cccccccc} -k-1 & -k-1 & -k-1 & -k-1 & -k & -k & k & k \\ -k & k & -1 & -2k-1 & 1 & -2k-1 & -1 & 2k+1 \end{array} \tag{18}$$

This time the 4 awake indices are:

$$j_0 = 0, \quad j_1 = k, \quad j_2 = -k-1, \quad j_3 = -k. \tag{19}$$

Here is the pattern of zeros and poles.

$$(f,0,1,0), \qquad (f,1,7,6), \qquad (f,2,3,2), \qquad (f,3,5,4). \tag{20}$$

$$(g,0,5,6), \qquad (g,1,3,0), \qquad (g,2,7,4), \qquad (g,3,1,2). \tag{21}$$

The pictures in these cases look almost identical to the previous case. The reader can see these pictures by operating my computer program. Again, the zeros of f and g are located at the same places, and likewise the poles of f and g are located at the same places. Hence f/g is constant. This completes the proof the Factor Lemma II, which implies Lemma 2.2.

3 The Soul of the Bird

3.1 Goal of the Chapter

Given a polygon $P \subset \mathbf{R}^2$, let $\widehat{P}$ be the closure of the bounded components of $\mathbf{R}^2 - P$ and let P^I be the interior of $\widehat{P}$. (Eventually we will see that birds are embedded, so $\widehat{P}$ will be a closed topological disk and P^I will be an open topological disk.)

Suppose now that $P(t)$ for $t \in [0,1]$ is a path in $B_{n,k}$ starting at the regular n-gon $P(0)$. We can adjust by a continuous family of projective transformations so that $P(t)$ is a bounded polygon in $\mathbf{R}^2$ for all $t \in [0,1]$. We orient $P(0)$ counter-clockwise around $P^I(0)$. We extend this orientation choice continuously to $P(t)$. We let $P_{ab}(t)$ denote the diagonal through vertices $P_a(t)$ and $P_b(t)$. We orient $P_{a,b}(t)$ so that it points from $P_a(t)$ to $P_b(t)$. We take indices mod n.

We now recall a definition from the introduction: When P is embedded, we say that P is *strictly star shaped* with respect to $x \in P^I$ if each ray emanating from x intersects P exactly once.

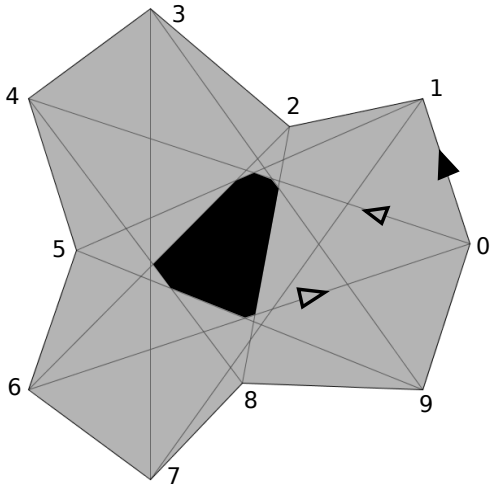

Figure 3.1: The soul of a 3-bird

Each such $(k+1)$-diagonal defines an oriented line that contains it, and also the (closed) *distinguished half plane* which lies to the left of the oriented line. These n half-planes vary continuously with t. The *soul* of $P(t)$, which we denote $S(t)$, is the intersection of the distinguished half-planes. Figure 3.1 shows the an example.

The goal of this chapter is to prove the following result.

Theorem 3.1. *Let P be a bird and let S be its soul. Then:*

1. *S is has non-empty interior.*

2. *$S \subset P^I$.*

3. *P is strictly star-shaped with respect to any point in S.*

Theorem 3.1 immediately implies Statement 1 of Theorem 1.1.

We are going to give a homotopical proof of Theorem 3.1. We say that a value $t \in [0,1]$ is a *good parameter* if Theorem 3.1 holds for $P(t)$. All three conclusions of Theorem 3.1 are open conditions. Finally, 0 is a good parameter. For all these reasons, it suffices to prove that the set of good parameters is closed. By truncating our path at the first supposed failure, we reduce to the case when Theorem 3.1 holds for all $t \in [0,1)$.

3.2 The Proof

For ease of notation we set $X = X(1)$ for any object X associated to $P(1)$.

Lemma 3.2. *If P is any k-bird, then P_0 and P_{2k+1} lie to the left of $P_{k,k+1}$. The same goes if all indices are cyclically shifted by the same amount.*

Proof: Consider the triangle with vertices $P_0(t)$ and $P_k(t)$ and $P_{k+1}(t)$. The k-niceness condition implies that this triangle is non-degenerate for all $t \in [0,1]$. Since $P_0(t)$ lies to to the left of $P_{k,k+1}(t)$, the non-degeneracy implies the same result for $t = 1$. The same argument works for the triple $(2k+1, k, k+1)$. ♠

Lemma 3.3. *S is non-empty and contained in P^I.*

Proof: By continuity, S is nonempty and contained in $P \cup P^I$. By the k-niceness property and continuity, P_1 lies strictly to the right of $P_{0,k+1}$. Hence the entire half-open edge $[P_0, P_1)$ lies strictly to the right of $P_{0,k+1}$. Hence $[P_0, P_1)$ is disjoint from S. By cyclic relabeling, the same goes for all the other half-open edges. Hence $S \cap P = \emptyset$. Hence $S \subset P^I$. ♠

Lemma 3.4. *P is strictly star-shaped with respect to any point of S.*

Proof: Since $P(t)$ is strictly star-shaped with respect to all points of $S(t)$ for $t < 1$, this lemma can only fail if there is an edge of P whose extending line contains a point $x \in S$. We can cyclically relabel so that the edge of $\overline{P_0 P_1}$.

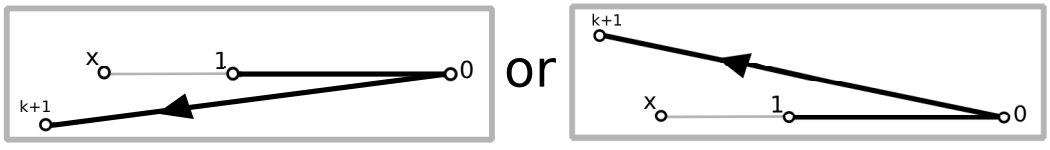

Figure 3.2: The diagonal $P_{0,k+1}$ does not separate 1 from x.

Since $x \notin P$, either P_1 lies between P_0 and x or P_0 lies in between x and P_1. In the first case, both P_1 and x lie on the same side of the diagonal $P_{0,k+1}$. This is a contradiction: P_1 is supposed to lie on the right and x is supposed to lie on the left. In the second case we get the same kind of contradiction with respect to the diagonal $P_{-k,1}$. ♠

We say that P has *opposing* $(k+1)$*-diagonals* if it has a pair of $(k+1)$-diagonals which lie in the same line and point in opposite directions. In this case, the two left half-spaces are on opposite sides of the common line.

Lemma 3.5. *P does not have opposing $(k+1)$-diagonals.*

Proof: We suppose that P has opposing diagonals and we derive a contradiction. In this case S, which is the intersection of all the associated left half-planes, must be a subset of the line L containing these diagonals. But then P intersects L in at least 4 points, none of which lie in S. But then P cannot be strictly star-shaped with respect to any point of S. This is a contradiction. ♠

We call three $(k+1)$-diagonals of $P(t)$ *interlaced* if the intersection of their left half-spaces is a triangle. See Figure 3.3.

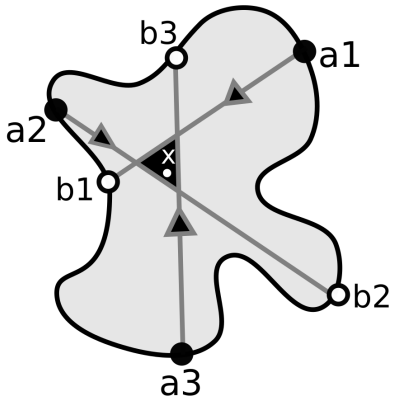

Figure 3.3: Interlaced diagonals on $P(t)$.

Given interlaced $(k+1)$-diagonals, and a point x in the intersection, the circle of rays emanating from x encounters the endpoints of the diagonals in an alternating pattern: $a_1, b_3, a_2, b_1, a_3, b_2$, where a_1, a_2, a_3 are the tail points and b_1, b_2, b_3 are the head points. Here a_1 names the vertex $P_{a_1}(t)$, etc.

Lemma 3.6. *$P(t)$ cannot have interlaced diagonals for $t < 1$.*

Proof: Choose $x \in S(t)$. The n-gon $P(t)$ is strictly star-shaped with respect to x. Hence, the vertices of P are encountered in order (mod n) by a family of rays that emanate from x and rotates around full-circle. Given the order these vertices are encountered, we have $a_{j+1} = a_j + \eta_j$, where $\eta_j \le k$. Here we are taking the subscripts mod 3 and the vertex values mod n. This tells us that $n = \eta_1 + \eta_2 + \eta_3 \le 3k$. This contradicts the fact that $n > 3k$. ♠

It only remains to show that S has non-empty interior. A special case of Helly's Theorem says the following: If we have a finite number of convex subsets of $\boldsymbol{R}^2$ then they all intersect provided that every 3 of them intersect. Applying Helly's Theorem to the set of interiors of our distinguished half-planes, we conclude that we can find 3 of these open half-planes whose triple intersection is empty. On the other hand, the triple intersection of the *closed* half-planes contains x. Since P has no opposing diagonals, this is only possible if the 3 associated diagonals are interlaced for t sufficiently close to 1. This contradicts Lemma 3.6. Hence S has non-empty interior.

4 The Feathers of the Bird

4.1 Goal of the Chapter

Recall that P^I is the interior of the region bounded by P. We call the union of black triangles in Figure 4.1 the *feathers* of the bird. the black region in the center is the soul.

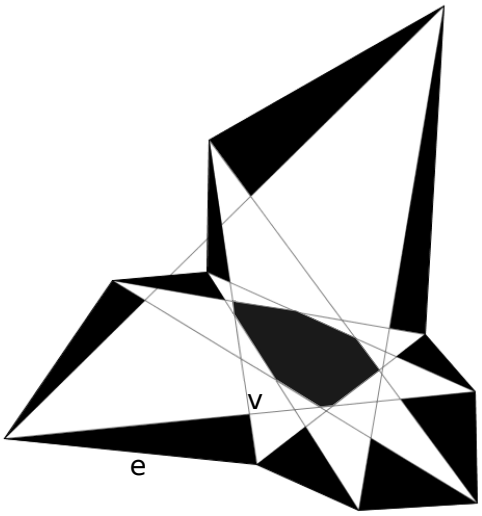

Figure 4.1 The feathers of a 3-bird.

Each feather F of a k-bird P is the convex hull of its *base*, an edge e of P, and its *tip*, a vertex of $\Delta_k(P)$.

The goal of this chapter is to prove the following result, which says that the simple topological picture shown in Figure 4.1 always holds.

Theorem 4.1. *The following is true.*

1. *Let F be an feather with base e. Then $F - \{e\} \subset P^I$.*

2. *Distinct feathers can only intersect at a vertex of P.*

3. *The line segment connecting two consecutive feather tips lies in P^I.*

When we apply Δ_k to P we are just specifying the points of $\Delta_k(P)$. We define the *polygon* $\Delta_k(P)$ so that the edges are the bounded segments connecting the consecutive tips of the feathers of P. With this definion, Statement 2 of Theorem 1.1 follows immediately from Theorem 4.1.

4.2 The Proof

There is one crucial idea in the proof of Theorem 4.1: The soul of P lies in the sector F^* opposite any of its feathers F. See Figure 4.2.

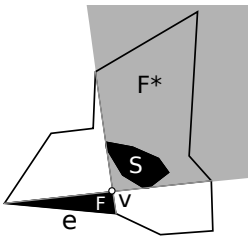

Figure 4.2 The soul lies in the sectors opposite the feathers.

We will give a homotopical proof of Theorem 4.1. By truncating our path of birds, we can assume that Theorem 4.1 holds for all $t \in [0,1)$. We set $P = P(1)$, etc.

Statement 1: Figure 4.3 shows the 2 ways that Statement 1 could fail:

1. The tip v of the feather F could coincide with some $p \in P$.
2. Some $p \in P$ could lie in the interior point of $\partial F - e$.

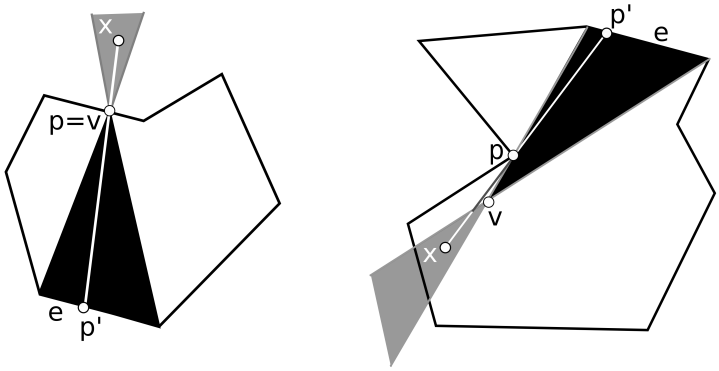

Figure 4.3: Case 1 (left) and Case 2 (right).

For all $x \in F^*$, the ray $\overrightarrow{xp}$ intersects P both at p and at a point $p' \in e$. This contradicts the fact that for any $x \in S \subset F^*$, the polygon P is strictly star-shaped with respect to x.

This establishes Statement 1 of Theorem 4.1.

Statement 2: Let F_1 and F_2 be two feathers of P, having bases e_1 and e_2. For Statement 2, it suffices to prove that $F_1 - e_1$ and $F_2 - e_2$ are disjoint.

The same homotopical argument as for Statement 1 reduces us to the case when F_1 and F_2 have disjoint interiors but $\partial F_1 - e_1$ and $\partial F_2 - e_2$ share a common point x. If ∂F_1 and ∂F_2 share an entire line segment then, thanks to the fact that all the feathers are oriented the same way, we would have two $(k+1)$ diagonals of P lying in the same line and having opposite orientation. Lemma 3.5 rules this out.

In particular x must be the tip of at least one feather. Figure 4.4 shows the case when $x = v_1$, the tip of F_1, but $x \neq v_2$. The case when $x = v_1 = v_2$ has a similar treatment.

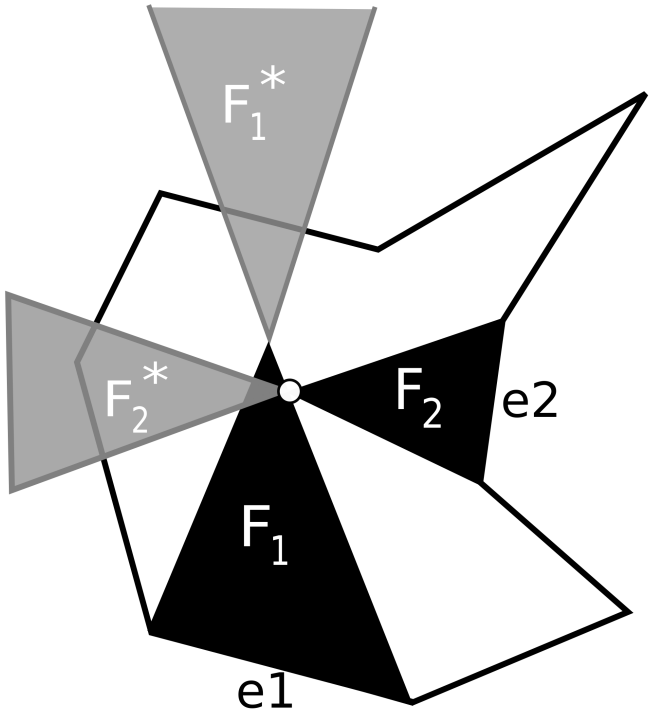

Figure 4.4: Opposiing sectors are disjoint

In this case, the two sectors F_1^* and F_2^* are either disjoint or intersect in a single point.

This contradicts the fact that $S \subset F_1^* \subset F_2^*$ has non-empty interior. This contradiction establishes Statement 2 of Theorem 4.1.

Statement 3: Recall that $\widehat{P} = P \cup P^I$. Let F_1 and F_2 be consecutive feathers with bases e_1 and e_2 respeectively. Let f be the edge connecting the tips of F_1 and F_2. Our homotopy idea reduces us to the case when $f \subset \widehat{P}$ and $f \cap P \neq \emptyset$. Figure 4.5 shows the situation.

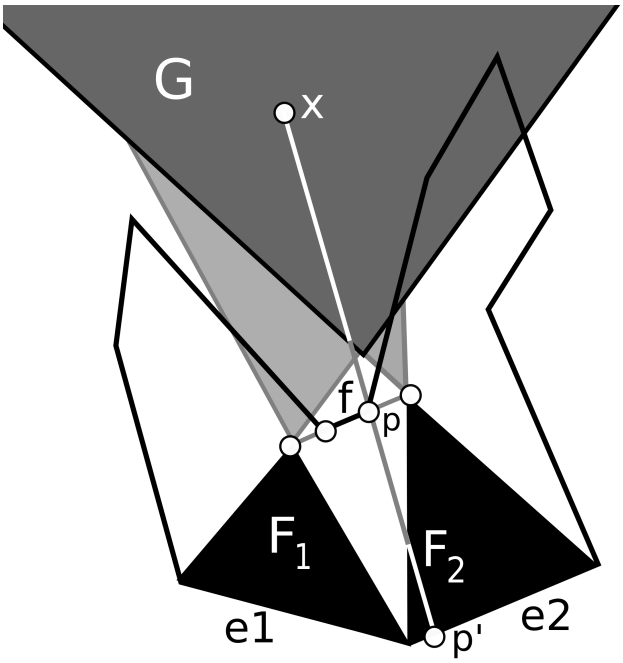

Figure 4.5: The problem a common boundary point

Note that $f \cap P$ must be strictly contained in the interior of f because (by Statement 1 of Theorem 4.1) the endpoints of f lie in P^I. But then, $f \cap P$ is disjoint from $F_1^* \cap F_2^*$, which is in turn contained in the shaded region G. For any $x \in G$ and each vertex p of f, the ray the ray $\overrightarrow{xp}$ also intersects P at a point $p' \in e_1 \cup e_2$. This gives the same contradiction as above when we take $x \in S \subset F_1^* \cap F_2^* \subset G$. This completes the proof of Statement 3 of Theorem 4.1.

5 The Degeneration of Birds

5.1 Statement of Result

Let $B_{k,n}$ denote the space of n-gons which are k-birds. Let χ_k denote the k-energy. With the value of k fixed in the background, we say that a *degenerating path* is a path $Q(t)$ of n-gons such that

1. $Q(t)$ is planar for all $t \in [0,1]$.
2. All vertices of $Q(t)$ are distinct for all $t \in [0,1]$.
3. $Q(t) \in B_{k,n}$ for all $t \in [0,1)$ but $Q(1) \notin B_{k,n}$.
4. $\chi_k(Q(t)) > \epsilon_0 > 0$ for all $t \in [0,1]$.

In this chapter we will prove the following result, which will help us prove that $\Delta_k(B_{k,n}) \subset B_{k,n}$ in the next chapter. The reader should probably just use the statement as a black box on the first reading.

Lemma 5.1 (Degeneration)**.** *If $Q(\cdot)$ is a degenerating path, then all but at most one vertex of $Q(1)$ lies in a line segment.*

Remark: Our proof only uses the fact that Q has nontrivial edges, nontrivial k-diagonals, and nontrivial $(k+1)$-diagonals. Some of the other vertices could coincide and it would not matter. Also, the same proof works if, instead of a continuous path, we have a convergent sequence $\{Q(t_n)\}$ with $t_n \to 1$ and a limiting polygon $Q(1) = \lim Q(t_n)$.

Example: Let us give an example for the case $k = 1$ and $n = 5$. Figure 5.0 shows a picture of a pentagon $Q(t)$ for $t = 1 - s$.

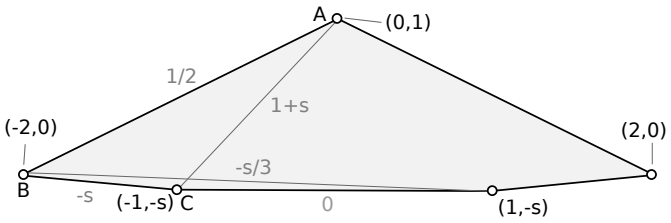

Figure 5.0: A degenerating path in the case $k = 1$ and $n = 5$.

Here s ranges from 1 to 0 as t ranges from 0 to 1. We have labeled some of the slopes to facility the calculation (which we leave to the reader) that $\chi_1(Q(t))$ remains uniformly bounded away from 0.

5.2 Distinguished Diagonals

We orient $Q(t)$ so that it goes counter-clockwise around the region it bounds. We orient the diagonal Q_{ab} so that it points from Q_a to Q_b. For $t < 1$ the vertices $Q_1(t)$ and $Q_k(t)$ lie to the right of the diagonal $Q_{0,k+1}(t)$, in the sense that a person walking along this diagonal according to its orientation would see that points in the right. This has the same proof as Lemma 3.2. The same rule holds for all cyclic relabelings of these points. The rule holds when $t < 1$. Taking a limit, we get a weak version of the rule: Each of $Q_1(1)$ and $Q_k(1)$ either lies to the right of the diagonal $Q_{0,k+1}(1)$ or on it. The same goes for cyclic relabeings. We call this the *Right Hand Rule*.

Say that a *distinguished diagonal* of $Q(t)$ is either a k-diagonal or a $(k+1)$-diagonal. There are $2n$ of these, and they come in a natural cyclic order:

$$Q_{0,k}(t) \quad Q_{0,k+1}(t), \quad Q_{1,k+1}(t), \quad Q_{1,k+2}(t), ... \tag{22}$$

The pattern alternates between k and $(k+1)$-diagonals. We say that a *diagonal chain* is a consecutive list of these.

We say that one oriented segment L_2 lies *ahead* of another one L_1 if we can rotate L_1 by $\theta \in (0, \pi)$ radians counter-clockwise to arrive at a segment parallel to L_2, In this case we write $L_1 \prec L_2$. We have

$$Q_{0,k+1}(t) \prec Q_{1,k+1}(t) \prec Q_{1,k+2}(t) \prec Q_{2,k+2}(t). \tag{23}$$

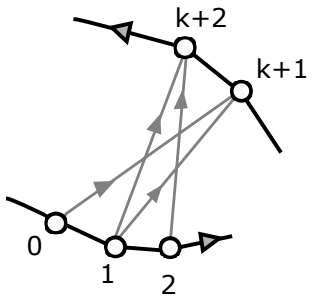

Figure 5.1: The turning rule

This certainly holds when $t = 0$. By continuity and the Right Hand Rule, this holds for all $t < 1$. Taking a limit, we see that the k-diagonals of $Q(1)$ weakly turn counter-clockwise in the sense that either $L_1 \prec L_2$ for consecutive diagonals or else L_1 and L_2 lie in the same line and point in the same direction. Moreover, the total turning is 2π. If we start with one distinguished diagonal and move through the cycle then the turning angle increases by jumps in $[0, \pi]$ until it reaches 2π. We call these observations *the Turning Rule*.

5.3 Collapsed Diagonals

Figure 5.2 shows the distinguished diagonals incident to Q_0. We always take indices mod n. Thus $-k - 1 = n - k - 1 \bmod n$.

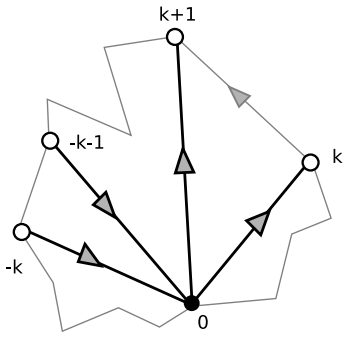

Figure 5.2: The 4 distinguished diagonals incident to $Q_0(t)$.

We say that Q has *collapsed diagonals* at a vertex if Q if the 4 distinguished diagonals incident to Q_k do not all lie on distinct lines. We set $Q = Q(1)$. We set $X = X(1)$ for each object X associated to $Q(1)$.

Since Q is planar but not k-nice, Q must have collapsed diagonals at some vertex. We relabel so that the collapsed diagonals are at Q_0.

Lemma 5.2. *If Q has collapsed diagonals at Q_0 then $Q_{-k-1,0}$ and $Q_{0,k+1}$ point in opposite directions or $Q_{-k,0}$ and $Q_{0,k}$ point in the same direction.*

Proof: Associated to each diagonal incident to Q_0 is the ray which starts at Q_0 and goes in the direction of the other endpoint of the diagonal. (Warning: The ray may have the opposite orientation than the diagonal it corresponds to.) If the angle between any of the rays tends to π as $t \to 1$ then the angle between the outer two rays tends to π. In this case $Q_{-k,0}$ and $Q_{0,k}$ point in the same directions. If the angle between non-adjacent rays tends to 0 then $Q_{-k-1,0}$ and $Q_{0,k+1}$ are squeezed together and point in opposite directions.

Suppose that the angle between adjacent rays tends to 0. If the two adjacent rays are the middle ones, we have the case just considered. Otherwise, either the angle between the two left rays tends to 0 or the angle between the two right rays tends to 0. In either case, the uniform lower bound on the cross ratio forces a third diagonal to point either in the same or the opposite direction as these adjacent diagonals when $t = 1$. Any situation like this leads to a case we have already considered. ♠

5.4 The Case of Aligned Diagonals

We say that Q has *aligned diagonals* at the vertex Q_0 if $Q_{-k,0}$ and $Q_{0,k}$ are parallel. This is the second option in Lemma 5.2. We make the same kind of definition at other vertices, with the indices shifted in the obvious way,.

Lemma 5.3. *Suppose Q does not lie in a single line. Suppose also that Q has aligned diagonals at Q_0. Then the diagonals $Q_{-k,0}, Q_{-k,1}, ..., Q_{-1,k}, Q_{0,k}$ all are parallel and (hence) the $2k+1$ points $Q_{-k}, ..., Q_0, ..., Q_k$ are contained in the line defined by these diagonals.*

Proof: These two diagonals define a short chain of diagonals, which starts with the first listed diagonal and ends with the second one. They also define a long chain, which starts

with the second and ends with the first. The total turning of the diagonals is 2π, so one of the two chains defined by our diagonals turns 2π and the other turns 0. Suppose first that the long chain has 0 turning. This chain involves all points of Q, and forces all points of Q to be on the same line. So, the short chain must consist of parallel diagonals. ♠

All we use in the rest of the proof is that $Q_{-k}, ..., Q_k$ are all contained in a line L. By shifting our indices, we can assume that $Q_{k+1} \notin L$. This relabeling trick comes with a cost. Now we cannot say whether the points $Q_{-k}....Q_k$ come in order on L. We now regain this control.

Lemma 5.4. *The length $2k$-diagonal chain $Q_{-k,0} \to ... \to Q_{0,k}$ consists entirely of parallel diagonals. There is no turning at all.*

Proof: The diagonals $Q_{-k,0}$ and $Q_{0,k}$. are either parallel or anti-parallel. If they are anti-parallel, then the angle between the corresponding rays incident $Q_0(t)$ tends to 0 as $t \to 1$. But these are the outer two rays. This forces the angle between all 4 rays incident to $Q_0(t)$ to tend to 0. The whole picture just folds up like a fan. But one or these rays corresponds to $Q_{0,k+1}(t)$. This picture forces $Q_{k+1} \in L$. But this is not the case.

Now we know that $Q_{-k,0}$ and $Q_{0,k}$ are parallel. All the diagonals in our chain are either parallel or anti-parallel to the first and last ones in the chain. If we ever get an anti-parallel pair, then the diagonals in the chain must turn 2π around. But then none of the other distinguished diagonals outside our chain turns at all. As in Lemma 5.3, this gives $Q \subset L$, which is false. ♠

We rotate the picture so that L coincides with the X-axis and so that $Q_{0,k}$ points in the positive direction. Since we are already using the words *left* and *right* for another purpose, we say that $p \in L$ is *forward of* of $q \in L$ if p has larger X-coordinate. Likewise we say that q is *backwards of* p in this situation. We say that $Q_{0,k}$ points *forwards*. We have established that $Q_{-k,0}, ..., Q_{0,k}$ all point forwards.

Lemma 5.5. *$Q_{k+2} \in L$ and both $Q_{1,k+2}$ and $Q_{2,k+2}$ point backwards.*

Proof: We have arranged that $Q_{k+1} \notin L$. Let us first justify the fact that Q_{k+1} lies above L. This follows from Right Hand Rule applied to $Q_{0,k+1}$ and Q_k and the fact that $Q_{0,k}$ points forwards. Since Q_{-k}, Q_{-k+1}, Q_1 are collinear, Q has collapsed diagonals at Q_1. But Q cannot have aligned diagonals because $Q_{1,k+1}$ is not parallel to $Q_{-k,1}$. Hence Q has folded diagonals at 1. This means that the diagonals $Q_{-k,1}$ and $Q_{1,k+2}$ point in opposite directions. This forces $Q_{k+2} \in L$ and morever we can say that $Q_{1,k+2}$ points backwards.

We have $Q_2 \in L$ because $2 \le k$. We want to see that $Q_{2,k+2}$ points forwards and they Suppose not. We consider the 3 distinguished diagonals

$$Q_{0,k}, \quad Q_{1,k+2}, \quad Q_{2,k+2}.$$

These diagonals respectively point forwards, backwards, forwards and they all point one direction or the other along L. But then, in going from $Q_{0,k}$ to $Q_{2,k+2}$, the diagonals have already turned 2π. Since the total turn is 2π, the diagonals $Q_{2,k+2}$, $Q_{3,k+3}, ..., Q_{n,n+k}$ are all parallel. But then $Q_2, ..., Q_n \in L$. This contradicts the fact that $Q_{k+1} \notin L$. ♠

Lemma 5.6. *For at least one of the two indices $j \in \{2k+2, 2k+3\}$ we have $Q_j \in L$ and $Q_{k+2,j}$ points forwards.*

Proof: Since Q_1, Q_2, Q_{k+2} are collinear, Q has collapsed diagonals at Q_{k+2}. So, by Lemma 5.2, we either have folded diagonals at Q_{k+2} or aligned diagonals at Q_{k+2}. The aligned case gives $Q_{2k+2} \in L$ and the folded case gives $Q_{2k+3} \in L$. We need to work out the direction of pointing in each case.

Consider the aligned case. Suppose $Q_{k+2,2k+2}$ points backwards, as shown in Figure 5.3.

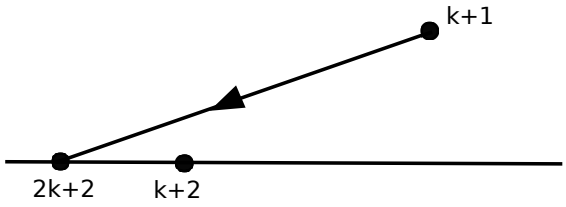

Figure 5.3: Violation of the Right Hand Rule

This violates the Right Hand Rule for Q_{k+2} and $Q_{k+1,2k+2}$ because Q_{k+1} lies above L.

Consider the folded case. Since $Q_{k+2,2k+3}$ and $Q_{1,k+2}$ point in opposite directions, and $Q_{1,k+2}$ points backwards (by the previous lemma), $Q_{k+2,2k+3}$ points forwards. ♠

Let $j \in \{2k+2, 2k+3\}$ be the index from Lemma 5.6. Consider the 3 diagonals

$$Q_{0,k}, \quad Q_{1,k+1}, \quad Q_{k+2,j}.$$

These diagonals are all parallel to L and respectively point in the forwards, backwards, forwards direction. This means that the diagonals in the chain $Q_{0,k} \to ... \to Q_{k+2,j}$ have already turned 2π radians. But this means that the diagonals

$$Q_{k+2,2k+3}, \quad Q_{k+3,2k+3}, \quad Q_{k+3,2k+4}, \quad ... \quad Q_{0,k} = Q_{n,n+k}$$

are all parallel and point forwards along L. Hence $Q_{k+2}, Q_{k+3}, ..., Q_n \in L$. Hence all points but Q_{k+1} lie in L.

5.5 The Case of Double Folded Diagonals

We fix a value of k. Say that two indices $a, b \in \mathbf{Z}/n$ are *far* if their distance is at least k in $\mathbf{Z}/n$. We say that Q has *far folded diagonals* if Q has folded diagonals at Q_a and Q has folded diagonals at b and a, b are far.

In this case we have two parallel diagonals $Q_{a,a+k+1}$ and $Q_{b,b+k+1}$. As in the proof of Lemma 5.3, one of the two diagonal chains defined by these diagonals consists of parallel diagonals. The far condition guarantees that at least $2k+1$ consecutive points are involved in each chain. But then we get $2k+1$ collinear points. So, if Q has far folded diagonals, then the same proof as in the previous section shows that the conclusion of the Degeneration Lemma holds for Q.

5.6 Good Folded Diagonals

We say that the folded diagonals $Q_{-k-1,0}$ and $Q_{0,k+1}$ are *good* if all the points $Q_{k+1}, Q_{k+2}, ..., Q_{n-k-1}$ are collinear. This notion is empty when $k = 2$ and $n = 7$ but otherwise it has content. In

this section we treat the case when Q has a pair of good folded diagonals. We start by discussing an auxiliary notion.

We say that Q has *backtracked edges* at Q_a if the angle between the edges $Q_{a,a+1}$ and $Q_{a,a-1}$ is either 0 or 2π.

Lemma 5.7. *If Q has backtracked edges at Q_a then Q has folded diagonals at Q_a.*

Proof: For $t \in [0,1)$, the edges of Q emanating from a divide the plane into 4 sectors, and one of these sectors, $C(t)$ contains all the distinguished diagonals emanating from $Q_a(t)$. The sector $C(t)$ is the one which locally intersects $Q(t)$ near $Q_a(t)$. The angle of $C(t)$ tends to 0 as $t \to 1$, forcing all the distinguished diagonals emanating from $Q_a(t)$ to squeeze down as $t \to 1$. This gives us the folded diagonals. ♠

We will use Lemma 5.7 in our analysis of good folded edges. Now we get to it. We rotate so that our two diagonals are in the line L, which is the X-axis. We normalize so that Q_0 is the origin, and Q_{k+1} and Q_{-k-1} are forward of Q_0.

Lemma 5.8. *If $n > 3k+1$ and $Q_{-k-1,0}, Q_{0,k+1}$ are good folded diagonals, then the Degeneration Lemma is true for Q.*

Proof: Suppose first that $Q_1 \in L$. Then Q has folded diagonals at Q_{k+1}. When $n > 3k+1$ the indices $(k+1)$ and $(-k-1)$ are k-far. This gives Q far folded diagonals, a case we have already treated.

To finish our proof, we show that $Q_1 \in L$. We explore some of the other points. We know that $Q_{k+1}, ..., Q_{n-k-1} \in L$. We can relabel dihedrally so that Q_{n-k-1} is forwards of Q_{k+1}. We claim that Q_{k+2} is forwards of Q_{k+1}. Suppose not. Then there is some index $a \in \{k+2, ..., -k-2\}$ such that Q_a is backwards of $Q_{a\pm1}$. What is going on is that our points would start by moving backwards on L and eventually they have to turn around. The index a is the turn-around index. This gives us backtracked edges at Q_a. By Lemma 5.7, we have folded diagonals at Q_a. But a and 0 are k-far indices. This gives Q far-folded diagonals.

The only way out of the contradiction is that Q_{k+2} is forwards of Q_{k+1}.

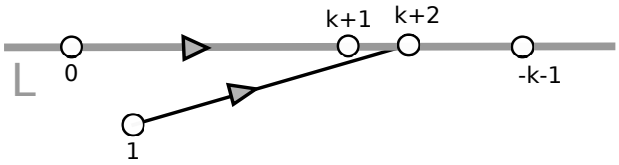

Figure 5.4: A contradiction involving Q_1.

Suppose $Q_1 \notin L$. by the Right Hand Rule applied to the diagonal $Q_{0,k+1}$, the point Q_1 lies beneath L, as shown in Figure 5.4. But then Q_{k+1} lies to the left of the diagonal $Q_{1,k+2}$. This violates the Right Hand Rule. Now we know that $Q_1 \in L$. ♠

Lemma 5.9. *Suppose $n = 3k+1$ and $k > 2$. If $Q_{-k-1,0}, Q_{0,k+1}$ are good folded diagonals, then the Degeneration Lemma is true for Q.*

Proof: The same argument as in Lemma 5.8 establishes the key containment $Q_1 \in L$. (We need $k > 2$ for this.) From here, as in Lemma 5.8, we deduce that $Q_{-k-1,0}$ and $Q_{k+1,2k+2}$ are parallel. This time the conclusion we get from this is not as good. We get a run of k points in L, and then a point not necessarily in L, and then a run of k additional points in L.

The points are $Q_{k+1}, ..., Q_{2k+1}, ..., Q_0$ with the point Q_{-k} omitted. But then Q has folded diagonals at each of these points except the outer two, Q_{k+1} and Q_0. But then For each such index h, we see that both $Q_{h\pm(k+1)}$ belong to L. This gives us all but one point in L.

It is instructive to consider an example, say $k = 4$ and $n = 13$. In this case, our initial run of points in L is $Q_5, Q_6, Q_7, Q_8, Q_{10}, Q_{11}, Q_{12}, Q_{13}$. The folded diagonals at Q_6, Q_7, Q_8 respectively give $Q_1, Q_2, Q_3 \in L$. The folded diagonals at Q_{10}, Q_{11}, Q_{12} respectively give $Q_2, Q_3, Q_4 \in L$. ♠

Finally we consider the case $k = 2$ and $n = 7$. In this case all we know is that $Q_0, Q_3, Q_4 \in L$ with Q_3, Q_4 forwards of Q_0. We can dihedrally relabel to that Q_4 is forwards of Q_3. Here $Q_3 = Q_{k+1}$ and $Q_4 = Q_{k+2}$. So, now we can run the same argument as in Lemma 5.9 to conclude that $Q_1 \in L$. Now we proceed as in the proof of Lemma 5.9.

5.7 Properties of the Soul

We define $S = S(1)$ to be the set of all accumulation points of sequences $\{p(t_n)\}$ where $p(t_n) \in S(t_n)$ and $t_n \to 1$. Here $S(t_n)$ is the soul of $P(t_n)$. We have one more case to analyze, namely ungood folded diagonals. To make our argument go smoothly, we first prove some properties about S.

Lemma 5.10. *Suppose that Q has folded diagonals at Q_0. If the Degeneration Lemma is false for Q, then S is contained in the line segment joining Q_0 to Q_{k+1}*

Proof: Here is a general statement about S. Since $S(t)$ is non-empty and closed for all $t < 1$, we see by compactness that S is also a non-empty closed subset of the closed region bounded by Q. By continuity S lies to the left of all the closed half-planes defined by the oriented $(k+1)$ diagonals (or in their boundaries). Since S lies to the left of (or on) each $(k+1)$ diagonal, S is a subset of the line L common to the folded diagonals and indeed S lies to one side of the fold point Q_0. From the way we have normalized, S lies in the X-axis forward of Q_0. (The point Q_0 might be an endpoint of S.)

If S contains points of L that lie forward of Q_{k+1} then either the diagonal $Q_{k+1,2k+2}$ points along the positive X-axis or into the lower half-plane. In the former cases, the diagonals $Q_{0,k+1}, Q_{k+1,2k+2}$ are parallel and we get at least $2k+1$ collinear points and so the Degeneration Lemma holds for Q.

If $Q_{k+1,2k+2}$ points into the negative half-plane, then the diagonal $Q_{0,k+1}$ turns more than π degrees before reaching $Q_{k+1,2k+2}$. But then the diagonals in the chain $Q_{-k-1,0} \to \ldots \to Q_{0,k+1} \ldots \to Q_{k+1,2k+2}$ turn more than 2π degrees. This is a contradiction. ♠

Remark: The same argument works with Q_{-k-1} in place of Q_{k+1}.

Lemma 5.11. *If the Degeneration Lemma is false for Q then S cannot intersect Q in the interior of an edge of Q.*

Proof: Suppose this happens. We relabel so that the edge is $Q_{0,1}$. By the Right Hand Rule, the point Q_1 is not on the left of the diagonal $Q_{0,k+1}$. At the same time, S is not on the right

of the diagonal. The only possibility is that Q_1, Q_0, Q_{k+1} are collinear. Likewise Q_{-k}, Q_0, Q_1 are collinear. Furtheremore, the $(k+1)$-diagonals $Q_{-k,1}$ and $Q_{0,k+1}$ are parallel. Figure 5.5 shows the situation for $Q(t)$ and $S(t)$ when t is very near 1.

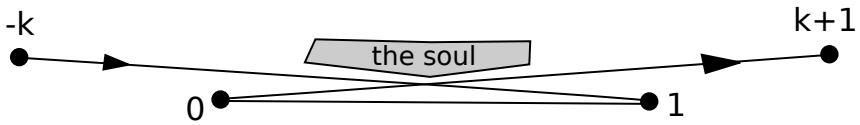

Figure 5.5: The relevant points and lines.

But now we have two $(k+1)$-diagonals that are parallel and which start at indices that are k apart in $\boldsymbol{Z}/n$. This gives us $2k+1$ consecutive collinear points on the line containing our edge. We know how to finish the Degeneration Lemma in this case. The only way out is that S cannot intersect Q in the interior of an edge of Q. ♠

Lemma 5.12. *If the Degeneration Lemma is false for Q, then S cannot contain a vertex of Q.*

Proof: We relabel so that $Q_0 \in S$. The same analysis as in the previous lemma shows that Q_1, Q_0, Q_{-k} are collinear. Figure 5.6. shows the situation for t near 1. At the same time, the points Q_{-1}, Q_0, Q_k are collinear.

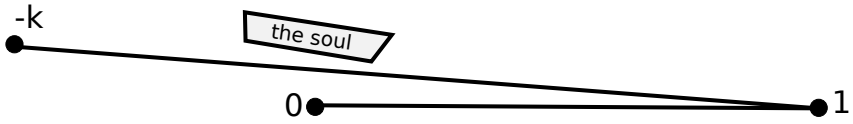

Figure 5.6: The relevant points and lines

To avoid a case of the Degeneration Lemma we have already done, Q must have folded diagonals at Q_{-k}. Likewise Q must have folded diagonals at Q_k. But then Q has far folded diagonals, and the Degeneration Lemma holds for Q. ♠

Now let us bring back our assumptions: Q has folded diagonals at Q_0 and the points Q_0, Q_{k+1}, Q_{-k-1} all lie in the X-axis in the forward order listed.

Corollary 5.13. *If the Degeneration Lemma is false for Q then S lies in the open interval bounded by Q_0 and Q_{k+1} and no point of S lies in Q. In particular, S contains a point x, forwards of Q_0 and backwards of both Q_{k+1} and Q_{-k-1}, that is disjoint from Q.*

5.8 Ungood Folded Diagonals

The only case left is when Q does not have $2k+1$ consecutive collinear points, and when all folded diagonals of Q are ungood. Without loss of generality, we will consider the case when Q has ungood folded diagonals at Q_0. We normalize as in the previous section, so that Q_0, Q_{k+1}, Q_{-k-1} lie in forward order on L, which is the X-axis. Let x be a point from Corollary 5.13.

We call an edge of Q *escaping* if $e \cap L$ is a single point. We call two different edges of Q, in the labeled sense, *twinned* if they are both escaping and if they intersect in an open interval. Even if two distinctly labeled edges of Q coincide, we consider them different as labeled edges.

Lemma 5.14. *Q cannot have twinned escaping edges.*

Proof: Consider $Q(t)$ for t near 1. This polygon is strictly star shaped with respect to a point $x(t)$ near x.

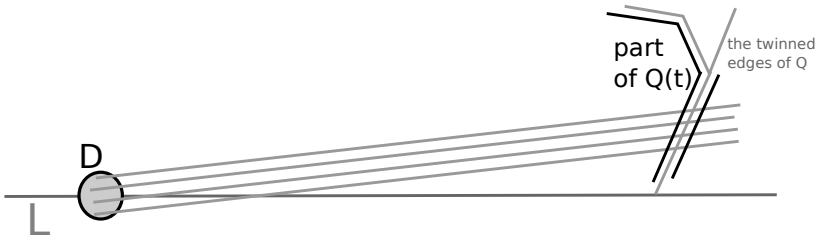

Figure 5.7: Rays intersecting the twinned segments

There is a disk D about x such that every $p \in D$ contains a ray which intersects the twinned edges in the middle third portion of their intersection. Figure 5.7 shows what we mean. Once t is sufficiently near 1, the soul $S(t)$ will intersect D, and for all points $p \in D$ there will be a ray which intersects $Q(t)$ twice. This contradicts the fact that $Q(t)$ is

strictly star-shaped with respect to all points of $S(t)$. ♠

We say that an escape edge *rises above* L if it intersects the upper half plane in a segment.

Lemma 5.15. *Q cannot have two escape edges which rise above L and intersect Q on the same side of the point x.*

Proof: This situation is similar to the previous proof. In this case, there is a small disk D about x such that every point $p \in D$ has a ray which intersects both rising escape edges transversely, and in the middle third of each of the two subsegments of these escape edges that lie above L. Figure 5.8 shows this situation.

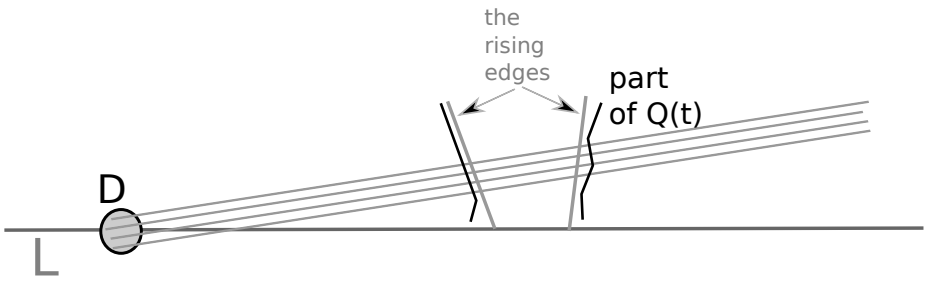

Figuren 5.8: Rays intersecting the rising segments.

In this case, some part of $Q(t)$ closely shadows our two escape edges for t near 1. But then, once t is sufficiently near 1, each ray we have been talking about intersects $Q(t)$ at least twice, once by each escaping edge. This gives the same contradiction as in the previous lemma. ♠

We define falling escape segments the same way. The same statement as in Lemma 5.15 works for falling escape segments. Since $x \notin Q$ we conclude that Q can have at most 4 escaping segments total.

But $Q = Q_+ \cup Q_-$, where $Q_\pm$ is an arc of Q that starts at Q_{k+1} and ends at Q_{-k-1}. Since both these arcs start and end on L, and since both do not remain entirely on L, we see

that each arc has at least 2 escape edges, and none of these are twinned. This means that both Q_+ and Q_- have exactly two escape edges.

Now for the moment of truth: Consider Q_+. Since Q_+ just has 2 escape edges, they both have to be either rising or falling. Also, since Q_+ starts and ends on the same side of x, and cannot intersect x, both the escape edges for Q_+ are on the same side of x. This is a contradiction. The same argument would work for Q_- but we don't need to make it.

6 The Persistence of Birds

In this chapter we prove Statement 3 of Theorem 1.1, namely the fact that $\Delta_k(B_{n,k}) = B_{n,k}$. First we use the Degeneration Lemma to prove that $\Delta_k(B_{n,k}) \subset B_{n,k}$. Then we deduce the opposite containment from projective duality and from the factoring of Δ_k given in §2.2.

6.1 Containment

Suppose for the sake of contradiction that there is some $P \in B_{k,n}$ such that $\Delta(P) \notin B_{k,n}$. Recall that there is a continuous path $P(t)$ for $t \in [0,1]$ such that $P(0)$ is the regular n-gon.

Define $Q(t) = \Delta_k(P(t))$. There is some $t_0 \in [0,1]$ such that $Q(t_0) \notin B_{k,n}$. We can truncate our path so that $t_0 = 1$. In other words, $Q(t) \in B_{n,k}$ for $t \in [0,1)$ but $Q(1) \notin B_{k,n}$.

Lemma 6.1. *$Q(\cdot)$ is a degenerating path.*

Proof: Note that $Q(\cdot)$ is planar and hence satisfies Property 1 for degenerating paths. Let $P = P(1)$ and $Q = Q(1)$. If Q doe not have all distinct vertices then two different feathers of P intersect at a point which (by Statement 2 of Theorem 1.1) lies in P^I. This contradicts Statement 2 of Theorem 4.1. Hence $Q(\cdot)$ satisfies Property 2 for degenerating paths. By construction, $Q(t) \in B_{n,k}$ for all $t \in [0,1)$. Hence $Q(\cdot)$ satisfies Property 3. The energy χ_k is well-defined and continuous on $B_{k,n}$. Hence, by compactness, $\chi_k(P(t)) > \epsilon_0$ for some $\epsilon_0 > 0$ and all $t \in [0,1]$. Now for the crucial step: We have already proved that $\chi_k \circ \Delta_k = \chi_k$. Hence $\chi_k(Q(t)) > \epsilon_0$ for all $t \in [0,1]$. That is, $Q(\cdot)$ satisfies Property 4 for degenerating

paths. ♠

Now we apply the Degeneration Lemma to $Q(\cdot)$. We conclude that all but at most 1 vertex of $Q(1)$ lies in a line L. Stating this in terms of $P(1)$, we can say that all but at most one of the feathers of $P(1)$ have their tips in a single line L. Call an edge of $P(1)$ *ordinary* if the feather associated to it has its tip in L. We call the remaining edge, if there is one, *special*. Thus, all but at most one edge of P is ordinary.

Let $S(t)$ be the soul of $P(t)$. We know that $S(1)$ has non-empty interior by Theorem 3.1. For ease of notation we set $P = P(1)$ and $S = S(1)$.

Lemma 6.2. *P cannot have ordinary edges e_1 and e_2 that lie on opposite sides of L and are disjoint from L.*

Proof: Suppose this happens. Figure 6.1 shows the situation.

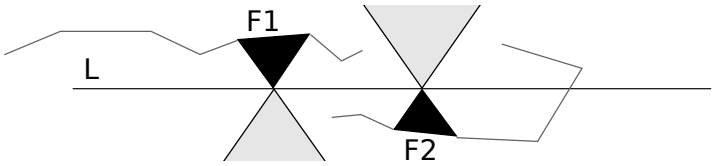

Figure 6.1: Two feathers on opposite sides of L.

Let F_1 and F_2 be the two associated feathers. Then the opposite sector F_1^* lies above L, and the opposite sector F_2^* lies below L and the two tips are distinct. But then $S(1)$, which must lie in the intersection of these sectors, is empty. ♠

Lemma 6.3. *P cannot have more than 2 ordinary edges which intersect L.*

Proof: Note that an ordinary edge cannot lie in L because then the tip would not. So, an ordinary edge that intersects L does so either at a single vertex or at an interior point. As we trace along L in one direction or the other we encounter the first intersecting edge and then the last one and then some other intersecting edge. Let $F_1.F_2.F_3$ be the two feathers,

as shown in Figure 6.3. Let e_j be the edge of F_j that belongs to P. Let v_j be the tip of F_j. (Figure 6.3 shows the case when $e_j \cap L$ is an interior point of e_j for each $j = 1, 2, 3$, but the same argument would work if some of these intersection points were vertices.)

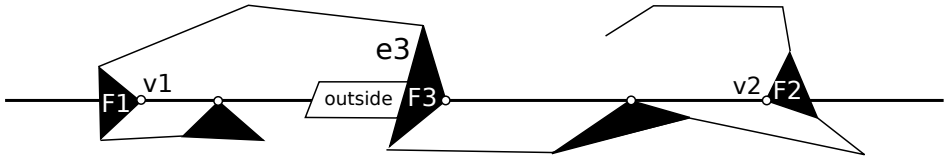

Figure 6.2: Three or more crossing edges

One of the two arcs α of Q joining v_1 to v_2 stays in L, namely the one avoiding the one point of Q not on L. However, α passes right through F_3 and in particular crosses e_3 transversely. However, one side of F_3 is outside P. Hence α is not contained in P^I, the interior of the region bounded by P. This contradicts Statement 2 of Theorem 1.1, which says that $Q \subset P^I$. ♠

The line L divides the plane into two open half-planes, which we call the *sides* of L. Lemma 6.2 says that P cannot have ordinary edges contained in opposite sides of L. Lemma 6.3 says that at most 2 ordinary edges can intersect L. Hence, all but at most 2 of the ordinary edges of P lie on one side of L. Call this the *abundant side* of L. Call the other side the *barren side*. The barren side contains no ordinary edges at all, and perhaps the special edge. In particular, at most two vertices of P lie in the barren side.

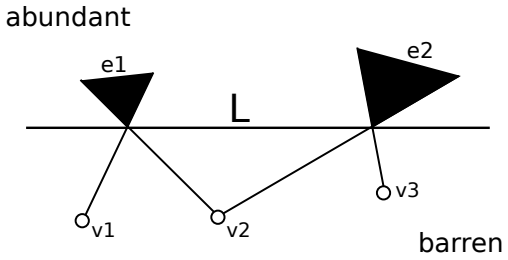

Figure 6.3: Following the diagonals bounding a feather

At the same time, each ordinary edge on the abundant side contributes two vertices to the barren side: We just follow the diagonals comprising the corresponding feather. These

diagonals cross L from the abundant side into the barren side. Two different ordinary edges contribute at least 3 distinct vertices to the barren side. This is a contradiction.

We have ruled out all possible behavior for $P = P(1)$ assuming that $Q = Q(1)$ is degenerate. Hence, $Q(1)$ is not degenerate. This means that $Q(1)$ is a bird. This completes the proof that

$$\Delta_k(B_{k,n}) \subset B_{k,n}. \tag{24}$$

6.2 Equality

We use the notation from §2.2. Equation 8 implies that

$$\Delta_k^{-1} = D_{k+1} \circ \Delta_k \circ D_{k+1}. \tag{25}$$

So far, Equation 25 makes sense in terms of PolyPoints and PolyLines.

Below we will explain how to interpret D_{k+1} as a map from polygons in $\boldsymbol{P}$ to polygons in $\boldsymbol{P}^*$ and also as a map from polygons in $\boldsymbol{P}^*$ to polygons in $\boldsymbol{P}$. Since the dual projective plane $\boldsymbol{P}^*$ is an isomorphic copy of $\boldsymbol{P}$, it makes sense to define $B^*_{k.n}$. This space is just the image of $B_{k,n}$ under any projective duality. Below we will prove

Theorem 6.4. $D_{k+1}(B_{k,n}) \subset B^*_{k,n}$.

It then follows from projective duality that $D_{k+1}(B^*_{k,n}) \subset B_{k,n}$. Combining these equations with Equation 25 we see that $\Delta_k^{-1}(B_{n,k}) \subset B_{n,k}$. This combines with Equation 24 to finish the proof of Theorem 1.1.

Now we prove Theorem 6.4.

Lemma 6.5. *If $P \in B_{k,n}$, then we can enhance $D_{k+1}(P)$ in such a way that $D_{k+1}(P)$ is a planar polygon in $\boldsymbol{P}^*$. The enhancement varies continuously.*

Proof: A *polygon* is a PolyPoint together with additional data specifying an edge in $\boldsymbol{P}$ joining each consecutive pair of points. Dually, we get a polygon in $\boldsymbol{P}^*$ from a PolyLine by specifying, for each pair of consecutive lines L_j, L_{j+1}, an arc of the pencil of lines through the intersection point which connects L_j to L_{j+1}.

Specifying an enhancement of $D_{k+1}(P)$ is the same as specifing, for each consecutive pair L_1, L_2 of $(k+1)$ diagonals of P, an arc of the pencil through their intersection that connects L_1, L_2. There are two possible arcs. One of them avoids the interior of the soul of P and the other one sweeps through the soul of P. We choose the arc that avoids the soul interior. Figure 6.4 shows that we mean for a concrete example.

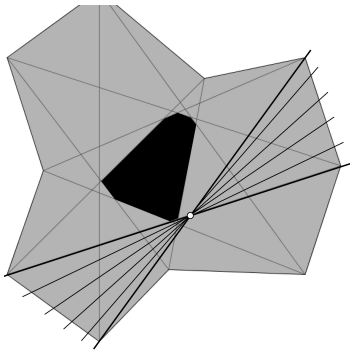

Figure 6.4: Enhancing a PolyLine to a polygon: Avoid the soul.

Since the soul of P has non-empty interior, there exists a point $x \in P$ which is disjoint from all these pencil-arcs. Applying duality, this exactly says that there is some line in $\boldsymbol{P}^*$ which is disjoint from all the edges of our enhanced $D_{k+1}(P)$. Hence, this enhancement makes $D_{k+1}(P)$ planar. Our choice also varies continuously on $B_{n,k}$. ♠

Lemma 6.6. *D_{k+1} maps a member of $B_{k,n}$ to an n-gon which is k-nice.*

Proof: Let $Q = D_{k+1}(P)$. A $(k+1)$-diagonal of Q is just a vertex of P. A k diagonal of Q is a vertex of $\Delta_k(p)$. Thus, to check the k-nice property for Q we need to take n-collections of 4-tuples of points and check that they are distinct. In each case, the points are collinear because the lines of Q are coincident.

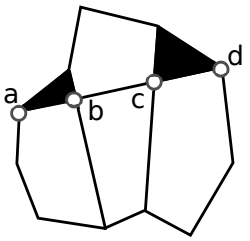

Figure 6.5 One of the n different 4-tuples we need to check.

Once we make this specification, there is really combinatorially only possibility for which collections we need to check. Figure 6.5 shows one such 4-tuple, a, b, c, d. The shaded triangles are the two feathers of P whose tips are b, c. But a, b, c, d are distinct vertices of $P \cup \Delta_k(P)$ and so they are distinct. That is all there is to it. ♠

To show that $Q = D_{k+1}(P)$ is a k-bird, we consider a continuous path $P(t)$ from the regular n-gon $P(0)$ to $P = P(1)$. We set $Q(t) = P(t)$. By construction, $Q(0)$ is a copy of the regular n-gon in $\boldsymbol{P}^*$, and $Q(t)$ is k-nice for all $t \in [0,1]$, and $Q(t)$ is a planar polygon for all $t \in [0,1]$. By definition $Q = Q(1)$ is a k-bird. This completes the proof of Theorem 6.4.

7 The Triangulation

7.1 Basic Definition

In this section we gather together the results we have proved so far and explain how we construct the triangulation τ_P associated to a bird $P \in B_{k,n}$.

Since $\Delta_k(B_{k,n}) \subset B_{k,n}$, we know that $\Delta_k(P)$ is also a k-bird. Combining this with Theorem 3.1 and Theorem 4.1 we can say that $\Delta_k(P)$ is one embedded n-gon contained in P^I, the interior of the region bounded by the embedded P. The region between P and $\Delta_k(P)$ is a topological annulus. Moreover, $\Delta_k(P)$ is obtained from P by connecting the tips of the feathers of P. The left side Figure 7.1 shows how this region is triangulated. The black triangles are the feathers of P and each of the white triangles is made from an edge of $\Delta_k(P)$ and two edges of adjacent feathers.

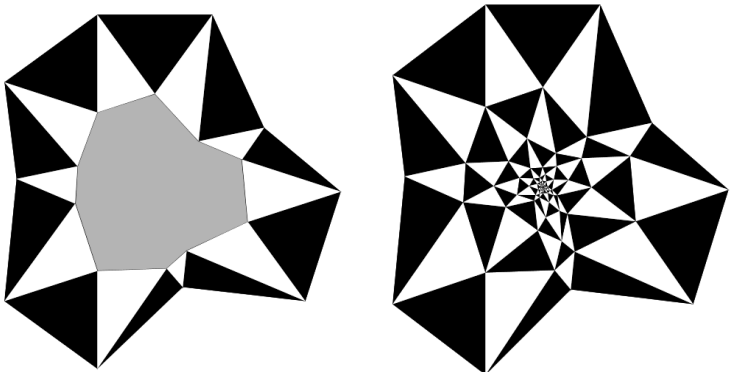

Figure 7.1: The triangulation of the annulus

Lemma 7.1. *For every member $P \in B_{k,n}$, the associated $2n$ triangles have pairwise disjoint interiors, and thus triangulate the annular region between P and $\Delta_k(P)$.*

Proof: As usual, we make a homotopical argument. If this result is false for some P, then we can look at path which starts at the regular n-gon (for which it is true) and stop at the first place where it fails. Theorem 4.1 tells us that nothing goes wrong with the feathers of P. The only thing that can go wrong is $\Delta_k(P)$ fails to be an embedded polygon. Since this does not happen, we see that in fact there is no counter-example at all. ♠

We can now iterate, and produce $2n$ triangles between $\Delta_k(P)$ and $\Delta_k^2(P)$, etc. The right side of Figure 7.1 shows the result of doing this many times. The fact that $\Delta_k(B_{k,n}) = B_{k,n}$ allows us to extend outward as well. When we iterate forever in both directions, we get an infinite triangulation of a (topological) cylinder that has degree 6 everywhere. This is what Figure 1.6 is showing. We call this bi-infinite triangulation τ_P.

7.2 Some Structural Results

The following result will help with the proof of Theorem 1.3.

Theorem 7.2. *Let $P \in B_{n,k}$. Let S be the soul of B. Then for $\ell \geq n$ we have $\Delta_k^\ell(P) \subset S$.*

Proof: We first note the existence of certain infinite polygonal arcs in τ_P. We start at a vertex of P and then move inward to a vertex of $\Delta_k(P)$ along one of the edges. We then continue through this vertex so that 3 triangles are on our left and 3 on our right. Figure 7.2 below shows the two paths like this that emanate from the same vertex of P.

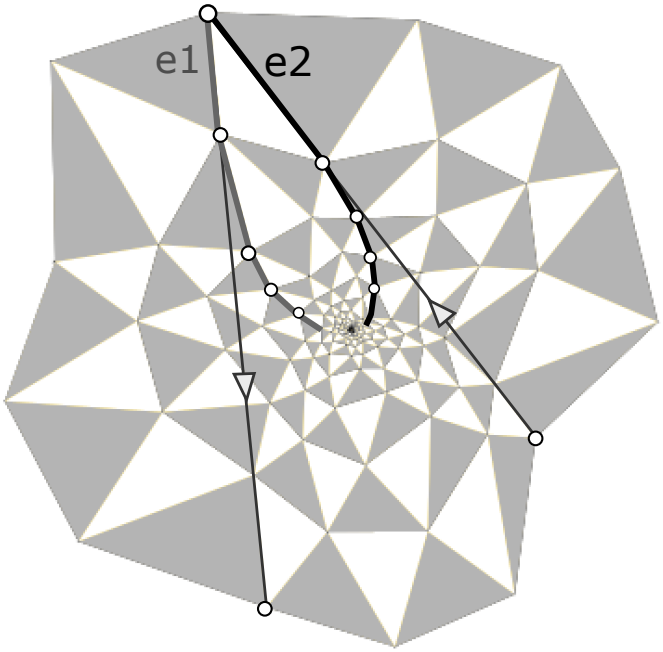

Figure 7.2: The spiral paths.

The usual homotopical argument establishes the fact that the spiral paths are locally convex. One can understand their combinatrics, and how they relate to the polygons in the orbit, just by looking at the case of the regular n-gon. We call the two spiral paths in Figure 7.2 *partners*. In the regular n-gon the partners intersect infinitely often. So this is true in general. Each spiral path has an initial segment joining the initial endpoint on P to the first intersection point with the partner. We define a *petal* to be the region bounded by the initial paths of the two partners.

It is convenient to write $P^\ell = \Delta_k^\ell(P)$. In the regular case, P^ℓ is contained in the petal for $\ell > n - 1$.. Hence, the same goes in the general case. Because the initial segments are locally convex, the petal lies to the left of the lines extending the edges e_1 and e_2 when

these edges are oriented according to the $(k+1)$-diagonals of P. But this argument works for every pair of partner spiral paths which start at a vertex of P. We conclude that for $\ell \geq n$, the polygon P^ℓ lies to the left of all the $(k+1)$-diagonals of P. But the soul of P is exactly the intersection of all these left half planes. ♠

Theorem 7.2 in turn gives us information about the nesting properties of birds within an orbit. Let S_ℓ denote the soul of P^ℓ. Let

$$S_\infty = \bigcap_{\ell \in \mathbf{Z}} S_\ell, \qquad S_{-\infty} = \bigcup_{\ell \in \mathbf{Z}} S_\ell. \tag{26}$$

It follows from Theorem 7.2 that $\widehat{P}_\infty = S_\infty$ and $\widehat{P}_{-\infty} = S_{-\infty}$, because

$$S_{\ell+n} \subset P^{\ell+n} \subset S_\ell \subset P^\ell. \tag{27}$$

Hence these sets are all convex subsets of an affine plane.

Corollary 7.3. *Any $P \in B_{k,n}$ is strictly star-shaped with respect to all points in the convex hull of $\Delta_k^n(P)$.*

Proof: Since $P^{\ell+n} \subset S_\ell$, and P^ℓ is strictly star shaped with respect to all points of S^ℓ, we see that P^ℓ is strictly star shaped with respect to all points of $P^{\ell+n}$. Since S_ℓ is convex, we can say more strongly that P^ℓ is strictly star-shaped with respect to all points of the convex hull of $P^{\ell+n}$. Now we just set $\ell = 0$ and recall the meaning of our notation, we get the exact statement of the result. ♠

An immediate corollary is that P is strictly star-shaped with respect to $\widehat{P}_\infty$. (Theorem 1.3 says that this is a single point.)

8 Nesting Properties of Birds

8.1 Duality

In this chapter we prove Theorem 1.3. In this first section we show how Statement 1 of Theorem 1.3 implies Statement 2. We want to prove that the "backwards union" $\widehat{P}_{-\infty}$ is an affine plane. Here $P \in B_{n,k}$ is a k-bird.

We take $\ell \geq 0$ and consider $P^{-\ell} = \Delta_k^{-\ell}(P)$. Since $P^{-\ell}$ is planar, there is a closed set Λ_ℓ of lines in $\boldsymbol{P}$ which miss $P^{-\ell}$. These sets of lines are nested: $\Lambda_1 \supset \Lambda_2 \supset \Lambda_3 ....$ The intersection is non-empty and contains some line L. We can normalize so that L is the line at infinity. Thus all $P^{-\ell}$ lie in $\boldsymbol{R}^2$. We want to see that $\widehat{P}_{-\infty} = \boldsymbol{R}^2$.

Let D_{k+1} be the map from §2.2 and §6.2. From Equation 8 we see that D_{k+1} conjugates Δ_k to Δ_k^{-1}. With Theorem 6.4 in mind, define the following "dual" k-birds:

$$\Pi^\ell = \Delta_k^\ell(D_{k+1}(P)) = D_{k+1}(P^{-\ell}). \tag{28}$$

From Statement 1 of Theorem 1.3, the sequence of k-birds $\{\Pi^\ell\}$ shrinks to a point in the dual plane $\boldsymbol{P}^*$. The vertices of Π^ℓ are the $(k+1)$-diagonals of $P^{-\ell}$. Because the vertices of Π^ℓ shrink to a single point, all the $(k+1)$-diagonals of $P^{-\ell}$ converge to a single line L'.

Lemma 8.1. *L' is the line at infinity.*

Proof: Suppose not. When ℓ is large, all the $(k+1)$-diagonals point nearly in the same direction as L'. In particular, this is true of the subset of these diagonals which define the soul $S^{-\ell}$. But these special diagonals turn monotonically and by less than π radians as we move from one to the next. Hence, some of these diagonals nearly point in one direction along L' and some point nearly in the opposite direction. But then $S^{-\ell}$ converges to a subset of L'. This is a contradiction, ♠

The soul $S^{-\ell}$ is a convex set, containing the origin, and is bounded by some of the $(k+1)$ diagonals. If $S^{-\ell}$ does not converge to the whole plane, then some $(k+1)$-diagonal

intersects a uniformly bounded region in $\boldsymbol{R}^2$ for each ℓ. But this produces a sequence of $(k+1)$-diagonals that does not converge to the line at infinity. This is a contradiction. Hence $S^{-\ell}$ converges to all of $\boldsymbol{R}^2$. But then so does $P^{-\ell}$.

8.2 The Pre-Compact Case

The rest of the chapter is devoted to proving Statrement 1 of Theorem 1.3. Let $P \in B_{n,k}$ and let $P^\ell = \Delta^\ell(P)$. We take $\ell = 0, 1, 2, 3....$

Conjecture 8.2. *The sequence $\{P^\ell\}$ is pre-compact modulo affine transformations. That is, this sequence has a convergent subsequence which converges to another element of $B_{n,k}$.*

In this section I will prove the $\widehat{P}_\infty$ is a single point under the assumption that $\{P^\ell\}$ is pre-compact.

We would like to see that the diameter of P^ℓ steadily shrinks, but the notion of diameter is not affinely natural. We first develop a notion of affinely natural diameter. For each direction v in the plane, we let $\|S\|_v$ denote the maximum length of $L \cap S$ where L is a straight line parallel to v. We then define

$$\delta(S_1, S_2) = \sup_v \frac{\|S_1\|_v}{\|S_2\|_v} \in [0, 1]. \tag{29}$$

The quantity $\delta(S_1, S_2)$ is affine invariant, and (choosing a direction μ which realizes the diamater of S_1) we have

$$\frac{\operatorname{diam}(S_1)}{\operatorname{diam}(S_2)} \le \frac{\|S_1\|_\mu}{\|S_2\|_\mu} \le \delta(S_1, S_2). \tag{30}$$

Let S^ℓ be the soul of P^ℓ. By Theorem 5.11 we have $S^{\ell+n} \subset S^\ell$. More precisely, the former set is contained in the interior of the latter set. Under the pre-compactness assumption, there are infinitely many indices ℓ_j and some $\epsilon > 0$ such that

$$\delta(S^{\ell_j+n}, S^{\ell_j}) < 1 - \epsilon. \tag{31}$$

But then

$$\frac{\operatorname{diam}(S^{\ell_j+n})}{\operatorname{diam}(S^{\ell_j})} < 1 - \epsilon \tag{32}$$

infinitely often. This forces $\mathrm{diam}(S^\ell) \to 0$. But $\widehat{P}_\infty$ is contained in this nested intersection and hence is a point.

If we knew the truth of Conjecture 8.2 then our proof of Theorem 1.3 would be done. Since we don't know this, we have to work much harder to prove Statement 1 in general.

8.3 Normalizing by Affine Transformations

Henceforth we assume that the forward orbit $\{P^\ell\}$ of P under Δ_k is not pre-compact modulo affine transformations.

Lemma 8.3. *There is a sequence $\{T_\ell\}$ of affine transformations such that*

1. *$T_\ell(P^\ell)$ has (the same) 3 vertices which make a fixed equilateral triangle.*
2. *T_ℓ expands distances on P^ℓ for all ℓ.*
3. *$T_\ell(P^\ell)$ is contained in a uniformly bounded subset of $\mathbf{R}^2$.*

Proof: To P^ℓ we associate the triangle τ_ℓ made from 3 vertices of P^ℓ and having maximal area. The diameter of τ_ℓ is uniformly small, so we can find a single equilateral triangle T and an expanding affine map $T_\ell : \tau_\ell \to T$. Let d be the side length of T. Every vertex of $T_\ell(P^\ell)$ is within d of all the sides of T, because otherwise we'd have a triangle of larger area. The sequence $\{T_\ell\}$ has the advertised properties. ♠

Let $Q^\ell = T_\ell(P^\ell)$. By compactness we can pass to a subsequence so that the limit polygon Q exists, in the sense that the vertices and the edges converge. Let Q_0, Q_1, etc. be the vertices of Q. Perhaps some of these coincide. Each distinguished diagonal of Q^ℓ defines the unit vector which is parallel to it. Thus Q^ℓ defines a certain list of $2n$ unit vectors. We can pass to a subsequence so that all these unit vectors converge. Thus Q still has well defined distinguished diagonals even when the relevant points coincide.

We now define the "limiting soul". Let $S^\ell = S(Q^\ell)$, the soul of Q^ℓ. As in §5.7. let S be the set of accumulation points of sequences $\{p^\ell\}$ with $p^\ell \in S^\ell$. Since $S^\ell \subset Q^\ell$ for all ℓ we

have $S \subset Q$. Now we define a related object. We have a left half-plane associated to each diagonal of Q. We define Σ to be the intersection of all these half-planes. We will use the set Σ at various places below to get control over the set S.

Lemma 8.4. $S \subset \Sigma$.

Proof: Fix $\epsilon > 0$. If this is not the case, then by compactness we can find a convergent sequence $\{p^\ell\}$, with $p^\ell \in S^\ell$, which does not converge to a point of Σ. But p^ℓ lies in every left half plane associated to Q^ℓ. But then, by continuity, the accumulation point p lies in every left half plane associated to Q. Hence $p \in \Sigma$. ♠

8.4 Structure of the Normalized Limits

We work under the assumption that $\widehat{P}_\infty$ is not a single point. The goal of this section is to establish several structural properties about the sets S and Q. Our first property guarantees that there is a chord S^* of S connecting vertices of Q. Once we establish this, we show that Q is a union of two "monotone" arcs joining the endpoints of S^*. These structural properties will be used repeatedly in subsequent sections of this chapter.

Let H_Q denote the convex hull of Q. Note that $S \subset Q \subset H_Q$.

Corollary 8.5. *Suppose that $\widehat{P}_\infty$ is not a single point. Then $\delta(S, H_Q) = 1$.*

Proof: Suppose not. Note that $H_{Q^\ell} \subset S^{\ell-n}$ by Theorem 7.2 and convexity. Then for ℓ large we have

$$\delta(Q^{\ell-n}) = \delta(S^\ell, S^{\ell-n}) \le \delta(S^\ell, H_{Q^\ell}) < \delta(S, H_Q) + \epsilon,$$

and we can make ϵ as small as we like. This gives us a uniform $\delta < 1$ such that $\delta(Q^\ell) < \delta$ once ℓ is large enough. The argument in the compact case now shows that $\widehat{P}_\infty$ is a single point. ♠

Corollary 8.5 says that S and Q have the same diameter. Hence there is a chord $S^* \subset S$ which has the same diameter as Q. Since Q is a polygon, this means that Q must have vertices at either endpoint of S^*. We normalize so that S^* is the unit segment joining $(0,0)$ to $(1,0)$.

Lemma 8.6. *Let $Q' \subset Q$ be an arc of Q that joins $(0,0)$ to $(1,0)$.*

1. *The vertices of Q' must have non-decreasing x-coordinates.*
2. *If consecutive vertices of Q' have the same x-coordinate, they coincide.*
3. *Either $Q' \subset S^*$ or Q' intersects S^* only at $(0,0)$ and $(1,0)$.*

Proof: Suppose the Statement 1 is false. Then we can find a vertical line Λ which intersects S^* at a relative interior point and which intersects Q' transversely at 3 points. But then once ℓ is sufficiently large, Q^ℓ will intersect all vertical lines sufficiently close to Λ in at least 3 points and moreover some of these lines will contain points of S^ℓ. This contradicts the fact that Q^ℓ is strictly star-shaped with respect to all points of Q^ℓ.

For Statement 2, we observe that Q' does not contain any point of the form $(0,y)$ or $(1,y)$ for $y \neq 0$. Otherwise Q has larger diameter than 1. This is to say that once Q' leaves $(0,0)$ it immediately moves forward in the X-direction. Likewise, once Q' (traced out the other way) leaves $(1,0)$ it immediately moves backward in the X-direction. If Statement 2 is false, ten we can find a non-horizontal line Λ' which intersects S^* in a relative interior point and which intersects Q' transversely at 3 points. The slope is Λ' depends on which of the two vertices of Q' lies above the other. Once we have Λ' we play the same game as for the first statement, and get the same kind of contradiction.

Suppose Statement 3 is false. We use the kind of argument we had in §5.8. By Statements 1 and 2 together, Q' must have an escape edge which touches S^* in a relative interior point. Moreover, this one escape edge is paired with another escape edge. Thus we can find a point $x \in S^*$ which strictly lies on the same side of both of these same-type escape edges. The argument in §5.8 now shows that Q^ℓ is not strictly star-shaped with

respect to points of S^ℓ very near x. ♠

Corollary 8.7. *Suppose* $0 \le a < b < n$ *and* $Q_a = Q_b$. *Then either we have* $Q_a = Q_{a+1} = ... = Q_b$ *or else we have* $Q_b = Q_{b+1} = ... = Q_{a+n}$.

Proof: In view of Lemma 8.6 it suffices to show that our two monotone arcs comprising Q are disjoint except at their endpoints.

Let U denote the open upper halfplane, bounded by the X-axis. After reflecting in the X-axis we can guarantee that one of our monotone arcs α has a point in U. But then, by Lemma 8.6, all of α lies in U except for its endpoints. If the other monotone arc β intersects α away from the endpoints, then β has a point in U, but then, by Lemma 8.6, all of β lies in U except for the endpoints. But then S lies in U, except for the points $(0,0)$ and $(1,0)$. This contradicts the fact that $S^* \subset S$. ♠

Our argument shows in particular that Q is embedded, up to adding repeated vertices. However, we will not directly use this property in our proof below.

8.5 The Triangular Case

We continue with the assumption that $\widehat{P}$ is not a single point. Here we pick off a special case:

- There is a line L such that $Q_0 \notin L$.
- $Q_k, Q_{k+1}, ..., Q_{n-k-1}, Q_{n-k} \in L$ and
- $Q_k \ne Q_{n-k}$.

Figure 8.1 shows the situation. As always, the notation Q_{-k} and Q_{n-k} names the same point. All but $2k-1$ points are on L, and except for Q_0 we don't know where these other $2k-1$ points are.

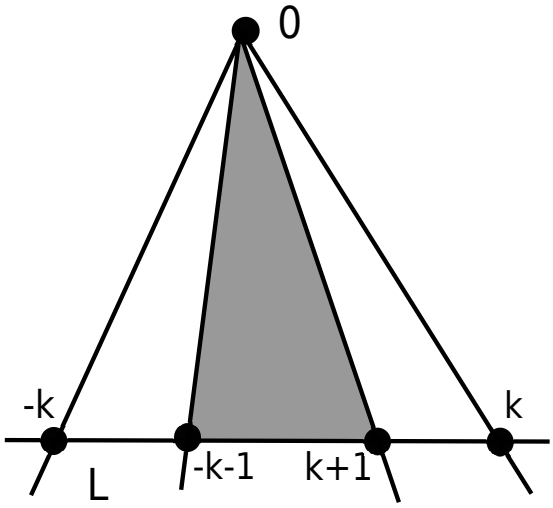

Figure 8.1: The triangular limit Q.

Given the constant energy of our orbit, the cross ratio of the lines

$$Q_{0,k},\ Q_{0,k+1},\ Q_{n-k-1,0},\ Q_{n-k,0}$$

is at least ϵ_0. Also, these lines are cyclically ordered about 0 as indicated in Figure 8.1, thanks to the k-niceness property and continuity. Also, the two lines containing $Q_{0,k}$ and $Q_{-k,0}$ are not parallel because $Q_0 \notin L$. Hence S is contained in the shaded region in Figure 8.1, namely the triangle with vertices Q_0 and $Q_{\pm(k+1)}$. But this shaded region has diameter strictly smaller than the triangle τ with vertices Q_0 and $Q_{\pm k}$. Hence $\mathrm{diam}(S) < \mathrm{diam}(\tau) \le \mathrm{diam}(Q)$. This contradicts Corollary 8.5 which says, in particular, that S and Q have the same diameter.

8.6 The Case of No Folded Diagonals

We work under the assumption that $\widehat{P}_\infty$ is not a single point. The notions of collapsed diagonals, folded diagonals, and aligned diagonals from §5 make sense for Q because the concepts just involve the directions of the diagonals. The proof of Lemma 5.3 also works the same way.

Lemma 8.8. *Q must either have a trivial edge, a trivial distinguished diagonal, or collapsed diagonals,*

Proof: As remarked in §5, the proof of the Degeneration Lemma works for sequences as well as paths, and only uses the fact that the limiting polygon has nontrivial edges and nontrivial distinguished diagonals. So, if Q has no trivial edges and no trivial distinguished diagonals, then all but one vertex of Q lies in a single line. But then Q has collapsed diagonals. ♠

Remark: Here is a second, more direct proof. If Lemma 8.8 is false then we have a picture as in the left side of Figure 7.1. The feathers defined in §4.1 would be all non-degenerate and the segments joining the tips of consecutive feathers would be nontrivial. This would force S to lie in the interior of Q. But then $\text{diam}(S) < \text{diam}(Q)$, contradicting Corollary 8.5.

If Q has a trivial distinguished diagonal, then by Lemma 8.7, we see that Q also has a trivial edge. If Q has a trivial edge, say $Q_{-1} = Q_0$, then the diagonals at Q are collapsed at Q_k. So, in all cases, Q has collapsed diagonals. We assume in this section that Q has no folded diagonals anywhere. This means that Q has aligned diagonals, say at Q_k. Thus $Q_{0,k}$ and $Q_{k,2k}$ are parallel. Since Q does not lie in a line, Lemma 5.3 tells us that the chain of $2k+1$ parallel distinguished diagonals:

$$Q_{0,k}, Q_{0,k+1}, Q_{1,k+1}, Q_{1,k+2}, ..., Q_{k-1,2k}, Q_{k,2k} \tag{33}$$

Now we have a "runaway situation". The two diagonals $Q_{2k,k}$ and $Q_{2k,k-1}$ (which are just the reversals of the last two in Equation 33) are parallel. Thus Q has collapsed diagonals at Q_{2k}. Since Q has no folded diagonals, Q has aligned diagonals at Q_{2k}. But then, applying Lemma 5.3 again, we can extend that chain in Equation 33 so that it contines as $, ..., Q_{2k-1,3k}, Q_{2k,3k}$. But now Q has collapsed diagonals at Q_{3k}. And so on. Continuing this way, we end up with all points on Q. This is a contradiction.

The only way out is that Q must have folded diagonals somewhere

8.7 The Case of Folded Diagonals

We continue to work under the assumption that $\widehat{P}_\infty$ is not a single point. Now we consider the case when Q has folded diagonals at, say, Q_0. What this means that the diagonals $Q_{0,k+1}$, $Q_{0,-k-1}$ are parallel. (Again, these diagonals are well defined even when their endpoints coincide; we are just using a notational convention to name them here.) But then the corresponding half planes intersect along a single line L, forcing $\Sigma \subset L$. By Lemma 8.4, the soul S is contained in Σ. Hence, $S \subset L$. Letting S^* be the chord from §8.4, we also have $S = S^*$. This is because S and S^* are segments of the same diagonal and in the same line. We will use S and S^* interchangeably below.

We normalize so that S is the line segment connecting $(0,0)$ to $(1,0)$. As in §8.4, both these points are vertices of Q. The folding condition forces Σ (and hence S) to lie to one side of these points. Hence, we have either $Q_0 = (0,0)$ or $Q_0 = (1,0)$. Without loss of generality we consider the case when $Q_0 = (0,0)$. Note that points of $Q - S$ do not belong to L, because Q and S have the same diameter. We break the analysis down into cases.

Case 1: Suppose that Q_{k+1} is not an endpoint of S^* and $Q_{n-k-1} \neq (0,0)$. Consider the arc Q' given by $Q_0 \to ... \to Q_{k+1} \to ... \to Q_\beta = (1,0)$. Here β is some index we do not know explicitly, but we take β as large as possible, in the sense that $Q_{\beta+1} \neq (1,0)$. The arc Q' connects $(0,0)$ to $(1,0)$ and intersets S^* at Q_{k+1}, a point which is neither $(0,0)$ or $(1,0)$. By Lemma 8.6, we have $Q' \subset S^*$. We conclude that $Q_0, ..., Q_\beta \subset S^*$.

If β does not lie in the index interval $(k+1, n-k-1)$ then we have just shown that $Q_{k+1}, ..., Q_{n-k-1} \in S^*$. If $\beta = n-k-1$ we have the same result. Here is what we do if β does lie in $(k+1, n-k-1)$. We apply our same argument as in the previous paragraph to the arc $Q_\beta \to ... \to Q_{n-k-1}$, and see that $Q_\beta, ..., Q_{n-k-1} \in S$. So, in all cases, we see that $Q_{k+1}, ..., Q_{n-k-1} \in S$.

In short, $Q_j \in L$ unless $j \in \{-k, ..., -1\}$. All but k vertices belong to L. In particular, we have an index $h \in \{-k, ..., -1\}$ such that $Q_h \notin L$ but $Q_{h+k}, Q_{h+k+1}, ..., Q_{h+n-k-1}, Q_{h+n-k} \in L$. Now we are close to the Triangular case from §8.5 except that all the indices are shifted

by h. If it happens that $Q_{h+k} \neq Q_{h+n-k}$ then we have the Triangular Case and we are done.

The other possibility is that $Q_{h+k} = Q_{h+n-k}$. In this case, Lemma 8.7 gives us $Q_{h+k} = Q_{h+k+1} = Q_{h+n-k-1} = Q_{h+n-k}$. In particular, the diagonals $Q_{h,h+k+1}$ and $Q_{h,h+n-k-1}$ are folded at Q_h. Since $Q_h \notin L$ this means that there is some other line L' such that $S \subset L'$. This is a contradiction.

Case 2: Suppose $Q_{-k-1} = Q_{k+1} = (1,0)$. Before analyzing this case, we remember a lesson from the end of Case 1: It is not possible for Q to have folded diagonals at a point not on S.

Corollary 8.7 says that $Q_{k+1} = ... = Q_{n-k-1} = (1,0)$. This is a run of $k+\beta$ points, where $\beta = n - (3k+1) \geq 0$. There is some index $h \in \{\pm 1, ... \pm k\}$ such that $Q_h \notin L$. Without loss of generality we will take $h \in \{1, ..., k\}$.

Suppose first that $n > 3k+1$. Then there are at least $k+1$ consecutive vertices sitting at $(1,0)$ and so both diagonals $Q_{h,k+h}$ and $Q_{h,k+h+1}$ point from Q_h to $(1,0) \neq Q_h$. This means that Q has collapsed diagonals at Q_h. Remembering our lesson, we know that Q does not have folded diagonals at Q_h. Hence Q has aligned diagonals at Q_h.

Now we have the same runaway situation we had in §8.6. The diagonals in the chain $Q_{h-k,h}...Q_{h,h+k}$ point are all pointing along the line connecting $(1,0)$ to Q_h, and they are pointing away from $(1,0)$. This gives us collapsed diagonals at Q_{h+k}. Remembering our lesson, we see that Q has aligned diagonals at Q_{h+k}. And so on. All the points after Q_h get stuck on L' and we have a contradiction.

If $n = 3k+1$, then the same argument works as long as $h \neq \pm k$. So, we just have to worry about the case when all points of Q belong to S except for Q_k and Q_{-k}, which do not belong to S. Applying Lemma 8.6 to the arc $Q_0 \to Q_1 \to ... \to Q_k \to (1,0)$ we conclude that $Q_0 = ... = Q_{k-1} = (0,0)$. Applying Lemma 8.6 to the arc $Q_0 \to Q_{-1} \to ... \to Q_{-k} \to (1,0)$ we conclude that $Q_0 = ... = Q_{k-1} = (0,0)$. But now we have a run of $2k-1 \geq k+1$ points sitting at $(0,0)$ and we can run the same argument as in the case $n > 3k+1$, with $(0,0)$ in place of $(1,0)$.

Case 3: The only cases left to consider is when one or both of $Q_{\pm(k+1)}$ equals $(0,0)$. We suppose without loss of generality that $Q_{-k-1} = (0,0)$. Since we also have $Q_0 = (0,0)$, Lemma 8.7 gives $Q_{-k-1} = ... = Q_0 = (0,0)$. This is a run of $k+2$ consecutive points sitting at $(0,0)$.

There is some smallest $h > 0$ so that $Q_h \notin S$. Applying Lemma 8.6 to the arc $Q_0 \to ... \to Q_k \to ... \to (1,0)$, we conclude that $Q_{h-1} = ... = Q_1 = (0,0)$. (Otherwise Lemma 8.6 would force $Q_h \in S$.)

Now we know that Q has collapsed diagonals at $Q_h \notin L$. We now get a contradiction from the same runaway situation as in Case 2.

9 Appendix

9.1 The Energy Invariance Revisited

In this section we sketch Anton Izosimov's proof that $\chi_k \circ \Delta_k = \chi_k$. This proof requires the machinery from [6]. (The perspective comes from [8], but the needed result for Δ_k is in the follow-up paper [6].)

Let P be an n-gon. We let $V_1, ..., V_n$ be points in $\boldsymbol{R}^3$ representing the consecutive vertices of P. Thus the vertex P_j is the equivalence class of V_j. We can choose periodic sequences $\{a_i\}, \{b_i\}, \{c_i\}, \{d_i\}$ such that

$$a_i V_i + b_i V_{i+k} + c_i V_{i+k+1} + d_i V_{i+2k+1} = 0, \qquad \forall i. \tag{34}$$

Recall from §2.2 that $\Delta_k = D_k \circ D_{k+1}$.

Lemma 9.1. *One of the cross ratio factors of $\chi_k \circ D_{k+1}$ is $(a_0 d_{-k})/(c_0 b_{-k})$.*

Proof: One of the factors is the cross ratio of P_0, y, x, P_{k+1}, where

$$x = P_{0,k+1} \cap P_{k,2k+1}, \qquad y = P_{-k,1} \cap P_{0,k+1}.$$

(Compare the right side of Figure 2.1, shifting all the indices there by $k+1$.)

The points x and y respectively are represented by vectors

$$X = a_0 V_0 + c_0 V_{k+1} = -b_0 V_k - d_0 V_{2k+1},$$

$$Y = -a_{-k} V_{-k} - c_{-k} V_1 = b_{-k} V_0 + d_{-k} V_{k+1}.$$

The point here is that the vector X lies in the span of $\{V_0, V_{k+1}\}$ and in the span of $\{V_k, V_{2k+1}\}$ and projectively this is exactly what is required. A similar remark applies to Y.

Setting $\Omega = V_0 \times V_{k+1}$, we compute the relevant cross ratio as

$$\frac{V_0 \times Y}{V_0 \times X} \cdot \frac{X \times V_{k+1}}{Y \times V_{k+1}} = \frac{d_{-k}\Omega}{c_0 \Omega} \times \frac{a_0 \Omega}{b_{-k}\Omega} = \frac{d_{-k} a_0}{b_{-k} c_0}, \tag{35}$$

which is just a rearrangement of the claimed term. ♠

The other cross ratio factors are obtained by shifting the indices in an obvious way. As an immediate corollary, we see that

$$\chi_k(D_{k+1}(P)) = \prod_{i=1}^{n} \frac{a_i d_i}{b_i c_i}. \tag{36}$$

Let us call this quantity $\mu_k(P)$.

Lemma 9.2. *If $\mu_k \circ \Delta_k = \mu_k$ then $\chi_k \circ \Delta_k = \chi_k$.*

Proof: If $\mu_k \circ \Delta_k = \mu_k$ then $\mu_k \circ \Delta_k^{-1} = \mu_k$. Equation 36 says that

$$\chi_k \circ D_{k+1} = \mu_k, \qquad \mu_k \circ D_{k+1} = \chi_k. \tag{37}$$

The first equation implies the second because D_{k+1} is an involution. Since D_{k+1} conjugates Δ_k to Δ_k^{-1} we have

$$\chi_k \circ \Delta_k = \chi_k \circ D_{k+1} \circ \Delta_k^{-1} \circ D_{k+1} = \mu_k \circ \Delta_k^{-1} \circ D_{k+1} = \mu_k \circ D_{k+1} = \chi_k.$$

This completes the proof. ♠

Let $\widetilde{P} = \Delta_k(P)$. Let $\{\widetilde{a}_i\}$, etc., be the sequences associated to $\widetilde{P}$. We want to show that

$$\prod_{i=1}^{n} \frac{a_i d_i}{b_i c_i} = \prod_{i=1}^{n} \frac{\widetilde{a}_i \widetilde{d}_i}{\widetilde{b}_i \widetilde{c}_i}. \tag{38}$$

This is just a restatement of the equation $\mu_k \circ \Delta_k = \mu_k$.

Now we use the formalism from [6] to establish Equation 38. We associate to our polygon P operator D on the space $\mathcal{V}$ of bi-infinite sequences $\{V_i\}$ of vectors in $\boldsymbol{R}^3$. The definition of D is given coordinate-wise as

$$D(V_i) = a_i V_i + b_i T^k(V_i) + c_i T^{k+1}(V_i) + d_i T^{2k+1}(V_i). \tag{39}$$

Here T is the shift operator, whose action is $T(V_i) = V_{i+1}$. If we take $\{V_i\}$ to be a periodic bi-infinite sequence of vectors corresponding to our polygon P, then D maps $\{V_i\}$ to the 0-sequence.

Next, we write $D = D_+ + D_-$ where coordinate-wise

$$D_+(V_i) = a_i V_i + c_i T^{k+1}(V_i), \qquad D_-(V_i) = b_i T^k(V_i) + d_i T^{2k+1}(V_i). \tag{40}$$

The pair (D_+, D_-) is associated to the polygon P.

Let $\widetilde{D}$ and $(\widetilde{D}_+, \widetilde{D}_-)$ be the corresponding operators associated to $\widetilde{P}$. One of the main results of [6] is that the various choices can be made so that

$$\widetilde{D}_+ D_- = \widetilde{D}_- D_+. \tag{41}$$

This is called *refactorization*. Equating the lowest (respectively highest) terms of the relation in Equation 41 gives us the identity $\widetilde{a}_i b_i = \widetilde{b}_i a_{i+k}$ (respectively $\widetilde{c}_i d_{i+k+1} = \widetilde{d}_i c_{i+2k+1}$.) These relations hold for all i and together imply Equation 38.

9.2 Extensions of Glick's Formula

Theorem 1.1 in [3] says that the coordinates for the collapse point of the pentagram map Δ_1 are algebraic functions of the coordinates of the initial polygon. In Equation 1.1 of [3], Glick goes further and gives a formula for the collapse point. I will explain his

formula. Let (x^*, y^*) denote the accumulation point of the forward iterates of P under Δ_1. Let $\widehat{P}_\infty = (x^*, y^*, 1)$ be the collapse point. In somewhat different notation, Glick introduces the operator

$$T_P = nI_3 - G_P, \qquad G_P(v) = \sum_{i=1}^{n} \frac{|P_{i-1}, v, P_{i+1}|}{|P_{i-1}, P_i, P_{i+1}|} P_i. \tag{42}$$

Here $|a, b, c|$ denotes the determinant of the matrix with rows a, b, c and I_3 is the 3×3 identity matrix. It turns out T_P is a Δ_1-invariant operator, in the sense that $T_{\Delta_0(P)} = T_P$. Moreover P_∞ is an eigenvector of T_P. This is Glick's formula for $\widehat{P}_\infty$. Actually, one can say more simply that G_P is a Δ_0-invariant operator and that $\widehat{P}_\infty$ is a fixed point of the projective action of G_p. This means that the vectors representing these points in $\boldsymbol{R}^3$ are eigenvectors for the operator. The reason Glick uses the more complicated expression $nI_3 - G_P$ is that geometrically it is easier to work with.

Define $G_{P,a,b}$ by the formula

$$G_{P,a,b}(v) = \sum_{i=1}^{n} \frac{|P_{i-a}, v, P_{i+b}|}{|P_{i-a}, P_i, P_{i+b}|} P_i. \tag{43}$$

Let $\widehat{P}_{\infty,k}$ be the limit point of the forward iterates of P under Δ_k.

A lot of experimental evidence suggests the following conjecture.

Conjecture 9.3. *Let $k \geq 2$. If $n = 3k+1$ the point $\widehat{P}_\infty$ is a fixed point for the projective action of $G_{P,k,k}$. If $n = 3k+2$ the point $\widehat{P}_\infty$ is a fixed point for the projective action of $G_{P,k+1,k+1}$. In particular, in these cases the coordinates of $\widehat{P}_\infty$ are algebraic functions of the vertices of P.*

Anton Izosimov kindly explained the following lemma, which seems like a big step in proving the conjecture. (I am still missing the geometric side of Glick's argument in this new setting.)

Lemma 9.4. *When $n = 3k+1$ the operator $G_{P,k,k}$ is invariant under Δ_k. When $n = 3k+2$ the operator $G_{P,k+1,k+1}$ is invariant under Δ_k.*

Proof: These operators are Glick's operator in disguise. When $n = 3k+1$ we can relabel our n-gons in a way that converts Δ_k to the pentagram map. The corresponding space of

birds $B_{n,k}$ corresponds to some strange set of "relabeled k-birds". This relabeling converts $G_{P,k,k}$ respectively to Glick's original operator. This proves the invariance of $G_{P,k,k}$ under Δ_k when $n = 3k+1$. A similar thing works for $n = 3k+2$, but this time the relabeling converts Δ_k to the inverse of the pentagram map. ♠

I was not able to find any similar formulas when $n > 3k+2$.

Question 9.5. *When $n > 3k+2$ and P is a k-bird, are the coordinates of the collapse point $\widehat{P}_\infty$ algebraic functions of the vertices of P?*

Here is one more thing I have wondered about. Suppose that n is very large and P is a convex n-gon. Then P can be considered as a k-bird for all $k = 1, 2, ..., \beta$, where β is the largest integer such that $n \geq 3\beta + 1$. When we apply the map Δ_k for these various values of k we get potentially β different collapse points. All I can say, based on experiments, is that these points are not generally collinear.

Question 9.6. *Does the collection of β collapse points in this situation have any special meaning?*

9.3 Star Relabelings

Let us further take up the theme in the proof of Lemma 9.4. Given an n-gon P and and some integer r relatively prime to n, we define a new n-gon P^{*r} by the formula

$$P^{*r}_j = P_{rj}. \tag{44}$$

Figure 1.5 shows the $P^{*(-3)}$ when P is the regular 10-gon.

As we have already mentioned, the action of Δ_1 on the $P^{*(-k)}$ is the same as the action of Δ_k on P when $n = 3k+1$. So, when $n = 3k+1$, the pentagram map has another nice invariant set (apart from the set of convex n-gons), namely

$$B^{*(-k)}_{k,n} = \{P^{*(-k)} \mid P \in B_{k,n}\}.$$

The action of the pentagram map on this set is geometrically nice. If we suitably star-relabel, we get star-shaped (and hence embedded) polygons. A similar thing works when $n = 3k + 2$.

Acknowledgments

I would like to thank Misha Gekhtman, Max Glick, Anton Izosimov, Boris Khesin, Valentin Ovsienko, and Serge Tabachnikov for many discussions about the pentagram zoo. I would like to thank Anton, in particular, for extensive discussions about the material in §9.

R.E.S. was supported by N.S.F. Grant DMS-21082802

References

[1] Q. Aboud and A. Izosimov, *The Limit Point of the Pentagram Map and Infinitesimal Monodromy*, I.M.R.N., Vol 7, (2022) 11

[2] M. Gekhtman, M. Shapiro, S. Tabachnikov, A. Vainshtein, *Integrable cluster dynamics of diected networks and pentagram maps*, Adv. Math. 300 (2016), pp 390-450 12

[3] M. Glick, *The Limit Point of the Pentagram Map*, International Mathematics Research Notices 9 (2020) pp. 2818–2831 11, 71

[4] M. Glick, *The pentagram map and Y-patterns*, Adv. Math. **227**, 2012, pp. 1019–1045. 12

[5] A. B. Goncharov and R. Kenyon, *Dimers and Cluster Integrable Systems*, Ann. Sc. Ec. Norm. Super. (4) 46 (2013) no. 5 pp 747–813 12

[6] A. Izosimov and B. Khesin, *Long Diagonal Pentagram Maps*, Bulletin of the L.M.S., vol. 55, no. 3, (2023) pp. 1-15 12, 13, 69, 71

[7] A. Izosimov, *The pentagram map, Poncelet polygons, and commuting difference operators*, Compos. Math. 158 (2022) pp 1084-1124

[8] A. Izosimov, *Pentagram maps and refactorization in Poisson-Lie groups*, Advances in Mathematics, vol. 404 (2022) 12, 69

[9] A. Izosimov, *Intersecting the Sides of the Polygon*, Proc. A.M.S. **150** (2022) 639-649. 11

[10] B. Khesin, F. Soloviev *Integrability of higher pentagram maps*, Mathem. Annalen. Vol. 357 no. 3 (2013) pp. 1005–1047 12

[11] B. Khesin, F. Soloviev *The geometry of dented pentagram maps*, J. European Math. Soc. Vol 18 (2016) pp. 147 – 179 12

[12] G. Mari Beffa, *On Generalizations of the Pentagram Map: Discretizations of AGD Flows*, Journal of Nonlinear Science, Vol 23, Issue 2 (2013) pp. 304–334 12

[13] G. Mari Beffa, *On integrable generalizations of the pentagram map* Int. Math. Res. Notices (2015) (12) pp. 3669-3693 12

[14] R Felipe and G. Mari-Beffa, *The pentagram map on Grassmannians*, Ann. Inst. Fourier (Grenoble) 69 (2019) no. 1 pp 421–456 12

[15] Th. Motzkin, *The pentagon in the projective plane, with a comment on Napier's rule*, Bull. Amer. Math. Soc. **52**, 1945, pp. 985–989. 11

[16] N. Ovenhouse, *The Non-Commutative Integrability of the Grassman Pentagram Map*, arXiv 1810.11742 (2019) 12

[17] V. Ovsienko, R. E. Schwartz, S. Tabachnikov, *The pentagram map: A discrete integrable system*, Comm. Math. Phys. **299**, 2010, pp. 409–446. 11, 17

[18] V. Ovsienko, R. E. Schwartz, S. Tabachnikov, *Liouville-Arnold integrability of the pentagram map on closed polygons*, Duke Math. J. Vol 162 No. 12 (2012) pp. 2149–2196 11, 17

[19] R. E. Schwartz, *The pentagram map*, Exper. Math. **1**, 1992, pp. 71–81. 11, 17, 21, 25

[20] R. E. Schwartz, *Discrete monodromy, pentagrams, and the method of condensation*, J. of Fixed Point Theory and Appl. **3**, 2008, pp. 379–409. 12, 17

[21] R. E. Schwartz, *A Textbook Case of Pentagram Rigidity*, arXiv 2108-07604 preprint (2021)[13

[22] R. E. Schwartz, *Pentagram Rigidity for Centrally Symmetric Octagons*, I.M.R.N. (2024) pp 9535–9561 13

[23] F. Soloviev *Integrability of the Pentagram Map*, Duke Math J. Vol 162. No. 15, (2012) pp. 2815 – 2853 11, 12

[24] M. Weinreich, *The Algebraic Dynamics of the Pentagram Map*, Ergodic Theory and Dynamical Systems 43 (2023) no. 10, pp. 3460 – 3505 12

AUTHOR

Richard Evan Schwartz
Department of Mathematics,
Brown University; Providence, RI, USA
email: Richard.Evan.Schwartz@gmail.com

Arnold Mathematical Journal
Volume 11, Issue 4, 2025

A Novel Geometric Realization of the Yajima-Oikawa Equations

Annalisa Calini Thomas Ivey

Received 17 Dec 2024; Accepted 23 May 2025

Abstract: We show that the Yajima-Oikawa (YO) equations, a model of short wave-long wave interaction, arise from a simple geometric flow on curves in the 3-dimensional sphere S^3 that are transverse to the standard contact structure. For the family of periodic plane wave solutions of the YO equations studied by Wright, we construct the associated transverse curves, derive their closure condition, and exhibit several examples with non-trivial topology.

Key words and phrases: Geometric evolution equations; integrable systems; contact structures; transverse curves; long wave-short wave models.

1 Introduction

This work is part of our investigation of curve flows in the 3-sphere S^3 that are invariant under the action of the group $SU(2,1)$ of pseudoconformal transformations, which

DOI: 10.56994/ARMJ.011.004.003

preserves the standard contact structure on the sphere. While the focus of our previous study [2] was Legendrian curves in the 3-sphere and geometric flows for such curves which are integrable (i.e., inducing integrable evolution equations for their fundamental differential invariants), in this note we discuss an interesting connection between an integrable model of short wave-long wave interaction and a geometric flow for curves that are transverse to the contact structure.

The pseudoconformal geometry of S^3 is inherited from the geometry of the space $\mathbb{C}^3$ endowed with the indefinite Hermitian form

$$\langle \mathbf{z}, \mathbf{w} \rangle := \mathrm{i}(z_3\overline{w_1} - z_1\overline{w_3}) + z_2\overline{w_2}. \tag{1}$$

(The coordinates are chosen so that the z_1, z_3 axes are null directions.) Given the standard action of $SL(3,\mathbb{C})$ on $\mathbb{C}^3$, let $SU(2,1)$ denote the subgroup that preserves this form. Let $\mathcal{N} \subset \mathbb{C}^3$ be the *null cone*, i.e., the set of nonzero null vectors for (1). The set of complex lines on the null cone is diffeomorphic to S^3, the unit sphere in $\mathbb{C}^2$ (see (30)). It follows that the linear action of $SU(2,1)$ on $\mathbb{C}^3$ induces an action on S^3 known as the group of pseudoconformal transformations. We will let π denote the complex projectivization map from $\mathbb{C}^3$ minus the origin to $\mathbb{C}P^2$, as well as its restriction to the null cone, giving a commutative diagram:

$$\begin{array}{ccc} \mathcal{N} & \subset & \mathbb{C}^3\backslash\{0\} \\ \downarrow\pi & & \downarrow\pi \\ S^3 & \subset & \mathbb{C}P^2 \end{array}$$

The pseudoconformal action preserves the standard contact structure on S^3, defined for curves in S^3 in terms of their lifts relative to π as follows.

Definitions. Let $\gamma : I \to S^3$ be a regular parametrized curve on an interval $I \subset \mathbb{R}$. Then γ is *Legendrian* if it has a lift $\Gamma : I \to \mathcal{N}$ satisfying

$$\mathrm{Im}\langle \Gamma_x, \Gamma \rangle = 0, \forall x \in I. \tag{2}$$

By contrast, γ is a *transverse curve* or *T-curve* if its lift satisfies

$$\mathrm{Im}\langle \Gamma_x, \Gamma \rangle \neq 0, \forall x \in I. \tag{3}$$

In other words, the tangent vector of a T-curve is everywhere transverse to the contact planes. (Note that both conditions (2),(3) are invariant under a change of lift, i.e., multiplying Γ by a nonzero complex-valued function.)

Let $\gamma : I \to S^3$ be a regular curve with lift $\Gamma : I \to \mathcal{N}$. Then Γ and its derivative Γ_x satisfy $\langle \Gamma, \Gamma \rangle = 0$ and $\mathrm{Re}\langle \Gamma_x, \Gamma \rangle = 0$. If γ is a transverse curve then $\mathrm{Im}\langle \Gamma_x, \Gamma \rangle \neq 0$, so we can assume the normalization $\langle \Gamma_x, \Gamma \rangle = \mathrm{i}$ or equivalently $\langle \mathrm{i}\Gamma, \Gamma_x \rangle = 1$; we can furthermore choose a lift that also satisfies $\langle \Gamma_x, \Gamma_x \rangle = 0$ (see §2 for more details). With these assumptions, we define a geometric flow based on the second derivative Γ_{xx} as

$$\Gamma_t = \mathrm{i}\left(\Gamma_{xx} - \langle \Gamma_{xx}, \Gamma_x \rangle \mathrm{i}\Gamma\right), \tag{4}$$

which induces a well-defined flow for the T-curve $\gamma = \pi \circ \Gamma$. Note that the vector field in parentheses on the right-hand side is a modification of Γ_{xx} that lies in $\{\Gamma_x\}^\perp$, the orthogonal complement of the complex span $\{\Gamma_x\}$. If we let $\mathrm{p}_{\{\Gamma_x\}^\perp}$ denote the orthogonal projection onto $\{\Gamma_x\}^\perp$, then writing (4) as $\Gamma_t = \mathrm{i}\mathrm{p}_{\{\Gamma_x\}^\perp}(\Gamma_{xx})$ suggests an analogy with the vortex filament flow $\gamma_t = \gamma_x \times \gamma_{xx}$ (or binormal flow) for an arc length parametrized curve γ in Euclidean space [10], with the skew-symmetric operator $\mathrm{i}\mathrm{p}_{\{\Gamma_x\}^\perp}$ the analogue of the symplectic operator $T_x\times$ for the binormal flow.

In Sections 2–4 we construct adapted frames for transverse curves—both local frames (akin to the Frenet frames of Euclidean geometry) and non-local 'natural' frames—and show that equation (4) can be rewritten in terms of a convenient non-local adapted frame (Γ, Γ_x, B) as

$$\Gamma_t = \mathrm{i}zB,$$

where B is a unit spacelike vector orthogonal to $\{\Gamma, \Gamma_x\}$ and z is a complex curvature, part of the set (z, m), $z \in \mathbb{C}, m \in \mathbb{R}$, of geometric invariants of Γ. After deriving the evolution equations for the geometric invariants induced by a general vector field on (lifts of) transverse curves, we show that the evolution induced by (4) on the invariants (z, m) is

the following system of nonlinear PDE

$$z_t = \mathrm{i}(z_{xx} - mz),$$
$$m_t = 2(|z|^2)_x,$$

known as the Yajima-Oikawa (YO) or Long-Wave-Short-Wave equations, a completely integrable model of interaction of long and short waves.

The YO system first appeared in work by Grimshaw [6] in the context of internal gravity waves, and was derived by Yajima & Oikawa [12] and by Djordjevic & Redekopp [5] as an integrable model of interaction of a long wave (of amplitude m) and a short wave (of complex amplitude z).

In Section 5, we use the connection between the Lax pair for the YO equations at given (z, m) and the adapted frame of the associated transverse curve to construct examples of geometric realizations of solutions of the YO equations. We focus on the family of plane wave YO solutions studied by Wright in [11], derive closure conditions for the associated curves, and construct explicit formulas. The plane wave solutions, though simple at the YO level, provide a wealth of closed transverse curves with non-trivial topology. We present visualizations of several examples, that illustrate how the knot type and the geometry relate to the parameters in the YO solutions.

In Section 6 we discuss some open questions and directions for future work.

2 Pseudoconformal Frames and Curvature

Let $\gamma : I \to S^3$ be a T-curve, and Γ be a lift satisfying $\mathrm{Im}\langle\Gamma_x, \Gamma\rangle > 0$. Since the restriction of the Hermitian form (1) to the complex span $\mathcal{S} = \mathrm{span}_{\mathbb{C}}\{\Gamma, \Gamma_x\}$ is non-degenerate, we construct a smooth adapted frame by selecting two linearly independent null vectors–Γ itself and a second vector $V \in \mathcal{S}$–and adding a third vector B which is spacelike and spans the complex line orthogonal to $\mathcal{S}$.

As described in Proposition 10 of [2], the ordered triple (Γ, B, V) of vectors in $\mathbb{C}^3$ can

be chosen to satisfy the following inner product relations

$$\langle \Gamma, \Gamma \rangle = \langle V, V \rangle = \langle B, \Gamma \rangle = \langle B, V \rangle = 0,$$

$$\langle \Gamma, V \rangle = -\mathrm{i}, \quad \langle V, \Gamma \rangle = \mathrm{i}, \quad \langle B, B \rangle = 1.$$

as well as the condition $\det(\Gamma, B, V) = 1$ (meaning that the vectors form the columns of a unimodular matrix). We call a triple that satisfies these relations a *unimodular null frame*. In the rest of this section we describe how a smoothly-varying unimodular null frame, including the lift Γ as its first member, can be chosen in an essentially unique way for a regular T-curve, allowing us to identify fundamental invariants.

Local frame.

In Corollary 1 of [2] it is shown that, under suitable nondegeneracy assumptions, any parametrized T-curve γ has a unimodular null frame field (Γ, B, V), constructed in terms of algebraic functions of the components of γ and its derivatives, that satisfies

$$\frac{d\widehat{F}}{dx} = \widehat{F} \begin{bmatrix} \frac{1}{3}\mathrm{i}p & -\mathrm{i}q & m \\ 0 & -\frac{2}{3}\mathrm{i}p & q \\ 1 & 0 & \frac{1}{3}\mathrm{i}p \end{bmatrix}. \tag{5}$$

where $\widehat{F}$ denotes the matrix with columns Γ, B, V, and m, p, q are real-valued *fundamental differential invariants* of the parametrized curve. We refer to this as the *local frame*, and it is unique up to multiplication of each column by the same cube root of unity. It is the analogue of the (local) Frenet frame for a unit-speed curve $\gamma : \mathbb{R} \to \mathbb{R}^3$ in Euclidean space.

Natural frame.

In the Euclidean case, one can also construct the (non-local) *relatively parallel* or *natural* frame (T, U_1, U_2), where $U_1 = \cos\theta\, N + \sin\theta\, B$ and $U_2 = -\sin\theta\, N + \cos\theta\, B$, with $\theta = -\int \tau\, ds$. (Here N and B are the unit normal and binormal vectors and s is arclength.) This frame, which is unique up to a choice of antiderivative θ, satisfies

$$\frac{dT}{ds} = k_1 U_1 + k_2 U_2, \quad \frac{dU_1}{ds} = -k_1 T, \quad \frac{dU_2}{ds} = -k_2 T,$$

so that the normal vectors U_1, U_2 rotate only in the direction of the tangent line. The functions $k_1 = k\cos\theta$ and $k_2 = k\sin\theta$ are *natural curvatures* [1].

By analogy with the Euclidean case, given the local frame $\widehat{F}$ for a T-curve γ we can use an antiderivative to neutralize the rotation of normal vector B in the normal plane, forming a new unimodular null frame field defined by

$$F = \widehat{F}\exp(\theta \mathsf{J}), \qquad \text{where } \theta = -\int p\,dx, \quad \mathsf{J} = \begin{pmatrix} \frac{1}{3}\mathrm{i} & 0 & 0 \\ 0 & -\frac{2}{3}\mathrm{i} & 0 \\ 0 & 0 & \frac{1}{3}\mathrm{i} \end{pmatrix}.$$

It follows that F satisfies the *nonlocal frame equations*

$$\frac{dF}{dx} = F\begin{bmatrix} 0 & -\mathrm{i}\bar{z} & m \\ 0 & 0 & z \\ 1 & 0 & 0 \end{bmatrix}, \tag{6}$$

where $z = e^{\mathrm{i}\theta}q$ and m is the same as in (5). One can interpret z as a complex curvature, measuring how the tangent line $\pi\{\Gamma, V\}$ bends within the complex projective plane. The real-valued invariant $m = \mathrm{Im}\langle V, V_x\rangle$ measures the deviation of the projectivization of V from being a Legendrian curve in S^3.

Companion λ-frames

Any two unimodular null frames at the same point of S^3 are linked by a transformation of the following form (see, e.g., Proposition 10 in [2])

$$\widetilde{\Gamma} = \nu\Gamma, \quad \widetilde{B} = \frac{\overline{\nu}}{\nu}(B + \mu\Gamma), \quad \widetilde{V} = \overline{\nu}^{-1}\left[V - \mathrm{i}\overline{\mu}B - (\lambda + \tfrac{1}{2}\mathrm{i}|\mu|^2)\Gamma\right], \tag{7}$$

where ν, μ are complex, with $\nu \neq 0$, and λ is real.

Given the local frame for a T-curve, we modify the frame using $\mu = 0$, $\nu = 1$ and λ constant in (7), to obtain the *companion λ-frame* $\widetilde{\Gamma} = \Gamma, \widetilde{B} = B, \widetilde{V} = V - \lambda\Gamma$. This modified frame satisfies

$$\widetilde{\Gamma}_x = \left(\frac{1}{3}\mathrm{i}p + \lambda\right)\widetilde{\Gamma} + \widetilde{V}, \quad \widetilde{B}_x = -\mathrm{i}q\widetilde{\Gamma} - \frac{2}{3}\mathrm{i}p\widetilde{B}, \quad \widetilde{V}_x = (m - \lambda^2)\widetilde{\Gamma} + (\frac{1}{3}\mathrm{i}p - \lambda)\widetilde{V}.$$

If we make a similar modification to a natural frame for a T-curve we obtain the *companion λ-natural frame*, which satisfies

$$\frac{d\widetilde{F}}{dx} = \widetilde{F}\begin{bmatrix} \lambda & -\mathrm{i}\overline{z} & m-\lambda^2 \\ 0 & 0 & z \\ 1 & 0 & -\lambda \end{bmatrix}. \tag{8}$$

Remark. Note that if the projection of the frame vector $\widetilde{V}$ of a companion λ-frame is a Legendrian curve in S^3 (so that $m-\lambda^2=0$), then the same is true for the companion frame constructed using $-\lambda$.

3 Curve Flows and the Yajima-Oikawa Equations

If $\gamma(x,t)$ is a smooth variation of a T-curve and (Γ, B, V) is a smoothly-varying choice of natural frame, then the vector field $\Gamma_t = f\Gamma + gB + hV$ must satisfy

$$h_x = -2\,\mathrm{Re}\, f \quad \text{and} \quad (\mathrm{Im}\, f)_x = \mathrm{Re}(g\overline{z}) \tag{9}$$

in order to keep the frame adapted, as shown in Proposition 11 of [2]. (Note that, since condition (3) is an open condition, such variations always exist.) It follows that the nonlocal invariants m and $z = k + \mathrm{i}\ell$ evolve by

$$\begin{bmatrix} k \\ \ell \\ m \end{bmatrix}_t = \mathcal{P}\begin{bmatrix} \mathrm{Im}\, g \\ -\mathrm{Re}\, g \\ \frac{1}{2}h \end{bmatrix}, \tag{10}$$

where

$$\mathcal{P} = \begin{pmatrix} -3\ell D^{-1}\circ\ell & 3\ell D^{-1}\circ k - D^2 + m & 2D\circ k + kD \\ 3kD^{-1}\circ\ell + D^2 - m & -3kD^{-1}\circ k & 2D\circ\ell + \ell D \\ 2kD + D\circ k & 2\ell D + D\circ\ell & 2(mD + D\circ m) - D^3 \end{pmatrix}$$

and $D = \partial_x$. The matrix operator $\mathcal{P}$ is skew-adjoint, and forms a Hamiltonian pair with

$$\mathcal{Q} = \begin{pmatrix} 0 & 1 & 0 \\ -1 & 0 & 0 \\ 0 & 0 & D \end{pmatrix}.$$

In particular, if Γ evolves by

$$\Gamma_t = \mathrm{i}zB, \tag{11}$$

then the invariants z and m satisfy the *Yajima-Oikawa* (YO) equations

$$\begin{aligned} z_t &= \mathrm{i}(z_{xx} - mz), \\ m_t &= 2(|z|^2)_x. \end{aligned} \tag{12}$$

Integrability

The YO system (12) is the compatibility condition of the following pair of linear systems

$$\boldsymbol{\phi}_x = U\boldsymbol{\phi}, \quad \boldsymbol{\phi}_t = V\boldsymbol{\phi}, \tag{13}$$

where

$$U = \begin{bmatrix} \lambda & 0 & 1 \\ \mathrm{i}z & 0 & 0 \\ m & \overline{z} & -\lambda \end{bmatrix}, \qquad V = \begin{bmatrix} -\frac{1}{3}\mathrm{i}\lambda^2 & -\mathrm{i}\overline{z} & 0 \\ \lambda z - z_x & \frac{2}{3}\mathrm{i}\lambda^2 & z \\ |z|^2 & \mathrm{i}(\lambda\overline{z} - \overline{z}_x) & -\frac{1}{3}\mathrm{i}\lambda^2 \end{bmatrix}, \tag{14}$$

with eigenfunction $\phi \in \mathbb{C}^3$, and spectral parameter $\lambda \in \mathbb{C}$. (We will show below that this is linearly equivalent to the Lax pair in [11].) When $\lambda \in \mathbb{R}$, U and V take value in the Lie algebra $\mathfrak{su}(2,1)$ of the subgroup of $SL(3,\mathbb{C})$ that preserves the Hermitian form (1). Taking the transpose of (13) and complex conjugating, we obtain

$$F_x = F\begin{bmatrix} \lambda & -\mathrm{i}\overline{z} & m \\ 0 & 0 & z \\ 1 & 0 & -\lambda \end{bmatrix}, \quad F_t = F\begin{bmatrix} \frac{1}{3}\mathrm{i}\lambda^2 & \lambda\overline{z} - \overline{z}_x & |z|^2 \\ \mathrm{i}z & -\frac{2}{3}\mathrm{i}\lambda^2 & \mathrm{i}(z_x - \lambda z) \\ 0 & \overline{z} & \frac{1}{3}\mathrm{i}\lambda^2 \end{bmatrix}. \tag{15}$$

Comparing the first of these equations to (8) shows that system (15) can be interpreted as the Frenet equations for the companion natural λ-frame of an T-curve with curvatures z and $\widetilde{m} = m + \lambda^2$, and which evolves by the flow

$$\Gamma_t = \mathrm{i}zB + \tfrac{1}{3}\mathrm{i}\lambda^2\Gamma. \tag{16}$$

This connection between the YO Lax pair and the evolution of (framed) curves allows the construction of interesting examples of transverse curves associated with simple solutions of the YO system, as shown in the rest of the article.

4 Plane wave solutions

In [11], Wright investigates the linear stability of plane wave solutions of the YO equations (17) and derives explicit solutions of the associated Lax pair in order to construct homoclinic orbits of unstable plane waves.

4.1 Equivalent Versions of YO

In [11] the YO system is given as

$$\begin{aligned} A_\tau &= -2\mathrm{i}(A_{xx} - AB), \\ B_\tau &= 4(|A|^2)_x \end{aligned} \tag{17}$$

for complex $A(x,\tau)$ and real $B(x,\tau)$, and its Lax pair is given as

$$\boldsymbol{\psi}_x = \mathbf{U}\boldsymbol{\psi}, \qquad \boldsymbol{\psi}_\tau = 2\mathbf{V}\boldsymbol{\psi} \tag{18}$$

with

$$\mathbf{U} = \begin{bmatrix} \mathrm{i}\zeta & A & \mathrm{i}B \\ 0 & 0 & -\overline{A} \\ -\mathrm{i} & 0 & -\mathrm{i}\zeta \end{bmatrix}, \quad \mathbf{V} = \begin{bmatrix} \frac{1}{3}\mathrm{i}\zeta^2 & \zeta A - \mathrm{i}A_x & \mathrm{i}|A|^2 \\ 2\overline{A} & -\frac{2}{3}\mathrm{i}\zeta^2 & \zeta\overline{A} - \mathrm{i}\overline{A_x} \\ 0 & -A & \frac{1}{3}\mathrm{i}\zeta^2 \end{bmatrix},$$

where ζ and τ denote Wright's spectral parameter and time variable respectively. (Wright's YO equations include an extra parameter which we omit because it can be removed by a simple change of variable.) The equations (17) are equivalent to (12) under the substitutions $A = \overline{z}$, $B = m$ and $\tau = \frac{1}{2}t$. Moreover, the linear systems (18) and (13) are equivalent under a change of gauge, since with these substitutions, $\mathbf{U} = MUM^{-1}$ and $\mathbf{V} = MVM^{-1}$, where

$$M = \begin{bmatrix} 0 & 0 & 1 \\ 0 & 1 & 0 \\ -\mathrm{i} & 0 & 0 \end{bmatrix}.$$

4.2 Wright's Solutions

In this section, we will present Wright's solutions, rewritten in terms of our variables. We will then make use of the eigenfunction formulas in [11], appropriately adapted to the geometric framework, to construct the associated transverse curves. We will then identify the parameter choices that give rise to closed transverse curves.

Proposition 1 ([11])**.** For real constants a, b, k and Λ such that $a > 0$, the functions

$$z(x,t) = a\mathrm{e}^{-\mathrm{i}N} \qquad m(x,t) = b, \quad \text{where } N := kx - \Lambda t$$

give a solution of (12) if and only if the *dispersion relation* $b + k^2 + \Lambda = 0$ is satisfied. When these z, m are substituted into (13), a non-trivial solution of (13) is given by

$$\boldsymbol{\phi}(x,t) = \mathrm{e}^{\mathrm{i}(\mu x + \nu t)} P \mathsf{r}, \tag{19}$$

where

$$P = \begin{bmatrix} 1 & 0 & 0 \\ 0 & \mathrm{e}^{-\mathrm{i}N} & 0 \\ 0 & 0 & 1 \end{bmatrix},$$

and r is a nonzero common eigenvector of the matrices

$$\begin{bmatrix} \lambda & 0 & 1 \\ \mathrm{i}a & \mathrm{i}k & 0 \\ b & a & -\lambda \end{bmatrix}, \qquad \begin{bmatrix} -\frac{1}{3}\mathrm{i}\lambda^2 & -\mathrm{i}a & 0 \\ a(\lambda + \mathrm{i}k) & \frac{2}{3}\mathrm{i}\lambda^2 - \mathrm{i}\Lambda & a \\ a^2 & a(k + \mathrm{i}\lambda) & -\frac{1}{3}\mathrm{i}\lambda^2 \end{bmatrix} \tag{20}$$

with eigenvalues $\mathrm{i}\mu$ and $\mathrm{i}\nu$, respectively.

It is easy to check that the matrices in (20) have a non-trivial common eigenvector if and only if μ and ν satisfy

$$(\mu^2 + b + \lambda^2)(\mu - k) + a^2 = 0, \tag{21a}$$

$$\nu = \mu^2 - k^2 - \Lambda + \tfrac{2}{3}\lambda^2. \tag{21b}$$

In order to construct a fundamental matrix solution for (13) using solutions of the form (19), let $\mu = m_1, m_2, m_3$ be three distinct roots of (21a) and let n_1, n_2, n_3 be the corresponding values of ν given by substituting these into (21b). Then a matrix solution is given by $\Phi = PRE$, where

$$R = \begin{pmatrix} -1 & -1 & -1 \\ \dfrac{a}{k-m_1} & \dfrac{a}{k-m_2} & \dfrac{a}{k-m_2} \\ \lambda - \mathrm{i}m_1 & \lambda - \mathrm{i}m_2 & \lambda - \mathrm{i}m_3 \end{pmatrix}, \quad E = \begin{pmatrix} \mathrm{e}^{\mathrm{i}(m_1 x + n_1 t)} & 0 & 0 \\ 0 & \mathrm{e}^{\mathrm{i}(m_2 x + n_2 t)} & 0 \\ 0 & 0 & \mathrm{e}^{\mathrm{i}(m_3 x + n_3 t)} \end{pmatrix}.$$

Our discussion in §3 implies that if Φ is a fundamental matrix solution of the YO Lax pair for a real value of λ, and taking value in the group $SU(2,1)$, then $F = \Phi^\dagger$ is a λ-natural frame matrix for a transverse curve evolving by (16). Since $\lambda \in \mathbb{R}$ implies that the coefficient matrices in (13) take value in $\mathfrak{su}(2,1)$, we can ensure that our fundamental matrix takes value in $SU(2,1)$ by modifying it to be equal to the identity matrix when $x = t = 0$:

$$\Phi = PRER^{-1}P_0^{-1}, \qquad \text{where } P_0 = P\big|_{x=t=0}. \tag{22}$$

Using this matrix to construct the natural frame, and taking the projectivization of the first frame vector Γ to obtain a transverse curve γ, we now consider the question of when the resulting curve is smoothly closed.

Proposition 2. Suppose the fundamental matrix $\Phi = PRE$ described above corresponds to a λ-natural frame for a T-curve γ. Then γ is closed of length L if and only if there is a cube root ω of unity such that

$$\mathrm{e}^{\mathrm{i}m_j L} = \overline{\omega}\mathrm{e}^{\mathrm{i}kL/3}. \tag{23}$$

Proof. Let F be a natural λ-frame along the curve, satisfying the spatial part of (15), and let $\widehat{F}$ be the local frame related to F by $\widehat{F} = F\exp(-\theta \mathsf{J})$. Because the local frame is uniquely determined by derivatives of γ, up to multiplying by a cube root of unity, then γ is closed of length L if and only if

$$\widehat{F}(x + L) = \omega \widehat{F}(x). \tag{24}$$

For the solutions of Prop. 1, $\theta = \arg z = -N$; rewriting (24) in terms of $F = \Phi^\dagger$, then in terms of the factors of Φ given by (22), and simplifying (using the fact that J commutes with M and P) gives the condition (23). □

Without loss of generality, we will take $L = 2\pi$ from now on, and assume the roots of (21a) are numbered in ascending order, i.e., $m_1 < m_2 < m_3$. Note that, for a given value of λ, these roots determine the coefficients in the polynomial via:

$$\begin{aligned} k &= m_1 + m_2 + m_3, \\ a^2 &= (k - m_1)(k - m_2)(k - m_3), \\ b &= m_1 m_2 + m_1 m_3 + m_2 m_3 - \lambda^2. \end{aligned} \tag{25}$$

Lemma 3. The above closure conditions (23) are satisfied if and only if there are positive integers p, q such that k satisfies either

$$-\tfrac{1}{2}(2p + q) < k < \tfrac{1}{2}(p - q) \tag{26a}$$

or

$$k > \tfrac{1}{2}(p + 2q). \tag{26b}$$

In either case, the roots are given by

$$m_1 = \tfrac{1}{3}(-2p - q + k), \quad m_2 = \tfrac{1}{3}(p - q + k), \quad m_3 = \tfrac{1}{3}(p + 2q + k), \tag{27}$$

and $\omega = \mathrm{e}^{2\pi \mathrm{i}\epsilon/3}$ where $\epsilon = 0, 1, 2$ is such that $3m_j - k \equiv \epsilon$ modulo 3.

Proof. We can rewrite the closure condition (23) as

$$m_j = l_j + \tfrac{1}{3}\epsilon + \tfrac{1}{3}k, \tag{28}$$

for some integers $l_1 < l_2 < l_3$. The second relation in (25) is satisfied for $a > 0$ if and only if

$$m_1 < k < m_2 < m_3 \qquad \text{or} \qquad m_1 < m_2 < m_3 < k. \tag{29}$$

When written in terms of the positive integers $p = l_2 - l_1$ and $q = l_3 - l_2$, the two conditions in (29) become those in (26).

Conversely, suppose a pair positive integers p, q satisfy either of the equations in (26) for some real number k. Let $\epsilon = 0, 1, 2$ be chosen so that $p - q \equiv \epsilon$ modulo 3, and let

$$l_1 = \tfrac{1}{3}(-2p - q - \epsilon), \qquad l_2 = \tfrac{1}{3}(p - q - \epsilon), \quad l_3 = \tfrac{1}{3}(p + 2q) - \frac{1}{3}\epsilon.$$

Then with m_j given by (28), condition (29) is satisfied. □

4.3 Visualizing Examples

In this section we will exhibit examples of closed transverse curves in S^3, generated using the fundamental matrix Φ corresponding to Wright's solutions, with closure conditions imposed using Lemma 3. In particular, we will observe knotted transverse curves which, because their differential invariants are the same at each time, move by rigid motion under the flow (16).

In more detail, given two positive integers p, q one may select any value of λ and a real value of k satisfying one of the inequalities in (26). The other parameters involved in the solution are determined by equations (25) and (27). This yields two distinct 2-parameter families of closed curves for each pair (p, q). (Exactly how we construct these curves is explained below.) We will assume that p, q are relatively prime; experiments indicate that the knot types are the same when p, q are multiplied by a common integer factor.

In the case (26a) we observe that the curve in $\mathbb{R}^3$ is a right-handed $(q, p + q)$ torus knot. Recall that the type of a (m, n) torus knot depends only on the *unordered pair* $\{m, n\}$. However, for our examples we find that when k is close to its lower limit, the knot takes a shape with q strands that wind along the torus the long way (see Figure 1, top left, where $k = -3.85 \gtrsim -4$), while when k is close to its upper limit the knot has $p + q$ strands winding the long way (see Figure 1, bottom right, where $k = 0.2 \lesssim 0.5$.) In general, the knot shape is more compact and symmetric when $\lambda = 0$; Figure 2 shows two shapes for the same p, q, k but different λ values. Note that (25) shows that these curves have the same differential

invariant z but different constant values $m = b$.

We showed in Lemma 12 of [2] that transverse curves for which $z = 0$ identically are $SU(2,1)$-congruent to curves which run along the circular fibers of the Hopf fibration. Thus, when k approaches one of the roots m_j, $a = |z|$ will approach zero and the closed curve will approach a multiply-covered circle congruent to a Hopf fiber. In Figure 1, we show a family of right-handed $(2,5)$ torus knots, corresponding to a range of k-values, where at both ends of the family the curve approaches a multiply-covered circle.

In the case (26b) we observe that the curve in $\mathbb{R}^3$ is a left-handed (p,q) torus knot. (When $p = 1$ or $q = 1$ the curve is unknotted, as shown in Figure 4.) When k is close to its lower limit the curve has p strands winding around the torus the long way, and its shape approaches a circle covered p times. For large values of k, the curve approaches a flattened teardrop shape, with the knot crossings compressed into a small region near where $x = \pi$. Both these limiting behaviors are illustrated in Figure 3.

4.4 Constructing Transverse Curves

Once we have a fundamental matrix solution Φ for the linear system (13), the first component of the λ-natural frame is then given by

$$\Gamma = F\mathsf{e}_1 = \Phi^\dagger \mathsf{e}_1,$$

taking value in the null cone $\mathcal{N}$. We produce curves in S^3 using a projection $\hat{\pi} : \mathcal{N} \to S^3$ given in terms of the components of Γ by

$$z_1 = \frac{\Gamma_3 - \mathrm{i}\Gamma_1}{\Gamma_3 + \mathrm{i}\Gamma_1}, \qquad z_2 = \frac{\sqrt{2}\,\Gamma_2}{\Gamma_3 + \mathrm{i}\Gamma_1}, \tag{30}$$

where (z_1, z_2) lie on the unit sphere in $\mathbb{C}^2$ equipped with its standard Hermitian inner product. For purposes of visualization, we in turn apply stereographic projection into $\mathbb{R}^3$ (using the point $z_1 = 0$, $z_2 = \mathrm{i}$ as pole) given by

$$\sigma : (z_1, z_2) \longmapsto \left(\frac{\operatorname{Re} z_1}{1 - \operatorname{Im} z_2}, \frac{\operatorname{Im} z_1}{1 - \operatorname{Im} z_2}, \frac{\operatorname{Re} z_2}{1 - \operatorname{Im} z_2} \right).$$

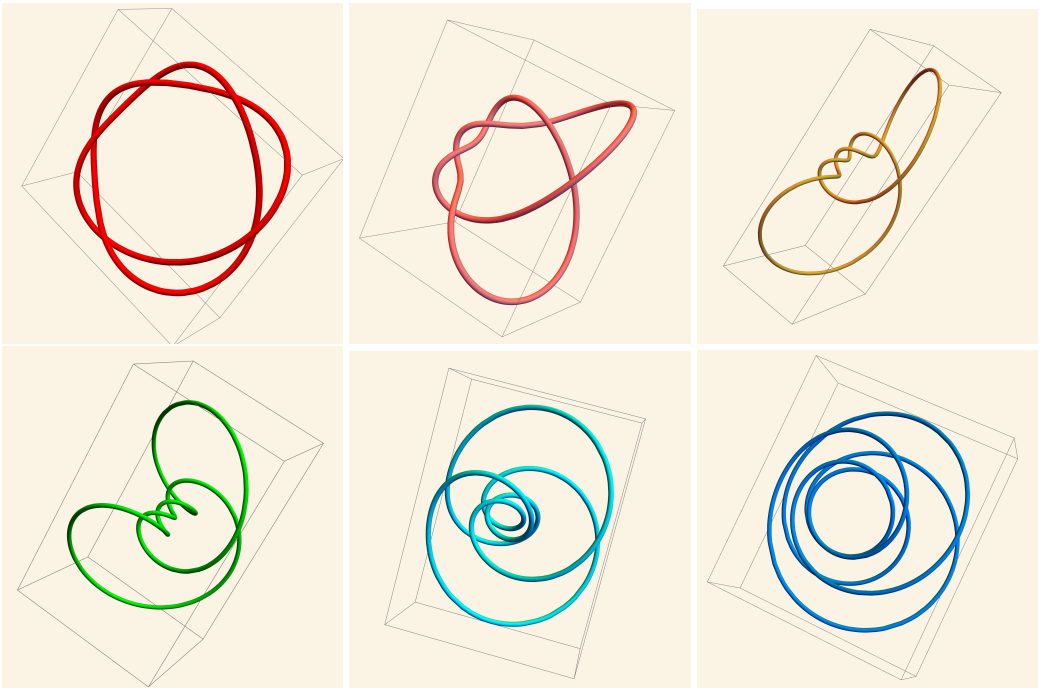

Figure 1: A family of $(2,5)$ torus knots obtained using $p=3$, $q=2$, $\lambda=0$ and the values $k=-3.85,-3.25,-2.5$ in the top row and $k=-1.75,-0.7,0.2$ in the bottom row. The first and last figure show knots near the limiting values of k, since $k\in(-4,0.5)$ from (26a).

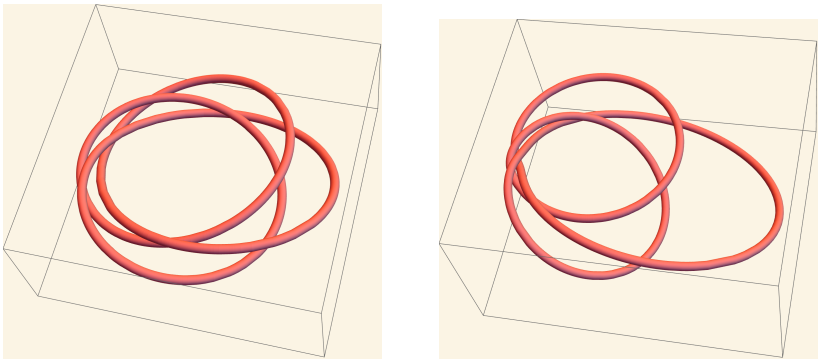

Figure 2: Right-handed $(3,4)$ torus knots obtained using $p=1$, $q=3$ and $k=-2.2$; on the left $\lambda=0$, while on the right $\lambda=3.1$.

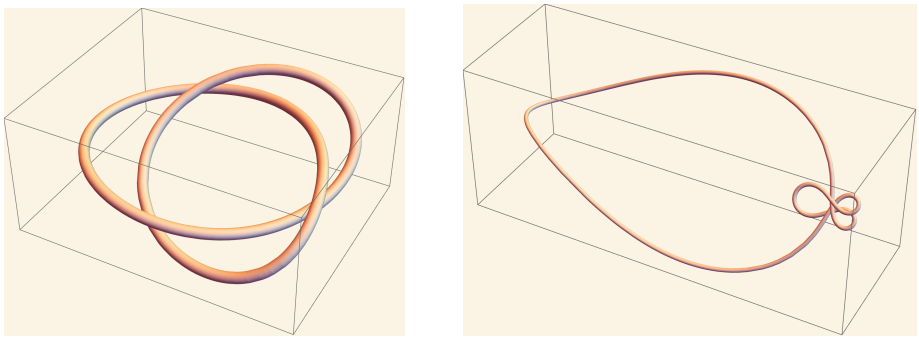

Figure 3: Left-handed $(2,3)$ torus knots (i.e., trefoils) obtained using $p=1$, $q=2$ and $\lambda=0$; on the left $k=4.6$, while on the right $k=31$.

Remark. The action of $SU(2,1)$ on the null cone preserves the 1-form $\alpha_N=(dg,g)$, which is the pullback under $\hat{\pi}$ of the standard contact form on S^3, given by $\alpha_S=\frac{1}{2}\operatorname{Im}(\overline{z}_1dz_1+\overline{z}_2dz_2)$. The contact planes in S^3 annihilated by this 1-form are orthogonal to the Hopf fibers. Since S^3 is parallelizable, we can choose an globally defined orthogonal frame $(\mathsf{v}_0,\mathsf{v}_1,\mathsf{v}_2)$ such that $\mathsf{v}_1,\mathsf{v}_2$ are tangent to the contact planes. For purposes of visualizing the contact distribution, we will use the following vectors in $\mathbb{R}^3$ which are tangent to the image of this distribution under stereographic projection:

$$\sigma_*\mathsf{v}_1=-(z+xy)\frac{\partial}{\partial x}+\tfrac{1}{2}(x^2-y^2+z^2-1)\frac{\partial}{\partial y}+(x-yz)\frac{\partial}{\partial z},$$
$$\sigma_*\mathsf{v}_2=\tfrac{1}{2}(x^2-y^2-z^2+1)\frac{\partial}{\partial x}+(xy-z)\frac{\partial}{\partial y}+(xz+y)\frac{\partial}{\partial z}.$$

Figure 4 shows how the curve γ is transverse to the planes spanned by these vector fields.

Recall from (6) that when $m=0$ the frame vector V projects to a Legendrian curve in S^3. Figure 4 also shows this companion curve which in this example is linked with γ and tangent to the contact planes.

5 Discussion

We have shown how the YO equations arise, somewhat unexpectedly, from a simple geometric flow for curves in S^3 that are transverse to the standard contact structure. The

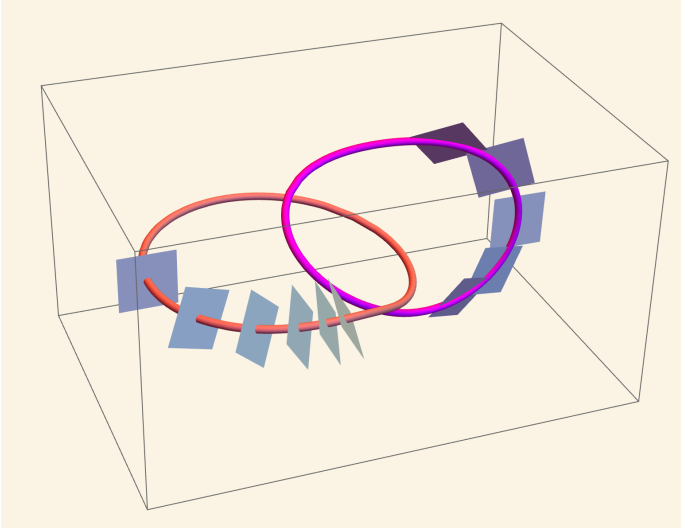

Figure 4: At left, in orange, is an unknotted T-curve γ generated using parameter values $p = q = 1$, $k = 2$ and $\lambda = 1/\sqrt{3}$. Substituting these values into (27) and (25) shows that $m = b = 0$, hence the curve traced by the projectivization of frame vector V (shown at right in magenta) is a Legendrian curve. Along both curves we have drawn some planes of the contact distribution.

recent renewed interest in the YO equations and related systems (see, e.g., [3, 4, 7]), the analogies between the geometric flow considered in this work and the vortex filament flow, and the relatively simple reconstruction of the transverse curve in terms of solutions of the YO Lax pair, makes this a good case for exploring questions such as recursion schemes and the geometric and topological properties of transverse curves related to special solutions of the YO equations.

A natural direction of investigation is the study of the integrable hierarchy of vector fields for transverse curves associated with the YO hierarchy. These are generated by beginning with a conserved density for the YO equations, e.g.,

$$\rho_1 = \tfrac{1}{2}m, \quad \rho_2 = \tfrac{1}{2}|z|^2, \quad \rho_3 = \tfrac{1}{2}\,\mathrm{Im}(\overline{z}z_x) - \tfrac{1}{8}m^2, \quad \rho_4 = -\tfrac{1}{2}\left(m|z|^2 + |z_x|^2\right), \ldots$$

and forming the vector field $X_n = f_n\Gamma + g_nB + h_nV$ where (Γ, B, V) is a natural frame. The coefficients are determined by the corresponding density as follows. As in (10)

write $z = k + \mathrm{i}\ell$ and express the density ρ_n in terms of real invariants k, ℓ, m and their x-derivatives. Let

$$(a_n, b_n, c_n)^T = \mathsf{E}\rho_n$$

where E denotes the vector-valued Euler operator. Then the components of X_n are $h_n = 2c_n$, $g_n = \mathrm{i}(a_n + \mathrm{i}b_n)$ and $f_n = -(c_n)_x + \mathrm{i}d_n$, where $d_n = \int \mathrm{Re}(g_n\overline{z})\,dx$. (Thus, these vector fields satisfy the conditions in (9) to preserve the adapted frame.)

The first few vector fields generated this way are

$$\begin{aligned}
X_1 &= V = \Gamma_x,\\
X_2 &= \mathrm{i}zB = \mathrm{i}(\Gamma_{xx} - m\Gamma),\\
X_3 &= \left(\tfrac{1}{4}m_x + \tfrac{1}{2}\mathrm{i}|z|^2\right)\Gamma + z_x B - \tfrac{1}{2}mV,\\
X_4 &= \left(\tfrac{1}{2}|z|^2_x - \mathrm{i}\,\mathrm{Im}(\overline{z}z_x)\right)\Gamma + \mathrm{i}(z_{xx} - mz)B - |z|^2 V.
\end{aligned}$$

The fact that the antiderivative d_n is always expressible in terms of z, m and their derivatives is somewhat mysterious. However, we observe that these antiderivatives are expressible in terms of Hermitian inner products of the vector fields themselves:

$$d_{2j} = -\tfrac{1}{2}\sum_{k=1}^{2j-2}\langle X_{2j-k}, X_{1+k}\rangle, \qquad d_{2j+1} = -\tfrac{1}{2}\sum_{k=1}^{2j-1}(-1)^k\langle X_{2j+1-k}, X_{1+k}\rangle.$$

Since $d_n = \mathrm{Re}\langle X_n, V\rangle = \frac{1}{2}(\langle X_n, V\rangle + \langle V, X_n\rangle)$ and $V = X_1$, these identities are equivalent to

$$\sum_{k=0}^{2j-1}\langle X_{2j-k}, X_{1+k}\rangle = 0 \qquad \text{and} \qquad \sum_{k=0}^{2j}(-1)^k\langle X_{2j+1-k}, X_{1+k}\rangle = 0.$$

These show a remarkable parallel with the situation for vector fields in the hierarchy for the vortex filament flow [9], where the antiderivative required for the tangential component of X_{n+1} is expressible in terms of inner products of the vector fields up to X_n. In that case, the analogous identities were proved using the first-order 'geometric' recursion operator for the vector fields. In our case, it may be sufficient to have a second-order recursion operator that relates X_{n+2} to X_n.

Bäcklund and Darboux transformations as well as Miura transformations are other common features of integrable systems. In particular, the classical Bäcklund transformation for the sine-Gordon equation has its origins in relating pair of pseudospherical surfaces through line congruences (see, e.g., §7.5 in [8]). It is possible that an analogous transformation exists between T-curves evolving by the YO flow (11); one might expect that the curves would be joined by a congruence of circles in S^3 expressed in terms of the vectors of the natural frame.

In relation to a possible Miura transformation, one can investigate the evolution equations induced by (11) for the *tangent indicatrix*, i.e., the curve in S^3 traced out by the projectivization of the frame vector V. It is natural to ask how the invariants of these indicatrices are related to those of the primary curve, and furthermore whether, when the primary curve evolves by an integrable geometric flow, the invariants of the indicatrix evolve by a related integrable system.

Acknowledgments

We thank Emilio Musso for many fruitful discussions.

References

[1] R. L. Bishop, There is more than one way to frame a curve, American Math. Monthly, 822:46–51, 1975. 82

[2] A. Calini, T. Ivey, Integrable geometric flows for curves in pseudoconformal S^3, Journal of Geometry and Physics, 166, 104249, 2021. 78, 80, 81, 82, 83, 90

[3] M. Caso-Huerta, A. Degasperis, S. Lombardo, M. Sommacal, A new integrable model of long wave–short wave interaction and linear stability spectra, Proc. R. Soc. A. 477 (2021) 20210408. 93

[4] M. Caso-Huerta, A. Degasperis, S. Lombardo, M. Sommacal, Periodic and solitary wave solutions of the long wave– short wave Yajima-Oikawa-Newell model, Fluids 7 (7) (2022) 227. 93

[5] V. Djordjevic, L. Redekopp, On two-dimensional packets of capillary-gravity waves, Journal of Fluid Mechanics, 79(4), 703-714, 1977. 80

[6] R.H.J. Grimshaw, The modulation and stability of an internal gravity wave, Res. Rep. School Math. Sci., Univ. Melbourne, no. 32, 1975. 80

[7] R. Li, X. Geng, Periodic-background solutions for the Yajima–Oikawa long-wave–short-wave equation, Nonlinear Dyn. 109 (2) (2022) 1053–1067. 93

[8] T.A. Ivey, J.M. Landsberg, *Cartan for Beginners: Differential Geometry via Moving Frames and Exterior Differential Systems* (2nd ed.), Graduate Studies in Mathematics **175**, American Mathematical Society, 2016 95

[9] J. Langer, Recursion in Curve Geometry, New York J. Math. 5, 25–51 (1991). 94

[10] J. Langer, R. Perline, Poisson geometry of the filament equation, J Nonlinear Sci 1, 71–93 (1991). 79

[11] O. C. Wright, Homoclinic Connections of Unstable Plane Waves of the Long-Wave–Short-Wave Equations, Studies in Applied Mathematics 117:71–93, 2006. 80, 84, 85, 86

[12] N. Yajima, M. Oikawa, Formation and Interaction of Sonic-Langmuir Solitons, Progress of Theoretical Physics, 56(6), 1719–1739, 1976. 80

AUTHORS

Annalisa Calini
Department of Mathematics,
College of Charleston,
Charleston, SC, USA
email: calinia@cofc.edu

Thomas Ivey
Department of Mathematics,
College of Charleston,
Charleston, SC, USA
email: iveyt@cofc.edu

Arnold Mathematical Journal
Volume 11, Issue 4, 2025

On dual-projectively equivalent connections associated to second order superintegrable systems

Andreas Vollmer

Received 27 Dec 2024; Accepted 28 May 2025

Abstract: Pre-geodesics of an affine connection are the curves that are geodesics after a reparametrization (the analogous concept in Kähler geometry is known as J-planar curves). Similarly, dual-geodesics on a Riemannian manifold are curves along which the 1-forms associated to the velocity are preserved after a reparametrization.

Superintegrable systems are Hamiltonian systems with a large number of independent constants of the motion. They are said to be second order if the constants of the motion can be chosen to be quadratic polynomials in the momenta. Famous examples include the Kepler-Coulomb system and the isotropic harmonic oscillator.

DOI: 10.56994/ARMJ.011.004.004

We show that certain torsion-free affine connections which are naturally associated to certain second order superintegrable systems share the same dual-geodesics.

AMS Classification: 70G45, 53B10, 37J35, 53B12, 70H33

1 Introduction

We consider geometric structures (more precisely, certain affine connections) that naturally appear in the context of certain second order (maximally) superintegrable Hamiltonian systems. Such systems include famous models from mathematical physics, such as the Kepler-Coulomb system, the isotropic harmonic oscillator or the Smorodinski-Winternitz system. We obtain that the aforementioned geometric structures are dual-projectively equivalent, a concept which has been introduced in the context of statistical manifolds, Weylian structures and affine hypersurfaces.

Let (M, g) be a Riemannian (smooth) manifold. Assume that, for $\varepsilon > 0$, $\gamma : (-\varepsilon, \varepsilon) \to M$ is a (smooth) curve on M with tangent (velocity) vector field $\dot{\gamma}$. We denote the 1-form associated to $\dot{\gamma}$ (by virtue of g) by $\dot{\gamma}^\flat$. Here, $\flat : \mathfrak{X}(M) \to \Omega^1(M)$ denotes the usual musical isomorphism induced by g. Similarly, we denote by $\sharp : \Omega^1(M) \to \mathfrak{X}(M)$ the musical isomorphism induced by g^{-1}, when the underlying metric is clear.

Definition 1 ([Iva95]). *A curve γ on M is called* dual-geodesic *for an affine connection ∇ if*

$$\nabla_{\dot{\gamma}} \dot{\gamma}^\flat = q(t)\, \dot{\gamma}^\flat,$$

where $q : (-\varepsilon, \varepsilon) \to \mathbb{R}$. In particular, we say that γ is an affinely parametrized *dual-geodesic for ∇, if*

$$\nabla_{\dot{\gamma}} \dot{\gamma}^\flat = 0.$$

If ∇ is the Levi-Civita connection of the (Riemannian) metric g, then we also say that a curve is dual-geodesic for g, if it is dual-geodesic for ∇.

It is well-known that for every dual-geodesic curve, there exists an affine parametrization, see [Iva95, Prop. 2.1]. In this reference, dual-geodesics are introduced as a tool for the study of semi-conjugate connections and affine hypersurface immersions, and we refer the interested reader there for more detailed information on this perspective. Here, we mention only the following fact, which we need later: *Let $p \in M$ and $w \in T_pM$. Then there exists a (unique up to reparametrization and for sufficiently small $\varepsilon > 0$) dual-geodesic curve $\gamma : (-\varepsilon, \varepsilon) \to M$, $\gamma(0) = p$ with $\dot{\gamma}(0) = w$,* see [Iva95, Prop. 2.2] .

Definition 2 ([Iva95])**.** *Two connections are called dual-projectively equivalent, if they share the same dual-geodesic curves.*

Dual-geodesics and dual-projectively equivalent connections have been discussed, for instance, in [Iva95, Mat10], where they have been related to affine hypersurfaces, statistical manifolds and Weylian structures. The purpose of this paper is to demonstrate that dual-projectively equivalent connections naturally arise in the context of second order superintegrable Hamiltonian systems. Let (M, g) be a simply connected (connected) Riemannian manifold and denote its Levi-Civita connection by ∇. Then T^*M carries a natural symplectic structure ω induced by the tautological 1-form. We consider a natural Hamiltonian $H : T^*M \to \mathbb{R}$,

$$H(x, p) = g_x^{-1}(p, p) + V(x)\,,$$

where (x, p) are canonical Darboux coordinates on T^*M. For a function $f : T^*M \to \mathbb{R}$, we denote by X_f the Hamiltonian vector field with respect to the natural symplectic structure, i.e. $\iota_{X_f}\omega = df$.

Definition 3. *A (maximally)* superintegrable system *is given by a Hamiltonian H together with $2n-2$ functions $F^{(m)} : T^*M \to \mathbb{R}$, such that $(H, F^{(1)}, \dots, F^{(2n-2)})$ are functionally independent, and such that $X_H(F^{(m)}) = 0$ for all $1 \le m \le 2n-2$. We say that a superintegrable system is* second order *if the functions $F^{(m)}$ are quadratic polynomials in the momenta, i.e.*

$$F^{(m)}(x, p) = \sum_{i,j=1}^{n} K^{ij}_{(m)}(x) p_i p_j + W^{(m)}(x).$$

For the integrals of motion in a second order superintegrable system, it is easy to check that (omitting the subscript (m) for brevity) the tensor field $\sum g_{ai}g_{bi}K^{ab}\,dx^i\otimes dx^j$ is Killing, i.e. satisfies $\nabla_X K(X,X)=0$ for all $X\in\mathfrak{X}(M)$. We write $\mathcal{K}$ for the $\mathbb{R}$-linear space of Killing tensors associated to a second order superintegrable system, meaning that there is a function W on M such that $F=K(p^\sharp,p^\sharp)+W$ is an integral of the motion for H, i.e. $X_H(F)=0$.

Definition 4. *We say that a second order superintegrable system is* irreducible*, if the linear space generated by the endomorphisms K, $K^\flat\in\mathcal{K}$, form an irreducible set, i.e. do not share a common eigenspace. For the sake of brevity, an irreducible second order superintegrable system will simply be referred to as an* irreducible system *in the following.*

It was proven in [KSV23] that, for an irreducible system, there exists a tensor field $\hat{T}\in\Gamma(\mathrm{Sym}^2_\circ(T^*M)\otimes TM)$, trace-free in its covariant indices, such that

$$\nabla^2 V=\hat{T}(dV)+\frac{1}{n}\,g\,\Delta V, \tag{1}$$

where $\hat{T}$ depends on $\mathcal{K}$ only, and where Δ denotes the Laplace-Beltrami operator. In general, the tensor $\hat{T}$ is not unique, but here we confine ourselves to systems for which $\hat{T}$ is unique. Specifically, we consider *non-degenerate* second order superintegrable systems. These are irreducible systems with a $(n+2)$-parameter family of potentials (see Section 2 for a precise definition). The main results are Theorems 1 and 2 in Section 3, which show that three affine connections, which are naturally defined for non-degenerate systems, are dual-projectively equivalent:

⟨A⟩ the induced connection $\nabla^g\pm\hat{T}$ (“induced connections”),

⟨B⟩ the corresponding connection that endows the space with the information-geometric structure of a *statistical manifold*,

⟨C⟩ the connections that naturally arise when one restricts to an $(n+1)$-dimensional subspace of potentials (to be explained later).

These connections can also be found in [KSV23, KSV24, CV25, Vol25b, NV24], for example. Before we prove these dual-projective equivalences, we review some facts about

irreducible second order superintegrable Hamiltonian systems.

2 Irreducible second order superintegrable systems

Two specific kinds of irreducible systems are going to play a crucial role in the following, namely non-degenerate and (generalised) semi-degenerate systems. These are introduced in the following two subsections. The terminology goes back to the foundational work by Kalnins and coworkers, cf. [KKMJ18, KKM05a, KKM05b, KKM05c, KKM06a, KKM06b] and the references therein. For semi-degenerate systems, we also mention [ERJ17].

2.1 Non-degenerate systems

Non-degenerate systems are quadruples $(M, g, \mathcal{K}, \mathcal{V})$ such that (M, g) is as before, $\mathcal{K}$ is a linear space of Killing tensors (of dimension $2n-1$ or larger, with $g \in \mathcal{K}$) and $\mathcal{V} \subset \mathcal{C}^\infty(M)$ is a linear subspace (of dimension $n+2$), such that the space of endomorphisms associated to $\mathcal{K}$ is irreducible, and $d(K(dV)) = 0$ for all $V \in \mathcal{V}$ and $K \in \mathrm{End}(TM)$ with $K^\flat \in \mathcal{K}$. Such a system satisfies (1), which then implies the (closed) prolongation system (∇ denotes the Levi-Civita connection of g, and Δ its Laplace-Beltrami operator)

$$\nabla^2 V = \hat{T}(dV) + \frac{1}{n}\Delta V\, g$$
$$\nabla \Delta V = \hat{q}(dV) + (\mathrm{tr}(\hat{T}) - q)\Delta V$$

where $q(X,Y) = g(\hat{q}(X), Y)$ and $\hat{q}(X) = \mathrm{tr}_g(\nabla_{\cdot}\hat{T}(\cdot, X)) + \mathscr{T}(X) - \widehat{\mathrm{Ric}}^g(X)$ with $g(\widehat{\mathrm{Ric}^g}(X), Y) = \mathrm{Ric}^g(X,Y)$. Also, we introduce $\mathscr{T} \in \mathrm{End}(TM)$ via $\mathscr{T}(X) = \mathrm{tr}_g(\Theta(X,\cdot,\cdot))$, where $\Theta : \mathfrak{X}(M)^3 \to \mathfrak{X}(M)$,

$$\Theta(X,Y,Z)(\alpha) = \hat{T}(X,Y)(\hat{T}(Z)(\alpha)),$$

for $X, Y, Z \in \mathfrak{X}(M)$, $\alpha \in \Omega^1(M)$, where $\hat{T}(Z)(\alpha)$ is the 1-form $\hat{T}(\cdot, Z)(\alpha)$. For a non-degenerate system, we define the induced connections by

$$\nabla^{\pm\hat{T}} := \nabla \mp \hat{T}, \tag{2}$$

which is torsion-free and Ricci-symmetric, see [Vol25b]. For simplicity, we abbreviate $\nabla^{\hat{T}} = \nabla^{+\hat{T}}$. Following [KSV23], we furthermore introduce the totally symmetric and tracefree tensor field $S \in \Gamma(\mathrm{Sym}^3_\circ(T^*M))$ and the 1-form $t \in \Omega^1(M)$ by setting $S = \mathring{T}$ and $t = \frac{n}{(n-1)(n+2)}\mathrm{tr}(\hat{T})$, such that

$$T(X,Y,Z) = S(X,Y,Z) + t(X)g(Y,Z) + t(Y)g(X,Z) + t(Z)g(X,Y)\,,$$

where $T := \hat{T}^\flat$ and where $X, Y, Z \in \mathfrak{X}(M)$. Next, for dimension $n \geq 3$, we let

$$\mathcal{Z} = \mathscr{S} - (n-2)(S(t) + t \otimes t) - \mathrm{Ric}^g, \tag{3}$$

where $\mathscr{S}(X,Y) = \mathrm{tr}_g(\,\hat{S}(X,\cdot)(S(\cdot,Y))\,)$. It is shown in [KSV23] that, if $n \geq 3$ and if the underlying manifold is of constant sectional curvature, then

$$\mathring{\mathcal{Z}} = \mathring{\nabla}^2\zeta \tag{4}$$

for a function $\zeta \in \mathcal{C}^\infty(M)$. We can hence introduce the totally symmetric tensor field

$$\mathcal{F} = T + \frac{n+2}{n}\, g \otimes t + \frac{1}{2(n-2)}\,\Pi_{\mathrm{Sym}} g \otimes d\zeta\,.$$

which is then also a Codazzi tensor, c.f. [KSV23]. Note that the definition of $\mathcal{F}$ relies on the assumption of having a space of constant sectional curvature. For later use, we also introduce $\hat{\mathcal{F}} = \mathcal{F}g^{-1}$ and $\nabla^{\pm\hat{\mathcal{F}}} = \nabla \mp \hat{\mathcal{F}}$ (and $\nabla^{\hat{\mathcal{F}}} = \nabla^{+\hat{\mathcal{F}}}$).

Relaxing the curvature assumptions again, we introduce, for a non-degenerate system in dimension $n \geq 2$, the totally symmetric tensor field

$$B = T + \frac{n+2}{n}\, g \otimes t\,,$$

as well as the connections

$$\nabla^{\pm\hat{B}} := \nabla \mp \hat{B} \qquad (\nabla^{\hat{B}} = \nabla^{+\hat{B}}).$$

where $\hat{B} = Bg^{-1}$, c.f. [KSV23]. We remark that for so-called *abundant* systems, the connections $\nabla^{\pm\hat{\mathcal{F}}}$ and $\nabla^{\pm\hat{B}}$, respectively, coincide up to a suitable *gauge choice* of ζ. An abundant system is a non-degenerate system with $\frac{1}{2}n(n+1)$ linearly independent, compatible Killing

tensor fields. Note the non-trivial freedom for choosing the function ζ, satisfying (4). This gauge freedom is thoroughly discussed in [KSV23]. If $n \geq 3$ and g has constant sectional curvature, [KSV23] shows that one can choose $\zeta = 0$ without changing the data of S and t, i.e. without modifying the structure tensor $\hat{T}$.

2.2 Semi-degenerate systems

Generalized semi-degenerate systems, or $(n+1)$-parameter systems, are quadruples $(M, g, \mathcal{K}, \mathcal{V})$ such that (M, g) is as before, $\mathcal{K}$ is a linear space of Killing tensors (of dimension $2n-1$ or larger, with $g \in \mathcal{K}$) and $\mathcal{V} \subset \mathcal{C}^\infty(M)$ is a linear subspace (of dimension $n+1$), such that the space of endomorphisms associated to $\mathcal{K}$ is irreducible, and $d(K(dV)) = 0$ for all $V \in \mathcal{V}$ and $K \in \mathrm{End}(TM)$ with $K^\flat \in \mathcal{K}$. Moreover, we require that in addition to (1), an equation of the form

$$\Delta V = \hat{s}(dV) \tag{5}$$

holds, for some $\hat{s} \in \mathfrak{X}(M)$ that is determined by $\mathcal{K}$, and where Δ is the Laplace-Beltrami operator of the Levi-Civita connection ∇ of g. For the generalized semi-degenerate system subject to (5) we therefore have

$$\nabla^2 V = \hat{D}(dV)\,,$$

where we introduce the tensor field $\hat{D} = \hat{T} + \frac{1}{n}\, g \otimes \hat{s} \in \Gamma(\mathrm{Sym}^2(T^*M) \otimes TM)$. Note that $\hat{T}$ depends on the space $\mathcal{K}$ only. We also introduce $D = \hat{D}^\flat \in \Gamma(\mathrm{Sym}^2(T^*M) \otimes T^*M)$ for later use.

We say that a generalized semi-degenerate system, is *weak*, if there is $\mathcal{V}' \supset \mathcal{V}$ such that $(M, g, \mathcal{K}, \mathcal{V}')$ is non-degenerate. Otherwise, we call it a *strong* semi-degenerate system. For a (weak or strong) semi-degenerate system, we define the induced connection by

$$\nabla^{\pm\hat{D}} := \nabla \mp \hat{D}$$

(again abbreviating $\nabla^{\hat{D}} = \nabla^{+\hat{D}}$). It is shown in [Vol25b] that $\nabla^{\hat{D}}$ is torsion-free, Ricci-symmetric and projectively flat (the reference only discusses the case of strong semi-degeneracy, but it is easy to extend this result to generalized semi-degenerate systems).

We also introduce the tensor field, c.f. [NV24],

$$N(X,Y,Z) := \frac{1}{3}\left(2\,D(X,Y,Z) - D(X,Z,Y) - D(Y,Z,X)\right) \\ + \frac{1}{3(n-1)}\left(2g(X,Y)\mathtt{d}(Z) - g(X,Z)\mathtt{d}(Y) - g(Y,Z)\mathtt{d}(X)\right)$$

where $\mathtt{d} = (n+2)t - s$. It is shown in [NV24] that $N = 0$ characterizes precisely the situation of a generalized semi-degenerate system that is weak (i.e. it is strong if N does not vanish). This means, in the case $N = 0$, that

$$\hat{T} = \hat{D} - \frac{1}{n}\, g \otimes \hat{s}$$

satisfies the conditions of a non-degenerate structure tensor. For later use, and to keep the notation clean, we introduce the 1-form $s \in \Omega^1(M)$, $s = \hat{s}^\flat$.

3 Proof of the main results

In this section, we show the dual-geodesic equivalence of the connections ⟨A⟩–⟨C⟩. All of these connections are torsion-free. Indeed, denoting the Levi-Civita connection of g by ∇, the torsion-freeness of $\nabla \pm \hat{T}$ follows immediately from the symmetries of $\hat{T}$, cf. [Vol25b]. The torsion-freeness of $\nabla \pm \hat{B}$ follows immediately from the total symmetry of $B^\flat$. In the semi-degenerate case, the torsion-freeness of the connections $\nabla \pm \hat{D}$ follows similarly.

Before we proceed to the actual proof, we review some results from the literature that are going to be useful later.

Lemma 1 (Prop. 2.3 of [Iva95])**.** *Let (M,g) be a pseudo-Riemannian manifold. Then two torsion-free affine connections ∇, ∇' are dual-projectively equivalent if and only if there is a 1-form $\alpha \in \Omega^1(M)$ such that*

$$\nabla'_X Y = \nabla_X Y + \alpha^\sharp\, g(X,Y) \tag{6}$$

for any vector fields $X, Y \in \mathfrak{X}(M)$.

Torsion-freeness is a necessary requirement for (6), and in the presence of torsion counterexamples can easily be found.

For later use, we also introduce the concept of *semi-compatibility* for pairs (∇', h) consisting of an affine connection ∇' and a metric h.

Definition 5 ([Iva95])**.** *The pair (∇', h) is said to be* semi-compatible *(via α), if there exists a 1-form α such that*

$$\nabla'_X h(Y,Z) - \nabla'_Y h(X,Z) = \alpha(Y)h(X,Z) - \alpha(X)h(Y,Z)$$

for any $X, Y, Z \in \mathfrak{X}(M)$. The pair (∇', h) is called compatible*, if it is semi-compatible via $\alpha = 0$.*

We begin our investigation with the dual-projective equivalence of the connections ⟨A⟩ and ⟨B⟩. To this end, consider a non-degenerate system on (M, g) with structure tensor $\hat{T}$ as before. Observe that the induced connection $\nabla^{\hat{T}}$ and the structural connection $\nabla^{\hat{B}}$ are dual-projectively equivalent.

Theorem 1. *(i) The connections $\nabla^{\hat{T}}$ and $\nabla^{\hat{B}}$ share the same dual-geodesics.*

(ii) For a non-degenerate system with induced connection $\nabla^{\hat{T}}$, there is a unique dual-projectively equivalent connection $\nabla^\star$ such that $(\nabla^\star, g)$ is compatible. In fact, $\nabla^\star = \nabla^{\hat{B}}$.

The analogous statements hold, if we replace $\nabla^{\hat{T}}$ and $\nabla^{\hat{B}}$ by $\nabla^{-\hat{T}}$ and $\nabla^{-\hat{B}}$, respectively. We comment that the following proof also shows that $T = 0$, if $\nabla^{\hat{T}} = \nabla^\star$. This latter condition holds for the so-called non-degenerate harmonic oscillator system [KSV23].

Proof. We denote the Levi-Civita connection of g by ∇^g. We have $\nabla^{\hat{T}} - \nabla^{\hat{B}} = \nabla^g - \hat{T} - \nabla^g + \hat{B} = \hat{B} - \hat{T}$. Using the musical isomorphisms, we then compute

$$(B - T)(X, Y, Z) = \frac{n+2}{n}\, t(Z) g(X, Y)$$

and conclude $\nabla^{\hat{T}} - \nabla^{\hat{B}} = \frac{n+2}{n}\, g \otimes t^\sharp$. This proves the first claim. We next consider the connections that are dual-projectively equivalent to $\nabla^{\hat{T}}$. They are of the form, $\beta \in \Omega^1(M)$,

$$\nabla^\star_X Y = \nabla^{\hat{T}}_X Y + \beta^\sharp\, g(X, Y).$$

A short computation shows that

$$\nabla^{\star}_X g(Y,Z) - \nabla'_Y g(X,Z) = \alpha(Y) g(X,Z) - \alpha(X) g(Y,Z)$$

with the 1-form $\alpha = \frac{n+2}{n} t - \beta$. The connection $\nabla^{\star}$ therefore is compatible with g if and only if $\beta = \frac{n+2}{n} t$. We conclude

$$\nabla^{\star}_X Y = \nabla^{\hat{T}}_X Y + \frac{n+2}{n} t^{\sharp} g(X,Y) = \nabla^{\hat{B}}_X Y.$$

□

Remark 1. *We remark that an analogous computation shows* $\nabla^{\hat{F}}_X g(Y,Z) - \nabla^{\hat{F}}_Y g(X,Z) = 0$, *alongside* $\nabla^{\hat{B}}_X g(Y,Z) - \nabla^{\hat{B}}_Y g(X,Z) = 0$. *However, the connections* $\nabla^{\hat{F}}$ *and* $\nabla^{\hat{B}}$ *are, in general, different, as*

$$g(\nabla^{\hat{F}} - \nabla^{\hat{B}}) = \frac{1}{2(n-2)} \Pi_{\mathrm{Sym}} g \otimes d\zeta .$$

We infer that the connections ∇^{F} *and* $\nabla^{\hat{B}}$ *coincide precisely if* $d\zeta = 0$. *Note that the vanishing of* $d\zeta$ *implies* $\mathring{\mathcal{Z}} = 0$.

We now turn our attention to the dual-projective equivalence of the connections ⟨A⟩ and ⟨C⟩, i.e. we now consider systems with (n+1)-parameter potential. Again, we focus on $\nabla^{\hat{D}} = \nabla^{+\hat{D}}$ for conciseness, as the discussion for $\nabla^{-\hat{D}}$ is analogous. We introduce the connection

$$\nabla^{\dagger} = \nabla^{\hat{D}} - \frac{1}{n} s^{\sharp} g$$

which is clearly dual-projectively equivalent to $\nabla^{\hat{D}}$. We characterize weak semi-degeneracy via $\nabla^{\hat{D}}$.

Theorem 2. *(i) Consider a weak semi-degenerate system with induced connection* $\nabla^{\hat{D}}$. *Assume that the induced connection of the naturally associated non-degenerate system is* $\nabla^{\hat{T}}$. *Then* $\nabla^{\hat{D}}$ *and* $\nabla^{\hat{T}}$ *share the same dual-geodesics.*

(ii) Consider a (generalized) semi-degenerate system with induced connection $\nabla^{\hat{D}}$ *and semi-degeneracy* 1*-form* s. *Then* $(\nabla^{\hat{D}}, g)$ *are semi-compatible via*

$$\beta = \frac{1}{n} \left(s - (n+2)\, t \right) ,$$

if and only if the system is a weak semi-degenerate system.

The analogous statements hold, if we replace $\nabla^{\hat{T}}$ and $\nabla^{\hat{D}}$ by $\nabla^{-\hat{T}}$ and $\nabla^{-\hat{D}}$, respectively.

Proof. We have $\nabla^{\hat{T}} = \nabla^{\dagger}$, and hence $\nabla^{\hat{T}}$ and $\nabla^{\hat{D}}$ are dual-projectively equivalent, completing the first part of the theorem. For the second part, we first compute

$$\begin{aligned}\nabla^{\hat{D}}_X g(Y,Z) - \nabla^{\hat{D}}_Y g(X,Z) &= N(Y,Z,X) - N(X,Z,Y) \\ &\quad + \frac{1}{n}\left(s(X) - (n+2)\,t(X)\right) g(Y,Z) \\ &\quad - \frac{1}{n}\left(s(Y) - (n+2)\,t(Y)\right) g(X,Z) \\ &\overset{!}{=} \beta(X) g(Y,Z) - \beta(Y) g(X,Z) \end{aligned} \tag{7}$$

where the exclamation point indicates the requirement that $(\nabla^{\hat{D}}, g)$ be semi-compatible via s.

Part "⇒": Inserting the formula for β into (7), we obtain the condition

$$N(Y,Z,X) = N(X,Z,Y).$$

It follows that $N = 0$ and, invoking [NV24], we thus obtain the claim.

Part "⇐": If the system is weakly semi-degenerate, then $N = 0$, due to [NV24]. We immediately find that the condition at the exclamation point holds, if β is as claimed. □

4 Conclusion

We have seen here that certain affine connections that naturally appear in the theory of irreducible superintegrable systems are dual-projectively equivalent. In particular, the theorems stated in this paper imply that extendability (weak semi-degeneracy) for a $(n+1)$-parameter system is linked to the semi-compatibility (with the metric g) of its induced connection $\nabla^{\hat{D}}$. Weak semi-degeneracy in turn implies that there is a naturally associated non-degenerate system whose induced connection $\nabla^{\hat{T}}$ is dual-projectively equivalent to $\nabla^{\hat{D}}$. In this case there is also a connection $\nabla^{\hat{B}}$ that is compatible with g and dual-projectively equivalent to $\nabla^{\hat{D}}$. The observed occurrence of dual-projective geometry

is natural and linked to the underlying Weylian structure. The underlying Weylian structure was discussed in [Vol25a]. Note that, by a direct computation,

$$\nabla^{\hat{T}}_X g(Y,Z) - \frac{n+2}{n}\, t(X) g(Y,Z) \in \Gamma(\mathrm{Sym}^3(T^*M))$$

is totally symmetric. According to [Mat10], it was shown in [Mat07] that this implies the existence of a Weylian connection.

Acknowledgments

This research was funded by the German Research Foundation (Deutsche Forschungsgemeinschaft) through the research grant #540196982.

References

[CV25] Vicente Cortés and Andreas Vollmer. Affine hypersurfaces and superintegrable systems, 2025. arXiv:2504.05200. 101

[ERJ17] M. A. Escobar-Ruiz and W. Miller Jr. Toward a classification of semidegenerate 3d superintegrable systems. *Journal of Physics A: Mathematical and Theoretical*, 50(9), 2017. 102

[Iva95] Stefan Ivanov. On dual-projectively flat affine connections. *Journal of Geometry*, 53, 1995. 99, 100, 105, 106

[KKM05a] E. G. Kalnins, J. M. Kress, and W. Miller, Jr. Second-order superintegrable systems in conformally flat spaces. I. Two-dimensional classical structure theory. *J. Math. Phys.*, 46(5):053509, 28, 2005. 102

[KKM05b] E. G. Kalnins, J. M. Kress, and W. Miller, Jr. Second order superintegrable systems in conformally flat spaces. II. The classical two-dimensional Stäckel transform. *J. Math. Phys.*, 46(5):053510, 15, 2005. 102

[KKM05c] E. G. Kalnins, J. M. Kress, and W. Miller, Jr. Second order superintegrable systems in conformally flat spaces. III. Three-dimensional classical structure theory. *J. Math. Phys.*, 46(10):103507, 28, 2005. 102

[KKM06a] E. G. Kalnins, J. M. Kress, and W. Miller, Jr. Second order superintegrable systems in conformally flat spaces. IV. The classical 3D Stäckel transform and 3D classification theory. *J. Math. Phys.*, 47(4):043514, 26, 2006. 102

[KKM06b] E. G. Kalnins, J. M. Kress, and W. Miller, Jr. Second-order superintegrable systems in conformally flat spaces. V. Two- and three-dimensional quantum systems. *J. Math. Phys.*, 47(9):093501, 25, 2006. 102

[KKMJ18] E. G. Kalnins, J. M. Kress, and W. Miller Jr. *Separation of Variables and Superintegrability*. 2053-2563. IOP Publishing, 2018. 102

[KSV23] J. Kress, K. Schöbel, and A. Vollmer. An Algebraic Geometric Foundation for a Classification of Second-Order Superintegrable Systems in Arbitrary Dimension. *J. Geom. Anal.*, 33(360), 2023. 101, 103, 104, 106

[KSV24] Jonathan Kress, Konrad Schöbel, and Andreas Vollmer. Algebraic conditions for conformal superintegrability in arbitrary dimension. *Comm. Math. Phys.*, 405(92), 2024. 101

[Mat07] Hiroshi Matsuzoe. Geometry of statistical manifolds and its generalization. In *Topics in Contemporary Differential Geometry, Complex Analysis and Mathematical Physics. Proceedings of the 8th International Workshop on Complex Structures and Vector Fields*, pages 244–251. World Scientific, 2007. 109

[Mat10] Hiroshi Matsuzoe. Statistical manifolds and affine differential geometry. *Advanced Studies in Pure Mathematics*, 57:303–321, 2010. 100, 109

[NV24] Jeremy Nugent and Andreas Vollmer. A necessary and sufficient condition for a second-order superintegrable system with (n+1)-parameter potential

to extend to a non-degenerate second-order superintegrable system, 2024. arxiv:2411.06994. 101, 105, 108

[Vol25a] Andreas Vollmer. Second-order superintegrable systems and Weylian geometry. *Nuclear Physics B*, 1019:117095, 2025. 109

[Vol25b] Andreas Vollmer. Torsion-free connections of second-order maximally superintegrable systems. *Bulletin London Mathm. Soc.*, 57, 2025. 101, 103, 104, 105

AUTHOR

Andreas Vollmer
University of Hamburg,
Department of Mathematics,
Bundesstraße 55,
20146 Hamburg, Germany
email: andreas.vollmer@uni-hamburg.de

Arnold Mathematical Journal
Volume 11, Issue 4, 2025

Folding of quadrilaterals, zigzags, and Arnold-Liouville integrability

Anton Izosimov

Received 04 Apr 2025; Accepted 09 Jul 2025

Abstract: We put Darboux's porism on folding of quadrilaterals, as well as closely related Bottema's zigzag porism, in the context of Arnold-Liouville integrability.

AMS Classification: 37J70

Key words and phrases: folding, Darboux's porism, zigzag porism

1 Introduction

One of the historically first manifestations of integrability is *Poncelet's porism*, also known as *Poncelet's closure theorem*. Poncelet's theorem says that if a planar n-gon is inscribed in a conic C_1 and circumscribed about another conic C_2, then any point of C_1 is a vertex of such an n-gon, see Figure 1. The two arguably most standard proofs of this theorem are based, respectively, on complex and symplectic geometry. The complex proof goes

DOI: 10.56994/ARMJ.011.004.005

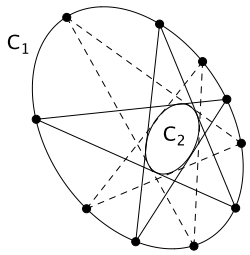

Figure 1: Every point of C_1 is a vertex of a pentagon inscribed in C_1 and circumscribed about C_2.

roughly as follows. One can identify the space of tangents dropped from a point on C_1 to C_2 with an elliptic curve. The successive sides of a polygon inscribed in C_1 and circumscribed about C_2 are points on that curve related to each by a fixed translation. This polygon closes up if and only if the translation vector is a torsion point on the elliptic curve. Whether or not that is the case depends only on C_1 and C_2, but not on the initial point, so all polygons inscribed in C_1 and circumscribed about C_2 will close up after the same number of steps [GH77].

The second, symplectic, proof is based on the fact that any two generic conics can be mapped, by a projective transformation, to confocal conics. In the confocal case, a polygon inscribed in C_1 and circumscribed about C_2 can be identified with a billiard trajectory in C_1. The billiard in a conic is an integrable system, and any two polygons inscribed in C_1 and circumscribed about C_2 correspond to trajectories belonging to the same level set of the first integral. Hence, by Arnold-Liouville theorem, if one of the trajectories is periodic with period n, then so is the other one, cf. [LT07].

A lesser known relative of Poncelet's porism is *Darboux's porism on folding of quadrilaterals*. *Folding* of a vertex of a planar polygon is the reflection of that vertex is the diagonal joining its neighbors, see Figure 2. Darboux's porism says that if a sequence of alternating foldings of adjacent vertices restores, after $2n$ steps, the initial polygon, then this is the case for any polygon with the same side lengths. For example, folding any polygon with side lengths $1, 3, 3\sqrt{5}, 5$ six times, we come back to the initial polygon, see

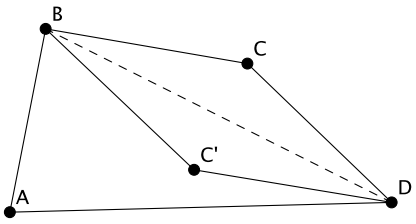

Figure 2: Folding of the vertex C of a quadrilateral $ABCD$. Its new position is C'.

[Izm23, Figure 2].

Just like Poncelet's porism, Darboux's theorem can be proved using elliptic curves. Specifically, one shows that the complexified moduli space of quadrilaterals with fixed side length is an elliptic curve. Composition of foldings at adjacent vertices amounts to a translation on that curve. Whether or not a sequence of foldings restores the initial polygon depends on whether the translation vector is a torsion point and is independent on the particular choice of a quadrilateral [Izm23].

What currently seems to be missing in the literature is a symplectic proof of Darboux's theorem. We provide such a proof in the present paper. Specifically, we show that, in an appropriate sense, Darboux's folding is Arnold-Liouville integrable, and deduce Darboux's porism.

Furthermore, we extend these results to Bottema's *zigzag porism* [Bot65], which can be stated as follows. Let C_a and C_b be two circles such that there exists a unit equilateral $2n$-gon whose odd-indexed vertices lie on C_a and even-indexed vertices lie on C_b. Then there exist infinitely many such $2n$-gons. The zigzag porism is equivalent to Darboux's porism when the circles are coplanar [CH00], but is in fact valid for any two circles in $\mathbb{R}^3$ [BHH74]. We construct the underlying Arnold-Liouville integrable system in this more general setting.

2 Arnold-Liouville integrability of folding

Let $\mathcal{P}$ be the space of quadrilaterals $ABCD$ with fixed side lengths, considered up to orientation-preserving isometries. There is abundant literature on the topology of such spaces for polygons with any number of vertices, see [KM95] and references therein. The space $\mathcal{P}$ is a smooth manifold assuming that there is no linear combination of side lengths with coefficients ± 1 which is equal to zero [KM95, Lemma 2]. In the case of quadrilaterals, this manifold is diffeomorphic to a circle or disjoint union of two circles, see [KM95, Theorem 1]. These circles are distinguished by the sign of the oriented area and are interchanged by an orientation-reversing isometry, cf. [KM95, Section 10].

Denote by $F_B : \mathcal{P} \to \mathcal{P}$ folding of the vertex B. This mapping is well-defined assuming that the vertices A and C cannot come together. This holds provided that the side lengths satisfy at least one of the following conditions: $|AB| \neq |BC|$ or $|AD| \neq |CD|$. Likewise, let $F_C : \mathcal{P} \to \mathcal{P}$ be folding of C, and let $F := F_C \circ F_B$ be the composition of the two foldings. Darboux's porism says that if $F^n(P) = P$ for some quadrilateral $P \in \mathcal{P}$, then F^n is the identity mapping on $\mathcal{P}$. We shall prove this by establishing Arnold-Liouville integrability of the mapping F.

Clearly, F cannot be Arnold-Liouville integrable on the space $\mathcal{P}$ of quadrilaterals with fixed side lengths, as the latter space is one-dimensional. So, we consider a bigger space $\mathcal{P}'$ of quadrilaterals with fixed lengths of the sides AB, BC, CD, again considered up to orientation-preserving isometries. This space is diffeomorphic to a two-dimensional torus and is parametrized by the oriented angles $\angle ABC$ and $\angle BCD$. The squared length of the side AD is a smooth function of the torus $\mathcal{P}'$. The space $\mathcal{P}$ of quadrilaterals with fixed lengths of all sides is a level set of that function.

Theorem 2.1. *The folding mapping $F = F_C \circ F_B$ is Arnold-Liouville integrable on the moduli space $\mathcal{P}'$ of quadrilaterals $ABCD$ with fixed lengths of the sides AB, BC, CD.*

Proof. Folding does not affect side lengths. In particular, $|AD|^2$ is a first integral of F.

Furthermore, the map $F : \mathcal{P}' \to \mathcal{P}'$ has an invariant symplectic structure given by

$$\Omega := d\angle ABC \wedge d\angle BCD.$$

To show invariance, consider, for instance, folding of the vertex C depicted in Figure 2. The pullback of the symplectic form Ω by this map is

$$F_C^*\Omega = d\angle ABC' \wedge d\angle BC'D = d(\angle ABC - 2\angle CBD) \wedge d(2\pi - \angle BCD) = -\Omega - 2d\angle CBD \wedge d\angle BCD.$$

Furthermore, since the side lengths $|BC|$ and $|CD|$ are fixed, the angle $\angle CBD$ is a function of the angle $\angle BCD$ and is independent of the angle $\angle ABC$. So, $d\angle CBD \wedge d\angle BCD = 0$, implying

$$F_C^*\Omega = -\Omega,$$

i.e., the form Ω is *anti-invariant* under a single folding, and hence invariant under F. □

3 Darboux's porism

Theorem 3.1 (Darboux's porism)**.** *Assume we are given a quadrilateral which restores its initial shape after $2n$ alternating foldings at adjacent vertices. Suppose its side lengths are such that no linear combination of them with coefficients ± 1 is equal to zero. Then any quadrilateral with the same side lengths restores its initial shape after $2n$ alternating foldings at adjacent vertices.*

Remark 3.2. The condition on linear combinations of side lengths cannot be avoided. Consider, for instance a quadrilateral with all four vertices along a line, shown in Figure 3. Here we have $|AB| = 2$, $|BC| = 1$, $|CD| = 2$, $|AD| = 3$. Clearly, this quadrilateral is invariant under any folding. However, that is not so for a generic quadrilateral with side lengths $2, 1, 2, 3$.

Proof of Theorem 3.1. The assumption on linear combinations of side lengths ensures that the moduli space $\mathcal{P}$ of quadrilaterals with such side lengths is a regular level set of the function $|AD|^2$ on the moduli space $\mathcal{P}'$ of polygons with fixed lengths of AB, BC, CD.

Figure 3: A degenerate polygon.

We are given that there is a quadrilateral $P \in \mathcal{P}$ on that level set such that $F^n(P) = P$. So, by Arnold-Liouville integrability of F, we have that F^n is the identity on the connected component of $\mathcal{P}$ containing P. Moreover, since there are at most two components, and they are interchanged by an orientation-reversing isometry which commutes with foldings, we must have that F^n is the identity of the whole of $\mathcal{P}$, as desired. □

4 A remark on polygons with more vertices

The F-invariant symplectic form on the moduli space $\mathcal{P}'$ of quadrilaterals with fixed lengths of the sides AB, BC, CD induces an F-invariant non-vanishing 1-form on any non-singular level set of the first integral $|AD|^2$, i.e., on the moduli space $\mathcal{P}$ of quadrilaterals with fixed side lengths. The existence of this 1-form is at heart of Arnold-Liouville theorem. It can be shown that, up to a constant factor, this form is given by

$$\frac{d\angle ABC}{\text{area of } \triangle ACD}.$$

This expression is invariant under cyclic permutation of vertices, up to sign. Likewise, the expression

$$\frac{d\phi_{i+2} \wedge \cdots \wedge d\phi_{i-2}}{\text{area of the triangle formed by vertices } i-1, i, i+1},$$

where ϕ_i is the angle subdued at ith vertex (the indices are understood cyclically, modulo n), gives a volume form on the moduli space of n-gons with fixed side lengths which is anti-invariant under each folding and hence invariant under an even number of foldings. However, for $n > 4$, this does not imply any kind of integrable behavior. Moreover, already for pentagons a random sequence of foldings has dense orbits on the moduli space $\mathcal{P}$ [CD23].

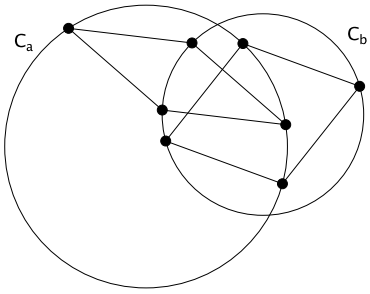

Figure 4: The zigzag porism: all zigzags with the same edge length close after the same number of steps.

5 The zigzag porism

Let C_a and C_b be two circles in $\mathbb{R}^3$. A *zigzag* between C_a and C_b is an equilateral polygon whose odd-indexed vertices lie on C_a and even-indexed vertices lie on C_b. The zigzag porism says that if there exists a closed $2n$-gonal zigzag between C_a and C_b, then any zigzag between C_a and C_b with the same edge length is also a closed $2n$-gon [Bot65, BHH74], see Figure 4.

A zigzag between two circles C_a, C_b may be built by iterating the *zigzag map* $Z : C_a \times C_b \to C_a \times C_b$ which sends a pair $A \in C_a$, $B \in C_b$ to a pair $A' \in C_a$, $B' \in C_b$ such that $|A'B'| = |A'B| = |AB|$, see Figure 5. This map is a composition of two involutions, namely $(A, B) \longmapsto (A', B)$, where $|A'B| = |AB|$, and $(A', B) \longmapsto (A', B')$, where $|A'B'| = |A'B|$. Observe

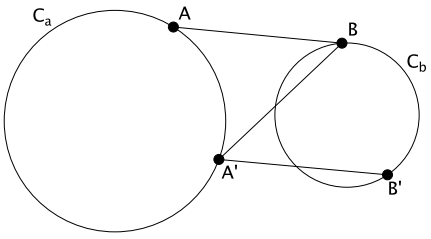

Figure 5: The zigzag map $Z : (A, B) \longmapsto (A', B')$.

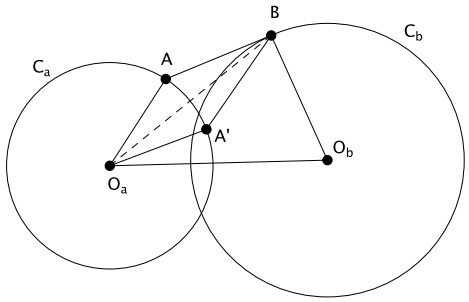

Figure 6: Two successive legs AB, BA' of a zigzag are related by folding.

that, in the case when the circles C_a, C_b are coplanar, these involutions are just foldings of the quadrilateral O_aABO_b, where O_a, O_b are centers of C_a, C_b, at A and B respectively, see Figure 6. So, the planar case of the zigzag porism is equivalent to Darboux's porism [CH00]. Here we show that the integrability result carries over to the spatial situation:

Theorem 5.1. *The zigzag map Z is Arnold-Liouville integrable for any circles C_a, C_b in $\mathbb{R}^3$.*

Proof. By definition, the map $Z : (A, B) \longmapsto (A', B')$ preserves the squared distance between A and B. So, it suffices to find an area form on $C_a \times C_b$ invariant under Z. Let $\phi_a, \phi_b \in \mathbb{R}/2\pi\mathbb{Z}$ be standard angular parameters on C_a, C_b. We will prove that the form $d\phi_a \wedge d\phi_b$ on $C_a \times C_b$ is preserved by Z. To that end, it suffices to establish anti-invariance of that form with respect to the involutions whose composition gives Z. Furthermore, since those involutions are related to each other by interchanging the roles of the circles

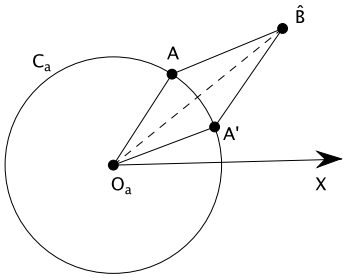

Figure 7: The involution $(A, B) \longmapsto (A', B)$ takes the form $d\phi_a \wedge d\phi_b$ to $-d\phi_a \wedge d\phi_b$.

C_a, C_b, it is sufficient to consider the involution $(A, B) \longmapsto (A', B)$ defined by the condition $|A'B| = |AB|$, where $A, A' \in C_a$. Let $\hat{B}$ be the orthogonal projection of B onto the plane containing C_a. Then $|A\hat{B}| = |A'\hat{B}|$, see Figure 7. Here O_aX is the reference direction used to define the angular coordinated ϕ_a on C_a. We have

$$\angle XO_aA + \angle XO_aA' = 2\angle XO_a\hat{B}.$$

So, the sum on the left only depends on the position of the point B but not A. Therefore, in coordinates ϕ_a, ϕ_b, the involution $(A, B) \longmapsto (A', B)$ has the form

$$(\phi_a, \phi_b) \longmapsto (f(\phi_B) - \phi_a, \phi_b)$$

for a certain smooth function f. So, the form $d\phi_a \wedge d\phi_b$ is indeed anti-invariant under this involution. □

In terms of the map Z, the zigzag porism says that if an orbit of $(A, B) \in C_a \times C_b$ under Z is n-periodic, then the same holds for any $(A', B') \in C_a \times C_b$ with $|A'B'| = |AB|$. This is derived from Theorem 5.1 in the same way as Darboux's porism is obtained from Theorem 2.1.

Acknowledgments

The author learned about the zigzag porism from the referee of the first version of this paper. The author is grateful to Max Planck Institute for Mathematics in Bonn for its hospitality and financial support. This work was partially supported by the Simons Foundation through the Travel Support for Mathematicians program. Figures were created with help of software package Cinderella.

References

[BHH74] W.L. Black, H.C. Howland, and B. Howland. A theorem about zig-zags between two circles. *The American Mathematical Monthly*, 81(7):754–757, 1974. 114, 118

[Bot65] O. Bottema. Ein schliessungssatz für zwei kreise. *Elemente der Mathematik*, 20:1–7, 1965. 114, 118

[CD23] S. Cantat and R. Dujardin. Random dynamics on real and complex projective surfaces. *Journal für die reine und angewandte Mathematik (Crelles Journal)*, 2023(802):1–76, 2023. 117

[CH00] B. Csikós and A. Hraskó. Remarks on the zig-zag theorem. *Periodica Mathematica Hungarica*, 39(1):201–211, 2000. 114, 119

[GH77] P. Griffiths and J. Harris. A Poncelet theorem in space. *Commentarii Mathematici Helvetici*, 52(2):145–160, 1977. 113

[Izm23] I. Izmestiev. Deformation of quadrilaterals and addition on elliptic curves. *Moscow Mathematical Journal*, 23:205–242, 2023. 114

[KM95] M. Kapovich and J. Millson. On the moduli space of polygons in the Euclidean plane. *Journal of Differential Geometry*, 42(2):430–464, 1995. 115

[LT07] M. Levi and S. Tabachnikov. The Poncelet grid and billiards in ellipses. *The American Mathematical Monthly*, 114(10):895–908, 2007. 113

AUTHOR

Anton Izosimov
Department of Mathematics,
University of Arizona
and
School of Mathematics & Statistics,
University of Glasgow;
email: Anton.Izosimov@glasgow.ac.uk

Arnold Mathematical Journal
Volume 11, Issue 4, 2025

Spirals, tic-tac-toe partition, and deep diagonal maps

Zhengyu Zou

Received 25 Dec 2024; Accepted 9 Aug 2025

Abstract: The deep diagonal map T_k acts on planar polygons by connecting the k-th diagonals and intersecting them successively. The map T_2 is the pentagram map, and T_k is a generalization. We study the action of T_k on two subsets of the so-called twisted polygons, which we term *type-α and type-β k-spirals*. For $k \geq 2$, T_k preserves both types of k-spirals. In particular, we show that for $k = 2$ and $k = 3$, both types of k-spirals have precompact forward and backward T_k-orbits modulo projective transformations. We derive a rational formula for T_3, which generalizes the y-variables transformation formula of the corresponding quiver mutation by M. Glick and P. Pylyavskyy. We also present four algebraic invariants of T_3. These special orbits in the moduli space are partitioned into cells of a 3×3 tic-tac-toe grid. This establishes the action of T_k on k-spirals as a geometric generalization of T_2 on convex polygons.

DOI: 10.56994/ARMJ.011.004.006

AMS Classification: 05E99, 37J70, 51A05

Key words and phrases: pentagram map, twisted polygons, cluster algebra, polygonal dynamics, projective geometry, integrable systems, Casimir functions, discrete dynamical systems

1 Introduction

1.1 Context and Motivation

Given a polygon P in the real projective plane, let T_k be the map that connects its k-th diagonals and intersects them successively to form another polygon P' whose vertices are given by the following formula:

$$P'_i = P_iP_{i+k} \cap P_{i+1}P_{i+k+1}. \tag{1}$$

Figure 1 demonstrates an example of the action of T_2 on a convex heptagon. The map T_2 is called the *pentagram map*, a well-studied discrete dynamical system (see [Sch92, Sch01, Sch08, OST10]). A well-known result is that T_2 preserves convexity.[1] The T_2-orbit of a convex polygon sits on a flat torus in the moduli space of projective equivalent convex polygons. On the other hand, the geometry of the map T_k is less well-behaved. For $k \geq 3$, the T_k images of convex polygons may not even be embedded. See Figure 1 for an example of T_3 taking a convex heptagon to a polygon that is not even embedded.

Previous results of T_k often had an algebraic and combinatorial flavor, motivated by two branches of studies. The first one was a sequence of works [Sch08, OST10, Sol13, OST13] that established that the T_2 action on the moduli space of projective convex polygons is a discrete completely integrable system; the second one was M. Glick's discovery in [Gli11] of the connection between T_2 and cluster algebras. In [GSTV12], M. Gekhtman, M. Shapiro, S. Tabachnikov, and A. Vainshtein generalized the cluster transformations in [Gli11] to the map T_k acting on so-called "corrugated polygons," which

[1] A projective polygon is *convex* if some projective transformation maps it to a planar convex polygon in the affine patch

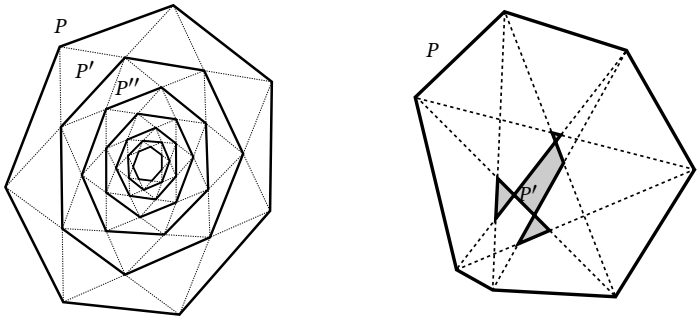

Figure 1: Left: The iterative images of a convex heptagon under the action of T_2. Right: A convex heptagon whose image under T_3 is not even embedded.

are polygonal curves in $\mathbb{RP}^k$ satisfying certain coplanarity conditions. [GSTV12] showed that T_k is a discrete integrable system. There are numerous integrability results for these higher-dimensional analogs. See [KS13, MB13, MB14, KS16, IK23]. These led to many applications and connections of T_k to other fields, such as octahedral recurrence [Sch08, FK12], the condensation method of computing determinants [Sch08, Gli18], cluster algebras [Gli11, GSTV12, GP16, FK12], Poisson Lie groups [FM16, Izo22b], T-systems [KV15, FK12], Grassmannians [FMB19], algebraically closed fields [Wei23], Poncelet polygons [Sch07, Sch21, Izo22a, Sch24], and integrable partial differential equations [Sch08, OST10, NS21].

The geometric aspects of T_k and other deep diagonal maps on planar polygons remain underexplored. There are only a few studies on the geometries of T_k that focused on small k or polygons with many symmetries. See [Sch21, Sch24]. There is no established general framework on the type of geometric properties preserved under T_k for $k \geq 3$ that is analogous to convexity under T_2. Even less is known for geometric objects that have precompact orbits under T_k.

The most relevant result to this endeavor is the discovery of *k-birds* under the map Δ_k in [Sch25]. A k-bird P is a planar n-gon with $n > 3k$, such that there exists a continuous

path of polygons $P^{(t)}$ connecting P to the regular n-gon where the four lines

$$P_i^{(t)}P_{i-k-1}^{(t)}, \quad P_i^{(t)}P_{i-k}^{(t)}, \quad P_i^{(t)}P_{i+k}^{(t)}, \quad P_i^{(t)}P_{i+k+1}^{(t)}$$

are distinct for all $i = 1, \dots, n$ and $t \in I$. The map Δ_k connects the $(k+1)$-th diagonal of a polygon and intersects the diagonals that are k clicks apart. See Figure 2 for the action of Δ_2 on 2-birds. In [Sch25], R. Schwartz showed that the k-birds are invariant under both Δ_k and Δ_k^{-1}. Experimentally, the k-birds seem to have toroidal orbits under Δ_k, which highly resembles the orbit of convex n-gons under T_2. Schwartz also showed that the k-birds have precompact forward Δ_k-orbits modulo affine transformations—a property satisfied by convex n-gons under T_2.

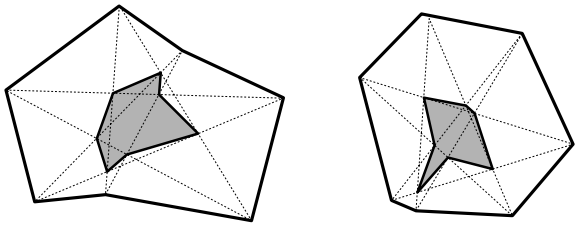

Figure 2: Action of Δ_2 on two heptagons that are 2-birds.

This paper has two main results. The first one is the discovery of two classes of geometric objects called type-α and type-β k-spirals that are preserved under T_k for all $k \geq 2$. These two classes of objects are subsets of *twisted polygons*: bi-infinite sequences $P : \mathbb{Z} \to \mathbb{RP}^2$ such that no three consecutive points are collinear, and $P_{i+n} = \phi(P_i)$ for some fixed projective transformation ϕ called the *monodromy*. The moduli space of projective equivalent twisted n-gons is conventionally denoted by $\mathcal{P}_n$. The type-α and type-β k-spirals are the first discovered classes of geometric constructions of T_k that generalize the pentagram map, which provides crucial evidence for a more general understanding of geometrically preserved classes under T_k.

The second result is the precompactness of both forward and backward T_k-orbits of type-α and type-β k-spirals modulo projective transformations for $k = 2$ and 3, a key property satisfied by convex polygons under the pentagram map discovered by Schwartz

in [Sch92]. We first examine the action of T_3 on type-α and type-β 3-spirals. We show that one can characterize type-α and type-β 3-spirals via linear constraints on the corner invariants. We also derive a birational formula of T_3 for the corner invariants, which is a generalization of the combinatorial formulas developed by [GP16]. Then, we present four global invariants under T_3, which we use to prove the precompactness of T_3-orbits modulo projective transformations. For the case $k = 2$, we show that there exists no type-α 2-spirals and that the type-β 2-spirals are distinct from closed convex polygons. We use the Casimir functions of the T_2-invariant Poisson structure developed in [Sch08] and [OST10] to show that type-β 2-spirals have precompact T_2-orbits modulo projective transformations.

1.2 The k-Spirals under the Map T_k

Here we describe the geometric picture of a k-spiral. For the formal definition, see §3.1. Geometrically, $[P] \in \mathcal{P}_n$ is a *k-spiral* if for all $N \in \mathbb{Z}$, we can find a representative P such that $\{P_i\}_{i \geq N}$ lies on the affine patch, and the triangles (P_i, P_{i+1}, P_{i+2}) and (P_i, P_{i+1}, P_{i+k}) have positive orientation for all $i \geq N$. We call P an *N-representative* of $[P]$.

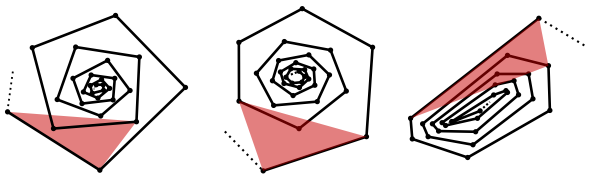

Figure 3: A gallery of 5-spirals. Left: $\mathcal{S}^{\alpha}_{5,3}$. Middle: $\mathcal{S}^{\beta}_{5,3}$. Right: $\mathcal{S}^{\beta}_{5,20}$. The red-shaded triangles indicate the defining orientations and containment relations of type-α and type-β k-spirals..

We are mainly interested in two types of k-spirals, which we term *type-α* and *type-β* (although there certainly exist many more types of spirals, we only consider these two types here). They are k-spirals with additional constraints on the arrangement of the four points $P_i, P_{i+1}, P_{i+k}, P_{i+k+1}$. For type-$\alpha$ spirals, we require P_{i+k} to be contained in the

interior of the triangle $(P_i, P_{i+1}, P_{i+k+1})$. For type-$\beta$ spirals, P_{i+k+1} needs to be contained in the interior of (P_i, P_{i+1}, P_{i+k}). We say P is a *type-α or type-β N-representative*. A class of twisted polygons $[P]$ is a type-α k-spiral (resp. β) if and only if it admits a type-α (resp. β) N-representative for all $N \in \mathbb{Z}$. Let $\mathcal{S}^{\alpha}_{k,n}$ and $\mathcal{S}^{\beta}_{k,n}$ denote the space of type-α and type-β k-spirals modulo projective equivalence. We will see in §3.1 that they are both open in $\mathcal{P}_n$ and hence have dimension $2n$. Figure 3 illustrates three examples of representatives of $\mathcal{S}^{\alpha}_{5,n}$ for $n = 3$, and 20.

It turns out that $\mathcal{S}^{\alpha}_{k,n}$ and $\mathcal{S}^{\beta}_{k,n}$ are invariant under both T_k and T_k^{-1}. Figure 4 shows the inward half of a representative P of $[P] \in \mathcal{S}^{\beta}_{5,3}$, with the red arc representing $P' = T_5(P)$. On the right we have five polygonal arcs by joining vertices of P that are 5 clicks apart. We call them *the transversals of P*. One way to distinguish type-α and type-β spirals is by looking at the orientations of transversals. The transversals of type-α spirals are counterclockwise, whereas those of type-β are clockwise (See Figure 11). In §3, we use the orientations of these transversals to prove the following main theorem.

Theorem 1.1. *For all $n \geq 2$ and $k \geq 2$, we have $T_k(\mathcal{S}^{\alpha}_{k,n}) = \mathcal{S}^{\alpha}_{k,n}$. The same is true for type-β.*

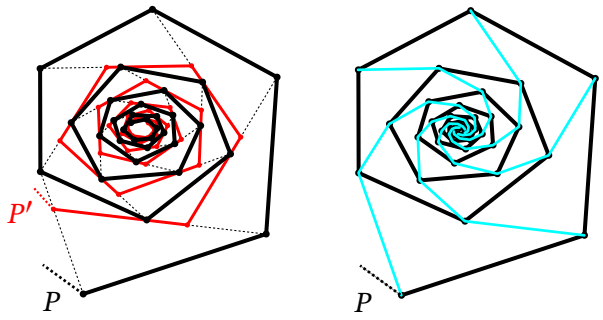

Figure 4: Left: T_5 acting on a representative P of $[P] \in \mathcal{S}^{\beta}_{5,3}$. Right: Transversals of P.

A key property satisfied by convex polygons under the pentagram map is that the forward and backward orbits of any convex polygon under the pentagram map are precompact modulo projective tranformations. See [Sch92, Lemma 3.2]. Experimental results suggest that the k-birds also have precompact Δ_k-orbits. In [Sch25, Conjecture 8.2]

Schwartz conjectured that the k-birds have precompact forward Δ_k-orbits modulo affine transformations. We observed experimentally that $\mathcal{S}^{\alpha}_{k,n}$ and $\mathcal{S}^{\beta}_{k,n}$ behave analogously under T_k.

Conjecture 1.2. *For $n \geq 2$ and $k \geq 2$, the forward and backward T_k-orbit of any $[P] \in \mathcal{S}^{\alpha}_{k,n}$ is precompact in $\mathcal{P}_n$. The same holds for type-β.*

In §6 and §7, we prove Conjecture 1.2 for $k = 2$ and $k = 3$.

1.3 Tic-Tac-Toe Partition and Precompact T_3 Orbits

Our main focus will be the case $k = 3$, which we prove in §6.2.

Theorem 1.3. *For $n \geq 2$, the forward and backward T_3-orbit of any $[P] \in \mathcal{S}^{\alpha}_{3,n}$ is precompact in $\mathcal{P}_n$. The same holds for type-β.*

We discovered several interesting properties of the two types of k-spirals and the map T_3 along our way to prove Theorem 1.3. One major discovery is that the sets $\mathcal{S}^{\alpha}_{3,n}$ and $\mathcal{S}^{\beta}_{3,n}$ fit well with a local parameterization of $\mathcal{P}_n \to \mathbb{R}^{2n}$ introduced by [Sch92] called *corner invariants* (See §2.4). The invariant sets of $\mathcal{P}_n$ under T_3 are partitioned by linear boundaries in the parameter space. The boundary lines give a grid pattern that resembles the board of the game "tic-tac-toe." Each of the four "side-squares" is invariant under T_3.

To construct the tic-tac-toe board, consider the three intervals I, J, K of $\mathbb{R}$ given by $I = (-\infty, 0)$, $J = (0, 1)$, $K = (1, \infty)$. The squares are of the form $I \times I$, $I \times J$, $I \times K$, $J \times I$, etc.. We mark the four side-squares $S_n(I, J)$, $S_n(J, I)$, $S_n(K, J)$, $S_n(J, K)$. See Figure 5 for a visualization of the tic-tac-toe grid. Given $[P] \in \mathcal{P}_n$, we say $[P] \in S_n(I, J)$ if all even corner invariants of $[P]$ are in I, and all odd ones are in J. This means if we plot all n pairs of corner invariants (x_{2i}, x_{2i+1}) onto $\mathbb{R}^2$, we would see n points lying in $I \times J$. The other three side squares are defined analogously.

Figure 6 shows vertices of a representative P of $[P] \in S_4(K, J)$ and the image $P' = T_3(P)$. On the right, we have the projection of the first 2^{11} iterations of the orbit of P under T_3. Each point corresponds to $P_3^{(m)}$ after normalizing $(P_{-2}^{(m)}, P_{-1}^{(m)}, P_0^{(m)}, P_1^{(m)})$ to the unit square

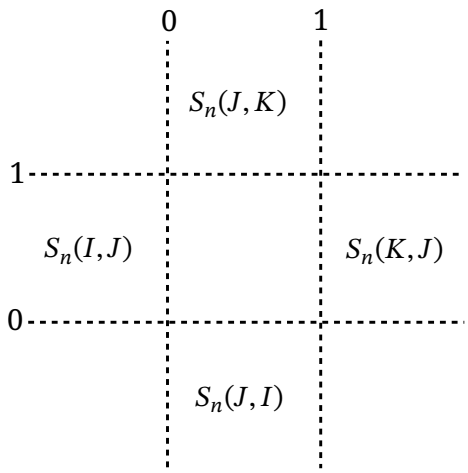

Figure 5: The partition of $\mathbb{R}^2$ into a 3×3 grid, and the four side-squares of our interest.

(here $P^{(m)} = T_3^m(P)$). We speculate that the orbit lies on a flat torus, where the map T_3 acts as a translation on the flat metric.

Twisted polygons that are assigned to these squares have geometric properties. For example, the closed convex polygons always lie in the center square; two of the side-squares are $\mathcal{S}^{\alpha}_{3,n}$ and $\mathcal{S}^{\beta}_{3,n}$; the other two side-squares are obtained by reverting the indexing of vertices of these two types of k-spirals. These facts will be proved in §4.

The proof of Theorem 1.3 is algebraic. In §5 I show that T_3 is a birational map on the corner invariants, which generalizes a direct application of [GP16, Theorem 1.6]. For the explicit formulas, see Equation (19). In §6, I derive four algebraic invariants of T_3, which allow me to show boundedness of the corner invariants of the T_3-orbits, thereby proving Theorem 1.3. This approach is reminiscent of Schwartz's second proof of precompactness of T_2-orbits of convex polygons in [Sch01, Section 3B & 3C].

1.4 The Type-β 2-Spirals and Precompact T_2 Orbits

We now proceed to the case $k = 2$, where the map T_2 is the classical pentagram map. In §3.1 we show that there exist no type-α 2-spirals (so Conjecture 1.2 is vacuously true for type-α 2-spirals). On the other hand, type-β 2-spirals are nontrivial geometric constructions that

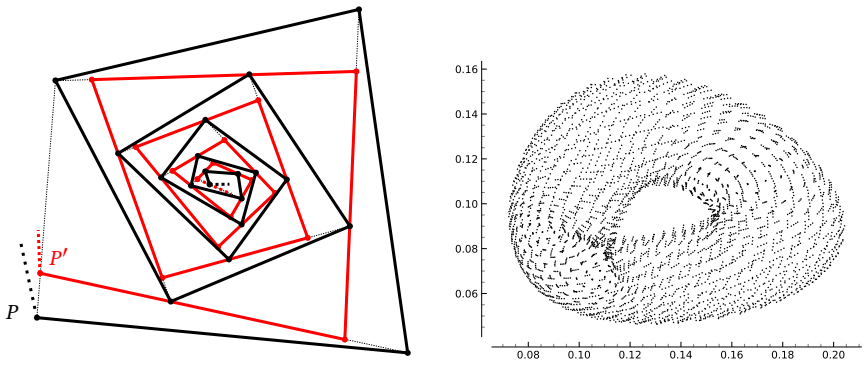

Figure 6: Left: T_3 acting on a representative of $[P] \in S_4(K,J)$. Right: The orbit of $P_3^{(m)}$ in $\mathbb{A}^2$ by fixing $P_{-2} = (0,0)$, $P_{-1} = (1,0)$, $P_0 = (1,1)$, $P_1 = (0,1)$.

are distinct from convex polygons. In §7.1, we show that the corner invariants of type-β 2-spirals are also partitioned by linear boundaries, and in particular $\mathcal{S}^{\alpha}_{3,n} \subset \mathcal{S}^{\beta}_{2,n}$.

We point out that the type-β 2-spirals are not related to the pentagram spirals in [Sch13]. The latter requires P to be a relabeling of $T_2^m(P)$ for some positive integer m.

In §7.2, we use the Casimir functions of the T_2-invariant Poisson structure on $\mathcal{P}_n$ from [Sch08] and [OST10] to prove Conjecture 1.2 for $k = 2$.

Theorem 1.4. *For $n \geq 2$, the forward and backward T_2-orbit of any $[P] \in \mathcal{S}^{\beta}_{2,n}$ is precompact in $\mathcal{P}_n$.*

1.5 Obstacles for $k > 3$ and Future Directions

Our algebraic method of proving Theorem 1.3 and 1.4 requires a complete characterization of the corner invariants of $\mathcal{S}^{\alpha}_{k,n}$ and $\mathcal{S}^{\beta}_{k,n}$ and enough algebraic invariants of T_k that uniformly bound the corner invariants away from the boundaries of $\mathcal{S}^{\alpha}_{k,n}$ and $\mathcal{S}^{\beta}_{k,n}$. However, the corner invariants seem to be not partitioned by linear boundaries for $k > 3$, which makes it difficult to analyze the boundaries of the corner invariants of $\mathcal{S}^{\alpha}_{k,n}$ and $\mathcal{S}^{\beta}_{k,n}$. Moreover, the map T_k for the corner invariants seems not birational from computer algebra. This makes it difficult to algebraically characterize the corner invariants.

One future direction is to look at the cross-ratio of different combinations of points other than the ones involved in the definition of corner invariants. In §8 we present a conjecture on a potential algebraic invariant of T_k, which can be interpreted as a Casimir function of a Poisson structure over the y-parameteris of a quiver Q_S. The quiver Q_S is associated to a Y-mesh of type S from [GP16] and is isomorphic to the quiver in [GSTV12], which corresponds geometrically to the map T_k.

Another direction is to analyze the two types of k-spirals geometrically. There are yet many open problems on the geometry of the two types of k-spirals that could hint at the behavior of their T_k-orbits. For open problems, see the end of §3.1. Answering these geometric problems may provide a new approach to tackle Conjecture 1.2.

Finally, for the case $k = 3$, the birational formula for T_3 could be applied to other settings such as the action of T_3 on Poncelet polygons [Sch24] or discovering T_3-compatible Poisson structures on $\mathcal{P}_n$ that generalizes the one in [GSTV12] for corrugated polygons.

1.6 Accompanying Program

I wrote a web-based program to visualize the orbits of twisted polygons under T_k. Readers can access it from the following link:

https://zzou9.github.io/pentagram-map/spiral.html

When reaching the website, you will see a representative of a twisted polygon displayed in the middle of the screen. You can click on the user manual button for instructions on how to use the program. I discovered most of the results by computer experiments using this program. The paper contains rigorous proofs of the beautiful pictures I observed from it.

1.7 Acknowledgements

This work was supported by a Brown University SPRINT/UTRA summer research program grant. I would like to thank my advisor, Richard Evan Schwartz, for introducing

the concept of deep diagonal maps, providing extensive insights throughout the project, and offering guidance during the writing process. I would like to thank Anton Izosimov and Sergei Tabachnikov for their insightful discussions on the tic-tac-toe partition. Finally, I am grateful to the referees for their helpful comments and for highlighting the connections between the birational formula and the work of Glick and Pylyavskyy.

2 Background

2.1 Projective Geometry

The real projective plane $\mathbb{RP}^2$ is the space of 1-dimensional subspaces of $\mathbb{R}^3$. *Points* of $\mathbb{RP}^2$ are lines in $\mathbb{R}^3$ that go through the origin. We say that $[x : y : z]$ is a *homogeneous coordinate* of $V \in \mathbb{RP}^2$ if the vector $\tilde{V} = (x, y, z)$ is a representative of V. Given two distinct points $V_1, V_2 \in \mathbb{RP}^2$, the *line* $l = V_1V_2$ connecting V_1 and V_2 is the 2-dimensional hyperplane spanned by the two 1-dimensional subspaces. Let l_1, l_2 be two lines in $\mathbb{RP}^2$. The *point of intersection* $l_1 \cap l_2$ is the 1-dimensional line given by the intersection of the two 2-dimensional subspaces. In $\mathbb{RP}^2$, there exists a unique line connecting each pair of distinct points and a unique point of intersection given two distinct lines. We call a collection of points $V_1, V_2, \dots, V_n \in \mathbb{RP}^2$ *in general position* if no three of them are collinear.

The *affine patch* $\mathbb{A}^2$ consists of points in $\mathbb{RP}^2$ with homogeneous coordinate $[x : y : 1]$. We call this canonical choice of coordinate $(x, y, 1)$ the *affine coordinate* of a point $V \in \mathbb{A}^2$. There is a diffeomorphism $\Phi : \mathbb{R}^2 \to \mathbb{A}^2$ given by $\Phi(x, y) = [x : y : 1]$. We often identify $\mathbb{A}^2$ as a copy of $\mathbb{R}^2$ in $\mathbb{RP}^2$. The line $\mathbb{RP}^2 - \mathbb{A}^2$ is called the *line at infinity*.

A map $\phi : \mathbb{RP}^2 \to \mathbb{RP}^2$ is a *projective transformation* if it maps points to points and lines to lines and is bijective. Algebraically, the group of projective transformations is $\mathrm{PGL}_3(\mathbb{R}) = \mathrm{GL}_3(\mathbb{R})/\mathbb{R}^*I$, where we are modding by the subgroup $\mathbb{R}^*I = \{\lambda I : \lambda \in \mathbb{R}^*\}$ and I is the 3×3 identity matrix. We state a classical result regarding projective transformations below with its proof omitted.

Theorem 2.1. *Given two 4-tuples of points* (V_1, V_2, V_3, V_4) *and* (W_1, W_2, W_3, W_4) *in* $\mathbb{RP}^2$*, both in general position, there exists a unique* $\phi \in \mathrm{PGL}_3(\mathbb{R})$ *such that* $\phi(V_i) = W_i$*.*

The group of *affine transformations* $\mathrm{Aff}_2(\mathbb{R})$ on $\mathbb{A}^2$ is the subgroup of projective transformations that fixes the line at infinity. It is isomorphic to a semidirect product of $\mathrm{GL}_2(\mathbb{R})$ and $\mathbb{R}^2$. Elements of $\mathrm{Aff}_2(\mathbb{R})$ can be uniquely expressed as a tuple (M', v) where $M' \in \mathrm{GL}_2(\mathbb{R})$ and $v \in \mathbb{R}^2$. Let $\mathrm{Aff}_2^+(\mathbb{R})$ denote the subgroup of $\mathrm{Aff}_2^+(\mathbb{R})$ where $(M', v) \in \mathrm{Aff}_2^+(\mathbb{R})$ iff $\det(M') > 0$. These are orientation-preserving affine transformations.

2.2 Orientation of Affine Triangles

Given an ordered 3-tuple (V_1, V_2, V_3) of points in $\mathbb{R}^2$ or $\mathbb{A}^2$, let $\mathrm{int}(V_1, V_2, V_3)$ denote the interior of the affine triangle with vertices V_1, V_2, V_3. There is a canonical way to define the orientation of an ordered 3-tuple. Let $\tilde{V}_i$ be the affine coordinate of V_i. We consider the *signed area* $\mathcal{O}(V_1, V_2, V_3)$ of the oriented triangle, which can be computed as

$$\mathcal{O}(V_1, V_2, V_3) = \det(\tilde{V}_1, \tilde{V}_2, \tilde{V}_3). \tag{2}$$

The determinant is evaluated on the 3×3 matrix with column vectors $\tilde{V}_i$. We say an ordered 3-tuple (V_1, V_2, V_3) is *positive* if $\mathcal{O}(V_1, V_2, V_3) > 0$. Figure 7 shows an example of a positive 3-tuple.

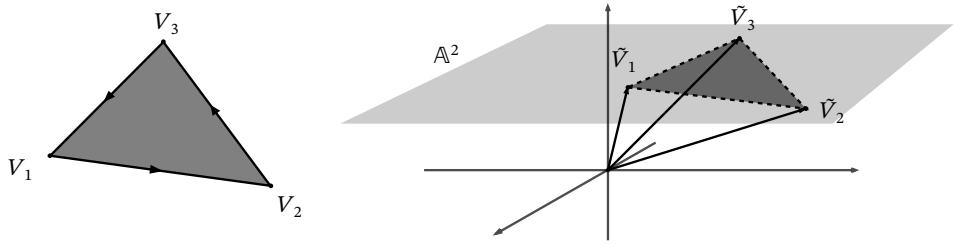

Figure 7: A positive 3-tuple of affine points (V_1, V_2, V_3).

Here is another way to compute $\mathcal{O}$ using the $\mathbb{R}^2$ coordinates of V_1, V_2, V_3:

$$\begin{aligned}\mathcal{O}(V_1, V_2, V_3) &= \det(V_1, V_2) + \det(V_2, V_3) + \det(V_3, V_1) \\ &= \det(V_i - V_{i-1}, V_{i+1} - V_i) \text{ for } i = 1, 2, 3\end{aligned} \tag{3}$$

where the determinant is evaluated on the 2×2 matrix.

$\mathcal{O}$ interacts with the action of $\mathrm{Aff}_2^+(\mathbb{R})$ and the symmetric group S_3 on planar/affine triangles in the following way: Given $M \in \mathrm{Aff}_2^+(\mathbb{R})$, let $V_i' = M(V_i)$. One can show that (V_1, V_2, V_3) is positive iff (V_1', V_2', V_3') is positive. On the other hand, for all $\sigma \in S_3$, $\mathcal{O}(V_{\sigma(1)}, V_{\sigma(2)}, V_{\sigma(3)}) = \mathrm{sgn}(\sigma)\mathcal{O}(V_1, V_2, V_3)$, so $\mathcal{O}(V_{\sigma(1)}, V_{\sigma(2)}, V_{\sigma(3)}) = \mathcal{O}(V_1, V_2, V_3)$ when σ is a 3-cycle.

Below are useful equivalence conditions for the positivity of (V_1, V_2, V_3). The proof is elementary, so we will omit it.

Proposition 2.2. *Given $V_1, V_2, V_3 \in \mathbb{R}^2$ in general position, and $W \in \mathrm{int}(V_1, V_2, V_3)$, the following are equivalent:*

1. *(V_1, V_2, V_3) is positive.*
2. *(V_i, V_{i+1}, W) is positive for some $i \in \{1, 2, 3\}$.*
3. *(V_i, V_{i+1}, W) is positive for all $i \in \{1, 2, 3\}$.*
4. *$\det(V_i - V_{i-1}, V_{i+1} - W) > 0$ for some $i \in \{1, 2, 3\}$.*
5. *$\det(V_i - V_{i-1}, V_{i+1} - W) > 0$ for all $i \in \{1, 2, 3\}$.*

2.3 The Cross-Ratio

The cross-ratio is used to construct a projective-invariant parametrization of the k-spirals. There are multiple ways to define the cross-ratio of four collinear points on the projective plane, each using its own permutation of the points. We follow the convention used in [Sch92]. Given four collinear points A, B, C, D on a line $\omega \subset \mathbb{RP}^2$, we choose a projective

transformation ψ that maps ω to the x-axis of $\mathbb{A}^2$. Let a, b, c, d be the x-coordinates of $\psi(A)$, $\psi(B)$, $\psi(C)$, $\psi(D)$. We define the *cross-ratio* to be the following quantity:

$$\chi(A, B, C, D) := \frac{(a-b)(c-d)}{(a-c)(b-d)}. \tag{4}$$

If A lies on the line at infinity, we let $\chi(A, B, C, D) = \frac{c-d}{b-d}$. One can check that given any $\phi \in \mathrm{PGL}_3(\mathbb{R})$,

$$\chi(A, B, C, D) = \chi(\phi(A), \phi(B), \phi(C), \phi(D)).$$

We also define the cross-ratio for four projective lines. Let l, m, n, k be four lines intersecting at a common point O. Normalize with a projective transformation so that $l, m, n, k \subset \mathbb{A}^2$ with slopes s_l, s_m, s_n, s_k. We define

$$\chi(l, m, n, k) = \frac{(s_l - s_m)(s_n - s_k)}{(s_l - s_n)(s_m - s_k)} \tag{5}$$

with $\chi(l, m, n, k) = \frac{s_n - s_k}{s_m - s_k}$ if $s_l = \infty$.

If ω is a line that does not go through O and intersects l, m, n, k at A, B, C, D respectively, we have

$$\chi(l, m, n, k) = \chi(A, B, C, D). \tag{6}$$

See Figure 8 for the configuration. The proof is elementary, so we will omit it.

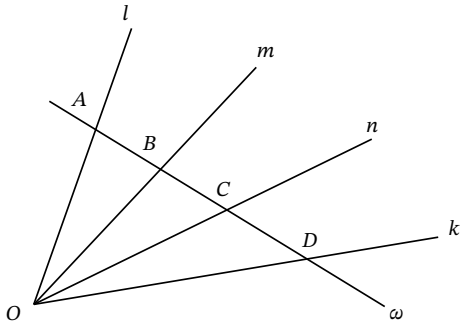

Figure 8: The configuration in Equation (6).

2.4 Twisted Polygons, Corner Invariants

Introduced in [Sch08], a *twisted n-gon* is a bi-infinite sequence $P : \mathbb{Z} \to \mathbb{RP}^2$, along with a projective transformation $M \in \mathrm{PGL}_3(\mathbb{R})$ called the *monodromy*, such that every three consecutive points of P are in general position, and $P_{i+n} = M(P_i)$ for all $i \in \mathbb{Z}$. When M is the identity, we get an ordinary closed n-gon. Two twisted n-gons P, Q are *equivalent* if there exists $\phi \in \mathrm{PGL}_3(\mathbb{R})$ such that $\phi(P_i) = Q_i$ for all $i \in \mathbb{Z}$. The two monodromies M_p and M_q satisfy $M_q = \phi M_p \phi^{-1}$. Let $\mathcal{P}_n$ denote the space of twisted n-gons modulo projective equivalence.

The cross-ratio allows us to parameterize $\mathcal{P}_n$ with coordinates in $\mathbb{R}^{2n}$. Given a twisted n-gon P, the *corner invariants* of P is a coordinate system $x_0(P), \dots, x_{2n-1}(P)$ given by

$$\begin{cases} x_{2i}(P) = \chi(P_{i-2},\, P_{i-1},\, P_{i-2}P_{i-1} \cap P_iP_{i+1},\, P_{i-2}P_{i-1} \cap P_{i+1}P_{i+2}); \\ x_{2i+1}(P) = \chi(P_{i+2},\, P_{i+1},\, P_{i+2}P_{i+1} \cap P_iP_{i-1},\, P_{i+2}P_{i+1} \cap P_{i-1}P_{i-2}). \end{cases} \tag{7}$$

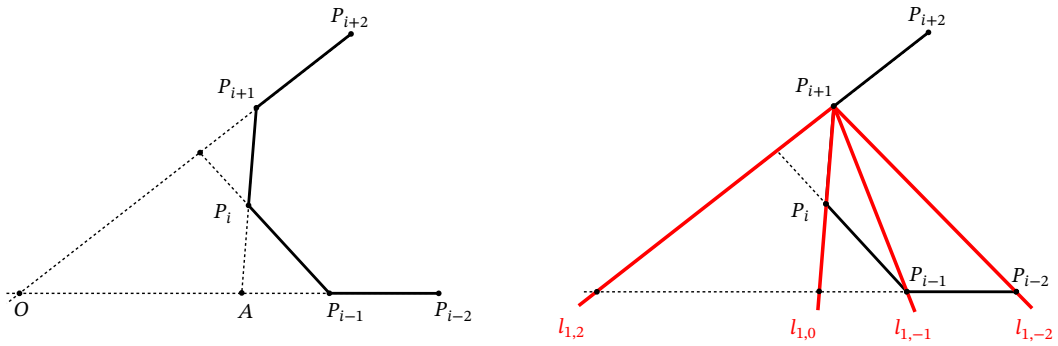

Figure 9: Left: The corner invariants $x_{2i}(P) = \chi(P_{i-2}, P_{i-1}, A, O)$ computed using Equation (7). Right: $x_{2i}(P) = \chi(l_{1,-2}, l_{1,-1}, l_{1,0}, l_{1,2})$ computed using Equation (8).

See the left side of Figure 9 for a geometric interpretation of the corner invariants. Let $l_{a,b} = P_{i+a}P_{i+b}$. By Equation (5), the corner invariants can be computed by

$$\begin{cases} x_{2i}(P) = \chi(l_{1,-2}, l_{1,-1}, l_{1,0}, l_{1,2}); \\ x_{2i+1}(P) = \chi(l_{-1,2}, l_{-1,1}, l_{-1,0}, l_{-1,-2}). \end{cases} \tag{8}$$

See the right side of Figure 9 for the line configurations.

Since χ is invariant under projective transformations, for all j we have $x_j(P) = x_{j+2n}(P)$, so a $2n$-tuple of corner invariants is enough to fully determine the projective equivalence class of a twisted n-gon. We use $x_j(P)$ to denote the corner invariants of $[P] \in \mathcal{P}_n$ without adding square brackets around P. To obtain the corner invariants of $[P] \in \mathcal{P}_n$, one can simply choose an arbitrary representative P and compute its corner invariants. [Sch08, Equation (19) & (20)] showed that one can also revert the process and obtain a representative twisted polygon of the equivalence class given its corner invariants.

3 The Spirals and T_k-Orbit Invariance

In this section, we explore the geometric properties of type-α and type-β k-spirals and prove Theorem 1.1. In §3.1, we give rigorous definitions of the two types of k-spirals and discuss their geometric properties. In §3.2, we introduce a construct associated to the two types of k-spirals called the transversals. In §3.3 and §3.4, we prove Theorem 1.1 using geometric properties of the transversals.

3.1 The Geometry of k-Spirals

Here we give the formal definition of a k-spiral and its two subsets called type-α and type-β. We then explore their geometric properties and present some open problems.

Definition 3.1. Given integers $k \geq 2$, $n \geq 2$, we say that $[P] \in \mathcal{P}_n$ is a *k-spiral* if for all $N \in \mathbb{Z}$, there exists a representative P that satisfies the following: For all $i \geq N$, P_i lies in $\mathbb{A}^2$, (P_i, P_{i+1}, P_{i+2}) is positive, and (P_i, P_{i+1}, P_{i+k}) is positive. Such a representative is called an *N-representative*. Saying that $[P]$ is a k-spiral means that $[P]$ admits an N-representative for all $N \in \mathbb{Z}$.

Remark 3.2. The idea of considering an N-representative for each $N \in \mathbb{Z}$ is new to the literature and may at first seem superfluous. Readers will see in §4 that this condition is natural when we examine the corner invariants of the two types of k-spirals. See the end of this section for open problems related to the geometry of N-representatives.

In practice, since $[P]$ is a twisted n-gon, it suffices to find a single N_0-representative P_0 for some $N_0 \in \mathbb{Z}$. One can then obtain other N-representatives for $N < N_0$ by applying the m-th power of the monodromy of $[P]$ to P_0, where $m > \frac{N_0 - N}{k} + 1$.

Definition 3.3. A k-spiral $[P] \in \mathcal{P}_n$ is of *type-α* or *type-β* if for all $N \in \mathbb{Z}$, it has an N-representative P that satisfies the following conditions:

- $[P]$ is of type-α if $P_{i+k} \in \operatorname{int}(P_i, P_{i+1}, P_{i+k+1})$ for all $i \geq N$;
- $[P]$ is of type-β if $P_{i+k+1} \in \operatorname{int}(P_i, P_{i+1}, P_{i+k})$ for all $i \geq N$.

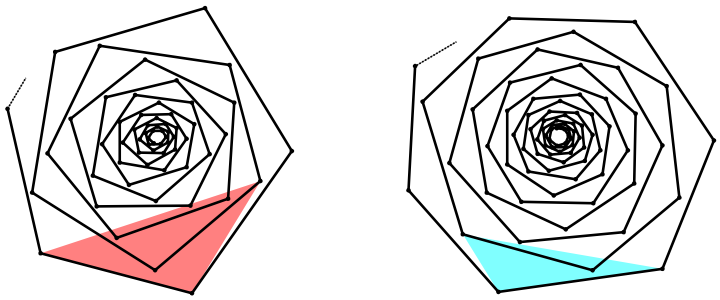

Figure 10: Left: The inward half of a 0-representative P of a type-α 6-spiral. The red triangle is joined by $(P_i, P_{i+1}, P_{i+k+1})$, which is positive by Proposition 3.4 and contains P_{i+k} in its interior. Right: The inward half of a 0-representative P of a type-β 6-spiral. The cyan triangle is joined by (P_i, P_{i+1}, P_{i+k}), which is positive and contains P_{i+k+1} in its interior.

See Figure 10 for 0-representatives of type-α and type-β 6-spirals. For the type-α k-spirals, we show that positivity of (P_i, P_{i+1}, P_{i+k}) is equivalent to positivity of $(P_i, P_{i+1}, P_{i+k+1})$. The latter condition turns out to be more convenient for showing T_k invariance.

Proposition 3.4. *$[P] \in \mathcal{P}_n$ is a type-α k-spiral if and only if for all $N \in \mathbb{Z}$, there exists a representative P that satisfies the following: for all $i \geq N$, P_i lies in $\mathbb{A}^2$, (P_i, P_{i+1}, P_{i+2}) is positive, $(P_i, P_{i+1}, P_{i+k+1})$ is positive, and $P_{i+k} \in \operatorname{int}(P_i, P_{i+1}, P_{i+k+1})$.*

Proof. Since $P_{i+k} \in \operatorname{int}(P_i, P_{i+1}, P_{i+k+1})$, we see that $\operatorname{int}(P_i, P_{i+1}, P_{i+k+1})$ is nonempty, so the three points P_i, P_{i+1}, P_{i+k+1} are in general position. It then follows from Proposition 2.2 that (P_i, P_{i+1}, P_{i+k}) is positive iff $(P_i, P_{i+1}, P_{i+k+1})$ is positive. □

Corollary 3.5. *There exists no type-α 2-spirals.*

Proof. It suffices to show that there exists no configuration of four points $A, B, C, D \in \mathbb{A}^2$ such that (A, B, D), (B, C, D) are both positive and $C \in \operatorname{int}(A, B, D)$. If (A, B, D) is positive and $C \in \operatorname{int}(A, B, D)$, then Proposition 2.2 implies (B, D, C) is positive, but that contradicts (B, C, D) positive because $\mathcal{O}(B, C, D) = -\mathcal{O}(B, D, C)$. □

On the other hand, type-β 2-spirals do exist. Geometrically, their N-representatives look like triangular spirals. See §7 for a more thorough discussion on type-β 2-spirals.

Remark 3.6. One may attempt to define the two types of k-spirals on bi-infinite sequences of points in $\mathbb{RP}^2$ with no periodicity constraints. The results in this section hold true for this more general definition. We restrict our attention to twisted polygons because it's a finite-dimensional space, which allows us to more easily keep track of the T_k-orbits.

We now proceed to discuss some geometric properties of type-α and type-β k-spirals. A twisted polygon P is called *k-nice* if the four points $P_i, P_{i+1}, P_{i+k}, P_{i+k+1}$ are in general position for all $i \in \mathbb{Z}$. The k-nice condition is projective invariant. Let $\mathcal{P}_{k,n}$ denote the space of k-nice twisted n-gons modulo projective equivalence.

Proposition 3.7. *For all $k \geq 2$, $\mathcal{P}_{k,n}$ is open in $\mathcal{P}_n$, so it has dimension $2n$.*

Proof. The condition that four points $P_i, P_{i+1}, P_{i+k}, P_{i+k+1}$ are in general position remains true if we perturb one of the points in a small enough neighborhood of $\mathbb{RP}^2$. The dimension of $\mathcal{P}_{k,n}$ comes from the fact that $\mathcal{P}_n$ has dimension $2n$, which is shown in [OST10, Lemma 2.2]. □

Proposition 3.8. *Both type-α and type-β k-spirals are k-nice.*

Proof. We give a proof to the type-α case. The type-β case is analogous, so we will omit it. Given a type-α k-spiral $[P]$ and an integer $i \in \mathbb{Z}$, let P be an i-representative of $[P]$. Since $(P_i, P_{i+1}, P_{i+k+1})$ is positive, these three points cannot be collinear. Also, since $P_{i+k} \in \operatorname{int}(P_i, P_{i+1}, P_{i+k+1})$, P_{i+k} does not lie in any of the lines joined by two of the three vertices P_i, P_{i+1}, P_{i+k+1}. This shows that $P_i, P_{i+1}, P_{i+k}, P_{i+k+1}$ are in general position. □

As stated in §1.2, we let $\mathcal{S}^{\alpha}_{k,n}$ and $\mathcal{S}^{\beta}_{k,n}$ denote the space of type-α and type-β k-spirals (By Corollary 3.5, $\mathcal{S}^{\alpha}_{2,n} = \emptyset$ for all $n \geq 2$).

Proposition 3.9. *Both $\mathcal{S}^{\alpha}_{k,n}$ and $\mathcal{S}^{\beta}_{k,n}$ are open in $\mathcal{P}_{k,n}$, so they both have dimension $2n$.*

Proof. The positivity conditions of (P_i, P_{i+1}, P_{i+2}) and (P_i, P_{i+1}, P_{i+k}) are open conditions from continuity of the determinant function. The condition $P_{i+k} \in \mathrm{int}(P_i, P_{i+1}, P_{i+k+1})$ for type-α (or $P_{i+k+1} \in \mathrm{int}(P_i, P_{i+1}, P_{i+k})$ for type-β) is equivalent to the positivity of certain determinants by Proposition 2.2, so this is also an open condition. Finally, $\mathcal{S}^{\alpha}_{k,n} \subset \mathcal{P}_{k,n}$ and $\mathcal{S}^{\beta}_{k,n} \subset \mathcal{P}_{k,n}$ follows from Proposition 3.8. □

A twisted polygon P is *closed* if there exists some positive integer n such that $P_{i+n} = P_i$, or $[P] \in \mathcal{P}_n$ with identity monodromy. We show that neither type-α nor type-β k-spirals are closed.

Proposition 3.10. *For all $k \geq 2$ and $n \geq 2$, if $[P] \in \mathcal{S}^{\alpha}_{k,n}$, then $[P]$ is not closed. The same holds for $\mathcal{S}^{\beta}_{k,n}$.*

Proof. Given any closed n-gon P on $\mathbb{A}^2$, let C be the convex hull of the vertices of P. Since P has finitely many vertices, there exists a vertex P_i such that $P_i \notin \mathrm{int}(C)$. Then, since $\mathrm{int}(P_{i-k}, P_{i-k+1}, P_{i+1}) \subset \mathrm{int}(C)$, we must have $P_i \notin \mathrm{int}(P_{i-k}, P_{i-k+1}, P_{i+1})$. It follows that P is not an N-representative of type-α k-spiral for any N or k. The proof for type-β is similar, so we omit it. □

The two types of k-spirals seem to possess rich geometric properties. We will present some open problems. In the discussion below, $[P]$ denotes a type-α or type-β k-spiral.

Problem 3.11. For all $N \in \mathbb{Z}$, is it always possible to find N-representatives P such that for all $j > i + 1$, (P_i, P_{i+1}, P_j) is positive (in other words, P_j always lies on the same side of the line P_iP_{i+1})?

Problem 3.12. Let P be an arbitrary representative of $[P]$. Is there a minimal $N \in \mathbb{Z}$ such that P is an N-representative on some affine patch of $\mathbb{RP}^2$? Does there exist P that is an N-representative for all $N \in \mathbb{Z}$?

Problem 3.13. Given an N-representative P, does P_i converge to a point in $\mathbb{A}^2$ as $i \to \infty$?

3.2 Transversals of the Spirals

In this section, we prove our remark in §1.2 that transversals for type-α spirals are oriented counterclockwise, whereas transversals for type-β are oriented clockwise. Recall that the *transversals* of an N-representative P of a k-spiral are k polygonal arcs joined by vertices $P_i, P_{i+k}, P_{i+2k}, \ldots$ for $i = N, \ldots, N+k-1$. See Figure 11 for one of the k transversals of the two representatives from Figure 10.

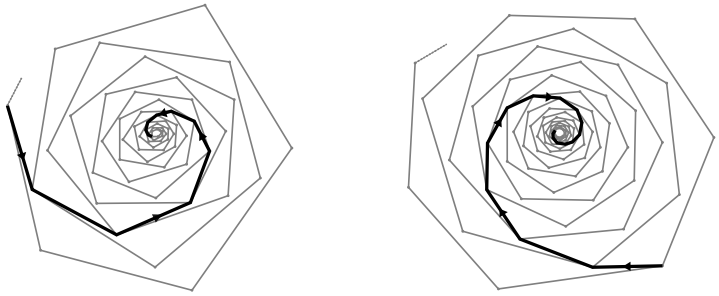

Figure 11: Transversals of two representatives from Figure 10.

Lemma 3.14. *Given $O, A, B, C, D \in \mathbb{A}^2$ (See Figure 12) such that (A,O,B), (A,O,D), (B,O,C), (C,O,D) are all positive. Then, (A,O,C) is positive iff (B,O,D) is positive.*

Proof. For the forward direction, normalize with $\mathrm{Aff}_2^+(\mathbb{R})$ so that $O = (0,0)$ and $A = (-1,0)$. Let $B = (x_b, y_b)$, $C = (x_c, y_c)$, and $D = (x_d, y_d)$. Since (A,O,B) is positive, Equation (3) gives us

$$\mathcal{O}(A,O,B) = \det(O-A, B-O) = \det(-A,B) = y_b > 0.$$

Similarly, positivity of (A,O,C) and (A,O,D) give us $y_c, y_d > 0$. Next, observe that

$$\mathcal{O}(B,O,C) = \det(-B,C) = -x_b y_c + x_c y_b;$$

$$\mathcal{O}(B,O,D) = \det(-B,D) = -x_b y_d + x_d y_b;$$

$$\mathcal{O}(C,O,D) = \det(-C,D) = -x_c y_d + x_d y_c.$$

Since $y_b, y_c, y_d > 0$, we have $\frac{y_b}{y_c}, \frac{y_d}{y_c} > 0$, which implies

$$\mathcal{O}(B,O,D) = -x_b y_d + x_d y_b = \frac{y_b}{y_c}\,\mathcal{O}(C,O,D) + \frac{y_d}{y_c}\,\mathcal{O}(B,O,C) > 0.$$

This shows positivity of (B,O,D).

The proof for the backward direction is analogous. Normalize so that $O = (0,0)$ and $D = (1,0)$. Let $A = (x_a, y_a)$, $B = (x_b, y_b)$, $C = (x_c, y_c)$. Positivity of (A,O,D), (B,O,D), and (C,O,D) implies $y_a, y_b, y_c > 0$. One can then check that

$$\mathcal{O}(A,O,C) = -x_a y_c + x_c y_a = \frac{y_c}{y_b}\,\mathcal{O}(A,O,B) + \frac{y_a}{y_b}\,\mathcal{O}(B,O,C) > 0.$$

This shows positivity of (A,O,C). □

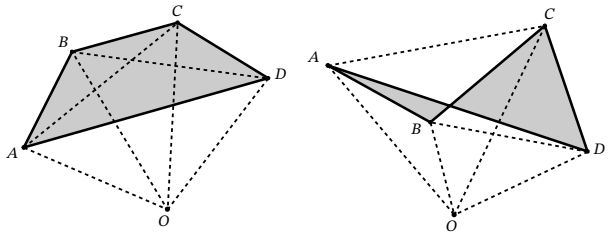

Figure 12: Examples of O, A, B, C, D in Lemma 3.14.

The next proposition formalizes our claim on the orientation of transversals.

Proposition 3.15. *Let P be an N-representative of a k-spiral $[P]$. For all $i > N$, if $[P]$ is type-α, then (P_i, P_{i+k}, P_{i+2k}) is positive; if $[P]$ is type-β, then (P_{i+2k}, P_{i+k}, P_i) is positive.*

Proof. The proof applies Lemma 3.14 with suitable choices of O, A, B, C, D. See Figure 13 for the configuration of points involved.

We start with P of type-α. Consider the following choices of vertices:

$$O = P_{i+k};\ A = P_i;\ B = P_{i+k-1};\ C = P_{i+2k};\ D = P_{i+k+1}.$$

It follows immediately from the definition of a type-α N-representative that (B,O,C) and (B,O,D) are positive. The other conditions follow from applications of Proposition

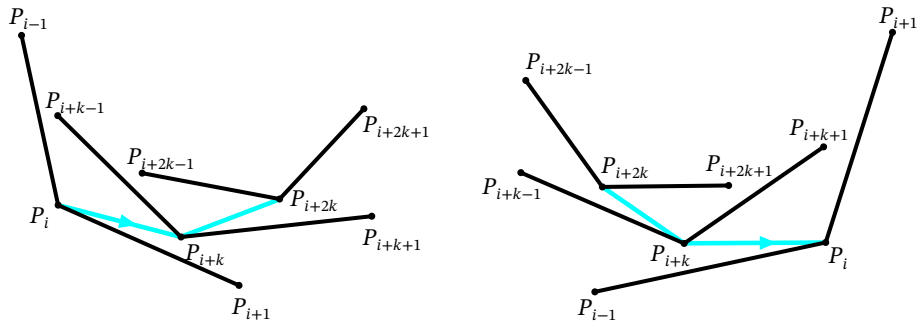

Figure 13: Left: $\mathcal{S}^{\alpha}_{k,n}$ configuration. Right: $\mathcal{S}^{\beta}_{k,n}$ configuration.

2.2. Apply Proposition 2.2 with (P_{i-1}, P_i, P_{i+k}) positive and $P_{i+k-1} \in \text{int}(P_{i-1}, P_i, P_{i+k})$ to get positivity of (A, O, B). Apply Proposition 2.2 with $(P_i, P_{i+1}, P_{i+k+1})$ positive and $P_{i+k} \in \text{int}(P_i, P_{i+1}, P_{i+k+1})$ to get positivity of (A, O, D). Apply Proposition 2.2 with $(P_{i+k}, P_{i+k+1}, P_{i+2k+1})$ positive and $P_{i+2k} \in \text{int}(P_{i+k}, P_{i+k+1}, P_{i+2k+1})$ to get positivity of (C, O, D). Then, the backward direction of Lemma 3.14 implies (P_i, P_{i+k}, P_{i+2k}) is positive.

The proof for type-β is analogous. Consider the following choices of vertices:

$$O = P_{i+k};\ A = P_{i+k-1};\ B = P_{i+2k};\ C = P_{i+k+1};\ D = P_i.$$

Positivity of (A, O, C) and (B, O, C) follows from the definition of a type-β N-representative. A similar application of Proposition 2.2 as in the case of type-α gives positivity of (A, O, B), (A, O, D), and (C, O, D), which we will omit. Finally, the forward direction of Lemma 3.14 implies (P_{i+2k}, P_{i+k}, P_i) is positive. □

3.3 Invariance of Forward Orbit

In this section, we prove that $\mathcal{S}^{\alpha}_{k,n}$ and $\mathcal{S}^{\beta}_{k,n}$ are T_k-invariant. We will use Equation (1) for our labeling convention. See Figure 14.

If P is k-nice, then P' is always well-defined. In particular, Proposition 3.8 implies T_k is well-defined on $\mathcal{S}^{\alpha}_{k,n}$ and $\mathcal{S}^{\beta}_{k,n}$.

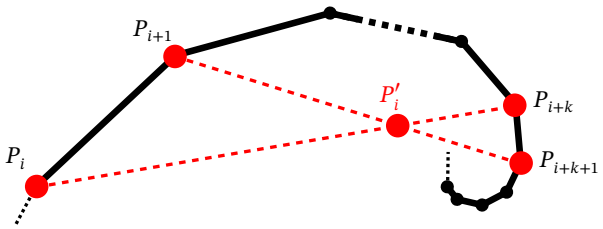

Figure 14: The labeling convention of the map T_k from Equation (1).

Remark 3.16. T_k doesn't necessarily send k-nice twisted polygons to k-nice twisted polygons. Here is an example provided by the anonymous referee: Fix $r \in (0,1)$. Consider the function $P : \mathbb{Z} \to \mathbb{C} \cong \mathbb{R}^2$ mapping $z \mapsto r^z \exp(z\pi i/k)$. One can check that P is a k-nice twisted n-gon for any $n \geq 2$ with monodromy that is a scale-rotation, but $T_k(P)$ is the zero function and hence not k-nice. What we will show is that in the case of type-α and type-β k-spirals, T_k does preserve k-niceness. This is a direct consequence of Theorem 1.1 and Proposition 3.8.

We proceed to prove the T_k-invariance of $\mathcal{S}^{\alpha}_{k,n}$ and $\mathcal{S}^{\beta}_{k,n}$ separately. We start with the following lemma.

Lemma 3.17. *Given four points A, B, C, D in $\mathbb{R}^2$ in general position with $D \in \text{int}(A,B,C)$. Let $O = AB \cap CD$. There exist $s \in (0,1)$ and $t \in (1,\infty)$ such that*

$$O = (1-s)A + sB = (1-t)C + tD.$$

Proof. Since $D \in \text{int}(A,B,C)$, there exists $\lambda_1, \lambda_2, \lambda_3 \in (0,1)$ such that

$$\lambda_1 + \lambda_2 + \lambda_3 = 1; \;\; D = \lambda_1 A + \lambda_2 B + \lambda_3 C.$$

Taking $s = \frac{\lambda_2}{1-\lambda_3}$ and $t = \frac{1}{1-\lambda_3}$ gives us the desired result. □

Proposition 3.18. *For all $k \geq 2$ and $n \geq 2$, $T_k(\mathcal{S}^{\alpha}_{k,n}) \subset \mathcal{S}^{\alpha}_{k,n}$.*

Proof. Given an N-representative P of some $[P] \in \mathcal{S}^{\alpha}_{k,n}$, we will show that $P' = T_k(P)$ is a type-α N-representative of $[T_k(P)]$ by proving that for all $i \geq N$, $(P'_i, P'_{i+1}, P'_{i+2})$ is positive,

$(P'_i, P'_{i+1}, P'_{i+k+1})$ is positive, and $P'_{i+k} \in \operatorname{int}(P'_i, P'_{i+1}, P'_{i+k+1})$. See the left side of Figure 15 for configurations of relevant vertices of P and P'.

Let $i \geq N$ be fixed. Since P is a type-α N-representative, $P_{j+k} \in \operatorname{int}(P_j, P_{j+1}, P_{j+k+1})$ for all $j \geq N$. Applying Lemma 3.17 with Equation (1) on P'_j for $j \in \{i, i+1, i+2, i+k, i+k+1\}$ gives us

$$\begin{aligned} P'_i &= (1-s_1)P_{i+1} + s_1 P_{i+k+1}; & P'_{i+1} &= (1-t_1)P_{i+1} + t_1 P_{i+k+1}; \\ P'_{i+1} &= (1-s_2)P_{i+2} + s_2 P_{i+k+2}; & P'_{i+2} &= (1-t_2)P_{i+2} + t_2 P_{i+k+2}; \\ P'_{i+k} &= (1-s_3)P_{i+k+1} + s_3 P_{i+2k+1}; & P'_{i+k+1} &= (1-t_3)P_{i+k+1} + t_3 P_{i+2k+1}, \end{aligned} \tag{9}$$

where $s_1, s_2, s_3 \in (0,1)$ and $t_1, t_2, t_3 \in (1, \infty)$. In particular, this shows $P'_{i+k+1} \notin P'_i P'_{i+1}$, so the three points $P'_i, P'_{i+1}, P'_{i+k+1}$ are in general position.

To see that $(P'_i, P'_{i+1}, P'_{i+2})$ is positive, Equation (3) and (9) give us

$$\begin{aligned} \mathcal{O}(P'_i, P'_{i+1}, P'_{i+2}) &= \det(P'_{i+1} - P'_i, P'_{i+2} - P'_{i+1}) \\ &= \det((s_1 - t_1)P_{i+1} + (t_1 - s_1)P_{i+k+1}, (s_2 - t_2)P_{i+2} + (t_2 - s_2)P_{i+k+2}) \\ &= (t_1 - s_1)(t_2 - s_2)\det(P_{i+k+2} - P_{i+2}, P_{i+1} - P_{i+k+1}). \end{aligned} \tag{10}$$

Then, since $\mathcal{O}(P_{i+1}, P_{i+2}, P_{i+k+2}) > 0$ and $P_{i+k+1} \in \operatorname{int}(P_{i+1}, P_{i+2}, P_{i+k+2})$, Proposition 2.2 implies $\det(P_{i+k+2} - P_{i+2}, P_{i+1} - P_{i+k+1}) > 0$, so $\mathcal{O}(P'_i, P'_{i+1}, P'_{i+2}) > 0$.

Next, we show that $P'_{i+k} \in \operatorname{int}(P'_i, P'_{i+1}, P'_{i+k+1})$. Let $r_1 = \frac{1-s_1}{t_1 - s_1}$ and $r_2 = \frac{s_3}{t_3}$. (9) implies $r_1, r_2 \in (0,1)$ and

$$\begin{aligned} P'_{i+k} &= (1-s_3)P_{i+k+1} + s_3 P_{i+2k+1} \\ &= \frac{(1-s_3)(t_1-1)}{t_1 - s_1} P'_i + \frac{(1-s_3)(1-s_1)}{t_1 - s_1} P'_{i+1} + \frac{s_3(t_3-1)}{t_3 - s_3} P'_{i+k} + \frac{s_3(1-s_3)}{t_3 - s_3} P'_{i+k+1}. \end{aligned}$$

It follows that

$$\begin{aligned} P'_{i+k} &= \frac{t_3 - s_3}{t_3(s_3 - 1)} \left(\frac{(1-s_3)(t_1-1)}{t_1 - s_1} P'_i + \frac{(1-s_3)(1-s_1)}{t_1 - s_1} P'_{i+1} + \frac{s_3(1-s_3)}{t_3 - s_3} P'_{i+k+1} \right) \\ &= \frac{(t_3 - s_3)(1-t_1)}{t_3(t_1 - s_1)} P'_i + \frac{(t_3 - s_3)(s_1 - 1)}{t_3(t_1 - s_1)} P'_{i+1} + \frac{s_3}{t_3} P'_{i+k+1} \\ &= (1-r_2)(1-r_1)P'_i + (1-r_2)r_1 P'_{i+1} + r_2 P'_{i+k+1}. \end{aligned}$$

Observe that the coefficients $(1-r_2)(1-r_1)$, $(1-r_2)r_1$, r_2 are all in $(0,1)$ and sum up to 1, so $P'_{i+k} \in \operatorname{int}(P'_i, P'_{i+1}, P'_{i+k+1})$.

Finally, using Equation (3) and (9), we have

$$\begin{aligned}\det(P'_{i+1}-P'_i, P'_{i+k+1}-P'_{i+k}) &= \det((t_1-s_1)(P_{i+k+1}-P_{i+1}), (t_3-s_3)(P_{i+2k+1}-P_{i+k+1})) \\ &= (t_1-s_1)(t_3-s_3)\det(P_{i+k+1}-P_{i+1}, P_{i+2k+1}-P_{i+k+1}) \\ &= (t_1-s_1)(t_3-s_3)\mathcal{O}(P_{i+1}, P_{i+k+1}, P_{i+2k+1}).\end{aligned} \tag{11}$$

Proposition 3.15 implies $\mathcal{O}(P_{i+1}, P_{i+k+1}, P_{i+2k+1}) > 0$, so $\det(P'_{i+1}-P'_i, P'_{i+k+1}-P'_{i+k}) > 0$ Since $P'_i, P'_{i+1}, P'_{i+k+1}$ are in general position and $P'_{i+k} \in \operatorname{int}(P'_i, P'_{i+1}, P'_{i+k+1})$, Proposition 2.2 and Equation (11) imply $\mathcal{O}(P'_i, P'_{i+1}, P'_{i+k+1}) > 0$. We conclude that P' is a type-α N-representative. □

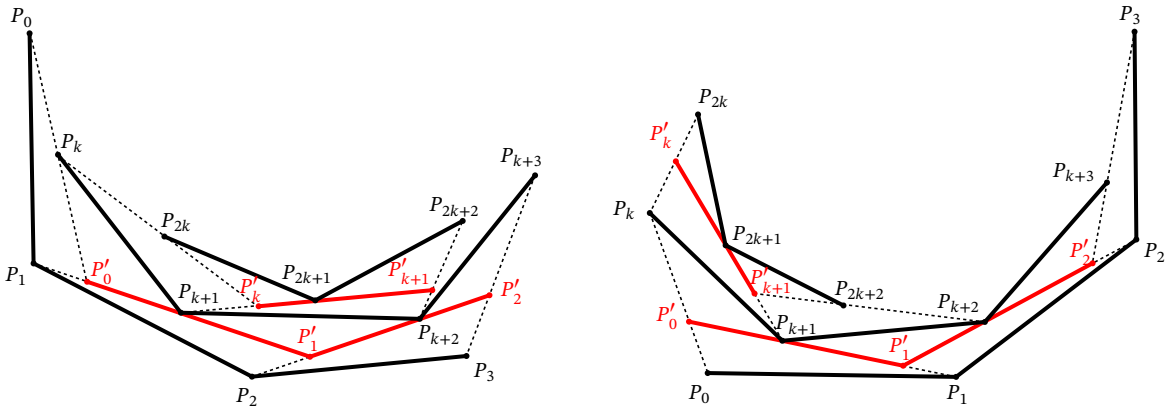

Figure 15: Left: Proposition 3.18 configuration. Right: Proposition 3.19 configuration.

Proposition 3.19. *For all $k \geq 2$ and $n \geq 2$, $T_k(\mathcal{S}^{\beta}_{k,n}) \subset \mathcal{S}^{\beta}_{k,n}$.*

Proof. The proof is analogous to the one for Proposition 3.18. Replacing α with β, we may work with the setup in the proof of Proposition 3.18. See the right side of Figure 15.

The key difference between type-α and type-β is that conditions for type-β k-spirals give us the following linear relations when we apply Lemma 3.17 with (1) on P'_j for

$j \in \{i, i+1, i+2, i+k, i+k+1\}$:

$$\begin{aligned} P'_i &= (1-t_1)P_{i+1} + t_1 P_{i+k+1}; & P'_{i+1} &= (1-s_1)P_{i+1} + s_1 P_{i+k+1}; \\ P'_{i+1} &= (1-t_2)P_{i+2} + t_2 P_{i+k+2}; & P'_{i+2} &= (1-s_2)P_{i+2} + s_2 P_{i+k+2}; \\ P'_{i+k} &= (1-t_3)P_{i+k+1} + t_3 P_{i+2k+1}; & P'_{i+k+1} &= (1-s_3)P_{i+k+1} + s_3 P_{i+2k+1}, \end{aligned} \tag{12}$$

where $s_1, s_2, s_3 \in (0,1)$ and $t_1, t_2, t_3 \in (1, \infty)$. We can see that $P'_{i+k} \notin P'_i P'_{i+1}$, so the three points P'_i, P'_{i+1}, P'_{i+k} are in general position.

A very similar computation as Equation (10) shows positivity of $(P'_i, P'_{i+1}, P'_{i+2})$, so we will omit it. Next, let $r_1 = \frac{t_1 - 1}{t_1 - s_1}$ and $r_2 = \frac{s_3}{t_3}$. Notice that $(1-r_2)(1-r_1)$, $(1-r_2)r_1$, and r_2 are all in $(0,1)$ and sum up to 1. Also, Equation (12) implies

$$P'_{i+k+1} = (1-r_2)(1-r_1)P'_i + (1-r_2)r_1 P'_{i+1} + r_2 P'_{i+k}.$$

This shows $P'_{i+k+1} \in \mathrm{int}(P'_i, P'_{i+1}, P'_{i+k})$. Finally, positivity of $(P'_i.P'_{i+1}, P'_{i+k})$ follows from a similar computation as Equation (11), $P'_{i+k+1} \in \mathrm{int}(P'_i, P'_{i+1}, P'_{i+k})$, the points P'_i, P'_{i+1}, P'_{i+k} are in general position, and Proposition 2.2. □

3.4 Invariance of Backward Orbit

In this section, we complete the proof of Theorem 1.1 by showing that $\mathcal{S}^{\alpha}_{k,n}$ and $\mathcal{S}^{\beta}_{k,n}$ are T_k^{-1}-invariant. One can derive a formula for T_k^{-1} from Equation (1). Given any k-nice twisted n-gon P', $P = T_k^{-1}(P')$ is given by

$$P_i = P'_{i-k-1}P'_{i-k} \cap P'_{i-1}P'_i. \tag{13}$$

Proposition 3.8 implies T_k^{-1} is well-defined on $\mathcal{S}^{\alpha}_{k,n}$ and $\mathcal{S}^{\beta}_{k,n}$. In general, T_k^{-1} needs not preserve k-niceness of twisted polygons.

Proposition 3.20. *For all $k \geq 2$ and $n \geq 2$, $T_k^{-1}(S^{\alpha}_{k,n}) \subset S^{\alpha}_{k,n}$.*

Proof. Given P' a type-α N-representative, we will show that $P = T_k^{-1}(P')$ is a type-α $(N+k+1)$-representative by proving that for all $i \geq N+k+1$, (P_i, P_{i+1}, P_{i+2}) is positive,

$(P_i, P_{i+1}, P_{i+k+1})$ is positive, the four points $P_i, P_{i+1}, P_{i+k}, P_{i+k+1}$ are in general position, and $P_{i+k} \in \operatorname{int}(P_i, P_{i+1}, P_{i+k+1})$. See the left side of Figure 16 for configurations of relevant vertices of P' and P.

Let $i \geq N + k + 1$ be fixed. Since P' is a type-α N-representative, we must have $P'_{j+k} \in \operatorname{int}(P'_j, P'_{j+1}, P'_{j+k+1})$ for all $j \geq N$. Applying Lemma 3.17 with Equation (13) on P_j for $j \in \{i, i+1, i+2, i+k, i+k+1\}$ gives us

$$\begin{aligned}
&P_i = (1-s_1)P'_{i-k} + s_1 P'_{i-k-1}; && P_i = (1-t_1)P'_i + t_1 P'_{i-1};\\
&P_{i+1} = (1-s_2)P'_{i-k+1} + s_2 P'_{i-k}; && P_{i+1} = (1-t_2)P'_{i+1} + t_3 P'_i;\\
&P_{i+2} = (1-s_3)P'_{i-k+2} + s_3 P'_{i-k+1}; && P_{i+k} = (1-s_4)P'_i + s_4 P'_{i-1};\\
&P_{i+k+1} = (1-s_5)P'_{i+1} + s_5 P'_i,
\end{aligned} \tag{14}$$

where $s_1, s_2, s_3, s_4, s_5 \in (0,1)$ and $t_1, t_2 \in (1, \infty)$.

We first show that $(P_i, P_{i+1}, P_{i+k+1})$ is positive. From Equation (14) we have

$$\mathcal{O}(P_i, P_{i+1}, P_{i+k+1}) = (t_1 t_2 (1-s_5) - t_1(1-t_2)s_5)\mathcal{O}(P'_{i-1}, P'_i, P'_{i+1}).$$

It follows that $\mathcal{O}(P_i, P_{i+1}, P_{i+k+1}) > 0$, so $(P_i, P_{i+1}, P_{i+k+1})$ is positive.

Next, we show that $P_{i+k} \in \operatorname{int}(P_i, P_{i+1}, P_{i+k+1})$. Let $r_1 = \frac{t_2 - 1}{t_2 - s_5}$ and $r_2 = \frac{s_4}{t_1}$. Equation (14) implies $r_1, r_2 \in (0,1)$ and

$$P_{i+k} = (1-r_2)(1-r_1)P_{i+1} + (1-r_2)r_1 P_{i+k+1} + r_2 P_i.$$

Observe that the coefficients $(1-r_2)(1-r_1)$, $(1-r_2)r_1$, and r_2 are all in $(0,1)$ and sum up to 1, so $P_{i+k} \in \operatorname{int}(P_i, P_{i+1}, P_{i+k+1})$.

Finally, we check (P_i, P_{i+1}, P_{i+2}) is positive. We aim to invoke Lemma 3.14 with the following choices of vertices:

$$O = P_{i+1};\ \ A = P_i;\ \ B = P_{i+k+1};\ \ C = P_{i+2};\ \ D = P'_{i-k+1}. \tag{15}$$

Positivity of (A, O, B) is a direct consequence of the above argument. Positivity of (B, O, C) follows from positivity of $(P_{i+1}, P_{i+2}, P_{i+k+2})$, $P_{i+k+1} \in \operatorname{int}(P_{i+1}, P_{i+2}, P_{i+k+2})$, and Proposition

2.2. Next, observe that

$$\begin{aligned}
\mathcal{O}(A,O,D) &= s_1 s_2 \mathcal{O}(P'_{i-k-1}, P'_{i-k}, P'_{i-k+1});\\
\mathcal{O}(C,O,D) &= (1-s_3) s_2 \mathcal{O}(P'_{i-k}, P'_{i-k+1}, P'_{i-k+2});\\
\mathcal{O}(B,O,D) &= s_2(1-s_5)\mathcal{O}(P'_{i-k}, P'_{i-k+1}, P'_{i+1}) + s_2 s_5 \mathcal{O}(P'_{i-k}, P'_{i-k+1}, P'_i);
\end{aligned} \tag{16}$$

Then, positivity of (A,O,D) and (C,O,D) follows from positivity of $(P'_{i-k-1}, P'_{i-k}, P'_{i-k+1})$ and $(P'_{i-k}, P'_{i-k+1}, P'_{i-k+2})$. To see that (B,O,D) is positive, apply Proposition 2.2 on $(P'_{i-k}, P'_{i-k+1}, P'_{i+1})$ positive and $P'_i \in \mathrm{int}(P'_{i-k}, P'_{i-k+1}, P'_{i+1})$ to get $(P'_{i-k}, P'_{i-k+1}, P'_i)$ positive. The backward direction of Lemma 3.14 then implies (P_i, P_{i+1}, P_{i+2}) is positive. We conclude that P is a type-α $(N+k+1)$-representative. □

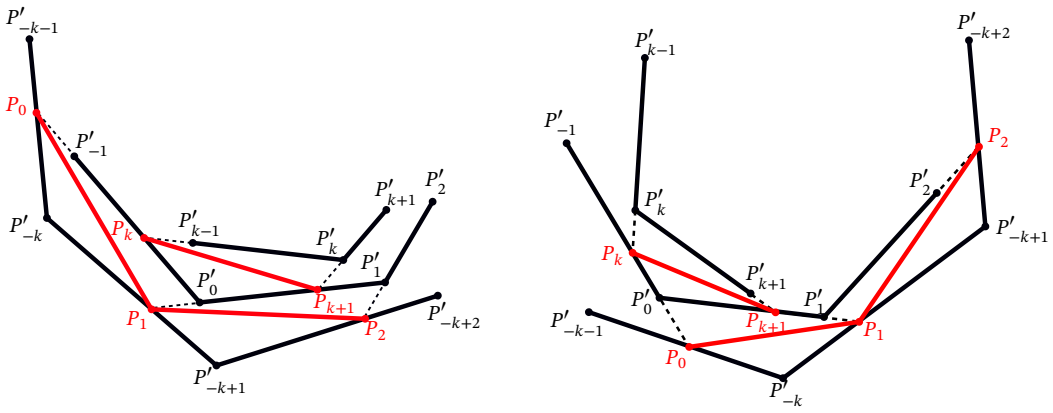

Figure 16: Left: Proposition 3.20 configuration. Right: Proposition 3.21 configuration.

Proposition 3.21. *For all $k \geq 2$ and $n \geq 2$, $T_k^{-1}(S^{\beta}_{k,n}) \subset S^{\beta}_{k,n}$.*

Proof. The proof is similar to that of Lemma 3.20 (See right side of Figure 16). We will point out some key differences. Replacing α with β, we may work with the setup in the proof of Proposition 3.20. Applying Lemma 3.17 with (13) on P_j for $j \in \{i, i+1, i+2, i+k, i+k+1\}$

gives us

$$\begin{aligned} P_i &= (1-s_1)P'_{i-k} + s_1 P'_{i-k-1}; & P_i &= (1-t_1)P'_{i-1} + t_1 P'_i; \\ P_{i+1} &= (1-s_2)P'_{i-k+1} + s_2 P'_{i-k}; & P_{i+1} &= (1-t_2)P'_i + t_3 P'_{i+1}; \\ P_{i+2} &= (1-s_3)P'_{i-k+2} + s_3 P'_{i-k+1}; & P_{i+k} &= (1-s_4)P'_{i-1} + s_4 P'_i; \\ P_{i+k+1} &= (1-s_5)P'_i + s_5 P'_{i+1}, \end{aligned} \tag{17}$$

where $s_1, s_2, s_3, s_4, s_5 \in (0,1)$ and $t_1, t_2 \in (1,\infty)$. Positivity of (P_i, P_{i+1}, P_{i+k}) follows from a similar computation as in (3.4). Next, let $r_1 = \frac{1-s_4}{t_1-s_4}$ and $r_2 = \frac{s_5}{t_2}$. Equation (17) implies

$$P_{i+k+1} = (1-r_2)(1-r_1)P_{i+k} + (1-r_2)r_1 P_i + r_2 P_{i+1}.$$

Observe that the coefficients $(1-r_2)(1-r_1)$, $(1-r_2)r_1$, and r_2 are all in $(0,1)$ and sum up to 1, so $P_{i+k+1} \in \operatorname{int}(P_i, P_{i+1}, P_{i+k})$.

Finally, assign O, A, B, C, D to be the same vertices as in (15). Positivity of (A,O,B), (B,O,C), (C,O,D), (A,O,D), and (B,O,D) follows from a very similar proof as that of Proposition 3.20, with (16) replaced by

$$\begin{aligned} \mathcal{O}(A,O,D) &= s_1 s_2 \mathcal{O}(P'_{i-k-1}, P'_{i-k}, P'_{i-k+1}); \\ \mathcal{O}(C,O,D) &= (1-s_3)s_2 \mathcal{O}(P'_{i-k}, P'_{i-k+1}, P'_{i-k+2}); \\ \mathcal{O}(B,O,D) &= s_2(1-s_5)\mathcal{O}(P'_{i-k}, P'_{i-k+1}, P'_i) + s_2 s_5 \mathcal{O}(P'_{i-k}, P'_{i-k+1}, P'_{i+1}). \end{aligned}$$

The backward direction of Proposition 3.14 then implies (P_i, P_{i+1}, P_{i+2}) is positive. □

We conclude this section by stating that Proposition 3.18, 3.19, 3.20, 3.21 together prove Theorem 1.1.

4 Coordinate Representation of 3-Spirals

4.1 The Tic-Tac-Toe Grids

Recall the intervals $I = (-\infty, 0)$, $J = (0,1)$, $K = (1,\infty)$ from §1.3. One can partition $\mathbb{R}^2$ into a 3×3 grid. See Figure 5. We make the following definition:

Definition 4.1. For $n \geq 2$, let $S_n(I,J)$ be the subset of $\mathcal{P}_n$ that satisfies the following: given $[P] \in S_n(I,J)$, for all $i \in \{0,\dots,n-1\}$, $(x_{2i}, x_{2i+1}) \in I \times J$. We similarly define $S_n(K,J)$, $S_n(J,I)$, and $S_n(J,K)$.

The following symmetries of the four grids follow directly from Definition 4.1.

Proposition 4.2. *For $i \in \mathbb{Z}$, define the map $\sigma_i : \mathbb{Z} \to \mathbb{Z}$ by $\sigma_i(x) = x + i$. Define the map $\iota : \mathbb{Z} \to \mathbb{Z}$ by $\iota(x) = -x$. Given $[P] \in \mathcal{P}_n$, the following are true:*

- *If $[P] \in S_n(I,J)$, then $[P \circ \sigma_i] \in S_n(I,J)$ for all $i \in \mathbb{Z}$. This also holds for $S_n(K,J)$, $S_n(J,I)$, and $S_n(J,K)$.*
- *$[P] \in S_n(I,J)$ if and only if $[P \circ \iota] \in S_n(J,I)$.*
- *$[P] \in S_n(K,J)$ if and only if $[P \circ \iota] \in S_n(J,K)$.*

To understand the geometry implied by the corner invariants, we need to examine what happens when the corner invariants take value from $0, 1, \infty$.

Proposition 4.3. *For all $[P] \in \mathcal{P}_n$ with corner invariants $x_j = x_j(P)$ and $i \in \mathbb{Z}$, we have the following correspondence between the position of P_{i+2} and the values of x_{2i} and x_{2i+1}:*

Configuration	*Coordinates*	*Configuration*	*Coordinates*
$P_{i+2} \in P_{i+1}P_i$	$x_{2i} = 0$	$P_{i+2} \in P_{i-1}P_{i+1}$	$x_{2i+1} = 0$
$P_{i+2} \in P_{i+1}P_{i-2}$	$x_{2i} = 1$	$P_{i+2} \in P_{i-1}P_{i-2}$	$x_{2i+1} = 1$
$P_{i+2} \in P_{i+1}P_{i-1}$	$x_{2i} = \infty$	$P_{i+2} \in P_{i-1}P_i$	$x_{2i+1} = \infty$

Proof. Consider the following lines:

$$l_1 = P_{i+1}P_{i-2}; \quad l_2 = P_{i+1}P_{i-1}; \quad l_3 = P_{i+1}P_i; \quad l_4 = P_{i+1}P_{i+2};$$
$$m_1 = P_{i-1}P_{i+2}; \quad m_2 = P_{i-1}P_{i+1}; \quad m_3 = P_{i-1}P_i; \quad m_4 = P_{i-1}P_{i-2}.$$

See Figure 17 for a visualization of the configurations of points and lines. Equation (8) implies $x_{2i} = \chi(l_1, l_2, l_3, l_4)$ and $x_{2i+1} = \chi(m_1, m_2, m_3, m_4)$. This yields

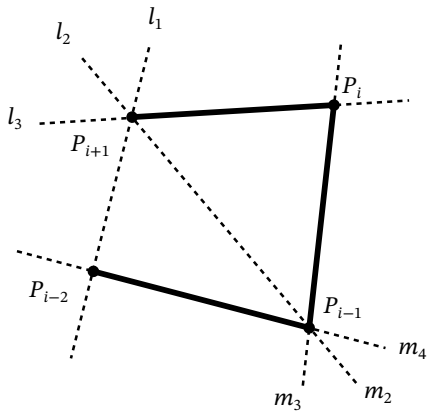

Figure 17: Configurations of points and lines in the proof of Proposition 4.3.

Configuration	Lines	Coordinates	Configuration	Lines	Coordinates
$P_{i+2} \in P_{i+1}P_i$	$l_4 = l_3$	$x_{2i} = 0$	$P_{i+2} \in P_{i-1}P_{i+1}$	$m_1 = m_2$	$x_{2i+1} = 0$
$P_{i+2} \in P_{i+1}P_{i-2}$	$l_4 = l_1$	$x_{2i} = 1$	$P_{i+2} \in P_{i-1}P_{i-2}$	$m_1 = m_4$	$x_{2i+1} = 1$
$P_{i+2} \in P_{i+1}P_{i-1}$	$l_4 = l_2$	$x_{2i} = \infty$	$P_{i+2} \in P_{i-1}P_i$	$m_1 = m_3$	$x_{2i+1} = \infty$

which is precisely the relationship described in the proposition. □

Remark 4.4. Proposition 4.3 also gives us a way to determine the position of P_{i+2} when neither x_{2i} nor x_{2i+1} takes value in $0, 1, \infty$. Suppose the four points $P_{i-2}, P_{i-1}, P_i, P_{i+1}$ are in general position. For $i, j, k \in \{1, 2, 3\}$ distinct, we define $U_{i,j}$ to be the connected component of $\mathbb{RP}^2 - (l_i \cup l_j)$ that does not intersect l_k. For $i, j, k \in \{2, 3, 4\}$ distinct, we define $V_{i,j}$ to be the connected component of $\mathbb{RP}^2 - (m_i \cup m_j)$ that does not intersect m_k. See Figure 18 for a visualization of the $U_{i,j}$'s and $V_{i,j}$'s using the point configurations given in Figure 17. By Proposition 4.3 and continuity of χ, we have the following:

Configuration	Coordinates	Configuration	Coordinates
$P_{i+2} \in U_{2,3}$	$x_{2i} = I$	$P_{i+2} \in V_{2,3}$	$x_{2i+1} = I$
$P_{i+2} \in U_{1,3}$	$x_{2i} = J$	$P_{i+2} \in V_{2,4}$	$x_{2i+1} = J$
$P_{i+2} \in U_{1,2}$	$x_{2i} = K$	$P_{i+2} \in V_{3,4}$	$x_{2i+1} = K$

Corollary 4.5. *Given $[P] \in \mathcal{P}_n$ with corner invariants $x_j = x_j(P)$, if $x_j \notin \{0, 1, \infty\}$ for all j, then P is 3-nice. Moreover, every four consecutive points of P are in general position.*

Proof. Using Proposition 4.3 we may check that

Collinearity	Coordinates	Collinearity	Coordinates
$P_{i-2}, P_{i-1}, P_{i+1}$	$x_{2i-1} = \infty$	P_{i-1}, P_i, P_{i+2}	$x_{2i+1} = \infty$
$P_{i-2}, P_{i-1}, P_{i+2}$	$x_{2i+1} = 1$	$P_{i-1}, P_{i+1}, P_{i+2}$	$x_{2i+1} = 0$
$P_{i-2}, P_{i+1}, P_{i+2}$	$x_{2i} = 1$	P_i, P_{i+1}, P_{i+2}	$x_{2i} = 0$
P_{i-1}, P_i, P_{i+1}	$x_{2i-2} = 0$		

All seven cases contradict the assumption in the corollary. Therefore, the four points $P_{i-2}, P_{i-1}, P_{i+1}, P_{i+2}$ are in general position, and the four consecutive points $P_{i-1}, P_i, P_{i+1}, P_{i+2}$ are in general position for all $i \in \mathbb{Z}$. This shows P is 3-nice, and every four consecutive points of P are in general position. □

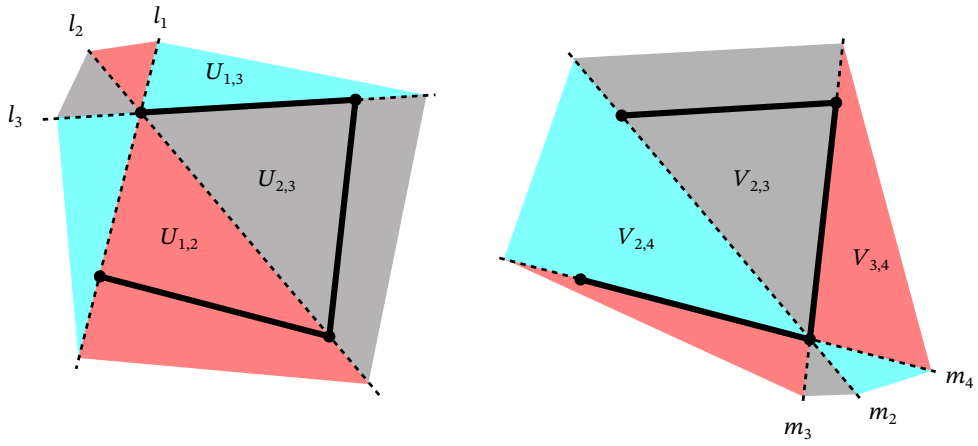

Figure 18: The connected components $U_{i,j}$'s and $V_{i,j}$'s in Remark 4.4. The corner invariants value in I if P_{i+2} lies in the black-shaded region, J if P_{i+2} lies in the red-shaded region, and K if P_{i+2} lies in the cyan-shaded region.

Our goal of this section is to prove the following correspondence theorem:

Theorem 4.6. *For all $n \geq 2$, $\mathcal{S}^{\alpha}_{3,n} = S_n(J,I)$, $\mathcal{S}^{\beta}_{3,n} = S_n(K,J)$.*

This theorem immediately produces the following important corollary.

Corollary 4.7. *For all $n \geq 2$, the four cells $S_n(I,J)$, $S_n(K,J)$, $S_n(J,I)$, $S_n(J,K)$ are both forward and backward invariant under T_3.*

Proof. The case $S_n(J,I)$ and $S_n(K,J)$ follows immediately from Theorem 1.1 and 4.6. We will prove the case $S_n(I,J)$. The case $S_n(J,K)$ is completely analogous, so we will omit.

Fix $[P] \in S_n(I,J)$. Recall the maps σ_i and ι from Proposition 4.2. Equation (1) implies $T_3(P \circ \iota) = T_3(P) \circ \iota \circ \sigma_4$. Then, Proposition 4.2 implies $[P \circ \iota] \in S_n(J,I)$, so $[T_3(P \circ \iota)] \in S_n(J,I)$. Finally, observe that

$$T_3(P) = (T_3(P) \circ \iota \circ \sigma_4) \circ (\sigma_{-4} \circ \iota) = T_3(P \circ \iota) \circ (\sigma_{-4} \circ \iota).$$

It follows that $[T_3(P)] \in S_n(I,J)$. We omit the proof of $[T_3^{-1}(P)] \in S_n(I,J)$. □

4.2 The Correspondence of $\mathcal{S}^{\alpha}_{3,n}$ and $S_n(J,I)$

Here we show that $\mathcal{S}^{\alpha}_{3,n}$ is equivalent to $S_n(J,I)$. We will first show that the corner invariants of a 0-representative P of some $[P] \in \mathcal{S}^{\alpha}_{3,n}$ satisfies $S_n(J,I)$. Then, we will show that we can find type-α N-representatives for all $N \in \mathbb{Z}$ given any $[P] \in S_n(J,I)$.

Lemma 4.8. *If P is an N-representative of $[P] \in \mathcal{S}^{\alpha}_{3,n}$, then $P_{i+2} \in \operatorname{int}(P_{i-1}, P_i, P_{i+1})$ for all $i > N+1$.*

Proof. Since (P_{i-1}, P_i, P_{i+1}) is positive, we may normalize with $\mathrm{Aff}_2^+(\mathbb{R})$ so that $P_{i-1} = (-1,0)$, $P_i = (0,0)$, and $P_{i+1} = (0,1)$. Let $P_{i+2} = (x,y)$. It suffices to show that $x < 0$, $y > 0$, and $y - x < 1$. We get $x < 0$ from positivity of (P_i, P_{i+1}, P_{i+2}), and we get $y > 0$ from positivity of (P_{i-1}, P_i, P_{i+2}). Finally, since $(P_{i-2}, P_{i-1}, P_{i+2})$ is positive and $P_{i+1} \in \operatorname{int}(P_{i-2}, P_{i-1}, P_{i+2})$, Proposition 2.2 implies $(P_{i+1}, P_{i-1}, P_{i+2})$ is positive, which gives us $y - x < 1$ as desired. □

Proposition 4.9. *For all $n \geq 2$, $\mathcal{S}^{\alpha}_{3,n} \subset S_n(J,I)$.*

Proof. Fix $i \in \mathbb{Z}$. Let P be an $(i-3)$-representative of $[P] \in \mathcal{S}^{\alpha}_{3,n}$ with corner invariants $x_j = x_j(P)$. Normalize with $\mathrm{Aff}^+_2(\mathbb{R})$ so that $P_{i-1} = (-1,0)$, $P_i = (0,0)$, and $P_{i+1} = (0,1)$. Let $s_{a,b}$ denote the slope of the line $P_{i+a}P_{i+b}$. See Figure 19 for the configuration of points.

We want to show that $(x_{2i}, x_{2i+1}) \in I \times J$. By Lemma 4.8, $P_{i+1} \in \mathrm{int}(P_{i-2}, P_{i-1}, P_i)$. This implies $s_{1,-2} > s_{-1,-2} > 1$. On the other hand, since $P_{i+1} \in \mathrm{int}(P_{i-2}, P_{i-1}, P_{i+2})$, we have $s_{1,2} > s_{1,-2} > 1$, and $s_{-1,2} \in (0,1)$. This gives us

$$x_{2i} = \frac{(s_{1,-2} - s_{1,-1})(s_{1,0} - s_{1,2})}{(s_{1,-2} - s_{1,0})(s_{1,-1} - s_{1,2})} = \frac{s_{1,-2} - 1}{s_{1,2} - 1} \in J \qquad \text{and}$$
$$x_{2i+1} = \frac{(s_{-1,2} - s_{-1,1})(s_{-1,0} - s_{-1,-2})}{(s_{-1,2} - s_{-1,0})(s_{-1,1} - s_{-1,-2})} = \frac{s_{-1,-2}(s_{-1,2} - 1)}{s_{-1,2}(s_{-1,-2} - 1)} \in I.$$

This concludes the proof. □

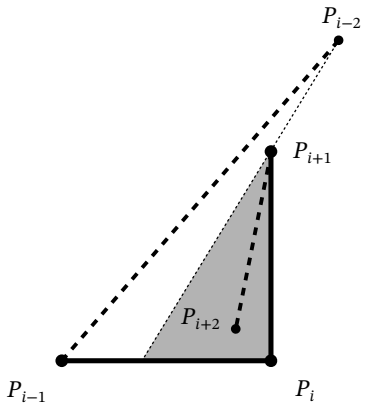

Figure 19: Configuration of Proposition 4.9 and 4.10.

Proposition 4.10. *For all $n \geq 2$, $\mathcal{S}^{\alpha}_{3,n} = S_n(I,J)$.*

Proof. Proposition 4.9 implies we only need to show $\mathcal{S}^{\alpha}_{3,n} \supset S_n(I,J)$. Given $[P] \in S_n(I,J)$, let P be a representative that satisfies $P_{-1} = (1,4)$, $P_0 = (-1,0)$, $P_1 = (0,0)$, $P_2 = (0,1)$. Say that P satisfies condition $(*)_i$ if the three triangles (P_{i-1}, P_i, P_{i+1}), (P_i, P_{i+1}, P_{i+2}), (P_{i-1}, P_i, P_{i+2}) are all positive, $P_{i+2} \in \mathrm{int}(P_{i-1}, P_i, P_{i+1})$, and $P_{i+2} \in \mathrm{int}(P_{i-2}, P_{i-1}, P_{i+1})$.

We show that for all $i > 0$, if P satisfies $(*)_{i-1}$, then P satisfies $(*)_i$. Since (P_{i-1}, P_i, P_{i+1}) is positive, we can normalize with $\mathrm{Aff}^+_2(\mathbb{R})$ so that $P_{i-1} = (-1,0)$, $P_i = (0,0)$, and $P_{i+1} =$

$(0,1)$. Let $s_{a,b}$ denote the slope of $P_{i+a}P_{i+b}$. Since $P_{i+1} \in \operatorname{int}(P_{i-2}, P_{i-1}, P_i)$, we know that $s_{1,-2} > s_{-1,-2} > 1$. Then, $x_{2i} \in J$ implies $0 < \frac{s_{1,-2}-1}{s_{1,2}-1} < 1$. This gives us $s_{1,2} > s_{1,-2} > 1$. On the other hand, $x_{2i+1} \in I$ implies $\frac{s_{-1,-2}(s_{-1,2}-1)}{s_{-1,2}(s_{-1,-2}-1)} < 0$. Since $s_{-1,-2} > 1$, this is equivalent to $1 - \frac{1}{s_{-1,2}} < 0$, which implies $s_{-1,2} \in (0,1)$. Thus, the two lines $P_{i-1}P_{i+2}$ and $P_{i+1}P_{i+2}$ must meet in the shaded triangle in Figure 19, which implies (P_i, P_{i+1}, P_{i+2}), (P_{i-1}, P_i, P_{i+2}) are positive, $P_{i+2} \in \operatorname{int}(P_{i-1}, P_i, P_{i+1})$, and $P_{i+2} \in \operatorname{int}(P_{i-2}, P_{i-1}, P_{i+1})$, so P satisfies $(*)_i$. Finally, since P clearly satisfies $(*)_0$, by induction P satisfies $(*)_i$ for all $i \geq 0$, so P is a type-α 0-representative of a 3-spiral. We conclude that $[P] \in \mathcal{S}^{\alpha}_{3,n}$. □

4.3 The Correspondence of $\mathcal{S}^{\beta}_{3,n}$ and $S_n(K,J)$

Here we show that $\mathcal{S}^{\beta}_{3,n}$ is equivalent to $S_n(K,J)$. The ideas behind the proofs are essentially the same as the ones in §4.2. We will focus on explaining how to modify the details of the proofs in §4.2 for type-β 3-spirals and $S_n(K,J)$.

Lemma 4.11. *If P is an N-representative of $[P] \in \mathcal{S}^{\beta}_{3,n}$, then the quadrilateral joined by vertices $(P_i, P_{i+1}, P_{i+2}, P_{i+3})$ is convex for all $i > N$.*

Proof. Normalize with $\operatorname{Aff}_2^+(\mathbb{R})$ so that $P_i = (-1,0)$, $P_{i+1} = (0,0)$, $P_{i+2} = (0,1)$, and $P_{i+3} = (x,y)$. Positivity of $(P_{i+1}, P_{i+2}, P_{i+3})$ and (P_i, P_{i+1}, P_{i+3}) implies $x < 0$ and $y > 0$. Positivity of (P_{i-1}, P_i, P_{i+2}), $P_{i+3} \in \operatorname{int}(P_{i-1}, P_i, P_{i+2})$, and Proposition 2.2 shows $y - x > 1$. □

Proposition 4.12. *For all $n \geq 2$, $\mathcal{S}^{\beta}_{3,n} \subset S_n(K,J)$.*

Proof. Let P be a (-3)-representative of $[P] \in \mathcal{S}^{\beta}_{3,n}$ with corner invariants $x_j = x_j(P)$. Lemma 4.11 implies the quadrilateral $(P_{i-2}, P_{i-1}, P_i, P_{i+1})$ is convex. Next, since P is a type-β (-3)-representative, $P_i \in \operatorname{int}(P_{i-2}, P_{i-1}, P_{i+1})$ for all $i \geq 0$ (See Figure 20). Referring back to Remark 4.4, convexity of $(P_{i-2}, P_{i-1}, P_i, P_{i+1})$ implies P_iP_{i+1} doesn't go through $P_{i-2}, P_{i-1}, P_{i+1}$, so $(x_{2i}, x_{2i+1}) \in K \times J$ whenever $P_{i+2} \in \operatorname{int}(P_{i-2}, P_{i-1}, P_{i+1})$. □

Lemma 4.13. *Given a 3-nice sequence $P : \mathbb{Z} \to \mathbb{RP}^2$ and an integer $i \in \mathbb{Z}$, let $x_{2i} = x_{2i}(P)$ and $x_{2i+1} = x_{2i+1}(P)$ be the corner invariants of P. If the following conditions are true:*

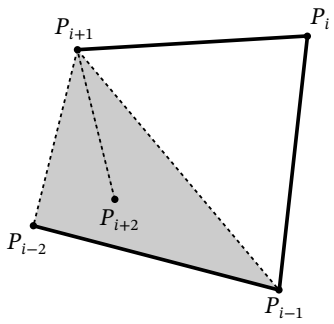

Figure 20: Configuration of Proposition 4.12 and Lemma 4.13.

- (P_{i-2}, P_{i-1}, P_i) *and* (P_{i-1}, P_i, P_{i+1}) *are both positive;*
- *The quadrilateral* $(P_{i-2}, P_{i-1}, P_i, P_{i+1})$ *is convex;*
- $(x_{2i}, x_{2i+1}) \in K \times J$.

Then, the following hold:

- $P_{i+2} \in \operatorname{int}(P_{i-2}, P_{i-1}, P_{i+1})$*;*
- *The quadrilateral* $(P_{i-1}, P_i, P_{i+1}, P_{i+2})$ *is convex;*
- (P_i, P_{i+1}, P_{i+2}) *and* (P_{i-1}, P_i, P_{i+2}) *are both positive.*

Proof. Recall that from the proof of Proposition 4.12, we claimed that if the quadrilateral $(P_{i-2}, P_{i-1}, P_i, P_{i+1})$ is convex, then the line P_iP_{i+1} doesn't go through $(P_{i-2}, P_{i-1}, P_{i+1})$. Since $(x_{2i}, x_{2i+1}) \in K \times J$, Remark 4.4 implies $P_{i+2} \in \operatorname{int}(P_{i-2}, P_{i-1}, P_{i+1})$, in which case all conclusions of this lemma will hold. See Figure 20 for a visualization of the five points. □

Proposition 4.14. $\mathcal{S}^{\beta}_{3,n} = S_n(K, J)$.

Proof. Proposition 4.12 gives us $\mathcal{S}^{\beta}_{3,n} \subset S_n(K, J)$, so we show the other containment. Given $[P] \in S_n(K, J)$, we can find a representative P that satisfies $P_N = (0, 0)$, $P_{N+1} = (1, 0)$, $P_{N+2} = (1, 1)$, $P_{N+3} = (0, 1)$. Corollary 4.5 shows that P is 3-nice. To see that (P_i, P_{i+1}, P_{i+2}), (P_i, P_{i+1}, P_{i+3}) are positive, and $P_{i+4} \in \operatorname{int}(P_i, P_{i+1}, P_{i+3})$, we may inductively apply Lemma 4.13. This implies $[P] \in \mathcal{S}^{\beta}_{3,n}$. □

5 A Birational Formula for T_3

Given two spaces X and Y, a *rational map* $f : X \dashrightarrow Y$ is an equivalence class of maps $f_U : U \to Y$ where U is a dense open in X, and the equivalence relation is given by $f_U \sim f_V$ if they restrict to the same map on $U \cap V$. A map $f : X \dashrightarrow Y$ is *birational* if there exists a rational map $g : Y \dashrightarrow X$ such that $g \circ f$ restricts to the identity on a dense open of X and $f \circ g$ restricts to an identity on a dense open of Y.

In this section, we show that $T_3 : \mathcal{P}_n \dashrightarrow \mathcal{P}_n$ is a birational map by finding an explicit formula using the corner invariants.

5.1 The Formula

Let P be a twisted n-gon, and $P' = T_3(P)$. In this section, we use a different labeling convention:

$$P'_i = P_{i-2}P_{i+1} \cap P_{i-1}P_{i+2}. \tag{18}$$

We let $x_j = x_j(P)$ and $x'_j = x_j(P')$ denote the corner invariants of P and P' respectively. Our goal is to show that T_3 is a birational map over the corner invariants. I discovered it using computer algebra and the reconstruction formula in [Sch08, Equation (19)].

Proposition 5.1. *Given* $[P] \in \mathcal{P}_{3,n}$*, the following formula holds* (*indices taken modulo* $2n$)*:*

$$\begin{cases} x'_{2i} = x_{2i-2} \cdot \dfrac{(x_{2i-4} + x_{2i-1} - 1)}{x_{2i-2}x_{2i-1} - (1 - x_{2i+1})(1 - x_{2i-4})}; \\ x'_{2i+1} = x_{2i+3} \cdot \dfrac{(x_{2i+2} + x_{2i+5} - 1)}{x_{2i+2}x_{2i+3} - (1 - x_{2i+5})(1 - x_{2i})}. \end{cases} \tag{19}$$

One can verify Equation (19) with the following procedure: Given the corner invariants of $[P]$, use the reconstruction formula from [Sch08, Equation (19)] to obtain a representative P. Apply T_3 on P as in Equation (18) to get $P' = T_3(P)$. Then, compute the corner invariants of P'. We present a geometric proof of Equation (19) using cross-ratio identities. We start with the following lemma, which is a classical observation in projective geometry called "quadrangular sets."

Lemma 5.2. *Let Q_1, Q_2, Q_3, Q_4 be four points in general position, and let ω be a line that contains none of the four points. For all $i \neq j$, let $l_{ij} = Q_iQ_j$ and $S_{ij} = \omega \cap l_{ij}$ Then,*

$$\chi(S_{12}, S_{13}, S_{14}, S_{24}) = \chi(S_{23}, S_{13}, S_{34}, S_{24}).$$

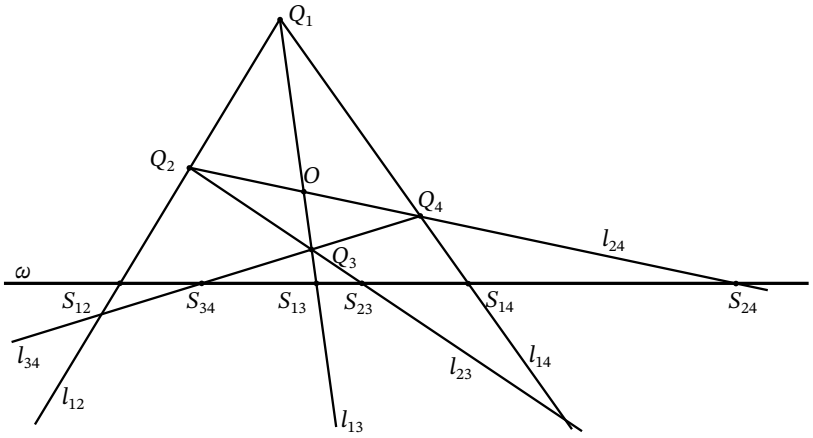

Figure 21: Point configurations of Lemma 5.2

Proof. Let $O = l_{13} \cap l_{24}$. See Figure 21 for an example of the point configurations. Applying Equation (6) on $(l_{12}, l_{13}, l_{14}, Q_1D)$ with respect to ω and Q_2Q_4 gives us

$$\chi(S_{12}, S_{13}, S_{14}, S_{24}) \overset{\omega}{=} \chi(l_{12}, l_{13}, l_{14}, Q_1D) \overset{l_{24}}{=} \chi(Q_2, O, Q_4, S_{24}).$$

Next, applying Equation (6) twice on $(l_{23}, l_{13}, l_{34}, Q_3D)$ with respect to l_{24} and ω gives us

$$\chi(Q_2, O, Q_4, S_{24}) \overset{l_{24}}{=} \chi(l_{23}, l_{13}, l_{34}, Q_3D) \overset{\omega}{=} \chi(S_{23}, S_{13}, S_{34}, S_{24}).$$

Combining the above two equations completes the proof. □

Proof of Proposition 5.1. From the symmetry of Equation (19), it suffices to prove the formula for x_0'. That is,

$$x_0' = \frac{x_{-2}(x_{-4} + x_{-1} - 1)}{x_{-2}x_{-1} - (1 - x_{-4})(1 - x_1)}. \tag{20}$$

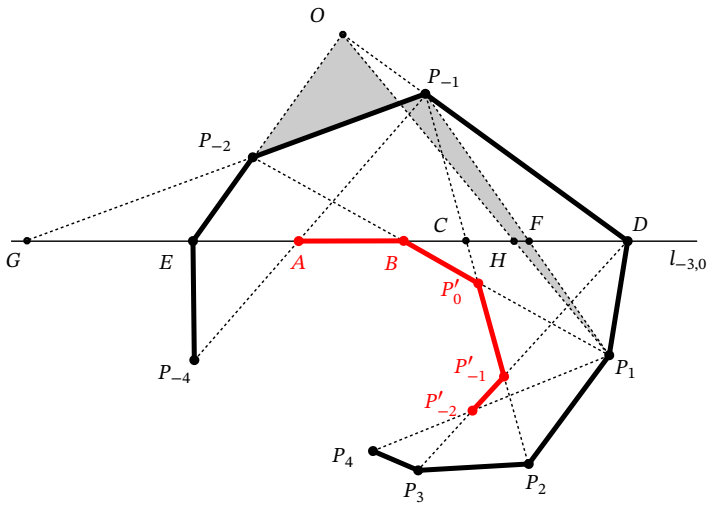

Figure 22: Visualization of Points Assigned in Equation (21). The thick black line segments are edges connecting vertices of P, and the thick red line segments are edges connecting vertices of P'.

Let $l_{i,j} = P_iP_j$ and $O = l_{-3,-2} \cap l_{-1,0}$. We label points as follows:

$$\begin{aligned} A &= P'_{-2}; & C &= l_{-3,0} \cap l_{-2,1}; & E &= P_{-3}; & G &= l_{-3,0} \cap l_{-2,-1}; \\ B &= P'_{-1}; & D &= P_0; & F &= l_{-3,0} \cap l_{-1,1}; & H &= l_{-3,0} \cap OP_1. \end{aligned} \tag{21}$$

Since $[P] \in \mathcal{P}_{3,n}$, every five consecutive points of $[P]$ are in general position. This ensures that point O and the points in Equation (21) are all distinct. See Figure 22 for a visualization of the assignment of labels to these points.

It follows from Equation (7) that $x'_0 = \chi(A, B, C, D)$. Using Equation (8), we have

$$\begin{aligned} x_{-4} &= \chi(l_{-1,-4}, l_{-1,-3}, l_{-1,-2}, l_{-1,0}) \overset{l_{-3,0}}{=} \chi(A, E, G, D); \\ x_{-2} &= \chi(l_{0,-3}, l_{0,-2}, l_{0,-1}, l_{0,1}) \overset{l_{-3,0}}{=} \chi(E, B, H, D); \\ x_{-1} &= \chi(l_{-2,1}, l_{-2,0}, l_{-2,-1}, l_{-2,-3}) \overset{l_{-3,0}}{=} \chi(B, D, G, E); \\ x_1 &= \chi(l_{-1,2}, l_{-1,1}, l_{-1,0}, l_{-1,-2}) \overset{l_{-3,0}}{=} \chi(C, F, D, G). \end{aligned} \tag{22}$$

We may further invoke Lemma 5.2 with $Q_1 = P_{-2}$, $Q_2 = O$, $Q_3 = P_1$, $Q_4 = P_{-1}$, and

$\omega = l_{-3,0}$. This gives us

$$x_{-2} = \chi(E, B, H, D) = \chi(G, B, F, D). \tag{23}$$

The rest of the proof is just algebraic verification. Normalize with a projective transformation so that $l_{-3,0}$ is the x-axis of $\mathbb{A}^2$. Let a, b, c, d, e, f, g, h be coordinates of A, B, C, D, E, F, G, H respectively. Plugging (22) and (23) into the numerator of (20) gives us

$$\begin{aligned} x_{-2}(x_{-4} + x_{-1} - 1) &= \chi(G, B, F, D)\,(\chi(A, E, G, D) + \chi(B, D, G, E) - 1) \\ &= \frac{(g-b)(f-d)}{(g-f)(b-d)}\left(\frac{(a-e)(g-d)}{(a-g)(e-d)} + \frac{(b-e)(g-d)}{(b-g)(e-d)}\right) \\ &= \frac{(a-b)(g-d)(e-g)(d-f)}{(a-g)(b-d)(e-d)(g-f)}. \end{aligned}$$

The denominator can be computed similarly. We skip the computation and list the results:

$$x_{-2}x_{-1} - (1 - x_{-4})(1 - x_1) = \frac{(a-c)(g-d)(d-f)(e-g)}{(a-g)(c-d)(d-e)(f-g)}.$$

Combining the above two equations gives us

$$\frac{x_{-2}(x_{-4} + x_{-1} - 1)}{x_{-2}x_{-1} - (1 - x_{-4})(1 - x_1)} = \frac{(a-b)(c-d)}{(a-c)(b-d)} = \chi(A, B, C, D) = x'_0,$$

which is precisely Equation (20). □

Next, we provide a formula for the inverse of T_3.

Proposition 5.3. *The map $T_3 : \mathcal{P}_n \dashrightarrow \mathcal{P}_n$ is birational. Its inverse is given by*

$$\begin{cases} x_{2i} = x'_{2i+2} \cdot \dfrac{(x'_{2i+4} + x'_{2i+1} - 1)}{x'_{2i+1}x'_{2i+2} - (1 - x'_{2i-1})(1 - x'_{2i+4})}; \\ x_{2i+1} = x'_{2i-1} \cdot \dfrac{(x'_{2i-3} + x'_{2i} - 1)}{x'_{2i}x'_{2i-1} - (1 - x'_{2i+2})(1 - x'_{2i-3})}. \end{cases} \tag{24}$$

We will give an algebraic proof. Consider two families of rational maps $\{\mu_{(s,t)} : \mathbb{R}^{2n} \dashrightarrow \mathbb{R}^{2n}\}_{(s,t)\in\mathbb{Z}^2}$ and $\{\nu_{(s,t)} : \mathbb{R}^{2n} \dashrightarrow \mathbb{R}^{2n}\}_{(s,t)\in\mathbb{Z}^2}$. Write $(a_0, \dots, a_{2n-1}) = \mu_{(s,t)}(x_0, \dots, x_{2n-1})$ and $(b_0, \dots, b_{2n-1}) = \nu_{(s,t)}(x_0, \dots, x_{2n-1})$. Then, we set

$$\begin{cases} a_{2i} = \dfrac{1 - x_{2i+s}}{x_{2i+s+t}} \\ a_{2i+1} = \dfrac{1 - x_{2i+1-s}}{x_{2i+1-s-t}}; \end{cases} \qquad \begin{cases} b_{2i} = \dfrac{1 - x_{2i+s}}{1 - x_{2i+s}x_{2i+s+t}} \\ b_{2i+1} = \dfrac{1 - x_{2i+1-s}}{1 - x_{2i+1-s}x_{2i+1-s-t}}. \end{cases} \tag{25}$$

Lemma 5.4. *Let $\varphi : \mathbb{Z}^2 \to \mathbb{Z}^2$ be the map given by*

$$\varphi(s,t) = ((-1)^{s+1}s,\ (-1)^s(2s+t)). \tag{26}$$

Then, φ is an involution. Moreover, when t is odd, $\mu_{(s,t)}^{-1} = \nu_{\varphi(s,t)}$ and $\nu_{(s,t)}^{-1} = \mu_{\varphi(s,t)}$.

Proof. To see φ is an involution, a direct computation shows that

$$\begin{aligned}\varphi^2(s,t) &= \varphi((-1)^{s+1}s,\ (-1)^s(2s+t)) \\ &= \Big((-1)^{(-1)^{s+1}s+s+2}s,\ (-1)^{(-1)^{s+1}s}\,(2(-1)^{s+1}s + (-1)^s(2s+t))\Big) = (s,t).\end{aligned}$$

Next, we show that when t is odd, $\mu_{(s,t)}^{-1} = \nu_{\varphi(s,t)}$. We will show by direct computation that $\mu_{(s,t)} \circ \nu_{\varphi(s,t)}$ is the identity on the $2i$-th coordinate when s is even. First, when s is even, $\varphi(s,t) = (-s, 2s+t)$. The $2i$-th coordinate of $\mu_{(s,t)} \circ \nu_{\varphi(s,t)}$ is given by

$$\begin{aligned}&\left(1 - \frac{1 - x_{2i+s+(-s)}}{1 - x_{2i+s+(-s)}x_{2i+s+(-s)+(2s+t)}}\right) \cdot \left(\frac{1 - x_{2i+s+t-(-s)}}{1 - x_{2i+s+t-(-s)}x_{2i+s+t-(-s)-(2s+t)}}\right)^{-1} \\ &= \left(1 - \frac{1 - x_{2i}}{1 - x_{2i}x_{2i+2s+t}}\right)\left(\frac{1 - x_{2i+2s+t}x_{2i}}{1 - x_{2i+2s+t}}\right) = x_{2i}.\end{aligned}$$

This is precisely what we want. One can similarly carry out the computation of $\nu_{\varphi(s,t)} \circ \mu_{s,t}$ for the $(2i+1)$-th coordinate, and s odd. We will omit these heavy computations and conclude that $\mu_{(s,t)}^{-1} = \nu_{\varphi(s,t)}$. Finally, to see $\nu_{(s,t)}^{-1} = \mu_{\varphi(s,t)}$, observe that $(-1)^s(2s+t)$ is odd iff t is odd. Therefore, $\nu_{s,t} \circ \mu_{\varphi(s,t)} = \nu_{\varphi^2(s,t)} \circ \mu_{\varphi(s,t)}$ is the identity map by the previous argument. The same argument shows that $\mu_{\varphi(s,t)} \circ \nu_{(s,t)}$ is the identity. □

The following corollary is immediate. We omit the proof.

Corollary 5.5. *For all $(s,t) \in \mathbb{Z}^2$ such that t is odd, $\mu_{(s,t)}$ and $\nu_{(s,t)}$ are birational maps.*

Proof of Proposition 5.3. We first claim that $T_3 = \nu_{(-1,-1)} \circ \mu_{(3,-3)}$. We will provide the computation for even coordinates. Let $(a_0, \dots, a_{2n-1})$ denote the image of $(x_0, \dots, x_{2n-1})$ under $\mu_{(3,-3)}$, and let $(b_0, \dots, b_{2n-1})$ denote the image of $(a_0, \dots, a_{2n-1})$ under $\nu_{(-1,-1)}$. Then, we have

$$\begin{aligned}b_{2i} = \frac{1 - a_{2i-1}}{1 - a_{2i-1}a_{2i-2}} &= \left(1 - \frac{1 - x_{2i-4}}{x_{2i-1}}\right) \cdot \left(1 - \frac{(1 - x_{2i-4})(1 - x_{2i+1})}{x_{2i-1}x_{2i-2}}\right)^{-1} \\ &= \frac{x_{2i-2}(x_{2i-1} + x_{2i-4} + 1)}{x_{2i-1}x_{2i-2} - (1 - x_{2i-4})(1 - x_{2i+1})}.\end{aligned}$$

Observe that this is precisely the first line of (19). The computation for b_{2i+1} is analogous, thus omitted. Then, by Corollary 5.5, $T_3^{-1} = \nu_{(3,-3)} \circ \mu_{(-1,3)}$. Finally, Equation (24) follows from a direct computation of $\nu_{(3,-3)} \circ \mu_{(-1,3)}$ using Equation (25), which we will omit. □

5.2 Conjugated Corner Invariants and Its T_3 Formula

To relate Equation (19) to parameters $(y_r)_{r \in \mathbb{Z}^2}$ in [GP16], it is convenient to consider another coordinate system of $\mathcal{P}_n$, which we define below.

Definition 5.6. Given $[P] \in \mathcal{P}_n$, define the *conjugated corner invariants* to be coordinate functions $\tilde{x}_0(P), \dots, \tilde{x}_{2n-1}(P)$ given by $\tilde{x}_j(P) = \frac{x_j(P)}{x_j(P)-1}$.

The conjugated corner invariants can be viewed as the image of the corner invariants under a birational map $\lambda : \mathbb{R}^{2n} \dashrightarrow \mathbb{R}^{2n}$ sending each coordinate $x_j \longmapsto \frac{x_j}{x_j-1}$. Observe that λ^2 restricted to the dense open set $(\mathbb{R} - \{0,1\})^{2n}$ is the identity map, so $\tilde{x}_j(P)$ is also a coordinate system for $\mathcal{P}_n$. Geometrically, the map λ corresponds to a different choice of permutation in the cross-ratio.

Throughout this section, we will use $\tilde{x}_j = \tilde{x}_j(P)$ and $\tilde{x}'_j = \tilde{x}_j(P')$ to denote the conjugate corner invariants of P and P'. We start by observing some symmetries of conjugating our factorization maps $\mu_{(s,t)}$ and $\nu_{(s,t)}$ from Equation (25).

Lemma 5.7. *For all $(s,t) \in \mathbb{Z}^2$, we have $\lambda \circ \mu_{(s,t)} \circ \lambda = \nu_{(s+t,-t)}$.*

Proof. We can check this by direct computation. We show that the equation holds on even coordinates. The $2i$-th coordinate of $\mu_{(s,t)} \circ \lambda$ is given by

$$\frac{1 - x_{2i+s} \cdot (x_{2i+s} - 1)^{-1}}{x_{2i+s+t} \cdot (x_{2i+s+t} - 1)^{-1}} = \frac{1 - x_{2i+s+t}}{x_{2i+s+t}(x_{2i+s} - 1)}$$

The $2i$-th coordinate of $\lambda \circ \mu_{(s,t)} \circ \lambda$ is given by

$$\left(\frac{1 - x_{2i+s+t}}{x_{2i+s+t}(x_{2i+s} - 1)}\right) \cdot \left(\frac{1 - x_{2i+s+t}}{x_{2i+s+t}(x_{2i+s} - 1)} - 1\right)^{-1} = \frac{1 - x_{2i+s+t}}{1 - x_{2i+s+t}x_{2i+s}},$$

which is precisely the $2i$-th coordinate of $\nu_{(s+t,-t)}$. The computation for the odd coordinates is similar. □

Since λ is an involution, it immediately follows that $\lambda\circ\nu_{(s,t)}\circ\lambda = \mu_{(s+t,-t)}$. This allows us to obtain a formula for T_3 with respect to the conjugated corner invariants.

Proposition 5.8. *Given any 3-nice twisted n-gon P, the following formula holds (indices taken modulo $2n$):*

$$\begin{cases} \tilde{x}'_{2i} = \tilde{x}_{2i-2} \cdot \dfrac{(1-\tilde{x}_{2i-1}\tilde{x}_{2i-4})(1-\tilde{x}_{2i+1})}{(1-\tilde{x}_{2i+1}\tilde{x}_{2i-2})(1-\tilde{x}_{2i-1})}; \\ \tilde{x}'_{2i+1} = \tilde{x}_{2i+3} \cdot \dfrac{(1-\tilde{x}_{2i+2}\tilde{x}_{2i+5})(1-\tilde{x}_{2i})}{(1-\tilde{x}_{2i}\tilde{x}_{2i+3})(1-\tilde{x}_{2i+2})}. \end{cases} \tag{27}$$

Proof. From the proof of Proposition 5.3, we saw that the formula for T_3 on the corner invariants is given by $\nu_{(-1,-1)}\circ\mu_{(3,-3)}$. It follows that the formula for conjugated corner invariants is $\lambda\circ\left(\nu_{(-1,-1)}\circ\mu_{(3,-3)}\right)\circ\lambda$. By Lemma 5.7,

$$\lambda\circ\left(\nu_{(-1,-1)}\circ\mu_{(3,-3)}\right)\circ\lambda = \left(\lambda\circ\nu_{(-1,-1)}\circ\lambda\right)\circ\left(\lambda\circ\mu_{(3,-3)}\circ\lambda\right) = \mu_{(-2,1)}\circ\nu_{(0,3)}.$$

It remains to check that $\mu_{(-2,1)}\circ\nu_{(0,3)}$ agrees with Equation (27). The $2i$-th coordinate of $\mu_{(-2,1)}\circ\nu_{(0,3)}$ is given by

$$\left(1-\frac{1-\tilde{x}_{2i-2}}{1-\tilde{x}_{2i-2}\tilde{x}_{2i+1}}\right)\cdot\left(\frac{1-\tilde{x}_{2i-1}}{1-\tilde{x}_{2i-1}\tilde{x}_{2i-4}}\right)^{-1} = \frac{\tilde{x}_{2i-2}(1-\tilde{x}_{2i-1}\tilde{x}_{2i-4})(1-\tilde{x}_{2i+1})}{(1-\tilde{x}_{2i-2}\tilde{x}_{2i+1})(1-\tilde{x}_{2i-1})}.$$

This is precisely $\tilde{x}'_{2i}$ from Equation (27). The computation for odd coordinates is omitted. □

Using Lemma 5.4, we can easily compute the formula of T_3^{-1} with respect to the conjugated corner invariants. The proof is again a direct computation, so we omit it.

Corollary 5.9. *The formula for T_3^{-1} with conjugated corner invariants is given by $\mu_{(0,3)}\circ\nu_{(2,-3)}$. More specifically,*

$$\begin{cases} \tilde{x}_{2i} = \tilde{x}'_{2i+2} \cdot \dfrac{(1-\tilde{x}'_{2i+1}\tilde{x}'_{2i+4})(1-\tilde{x}'_{2i-1})}{(1-\tilde{x}'_{2i-1}\tilde{x}'_{2i+2})(1-\tilde{x}'_{2i+1})}; \\ \tilde{x}_{2i+1} = \tilde{x}'_{2i-1} \cdot \dfrac{(1-\tilde{x}'_{2i}\tilde{x}'_{2i-3})(1-\tilde{x}'_{2i+2})}{(1-\tilde{x}'_{2i+2}\tilde{x}'_{2i-1})(1-\tilde{x}'_{2i})}. \end{cases} \tag{28}$$

5.3 Relation to Y-Variables

In this section, we discuss how Equation (18) generalizes the results from [GP16]. The propositions in this section hold for all four cells $S_n(I,J)$, $S_n(J,I)$, $S_n(K,J)$, $S_n(J,K)$. For notational convenience, our statements will only mention $S_n(J,I)$. The readers may assume that the propositions hold for the other three cells with the same proof.

The map T_3 along with the labeling convention of Equation (18) corresponds to the following construction in [GP16]. Let $a,b,c,d \in \mathbb{Z}^2$ be distinct and assume $a_2 \le b_2 \le c_2 \le d_2$. Say that $S = \{a,b,c,d\}$ is a *Y-pin* if $b_2 < c_2$ and the vectors $b-a$, $c-a$, $d-a$ generate all of $\mathbb{Z}^2$.

Definition 5.10 ([GP16, Definition 1.4])**.** Let $S = \{a,b,c,d\}$ be a Y-pin and suppose $D \ge 2$. A *Y-mesh of type S and dimension D* is a grid of points $\hat{P}_{i,j}$ in $\mathbb{RP}^D$ with $i,j \in \mathbb{Z}$ which together span all of $\mathbb{RP}^D$ and such that

- $\hat{P}_{r+a}, \hat{P}_{r+b}, \hat{P}_{r+c}, \hat{P}_{r+d}$ are distinct for all $r \in \mathbb{Z}^2$.
- Let $L_r = \hat{P}_{r+a}\hat{P}_{r+b}$. Then, $\hat{P}_{r+a}, \hat{P}_{r+b}, \hat{P}_{r+c}, \hat{P}_{r+d}$ all lie on L_r for all $r \in \mathbb{Z}^2$.
- The four lines $L_{r-a}, L_{r-b}, L_{r-c}, L_{r-d}$ (all of which contain $\hat{P}_r$) are distinct for all $r \in \mathbb{Z}^2$.

Let $S = \{(-1,0),(2,0),(0,1),(1,1)\}$, which is a Y-pin. Given a representative P of some $[P] \in S_n(J,I)$, we can consider a grid $(\hat{P}_{i,j})_{(i,j)\in\mathbb{Z}^2}$ where $\hat{P}_{i,j}$ is the i-th vertex of $T_3^j(P)$.

Proposition 5.11. *$(\hat{P}_{i,j})$ is a Y-mesh of type S and dimension 2.*

Proof. The first two conditions of Definition 5.10 are straightforward to verify using the identification $S_n(J,I) = \mathcal{S}^{\alpha}_{3,n}$ from Proposition 4.10. For the third condition, let $P^{(j)} = T_3^j(P)$. Then, we have

$$L_{r-a} = P^{(j)}_{i-1}P^{(j)}_{i+2}, \quad L_{r-b} = P^{(j)}_{i-1}P^{(j)}_{i-4}, \quad L_{r-c} = P^{(j)}_{i-1}P^{(j)}_{i}, \quad L_{r-d} = P^{(j)}_{i-1}P^{(j)}_{i-2}.$$

Notice also that $L_{r-a} = P^{(j+1)}_{i}P^{(j+1)}_{i+1}$ and $L_{r-b} = P^{(j+1)}_{i-2}P^{(j+1)}_{i-1}$, so 3-niceness of $P^{(j+1)}$ implies they are distinct. The other pairings are distinct because of 3-niceness of $P^{(j)}$. □

[GP16] then introduces the parameters $y_r(\hat{P})$ associated to a Y-mesh. Fix a Y-pin $S = \{a, b, c, d\}$ and a Y-mesh $\hat{P}$ of type S and dimension D. For all $r \in \mathbb{Z}^2$, consider

$$y_r(\hat{P}) = -\chi(\hat{P}_{r+a}, \hat{P}_{r+c}, \hat{P}_{r+d}, \hat{P}_{r+b}). \tag{29}$$

See the left side of Figure 23 for the setup using the Y-mesh from Proposition 5.11. [GP16, Theorem 1.6] give us the following relation on y_r:

$$y_{i+1,j}\, y_{i+1,j+2} = \frac{(1 + y_{i-1,j+1})(1 + y_{i+3,j+1})}{(1 + y_{i,j+1}^{-1})(1 + y_{i+2,j+1}^{-1})}. \tag{30}$$

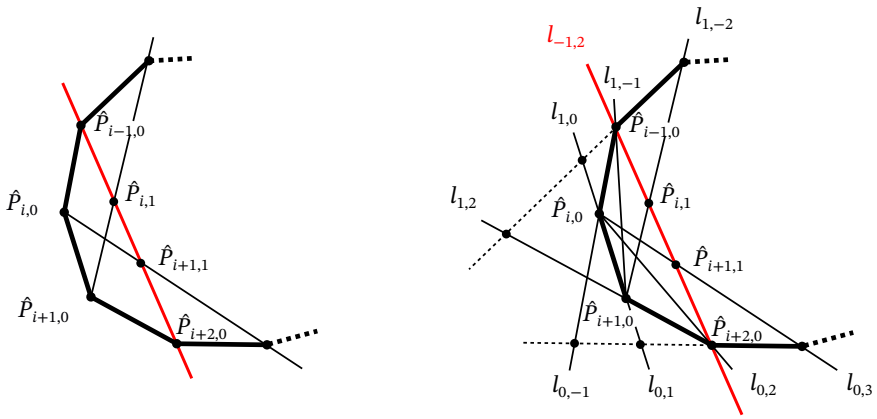

Figure 23: Left: Definition of $y_r(\hat{P})$ for the Y-mesh from Proposition 5.11. Right: Relationship between $y_r(\hat{P})$ and conjugated corner invariants.

Lemma 5.12. *Given a representative P of $[P] \in S_n(I, J)$ with conjugated corner invariants $\tilde{x}_j = \tilde{x}_j(P)$. Let $(\hat{P}_{i,j})$ be its corresponding Y-mesh with $y_r = y_r(\hat{P})$ for all $r \in \mathbb{Z}^2$. Then, for all $i \in \mathbb{Z}$,*

$$y_{i,0} = -\tilde{x}_{2i}\tilde{x}_{2i+3}. \tag{31}$$

Proof. Let $l_{a,b} = P_{i+a}P_{i+b}$. See right side of Figure 23 for the setup. Equation (8) gives us

$$\tilde{x}_{2i} = \frac{x_{2i}}{x_{2i} - 1} = \chi(l_{1,-2}, l_{1,-1}, l_{1,2}, l_{1,0}); \quad \tilde{x}_{2i+3} = \frac{x_{2i+3}}{x_{2i+3} - 1} = \chi(l_{0,3}, l_{0,2}, l_{0,-1}, l_{0,1}).$$

Notice that $(l_{1,-1} \cap l_{0,-1}) \cap (l_{1,2} \cap l_{0,2}) = P_{i-1}P_{i+2} = l_{-1,2}$. Then, from elementary cross ratio identities we have

$$\begin{aligned}\tilde{x}_{2i}\tilde{x}_{2i+3} &= \chi(l_{1,-1} \cap l_{-1,2}, l_{1,-2} \cap l_{-1,2}, l_{0,3} \cap l_{-1,2}, l_{0,2} \cap l_{-1,2}) \\ &= \chi(\hat{P}_{i-1,0}, \hat{P}_{i,1}, \hat{P}_{i+1,1}, \hat{P}_{i+2,0}) = -y_{i,0},\end{aligned}$$

which is precisely Equation (31). □

Remark 5.13. Equation (31) is very similar to the correspondence of y_r and corner invariants in the T_2 case. Let P be an arbitrary twisted n-gon with $P' = T_2(P)$. If we use the labeling convention $P'_i = P_{i-1}P_{i+1} \cap P_iP_{i+2}$, then the T_2-orbit $(\hat{P}_{i,j})_{(i,j)\in\mathbb{Z}^2}$, where $\hat{P}_{i,j}$ is the i-th vertex of $T_2^j(P)$, is a Y-mesh of type $S = \{(-1,0),(1,0),(-1,1),(0,1)\}$. Denote by $x_j = x_j(P)$ the corner invariants of P. Then, for all $i \in \mathbb{Z}$,

$$y_{i,0} = -x_{2i+1}x_{2i+2}. \tag{32}$$

For the proof of Equation (32), see [Gli11, Equation (2.2)].

Theorem 5.14. *For the Y-pin $S = \{(-1,0),(2,0),(0,1),(1,1)\}$, the transformation formula of y_r from* [GP16, Theorem 1.6] *is a direct consequence of the birational formula for the conjugated corner invariants under T_3.*

Proof. It suffices to show that we can use Equation (31) to derive (30) for $j = -1$. We first compute $y_{i+1,-1}$ and $y_{i+1,1}$ using Equation (27) and (28):

$$\begin{aligned} y_{i+1,-1} &= -\frac{\tilde{x}_{2i+4}(1-\tilde{x}_{2i+3}\tilde{x}_{2i+6})(1-\tilde{x}_{2i+1})}{(1-\tilde{x}_{2i+1}\tilde{x}_{2i+4})(1-\tilde{x}_{2i+3})} \cdot \frac{\tilde{x}_{2i+3}(1-\tilde{x}_{2i+1}\tilde{x}_{2i+4})(1-\tilde{x}_{2i+6})}{(1-\tilde{x}_{2i+3}\tilde{x}_{2i+6})(1-\tilde{x}_{2i+4})} \\ &= -\frac{\tilde{x}_{2i+3}\tilde{x}_{2i+4}(1-\tilde{x}_{2i+1})(1-\tilde{x}_{2i+6})}{(1-\tilde{x}_{2i+3})(1-\tilde{x}_{2i+4})}; \\ y_{i+1,1} &= -\frac{\tilde{x}_{2i}(1-\tilde{x}_{2i-2}\tilde{x}_{2i+1})(1-\tilde{x}_{2i+3})}{(1-\tilde{x}_{2i}\tilde{x}_{2i+3})(1-\tilde{x}_{2i+1})} \cdot \frac{\tilde{x}_{2i+7}(1-\tilde{x}_{2i+6}\tilde{x}_{2i+9})(1-\tilde{x}_{2i+4})}{(1-\tilde{x}_{2i+4}\tilde{x}_{2i+7})(1-\tilde{x}_{2i+6})} \\ &= -\frac{\tilde{x}_{2i}\tilde{x}_{2i+7}(1+y_{i-1,0})(1+y_{i+3,0})(1-\tilde{x}_{2i+3})(1-\tilde{x}_{2i+4})}{(1+y_{i,0})(1+y_{i+2,0})(1-\tilde{x}_{2i+1})(1-\tilde{x}_{2i+6})}. \end{aligned} \tag{33}$$

It follows that

$$\begin{aligned} y_{i+1,-1}\,y_{i+1,1} &= \frac{\tilde{x}_{2i}\tilde{x}_{2i+3}\tilde{x}_{2i+4}\tilde{x}_{2i+7}(1+y_{i-1,0})(1+y_{i+3,0})}{(1+y_{i,0})(1+y_{i+2,0})} \\ &= \frac{y_{i,0}y_{i+2,0}(1+y_{i-1,0})(1+y_{i+3,0})}{(1+y_{i,0})(1+y_{i+2,0})} = \frac{(1+y_{i-1,0})(1+y_{i+3,0})}{(1+y_{i,0}^{-1})(1+y_{i+2,0}^{-1})}. \end{aligned}$$

This concludes the proof. □

6 The Precompactness of T_3 Orbits

In this section, we establish four algebraic invariants of T_3. We then use them to prove Theorem 1.3. Having Theorem 4.6 in hand, we may fully work with $S_n(J,I)$ and $S_n(K,J)$. Our strategy is to use the algebraic invariants to show that the corner invariants are uniformly bounded.

6.1 The Four Invariants

Proposition 6.1. *Given $[P] \in \mathcal{P}_n$ with corner invariants $x_j = x_j(P)$, consider the following four quantities $\mathcal{F}_i = \mathcal{F}_i(P)$:*

$$\mathcal{F}_1 = \prod_{i=0}^{n-1} \frac{x_{2i}}{x_{2i}-1}; \quad \mathcal{F}_2 = \prod_{i=0}^{n-1} \frac{x_{2i+1}}{x_{2i+1}-1}; \quad \mathcal{F}_3 = \prod_{i=0}^{n-1} \frac{x_{2i}}{x_{2i+1}}; \quad \mathcal{F}_4 = \prod_{i=0}^{n-1} \frac{1-x_{2i}}{1-x_{2i+1}}. \tag{34}$$

Then, $\mathcal{F}_i$ is invariant under T_3 for $i = 1,2,3,4$.

Proof. We first show that $\mathcal{F}_3$ is invariant under T_3. Let $\mathcal{F}_3'$ denote the invariants obtained by plugging in x_i' from Equation (24). Observe that

$$\begin{aligned}\mathcal{F}_3' &= \mathcal{F}_3 \cdot \prod_{i=0}^{n-1} \frac{x_{2i-4}+x_{2i-1}-1}{x_{2i+2}+x_{2i+5}-1} \cdot \prod_{i=0}^{n-1} \frac{x_{2i+2}x_{2i+3}-(1-x_{2i+5})(1-x_{2i})}{x_{2i-2}x_{2i-1}-(1-x_{2i+1})(1-x_{2i-4})} \\ &= \mathcal{F}_3 \cdot \frac{\prod_{i=-3}^{n-4}(x_{2i+2}+x_{2i+5}-1)}{\prod_{i=0}^{n-1}(x_{2i+2}+x_{2i+5}-1)} \cdot \frac{\prod_{i=2}^{n+1}(x_{2i-2}x_{2i-1}-(1-x_{2i+1})(1-x_{2i-4}))}{\prod_{i=0}^{n-1}(x_{2i-2}x_{2i-1}-(1-x_{2i+1})(1-x_{2i-4}))} = \mathcal{F}_3.\end{aligned}$$

This shows $\mathcal{F}_3' = \mathcal{F}_3$. Next, we show that $\mathcal{F}_1$ and $\mathcal{F}_2$ are invariant. Using conjugated corner invariants, we see that $\mathcal{F}_1 = \prod_{i=0}^{n-1} \tilde{x}_{2i}$ and $\mathcal{F}_2 = \prod_{i=0}^{n-1} \tilde{x}_{2i+1}$. We let $\mathcal{F}_1' = \prod_{i=0}^{n-1} \tilde{x}_{2i}'$ be the first invariant of $T_3(P)$. Equation (27) gives us

$$\mathcal{F}_1' = \mathcal{F}_1 \cdot \prod_{i=0}^{n-1} \frac{(1-\tilde{x}_{2i-1}\tilde{x}_{2i-4})(1-\tilde{x}_{2i+1})}{(1-\tilde{x}_{2i+1}\tilde{x}_{2i-2})(1-\tilde{x}_{2i-1})} = \mathcal{F}_1,$$

where the last equality follows from cyclically permuting the numerator. This shows $\mathcal{F}_1' = \mathcal{F}_1$. The proof for $\mathcal{F}_2$ goes through the same computation, so we omit it.

Finally, observe that $\mathcal{F}_4 = \frac{\mathcal{F}_2\mathcal{F}_3}{\mathcal{F}_1}$, so by invariance of $\mathcal{F}_1, \mathcal{F}_2, \mathcal{F}_3$, we know that $\mathcal{F}_4$ must also be invariant. This concludes the proof. □

Remark 6.2. As shown in the proof of Proposition 6.1, $\mathcal{F}_1$ and $\mathcal{F}_2$ correspond to the product of conjugated corner invariants. $\mathcal{F}_3$ is the ratio of the two Casimirs $\frac{O_n}{E_n}$ of the T_2 invariant Poisson structure on $\mathcal{P}_n$. For discussions on $\mathcal{F}_3$ and the Casimirs, see [Sch24, §2.3]. Also, since $\mathcal{F}_1\mathcal{F}_4 = \mathcal{F}_2\mathcal{F}_3$, the four T_3 invariants are not algebraically independent.

Below is a direct consequence of the invariance of the $\mathcal{F}_i$'s. Since the $\mathcal{F}_i$'s are preserved by the forward action, it must also be preserved by the backward action.

Corollary 6.3. *The four invariants $\mathcal{F}_1, \mathcal{F}_2, \mathcal{F}_3, \mathcal{F}_4$ are also invariant under T_3^{-1}.*

6.2 Proof of Theorem 1.3

Recall that a subset A of a topological space X is precompact if the closure of A is compact. To show that the T_3-orbit is precompact, it suffices to show that the corner invariants of the orbit are uniformly bounded away from the singularities $0, 1, \infty$.

In this section, we let $[n] := \{1, \dots, n\}$. Given $[P] \in \mathcal{P}_n$, for all $j, m \in \mathbb{Z}$, let $x_{j,m} = x_j(T_3^m(P))$ whenever $T_3^m(P)$ exists. Let $\mathcal{F}_{i,m} = \mathcal{F}_i(T_3^m(P))$ for $i = 1, 2, 3, 4$. By Proposition 6.1, $\mathcal{F}_{i,m}$ is independent of m. All sequences are indexed by $\mathbb{Z}_{\geq 0}$ unless specified otherwise. Finally, when we say "$\{a_m\}$ converges/diverges on a subsequence, and $\{b_m\}$ converges/diverges on the same subsequence," we mean that a subsequence of $\{b_m\}$ with the same choice of indices as the subsequence of $\{a_m\}$ converges/diverges.

Lemma 6.4. *Given $[P] \in S_n(J, I)$, there exist $a, b \in J$ such that $x_{2i,m} \in [a, b]$ for all $i \in [n]$ and $m \in \mathbb{Z}_{\geq 0}$.*

Proof. We first claim that for each i, the sequence $\{x_{2i,m}\}$ is bounded above uniformly by some $b_i \in J$. If not, then $x_{2i,m} \to 1$ on a subsequence, which implies $1 - x_{2i,m} \to 0$ on the

same subsequence. Since $[T_3^m(P)] \in S_n(J,I)$ for all $m \in \mathbb{Z}_{\geq 0}$, we must have $1 - x_{2j,m} \in (0,1)$ and $(1 - x_{2j+1,m})^{-1} \in (0,1)$ for all $j \in [n]$. This implies $\mathcal{F}_{4,m} \to 0$ on the same subsequence, but that contradicts invariance of $\mathcal{F}_{4,m}$. Therefore, $\{x_{2i,m}\}$ is bounded above by $b_i = \sup_m\{x_{2i,m}\} \in J$. Taking $b = \max_{i\in[n]} b_i$ satisfies the condition in the lemma.

Next, we show $\{x_{2i,m}\}$ is bounded below uniformly by some $a_i > 0$. If not, then $x_{2i,m} \to 0$ on a subsequence, so $x_{2i,m} \cdot (x_{2i,m} - 1)^{-1} \to 0$ on the same subsequence. From the argument above, $x_{2j,m} \leq b$ for all $m \in \mathbb{Z}_{\geq 0}$ and $j \in [n]$, which gives us $|x_{2j,m} \cdot (x_{2j,m} - 1)^{-1}| \leq |\frac{b}{b-1}|$, so the sequences are uniformly bounded for all $j \neq i$. This together with $|x_{2i,m} \cdot (x_{2i,m} - 1)^{-1}| \to 0$ on a subsequence implies $|\mathcal{F}_{1,m}| \to 0$ on the same subsequence, but that contradicts invariance of $\mathcal{F}_{1,m}$. Therefore, $\{x_{2i,m}\}$ is bounded below by $a_i = \inf_m\{x_{2i,m}\} \in J$. Taking $a = \min_{i\in[n]} a_i$ completes the proof. □

Lemma 6.5. *With the same notation as in Lemma 6.6, there exist $c, d \in I$ such that $x_{2i+1,m} \in [c,d]$ for all $i \in [n]$ and $m \in \mathbb{Z}_{\geq 0}$.*

Proof. We first claim that for each i,the sequence $\{x_{2i+1,m}\}$ is bounded above uniformly by some $d_i \in I$. If not, then, $x_{2i+1,m} \cdot (x_{2i+1,m} - 1)^{-1} \to 0$ on a subsequence. Since $x_{2j+1,m} \cdot (x_{2j+1,m} - 1)^{-1} \in (0,1)$ for all $j \in [n]$, we must have $\mathcal{F}_{2,m} \to 0$ on the same subsequence, but that contradicts invariance of $\mathcal{F}_{2,m}$.

Next, we show that $\{x_{2i+1,m}\}$ is bounded below uniformly by some $c_i \in I$. If not, then a subsequence of $\{x_{2i+1,m}\}$ must diverge, so the same subsequence of $\{1 - x_{2i+1,m}\}$ also diverges. Lemma 6.4 and $x_{2i+1,m} \leq d_i < 0$ together implies $\mathcal{F}_{4,m}$ diverges on the same subsequence, but that contradicts invariance of $\mathcal{F}_{4,m}$. Finally, taking $c = \min_{i\in[n]} c_i$ and $d = \max_{i\in[n]} d_i$ completes the proof. □

The proofs of the following two lemmas are analogous to Lemma 6.4 and 6.5. We will omit the details and point out which invariants to use in each step.

Lemma 6.6. *Given $[P] \in S_n(K,J)$, there exist $a, b \in J$ such that $x_{2i+1,m} \in [a,b]$ for all $i \in [n]$ and $m \in \mathbb{Z}_{\geq 0}$.*

Proof. For each i, the sequence $\{x_{2i+1,m}\}$ is bounded below by some $a_i \in J$, for otherwise $\mathcal{F}_{3,m}$ diverges on a subsequence. Next, since $\{|\mathcal{F}_{3,m}|\}$ is bounded below by $\prod_{j=0}^{n-1} a_j > 0$, $\{x_{2i+1,m}\}$ is bounded above by some $b_i \in J$. Taking $a = \min_{i\in[n]} a_i$ and $b = \max_{i\in[n]} b_i$ completes the proof. □

Lemma 6.7. *With the same notation as in Lemma 6.6, there exist $c, d \in K$ such that $x_{2i,m} \in [c, d]$ for all $i \in [n]$ and $m \in \mathbb{Z}_{\geq 0}$.*

Proof. For each i, the sequence $\{x_{2i,m}\}$ must be bounded below by some $c_i \in K$, for otherwise $\mathcal{F}_{1,m} \to \infty$ on a subsequence. It's also bounded above by some d_i. To see this, Lemma 6.6 implies all corner invariants are bounded away from 0, so if $\{x_{2i,m}\}$ is not bounded above, then $\mathcal{F}_{3,m}$ diverges on a subsequence. Taking $c = \min_i c_i$ and $d = \max_i d_i$ completes the proof. □

Proof of Theorem 1.3. We will show that the forward T_3 orbit of $[P] \in \mathcal{S}^{\alpha}_{3,n} = S_n(J, I)$ has uniformly bounded corner invariants. By Proposition 4.10, $[P] \in S_n(J, I)$. Let $[a, b] \subset J$, $[c, d] \subset I$ be compact intervals derived from Lemma 6.4 and 6.5. Then, the sequence $\{(x_{0,m}, \dots, x_{2n-1,m})\}$ is contained in $\prod_{i=0}^{n-1}[a, b] \times [c, d]$, so it is uniformly bounded. To show precompactness of the backward T_3 orbit of $\mathcal{S}^{\alpha}_{3,n}$, one can adapt the proofs of Lemma 6.4 and 6.5 with very few changes. We omit the details. The case $\mathcal{S}^{\beta}_{3,n}$ follows from Lemma 6.6 and 6.7 by essentially the same argument, which we again omit. □

7 Type-β 2-Spirals and Precompact T_2 Orbits

7.1 The Corner Invariants of Type-β 2-Spirals

We finish this paper by discussing the type-β 2-spirals. Proposition 3.10 implies $\mathcal{S}^{\beta}_{2,n}$ is disjoint from the moduli space of closed convex polygons, so $\mathcal{S}^{\beta}_{2,n}$ is a new invariant geometric construction under the pentagram map by Theorem 1.1. In this section, we analyze the corner invariants of $\mathcal{S}^{\beta}_{2,n}$ and show that just like the type-α and type-β 3-spirals, it is cut out by linear boundaries.

Proposition 7.1. *For all $n \geq 2$, given any $[P] \in \mathcal{S}^{\beta}_{2,n}$ with corner invariants $x_j = x_j(P)$, we have $x_{2i} > 0$ and $x_{2i+1} < 0$ for all $i \in [n]$.*

Proof. Let P be an $(i-2)$-representative of $[P]$. Normalize by $\mathrm{Aff}^{+}_{2}(\mathbb{R})$ so that $P_{i-1} = (-1, 0)$, $P_i = (0, 0)$, $P_{i+1} = (0, 1)$ on the affine patch, which is possible because (P_{i-1}, P_i, P_{i+1}) is positive. Let $s_{a,b} \in \mathbb{R} \cup \{\infty\}$ denote the slope of $P_{i+a}P_{i+b}$. Positivity of (P_{i-2}, P_{i-1}, P_i) and $P_{i+1} \in \mathrm{int}(P_{i-2}, P_{i-1}, P_i)$ implies $s_{-1,-2} > 1$ and $s_{1,-2} > 1$. Similarly, since $P_{i+2} \in \mathrm{int}(P_{i-1}, P_i, P_{i+1})$, we have $s_{-1,2} \in (0, 1)$ and $s_{1,2} > 1$. It follows that

$$\begin{aligned} x_{2i} &= \frac{(s_{1,-2} - s_{1,-1})(s_{1,0} - s_{1,2})}{(s_{1,-2} - s_{1,0})(s_{1,-1} - s_{1,2})} = -\frac{s_{1,-2} - 1}{1 - s_{1,2}} > 0; \\ x_{2i+1} &= \frac{(s_{-1,2} - s_{-1,1})(s_{-1,0} - s_{-1,-2})}{(s_{-1,2} - s_{-1,0})(s_{-1,1} - s_{-1,-2})} = \frac{-s_{-1,-2}(s_{-1,2} - 1)}{s_{-1,2}(1 - s_{-1,-2})} < 0. \end{aligned} \tag{35}$$

This concludes the proof. □

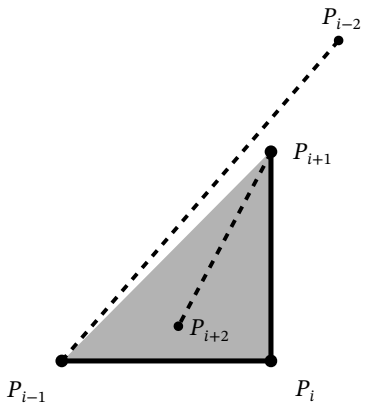

Figure 24: Configuration of Proposition 7.1 and 7.2.

Proposition 7.2. *For all $n \geq 2$, if $[P] \in \mathcal{P}_n$ has corner invariants $x_j = x_j(P)$ such that $x_{2i} > 0$ and $x_{2i+1} < 0$ for all $i \in [n]$, then $[P] \in \mathcal{S}^{\beta}_{2,n}$.*

Proof. Fix $N \in \mathbb{Z}$. Let P be a representative of $[P]$ such that $P_{N-2} = (\frac{1}{3}, \frac{3}{2})$, $P_{N-1} = (-1, 0)$, $P_N = (0, 0)$, and $P_{N+1} = (0, 1)$. We say P satisfies condition $(**)_i$ if (P_{i-1}, P_i, P_{i+1}) is positive and $P_{i+2} \in \mathrm{int}(P_{i-1}, P_i, P_{i+1})$. Then, P is a type-β N-representative of 2-spirals iff P satisfies

$(**)_i$ for all $i > N$. Notice that P satisfies $(**)_N$, so by an induction argument, it suffices to show that for $i \geq N$, if P satisfies $(**)_i$, then P satisfies $(**)_{i+1}$.

If P satisfies $(**)_i$, then (P_{i-1}, P_i, P_{i+1}) is positive. Normalize by $\mathrm{Aff}_2^+(\mathbb{R})$ so that $P_{i-1} = (-1, 0)$, $P_i = (0, 0)$, and $P_i = (0, 1)$. We will use the same notation $l_{a,b}$ and $s_{a,b}$ as Proposition 7.1. Since $P_{i+1} \in \mathrm{int}(P_{i-2}, P_{i-1}, P_i)$, we have $s_{-1,-2} > 1$ and $s_{1,-2} > 1$. Then, since $x_{2i} > 0$ and $x_{2i+1} < 0$, Equation (35) gives us

$$\frac{s_{1,-2} - 1}{s_{1,2} - 1} > 0 \text{ and } \frac{s_{-1,-2}(s_{-1,2} - 1)}{s_{-1,2}(s_{-1,-2} - 1)} < 0.$$

It follows that $s_{1,2} > 1$ and $1 - \frac{1}{s_{-1,2}} < 0$. The latter inequality implies $\frac{1}{s_{-1,2}} > 1$, so in particular $s_{-1,2} > 0$ and hence $s_{-1,2} \in (0, 1)$. The two conditions $s_{1,2} > 1$ and $s_{-1,2} \in (0, 1)$ implies $P_{i+2} \in \mathrm{int}(P_{i-1}, P_i, P_{i+1})$ and (P_i, P_{i+1}, P_{i+2}) positive, so P satisfies $(**)_{i+1}$ as desired. We conclude that $[P] \in \mathcal{S}_{2,n}^{\beta}$. □

7.2 The Precompactness of T_2 Orbits

We adapt the argument for Theorem 1.3 to give a quick proof of Theorem 1.4 using the Casimir functions of the T_2-invariant Poisson structure on $\mathcal{P}_n$ that were developed in [Sch08, Theorem 1.2]. One can find the proof of the following lemma in [Sch08, §2.2].

Lemma 7.3. *For the map T_2 acting on a twisted n-gon P with corner invariants $x_j = x_j(P)$, one has the following four invariant quantities.*

$$O_1(P) = \sum_{i=0}^{n-1}(-x_{2i+1} + x_{2i-1}x_{2i}x_{2i+1}); \quad O_n(P) = \prod_{i=0}^{n-1} x_{2i+1};$$
$$E_1(P) = \sum_{i=0}^{n-1}(-x_{2i} + x_{2i-2}x_{2i-1}x_{2i}); \quad E_n(P) = \prod_{i=1}^{n} x_{2i}.$$

We continue to use the notation from §6.2. In addition, we write $O_{1,m} = O_1(T_2^m(P))$. We define $O_{n,m}$, $E_{1,m}$, and $E_{n,m}$ analogously. By Lemma 7.3, the values of these four quantities are independent of the choice of m.

Lemma 7.4. *For all $n \geq 2$, given $[P] \in \mathcal{S}_{2,n}^{\beta}$, there exists $a, b > 0$ such that $x_{2i,m} \in [a, b]$ for all $i \in [n]$ and $m \in \mathbb{Z}_{\geq 0}$.*

Proof. Fix $i \in [n]$. We first show that $x_{2i,m}$ is uniformly bounded above by some $b > 0$. Since $T_2^m(P) \in \mathcal{S}^{\beta}_{2,n}$ for all $m \in \mathbb{Z}_{\geq 0}$, we must have $E_{1,m} < -x_{2i,m} < 0$. Then, if $x_{2i,m} \to \infty$ on a subsequence, $E_{1,m}$ also diverges on the same subsequence, but that contradicts invariance of $E_{1,m}$. This implies $x_{2i,m} < b_i$ for some $b_i > 0$. Taking $b = \max_{i\in[n]} b_i$ satisfies the condition in the lemma.

Next, we show that $x_{2i,m}$ is uniformly bounded below by some $a > 0$. We first notice that $E_{n,m} < b_i^n$. This implies if $x_{2i,m} \to 0$ on a subsequence, then $E_{n,m} \to 0$ on the same subsequence, but that contradicts invariance of $E_{n,m}$. Therefore, $x_{2i,m} > a_i$ for some $a_i > 0$. Taking $a = \min_{i\in[n]} a_i$ completes the proof. □

Lemma 7.5. *For all $n \geq 2$, given $[P] \in \mathcal{S}^{\beta}_{2,n}$, there exists $c, d < 0$ such that $x_{2i+1,m} \in [c, d]$ for all $i \in [n]$ and $m \in \mathbb{Z}_{\geq 0}$.*

Proof. The argument is analogous to the proof of Lemma 7.4. Fix $i \in [n]$. To find c_i that bounds $\{x_{2i+1,m}\}$ uniformly from below, we use the fact that $O_{1,m} > -x_{2i+1} > 0$. We then set $c = \min_{i\in[n]} c_i$. To find d_i that bounds $\{x_{2i+1,m}\}$ uniformly from above, we use the fact that $|O_n(P)| < |c^n|$. We then set $d = \max_{i\in[n]} d_i$ to complete the proof. □

Lemma 7.4 and 7.5 together implies that the forward T_2-orbit of any $[P] \in \mathcal{S}^{\beta}_{2,n}$ is precompact in $\mathcal{P}_n$. One can use the same argument to show that the backward T_2-orbit is also precompact. We have thus completed the proof of Theorem 1.4.

8 Appendix

8.1 Conjectures for Invariants

Given $[P] \in \mathcal{P}_{k,n}$, we may consider the following quantity:

$$y_i^{(k)}(P) = -\chi(P_i, P_iP_{i+k} \cap P_{i-1}P_{i+k-1}, P_iP_{i+k} \cap P_{i+1}P_{i+k+1}, P_{i+k}). \tag{36}$$

When $T_k^j(P)$ is well-defined, we write $y_{i,j}^{(k)} = y_i^{(k)}(T_k^j(P))$, or simply $y_{i,j}$ if the value of k is clear from the context. Let $Y_j^{(k)}$ (or simply Y_j) denote the product $\prod_{i=0}^{n-1} y_{i,j}^{(k)}$.

Proposition 8.1. *For all $k, n \geq 2$, given $[P] \in \mathcal{S}^{\alpha}_{k,n}$, there exists $C \in \mathbb{R}$, $C \neq 0$, such that*

$$Y^{(k)}_{j+1}\left(Y^{(k)}_{j}\right)^{-1} = C \tag{37}$$

for all $j \in \mathbb{Z}$. The same holds for $[P] \in \mathcal{S}^{\beta}_{k,n}$.

Proof. The grid $(\hat{P}_{i,j})_{(i,j)\in\mathbb{Z}^2}$ where $\hat{P}_{i,j}$ is the i-th vertex of $T^j_k(P)$ is a Y-mesh of type $S = \{(0,0),(k,0),(-1,1),(0,1)\}$ with $y_r = y_r(\hat{P})$ for $r \in \mathbb{Z}^2$. The proof is essentially the same as the one for Proposition 5.11, so we will omit it. Then, from [GP16, Theorem 1.6], we have

$$y_{i+k,j}y_{i-1,j+2} = \frac{(1+y_{i-1,j+1})(1+y_{i+k,j+1})}{(1+y^{-1}_{i,j+1})(1+y^{-1}_{i+k-1,j+1})}. \tag{38}$$

It follows that

$$\begin{aligned} Y_jY_{j+2} &= \prod_{i=0}^{n-1}(y_{i+k,j}y_{i-1,j+2}) = \prod_{i=0}^{n-1}\frac{(1+y_{i-1,j+1})(1+y_{i+k,j+1})}{(1+y^{-1}_{i,j+1})(1+y^{-1}_{i+k-1,j+1})} \\ &= \left(\prod_{i=0}^{n-1}(y_{i,j+1}\,y_{i+k-1,j+1})\right)\left(\prod_{i=0}^{n-1}\frac{(1+y_{i-1,j+1})(1+y_{i+k,j+1})}{(1+y_{i,j+1})(1+y_{i+k-1,j+1})}\right) = Y^2_{j+1}. \end{aligned} \tag{39}$$

This implies $Y_{j+2}/Y_{j+1} = Y_{j+1}/Y_j$ for all $j \in \mathbb{Z}$. Taking $C = Y_1/Y_0$ completes the proof. □

Remark 8.2. Combining the results of [GP16] and [GSTV12], we see that Proposition 8.1 is equivalent to [GSTV12, Theorem 2.1]. Specifically, the quantity in Equation (37) is shown to be a Casimir function with respect to a Poisson structure that is invariant under the y-variable transformation of a quiver Q_k, which we will define below.

Consider the infinite directed graph Q_k whose vertices are indexed by $\mathbb{Z}\times\{0,1\}$, with directed edges $(i,0)\to(i-1,1)$, $(i,0)\to(i-k,1)$, $(i,1)\to(i,0)$, and $(i-k-1,1)\to(i,0)$ for all $i \in \mathbb{Z}$. See Figure 25 for a visual representation of this quiver. We refer the readers to [GP16, §9] for the construction of this quiver and the proof that the y-variable transformations satisfy (38).

For all $n \geq 2$, the y-variables corresponding to $[P] \in \mathcal{P}_{k,n}$ are periodic modulo n. We may then identify vertices of Q_k via $(i,j) \sim (i+n,j)$, and similarly identify the corresponding edges. The resulting directed graph $Q_{k,n}$ is isomorphic to the quiver $\mathcal{Q}_{k,n}$ from [GSTV12]

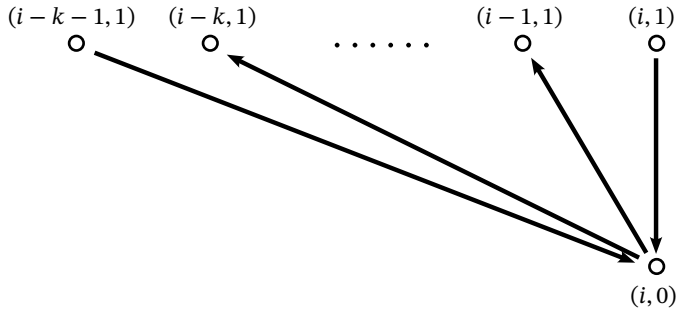

Figure 25: The quiver Q_k. Only edges into and out of the vertex $(i,0)$ are shown.

by applying a translation to the first entry of the vertices $(i,1)$. Moreover, the y-variables $(y_{i,0})_{i\in[n]}$ of the quiver in [GP16] transforms in the same way as the p-variables $(p_i)_{i\in[n]}$ of $\mathcal{Q}_{k,n}$ under the map $\overline{T_k}$ (see [GSTV12, §2]), and the q-variables $(q_i)_{i\in[n]}$ of $\mathcal{Q}_{k,n}$ correspond to the multiplicative inverse of $y_{i,-1}$. As a result, $Y_0^{(k)}/Y_{-1}^{(k)} = \prod_{i=1}^n p_i q_i$, which by [GSTV12, Theorem 2.1] is invariant under $\overline{T_k}$ and forms a Casimir function with respect to a Poisson structure that is invariant under $\overline{T_k}$.

Both [GP16] and [GSTV12] demonstrate that the quiver $Q_{k,n}$ is a bipartite graph that can be embedded into a torus. For further details, see [GP16, §9] and [GSTV12, §3]. This connection links $Q_{k,n}$ to the *Goncharov-Kenyon Dimer Integrable Systems* in [GK13], where a more general definition of Casimir functions is provided.

Conjecture 8.3. *The constant C in Proposition 8.1 equals 1 for all $k \geq 2$.*

We prove Conjecture 8.3 for $k = 2$ and $k = 3$. Let $x_j = x_j(P)$ be the corner invariants of $[P]$. The case $k = 2$ follows from $y_i^{(2)}(P) = -x_{2i+1}x_{2i+2}$ (see Equation (32)), so

$$\prod_{i=1}^n y_i^{(2)}(P) = (-1)^n \prod_{i=1}^n x_{2i+1}x_{2i+2} = (-1)^n\, O_n(P)\, E_n(P),$$

which is T_2-invariant by Lemma 7.3.

For the case $k = 3$, Equation (31) implies

$$\prod_{i=1}^n y_i^{(3)}(P) = (-1)^n \prod_{i=1}^n \frac{x_{2i}x_{2i+3}}{(x_{2i}-1)(x_{2i+3}-1)} = (-1)^n\, \mathcal{F}_1(P)\, \mathcal{F}_2(P),$$

which is T_3-invariant by Proposition 6.1.

References

[FK12] P. Di Francesco and R. Kedem. T-systems with boundaries from network solutions, 2012. 125

[FM16] V. V. Fock and A. Marshakov. *Loop groups, clusters, dimers and integrable systems*, pages 1–65. Springer International Publishing, Cham, 2016. 125

[FMB19] R. Felipe and G. Marí Beffa. The pentagram map on Grassmannians. *Annales de l'Institut Fourier*, 69(1):421–456, 2019. 125

[GK13] A. B. Goncharov and R. Kenyon. Dimers and cluster integrable systems. *Annales scientifiques de l'École Normale Supérieure*, Ser. 4, 46(5):747–813, 2013. 177

[Gli11] M. Glick. The pentagram map and y-patterns. *Advances in Mathematics*, 227(2):1019–1045, 2011. 124, 125, 168

[Gli18] M. Glick. The limit point of the pentagram map. *International Mathematics Research Notices*, 2020(9):2818–2831, 2018. 125

[GP16] M. Glick and P. Pylyavskyy. Y-meshes and generalized pentagram maps. *Proceedings of the London Mathematical Society*, 112(4):753–797, 2016. 125, 127, 130, 132, 164, 166, 167, 168, 176, 177

[GSTV12] M. Gekhtman, M. Shapiro, S. Tabachnikov, and A. Vainshtein. Higher pentagram maps, weighted directed networks, and cluster dynamics. *Electronic Research Announcements*, 19(0):1–17, 2012. 124, 125, 132, 176, 177

[IK23] A. Izosimov and B. Khesin. Long-diagonal pentagram maps. *Bulletin of the London Mathematical Society*, 55(3):1314–1329, 2023. 125

[Izo22a] A. Izosimov. The pentagram map, poncelet polygons, and commuting difference operators. *Compositio Mathematica*, 158(5):1084–1124, 2022. 125

[Izo22b] A. Izosimov. Pentagram maps and refactorization in poisson-lie groups. *Advances in Mathematics*, 404:108476, 2022. 125

[KS13] B. Khesin and F. Soloviev. Integrability of higher pentagram maps. *Mathematische Annalen*, 357(3):1005–1047, 2013. 125

[KS16] B. Khesin and F. Soloviev. The geometry of dented pentagram maps. *Journal of the European Mathematical Society*, 018(1):147–179, 2016. 125

[KV15] R. Kedem and P. Vichitkunakorn. T-systems and the pentagram map. *Journal of Geometry and Physics*, 87:233–247, 2015. Finite dimensional integrable systems: on the crossroad of algebra, geometry and physics. 125

[MB13] G. Marí Beffa. On generalizations of the pentagram map: discretizations of agd flows. *Journal of Nonlinear Science*, 23(2):303–334, 2013. 125

[MB14] G. Marí Beffa. On integrable generalizations of the pentagram map. *International Mathematics Research Notices*, 2015(12):3669–3693, 2014. 125

[NS21] D. Nackan and R. Speciel. Continuous limits of generalized pentagram maps. *Journal of Geometry and Physics*, 167:104292, 2021. 125

[OST10] V. Ovsienko, R. E. Schwartz, and S. Tabachnikov. The pentagram map: a discrete integrable system. *Communications in Mathematical Physics*, 299(2):409–446, 2010. 124, 125, 127, 131, 140

[OST13] V. Ovsienko, R. E. Schwartz, and S. Tabachnikov. Liouville-arnold integrability of the pentagram map on closed polygons. *Duke Mathematical Journal*, 162(12):2149 – 2196, 2013. 124

[Sch92] R. E. Schwartz. The pentagram map. *Experimental Mathematics*, 1(1):71 – 81, 1992. 124, 127, 128, 129, 135

[Sch01] R. E. Schwartz. The pentagram map is recurrent. *Experimental Mathematics*, 10:519–528, 2001. 124, 130

[Sch07] R. E. Schwartz. The poncelet grid. *Advances in Geometry*, 7(2):157–175, 2007. 125

[Sch08] R. E. Schwartz. Discrete monodromy, pentagrams, and the method of condensation. *Journal of Fixed Point Theory and Applications*, 3(2):379–409, 2008. 124, 125, 127, 131, 137, 138, 159, 174

[Sch13] R. E. Schwartz. Pentagram spirals. *Experimental Mathematics*, 22(4):384–405, 2013. 131

[Sch21] R. E. Schwartz. A textbook case of pentagram rigidity, 2021. 125

[Sch24] R. E. Schwartz. Pentagram rigidity for centrally symmetric octagons. *International Mathematics Research Notices*, 2024(12):9535–9561, 2024. 125, 132, 170

[Sch25] R. E. Schwartz. The flapping birds in the pentagram zoo. *Arnold Mathematical Journal*, page to appear, 2025. 125, 126, 128

[Sol13] F. Soloviev. Integrability of the pentagram map. *Duke Mathematical Journal*, 162(15):2815–2853, 2013. 124

[Wei23] M. H. Weinreich. The algebraic dynamics of the pentagram map. *Ergodic Theory and Dynamical Systems*, 43(10):3460–3505, 2023. 125

AUTHOR

Zhengyu Zou
Department of Mathematics,
Brown University
Providence, RI, USA
email: Zhengyu_Zou@brown.edu

Arnold Mathematical Journal
Volume 11, Issue 4, 2025

On symplectic linearizable actions

Eva Miranda

Received 27 Dec 2024; Accepted 24 Aug 2025

Abstract: We prove that linearizable actions are also symplectically linearizable (either smoothly or analytically) in a neighborhood of a fixed point. Specifically, the fundamental vector fields associated with the action can be simultaneously linearized in Darboux coordinates. This result extends equivariant symplectic local normal forms to non-compact group actions.

In both formal and analytic frameworks, the existence of linearizing coordinates is tied to a cohomological equation, which admits a solution for semisimple actions [9, 8]. Consequently, an analytic symplectic action of a semisimple Lie algebra can be locally linearized in Darboux coordinates, enabling the simultaneous analytic linearization of Hamiltonian vector fields near a shared zero. However, in the smooth setting, this result is restricted to semisimple Lie algebras of compact type. We construct an explicit example of a smooth, non-linearizable Hamiltonian action with a semisimple linear part, thereby answering in the negative a question posed by Eliasson [5].

DOI: 10.56994/ARMJ.011.004.007

1 Introduction

A classical result due to Bochner [1] establishes that a compact Lie group action on a smooth manifold is locally equivalent, in the neighbourhood of a fixed point, to its linearization. This result holds in the C^k category. It is worth exploring if similar results hold in the non-compact case.

As observed in [8], if the Lie group is connected, the linearization problem can be formulated in the following terms: find a linear system of coordinates for the vector fields corresponding to the one-parameter subgroups of G; or more generally, consider the representation of a Lie algebra and find coordinates on the manifold that simultaneously linearize the vector fields in the image of the representation vanishing at a point. This is the perspective we adopt in this note when referring to *linearization*.

In the formal and analytic cases, the existence of coordinates that linearize the action is related to a cohomological equation that can always be solved when the Lie group under consideration is semisimple [9], [8]. Guillemin and Sternberg also studied the problem in the C^∞ setting. At the end of [8], they presented the celebrated example of a non-linearizable action of $\mathfrak{sl}(2,\mathbb{R})$ on $\mathbb{R}^3$, constructed via a perturbation involving the radial vector field with flat coefficients. This example has been foundational in the literature, inspiring the construction of other examples with profound geometric implications, such as Weinstein's non-stable Poisson structure example [19].

When the semisimple Lie algebras are of compact type, the linearization of the action can be achieved by combining the local integration of the Lie group action with Bochner's theorem, leading to the linearization of the associated Lie algebra action [6].

Linearization techniques also play a significant role in Hamiltonian systems. When a Hamiltonian system arises from a symplectic action of a compact Lie group fixing a point, the equivariant version of Darboux's theorem ([18], [3]) ensures that the group action can be linearized in Darboux coordinates near the fixed point. It is worth exploring if similar results apply beyond the compact case.

For complete integrable systems, an associated abelian symplectic action emerges.

When the integrable system in local coordinates has a “linear part" linked to a Cartan subalgebra, this leads to non-degenerate singularities [4]. As shown in [5], [4], [10], [11] and [12], complete integrable systems near non-degenerate singular points are equivalent to their linear models. Consequently, the Hamiltonian system itself is equivalent to the linear one. This result provides normal forms for integrable systems near singular non-degenerate points and, specifically, ensures the simultaneous linearization of Hamiltonian vector fields near a common zero.

The next challenge involves Hamiltonian systems with a semisimple linear part, as proposed by Eliasson in [5]. In the formal or analytic setting, results by Guillemin and Sternberg [8] and Kushnirenko [9] demonstrate that such systems are equivalent to the linear model when the symplectic form is disregarded. In this note, we establish that not only can the Hamiltonian vector fields be linearized, but they can also be linearized in Darboux coordinates.

Following Guillemin and Sternberg’s approach, we prove that if a symplectic Lie algebra action of semisimple type fixes a point, there exist analytic Darboux coordinates in which the analytic vector fields generating the Lie algebra action are linear. This result also extends to complex analytic Lie algebra actions on complex analytic manifolds. Additionally, we construct an example of a Hamiltonian system with a semisimple linear part that is not C^∞-linearizable.

Organization of this article: In Section 2, we prove that linearizable actions on symplectic manifolds can be locally linearized in Darboux coordinates. In Section 3, we apply this to show that any real analytic symplectic action of a semisimple Lie algebra can be linearized in real analytic Darboux coordinates in a neighborhood of a fixed point. Furthermore, this result extends to analytic complex manifolds and complex analytic actions of semisimple Lie algebras. In Section 4, we present a counterexample proving that the linearization result does not hold in general for smooth Hamiltonian actions of semisimple Lie algebras.

Acknowledgements: I would like to thank Häkan Eliasson, Ghani Zeghib, David

Martínez-Torres and Marco Castrillón for their valuable feedback on an earlier version of this note.

2 Linearizable actions in Darboux coordinates

Let $\mathfrak{g}$ be a *Lie algebra* and let $\rho : \mathfrak{g} \longrightarrow L_{analytic}$ stand for a representation of $\mathfrak{g}$ in the algebra of real (or complex) analytic vector fields on a real (or complex) analytic manifold M.

We say that $p \in M$ is a **fixed point** for ρ if the vector fields in $\rho(\mathfrak{g})$ vanish at p. We say that ρ can be **linearized** in a neighborhood of a fixed point if there exist local coordinates in a neighbourhood of p such that the vector fields in the image of ρ can be simultaneously linearized (i.e, ρ is **equivalent to a linear representation**).

Assume that the Lie algebra action is (analytically/smoothly) linearizable and assume that M is endowed with a symplectic structure (smooth, analytic). We first prove that it is then symplectically linearizable.

Theorem 2.1. *Let $\mathfrak{g}$ be a Lie algebra and let (M, ω) be a (real or complex) analytic symplectic manifold. Let ρ be a representation by analytic symplectic vector fields. Let p be a fixed point for ρ and assume that ρ can be linearized. Then there exist local analytic coordinates $(x_1, y_1, \dots, x_n, y_n)$ in a neighborhood of p for ρ such that ρ is a linear representation and ω can be written as,*

$$\omega = \sum_{i=1}^{n} dx_i \wedge dy_i.$$

Proof. Let ρ be an analytic symplectic action of a Lie algebra on a manifold M, with a fixed point $p \in M$. Choose analytic coordinates $(x_1, y_1, \dots, x_n, y_n)$ centered at p in which the action ρ is linear. Let ω_1 denote the symplectic form in these coordinates. Although ρ is now linear, ω_1 need not be of Darboux type.

We denote by ω_0 the constant (degree-zero) term in the Taylor expansion of ω_1 at the origin. Since ω_1 is preserved by ρ and ρ is linear, it follows that ω_0 is preserved by the linearized action $\rho^{(1)} = \rho$. In particular, ω_0 is a constant symplectic form invariant under the action. Our goal is to construct a local analytic diffeomorphism ϕ, fixing the origin,

such that $\phi^*(\omega_1) = \omega_0$ and ϕ commutes with ρ. That is, we seek an equivariant analytic Darboux theorem for ω_1, linearizing the form while preserving the linear action ρ.

To this end, we apply the path method [16] for analytic symplectic structures. By the Poincaré lemma, there exists an analytic 1-form α such that

$$\omega_1 = \omega_0 + d\alpha.$$

Define a path of symplectic forms:

$$\omega_t = t\omega_1 + (1-t)\omega_0, \quad t \in [0,1].$$

Each ω_t is an analytic symplectic form in a neighbourhood of the origin. Moreover, the action ρ preserves both ω_0 and ω_1, hence it preserves the entire path ω_t.

We now define the time-dependent analytic vector field X_t by Moser's equation:

$$i_{X_t}\omega_t = -\alpha. \tag{2.1}$$

In order to ensure that X_t is invariant under ρ, it suffices to construct α invariant under ρ. For this purpose, we apply the standard homotopy operator used in the proof of the Poincaré lemma, adapted to our equivariant setting.

Let $R = \sum x_i\partial_{x_i} + y_i\partial_{y_i}$ be the radial vector field, and h_t the homothety $x \longmapsto tx$. Then, we define

$$\alpha := \int_0^1 \frac{1}{t} h_t^*(i_R\beta)\, dt, \quad \text{where } \beta = \omega_1 - \omega_0.$$

Because β is ρ-invariant and ρ commutes with R, it follows that α is also ρ-invariant. Thus, the vector field X_t is invariant under ρ.

Let ϕ_t denote the flow of X_t, satisfying the differential equation

$$\frac{\partial \phi_t}{\partial t}(q) = X_t(\phi_t(q)), \quad \phi_0 = \mathrm{id}. \tag{2.2}$$

Since X_t is ρ-invariant, the flow ϕ_t commutes with the action ρ. Moreover, because α vanishes at the origin, so does X_t, ensuring that each ϕ_t fixes the origin.

By construction, $\phi_t^*(\omega_t) = \omega_0$, and in particular $\phi_1^*(\omega_1) = \omega_0$. The diffeomorphism $\phi := \phi_1$ is then the desired equivariant analytic transformation taking ω_1 to ω_0 while preserving the linear action ρ.

This completes the proof. □

Remark 2.2. The theorem above is stated in the analytic category; however, if the linearization is assumed to hold in the smooth category, the symplectic diffeomorphism obtained from the proof is also smooth.

3 The case of analytic semisimple Lie algebra actions

Guillemin and Sternberg provided in [8] a complete characterization of analytically linearizable actions. They demonstrated that a necessary and sufficient condition for the representation

$$\rho : g \to L_{\text{analytic}}$$

to be locally analytically linearizable is the existence of an analytic vector field X, defined in a neighborhood of p, vanishing at p, with the identity matrix as its Jacobian at p, and commuting with all the vector fields in $\tilde{g}$.

This condition was elegantly recast in cohomological terms in [8]. They proved that the first cohomology group $H^1(g, V^*)$ acts as an obstruction to analytic linearization. For semisimple g, $H^1(g, V^*)$ vanishes for all representation spaces V, ensuring the possibility of analytic linearization. On the other hand, for non-semisimple g, one can construct a representation space V such that $H^1(g, V^*) \neq 0$, which precludes analytic linearization.

This result establishes the semisimple case as a natural candidate for analytic linearization.

Guillemin and Sternberg [8] and Kushnirenko [9] proved the following.

Theorem 3.1 (Guillemin-Sternberg, Kushnirenko)**.** *The representation $\rho : \mathfrak{g} \longrightarrow L_{analytic}$ with $\mathfrak{g}$ semisimple is locally equivalent, via an analytic diffeomorphism, to a linear representation of $\mathfrak{g}$ in a neighbourhood of a fixed point for ρ.*

As an application of theorem 2.1: When the representation is done by Hamiltonian vector fields (locally symplectic), the analytic diffeomorphism that gives the equivalence of the initial representation to the linear representation can be chosen to take the initial symplectic form to the Darboux one. Namely,

Corollary 3.2. *Let $\mathfrak{g}$ be a semisimple Lie algebra and let (M,ω) be a (real or complex) analytic symplectic manifold. Let $\rho : \mathfrak{g} \longrightarrow L_{analytic}$ be a representation by analytic symplectic vector fields. Then there exist local analytic coordinates $(x_1, y_1, \dots, x_n, y_n)$ in a neighbourhood of a fixed point p for ρ such that ρ is a linear representation and ω can be written as,*

$$\omega = \sum_{i=1}^{n} dx_i \wedge dy_i.$$

4 Non-linearizable semisimple smooth actions

4.1 The counterexample of Cairns and Ghys

In this section we recall the results of Cairns and Ghys concerning a C^∞-action of $SL(2,\mathbb{R})$ on $\mathbb{R}^3$ which is not linearizable. All results mentioned in this section are contained in section 8 of [2].

Consider the basis $\{X, Y, Z\}$ of $\mathfrak{sl}(2,\mathbb{R})$ satisfying the relations:

$$[X,Y] = -Z, \quad [Z,X] = Y, \quad [Z,Y] = -X$$

Now consider the representation on $\mathbb{R}^3$ defined on this basis as:

$$\begin{aligned} \rho(X) &= y\frac{\partial}{\partial z} + z\frac{\partial}{\partial y} \\ \rho(Y) &= x\frac{\partial}{\partial z} + z\frac{\partial}{\partial x} \\ \rho(Z) &= x\frac{\partial}{\partial y} - y\frac{\partial}{\partial x} \end{aligned} \tag{4.1}$$

The orbits of this action are the level sets of the quadratic form $Q = x^2 + y^2 - z^2 = r^2 - z^2$ (where $r^2 = x^2 + y^2$). These level sets are non-degenerate quadrics: one-sheeted hyperboloids for $Q > 0$, two-sheeted hyperboloids for $Q < 0$, and a quadratic cone for $Q = 0$.

Introduce the radial vector field

$$R = x\,\frac{\partial}{\partial x} + y\,\frac{\partial}{\partial y} + z\,\frac{\partial}{\partial z},$$

and perturb ρ by setting

$$\begin{aligned} \widetilde{X} &= \rho(X) + f\,R\,, \\ \widetilde{Y} &= \rho(Y) + g\,R\,, \\ \widetilde{Z} &= \rho(Z)\,, \end{aligned} \tag{4.2}$$

where

$$f(x,y,z) = x\,A\big(z,\sqrt{x^2+y^2}\big), \quad g(x,y,z) = -\,y\,A\big(z,\sqrt{x^2+y^2}\big),$$

and

$$A(z,r) \;=\; \frac{a\big(r^2-z^2\big)}{r^2},$$

with $a:\,\mathbb{R}\to\mathbb{R}$ any C^∞–function which vanishes for $r^2 - z^2 \le 0$ and is bounded.

By [2], the fields $\widetilde{X},\widetilde{Y},\widetilde{Z}$ still close under the Lie bracket to an $\mathfrak{sl}(2,\mathbb{R})$–algebra and are complete. Hence they integrate to an action $\hat{\rho}$ of the universal cover of $SL(2,\mathbb{R})$, which descends to $SL(2,\mathbb{R})$ itself since $\widetilde{Z} = \rho(Z)$ is unchanged. Moreover:

- On the "hyperbolic region" $\{x^2 + y^2 > z^2\}$, one has $a(r^2 - z^2) \neq 0$ and $\{\widetilde{X},\widetilde{Y},\widetilde{Z}\}$ are linearly independent, so $\hat{\rho}$–orbits are 3-dimensional.

- On and inside the "cone" $\{x^2 + y^2 \le z^2\}$, one has $a(r^2 - z^2) = 0$ so $\widetilde{X} = \rho(X)$, $\widetilde{Y} = \rho(Y)$, and $\hat{\rho}$ coincides with the linear action.

Since the original linear action never has 3-dimensional orbits, $\hat{\rho}$ cannot be conjugate to it. Therefore, the deformed action is not linearizable.

4.2 The counterexample of Guillemin and Sternberg

The construction of Guillemin and Sternberg [8] follows the guidelines outlined below. It is quite similar to the counterexample of Grant and Cairns; however, the key difference

is that the vector field the perturbation does not preserve Z, so it cannot be guaranteed that it lifts to $SL(2,\mathbb{R})$.

If we perturb the initial action of $\mathfrak{sl}(2,\mathbb{R})$ to the non-linear action:

$$\hat{\rho}(X) = \rho(X) + \frac{xz}{r^2} g(r^2 - z^2)R,$$
$$\hat{\rho}(Y) = \rho(Y) - \frac{yz}{r^2} g(r^2 - z^2)R,$$
$$\hat{\rho}(Z) = \rho(Z) + g(r^2 - z^2)R,$$

where $R = x\frac{\partial}{\partial x} + y\frac{\partial}{\partial y} + z\frac{\partial}{\partial z}$ is the radial vector field, and $g \in C^\infty(\mathbb{R})$ is such that $g(x) > 0$ if $x > 0$, and $g(x) = 0$ if $x \leq 0$.

Inside the cone $r^2 - z^2$, the two sets of vector fields are identical. However, if we choose $g(u) = e^{-1/u^2}$, $u > 0$, and $g(u) = 0$, $u \leq 0$, for example, then outside the cone $r^2 - z^2 = 0$, the vector field $\rho(X) = x\frac{\partial}{\partial y} - y\frac{\partial}{\partial x}$ has closed circular orbits, while the corresponding deformed vector field $\hat{\rho}(X)$ has orbits that spiral outward.

Therefore, it is impossible to find a C^∞-mapping defined in a neighborhood of the origin. Hence, ρ is not linearizable.

4.3 A Hamiltonian counterexample

We construct a counterexample to C^∞–linearization under the hypothesis that the action is Hamiltonian, thereby giving a negative answer to a question of Eliasson [5]. We keep the notation of the Cairns–Ghys construction from Section 4.1.

Proposition 4.1. *Let α be the $SL(2,\mathbb{R})$–action on $\mathbb{R}^3$ generated by*

$$\overline{X} = \rho(X) + fR, \qquad \overline{Y} = \rho(Y) + gR, \qquad \overline{Z} = \rho(Z),$$

where $R = x\,\partial_x + y\,\partial_y + z\,\partial_z$ and

$$f = x\,A\Big(z, \sqrt{x^2+y^2}\Big), \qquad g = -y\,A\Big(z, \sqrt{x^2+y^2}\Big), \qquad A(z,r) = \frac{a(r^2 - z^2)}{r^2},$$

with $a : \mathbb{R} \to \mathbb{R}$ smooth, bounded, and vanishing on $\mathbb{R}^-$. Let $\widehat{\alpha}$ be the cotangent lift of α to $T^*(\mathbb{R}^3)$. Then $\widehat{\alpha}$ is Hamiltonian and not C^∞–linearizable in a neighbourhood of the origin.

Proof. For a diffeomorphism $g : M \to M$, the cotangent lift is

$$\widehat{g}(q,p) = \big(g(q),\, (dg_q^{-1})^* p\big),$$

so

$$\pi \circ \widehat{g} = g \circ \pi \qquad \text{and} \qquad \widehat{g}(q,0) = (g(q),0). \tag{4.3}$$

Thus fibres map to fibres and the zero section is preserved by *every* cotangent lift. In particular, with

$$F := \pi^{-1}(0) = \{x = y = z = 0\}, \qquad Z := \{a = b = c = 0\}, \qquad O := (0,0,0;0,0,0),$$

both F and Z are invariant for the lifted linear action and for the lifted Cairns–Ghys action (note that 0 is fixed in the base, since ρ is linear and fR, gR vanish at 0).

Let $\alpha^{(1)}$ denote the linear part of α and $\widehat{\alpha}^{(1)}$ its cotangent lift. The latter is Hamiltonian for $\omega = d\theta$ ($\theta = a\,dx + b\,dy + c\,dz$), with moment map

$$\mu = (zb + cy,\ az + cx,\ -ay + bx) \in \mathfrak{sl}(2,\mathbb{R})^*,$$

whose Jacobian is

$$D\mu = \begin{pmatrix} 0 & c & b & 0 & z & y \\ c & 0 & a & z & 0 & x \\ b & -a & 0 & -y & x & 0 \end{pmatrix}.$$

For Hamiltonian actions one has $\dim(G{\cdot}m) = \operatorname{rank} d\mu_m$ (see, for instance, [7, §26]). A direct computation shows that

$$\operatorname{rank} D\mu = \begin{cases} 0, & p = O, \\ 2, & (x,y,z) \times (-a,-b,c) = 0,\ p \neq O, \\ 3, & \text{otherwise.} \end{cases}$$

Equivalently, the rank drops to 2 precisely when (x,y,z) is collinear with $(-a,-b,c)$, a locus

containing $F = \{x = y = z = 0\}$ and $Z = \{a = b = c = 0\}$ but strictly larger. Consequently,

$$\dim \mathcal{O}_{\widehat{\alpha}^{(1)}}(p) = \begin{cases} 0, & p = O, \\ 2, & (x, y, z) \times (-a, -b, c) = 0, \ p \neq O, \\ 3, & \text{otherwise}, \end{cases} \tag{4.4}$$

and, in particular, $\dim \mathcal{O}_{\widehat{\alpha}^{(1)}}(q, 0) = 2$ for all $q \neq 0$.

For any lifted action, the fundamental vector fields satisfy

$$\widehat{\xi}_X(q, p) = \big(\xi_X(q), \ -p \circ d\xi_X(q)\big). \tag{4.5}$$

Hence along Z one has $\widehat{\xi}_X(q, 0) = (\xi_X(q), 0)$, so every orbit starting in Z stays in Z. Conversely, no orbit through a point $(q, p) \notin Z$ can be contained in Z, since it already contains $(q, p) \notin Z$. Thus, near O, the orbits contained in Z are exactly those starting in Z. Moreover, from (4.5) we read off

$$\dim \mathcal{O}^{\widehat{\alpha}}(q, 0) = \dim \mathcal{O}^{\alpha}(q).$$

By [2, §8] there exist points $q \to 0$ in the base with 3–dimensional α–orbits. For such q, put $p = (q, 0) \in Z \setminus \{O\}$. Then

$$\dim \mathcal{O}^{\widehat{\alpha}}(q, 0) = \dim \mathcal{O}^{\alpha}(q) = 3. \tag{4.6}$$

Assume, for contradiction, that there exists a germ $\Phi : (T^*M, O) \to (T^*M, O)$ with $\Phi \circ \widehat{\alpha}^{(1)} = \widehat{\alpha} \circ \Phi$. Conjugacy carries orbits diffeomorphically to orbits, preserving their dimension. Since, near O, the orbits contained in Z are precisely those starting in Z for both lifted actions, necessarily $\Phi(Z) = Z$ and $\Phi(F) = F$. Hence $\Phi^{-1}(p) \in Z \setminus \{O\}$, so by (4.4)

$$\dim \mathcal{O}^{\widehat{\alpha}^{(1)}}\big(\Phi^{-1}(p)\big) = 2,$$

whereas by (4.6) $\dim \mathcal{O}^{\widehat{\alpha}}(p) = 3$, a contradiction. Therefore, $\widehat{\alpha}$ is not C^∞–linearizable near the zero section. □

Remark 4.2. We can employ the same strategy, adopting the counterexample by Guillemin and Sternberg in the process.

Consider the Lie algebra action of $\mathfrak{sl}(2,\mathbb{R})$, denoted by $\overline{\rho}$, on $\mathbb{R}^3$, generated by the vector fields:

$$\hat{\rho}(X) = \rho(X) + \frac{xz}{r^2} g(r^2 - z^2)R,$$
$$\hat{\rho}(Y) = \rho(Y) - \frac{yz}{r^2} g(r^2 - z^2)R,$$
$$\hat{\rho}(Z) = \rho(Z) + g(r^2 - z^2)R,$$

where $R = x\frac{\partial}{\partial x} + y\frac{\partial}{\partial y} + z\frac{\partial}{\partial z}$ is the radial vector field, and $g \in C^\infty(\mathbb{R})$ satisfies $g(u) = e^{-1/u^2}$ for $u > 0$ and $g(u) = 0$ for $u \leq 0$.

Using similar guidelines to those of Guillemin and Sternberg in [8], we can verify that the lifted action to $T^*(\mathbb{R}^3)$ is not C^∞-linearizable.

The lift of the action can be computed using the Liouville one-form. Let $\theta = a\,dx + b\,dy + c\,dz$. Then, the lift of the non-perturbed vector field is a Hamiltonian vector field with the Hamiltonian function

$$f = -ay + bx,$$

and the lifted vector field of the perturbed system is the Hamiltonian vector field with respect to the function

$$f' = -ay + bx + g(r^2 - z^2)(ax + by).$$

The Hamiltonian vector field of f is given by:

$$x\frac{\partial}{\partial y} - y\frac{\partial}{\partial x} + a\frac{\partial}{\partial b} - b\frac{\partial}{\partial a},$$

and it exhibits periodic orbits. In contrast, the corresponding deformed vector field, the Hamiltonian vector field of f', has orbits that spiral outward.

4.4 The case of semisimple Lie algebras of compact type

When the Lie algebra action is of compact type, it can be integrated into an action of a compact Lie group G (see [6] for a proof, which is based on the use of algebroids).

Given a fixed point for the action p, we can associate a linear action of the group in a neighbourhood of p, with the group action preserving the symplectic structure (which we can assume to be in Darboux coordinates). Applying the equivariant Darboux theorem [3], we obtain a diffeomorphism ϕ that linearizes the group action G in Darboux coordinates. By differentiation, this provides the linearization of the Lie algebra action ρ.

Acknowledgments

Eva Miranda is supported by the Catalan Institution for Research and Advanced Studies via an ICREA Academia Prize 2021 and by the Alexander Von Humboldt Foundation via a Friedrich Wilhelm Bessel Research Award. The author is also supported by the Spanish State Research Agency, through the Severo Ochoa and María de Maeztu Program for Centers and Units of Excellence in R&D (project CEX2020-001084-M) and the project PID2023-146936NB-I00 by the Spanish State Research Agency MCIU/AEI / 10.13039/501100011033/ FEDER, UE. She was also supported by the AGAUR project 2021 SGR 00603 Geometry of Manifolds and Applications, GEOMVAP.

References

[1] S. Bochner, *Compact groups of differentiable transformations.* Ann. of Math. (2) **46**, (1945). 372–381. 182

[2] G. Cairns and E. Ghys, *The local linearization problem for smooth $SL(n)$-actions*, Enseign. Math. (2) 43 (1997), no. 1-2, 133-171. 187, 188, 191

[3] M. Chaperon, *Quelques outils de la théorie des actions différentiables* Third Schnepfenried geometry conference, Vol. 1 (Schnepfenried, 1982), 259–275, Astérisque, 107-108, Soc. Math. France, Paris, 1983. 182, 193

[4] L. H. Eliasson, *Normal forms for Hamiltonian systems with Poisson commuting integrals*, Ph.D. Thesis (1984). 183

[5] L.H. Eliasson, *Normal forms for Hamiltonian systems with Poisson commuting integrals—elliptic case*, Comment. Math. Helv. **65** (1990), no. 1, 4–35. 181, 183, 189

[6] R. L. Fernandes and Ph. Monnier, *Linearization of Poisson brackets*, Lett. Math. Phys. 69, (2004) 89-114. 182, 193

[7] V. Guillemin and S. Sternberg, *Symplectic Techniques in Physics*, Cambridge University Press, Cambridge, 1990. 190

[8] V. Guillemin and S. Sternberg, *Remarks on a paper of Hermann*, Trans. Amer. Math. Soc. **130** (1968) 110–116. 181, 182, 183, 186, 188, 192

[9] A.G. Kushnirenko,*Linear-equivalent action of a semisimple Lie group in the neighbourhood of a stationary point*, Functional Anal. Appll, **1**, (1967) 89-90. 181, 182, 183, 186

[10] E. Miranda, *On symplectic linearization of singular Lagrangian foliations*, Ph.D. thesis, Universitat de Barcelona, ISBN: 9788469412374, 2003. 183

[11] E. Miranda, *Integrable systems and group actions.* Cent. Eur. J. Math. 12 (2014), no. 2, 240–270. 183

[12] E. Miranda and N.T. Zung, *Equivariant normal forms for nondegenerate singular orbits of integrable Hamiltonian systems*, Ann. Sci. Ecole Norm. Sup., 37, no. 6, 2004, pp. 819–839. 183

[13] E. Miranda and N. T. Zung, *A note on equivariant normal forms of Poisson structures*, Math. Research Notes, 2006, vol 13-6, 1001–1012.

[14] E. Miranda, *Some rigidity results for Symplectic and Poisson group actions*, XV International Workshop on Geometry and Physics, 177–183, Publ. R. Soc. Mat. Esp., 11, R. Soc. Mat. Esp., Madrid, 2007.

[15] E. Miranda, P. Monnier and N.T. Zung, *Rigidity of Hamiltonian actions on Poisson manifolds.* Adv. Math. 229, No. 2, 1136-1179 (2012).

[16] J. Moser, *On the volume elements on a manifold*, Trans. Am. Math. Soc. 120, 286-294 (1965). 185

[17] R. Palais, *Equivalence of nearby differentiable actions of a compact group.* Bull. Amer. Math. Soc. 67 1961 362–364.

[18] A. Weinstein, *Lectures on symplectic manifolds.* Regional Conference Series in Mathematics, No.**29**. American Mathematical Society, Providence, R.I., 1977. 182

[19] A. Weinstein, *The local structure of Poisson manifolds.*, J. Differential Geom. 18 (1983), no. 3, 523–557. 182

AUTHOR

Eva Miranda
Laboratory of Geometry and Dynamical Systems
and
SYMCREA research unit,
Department of Mathematics,
Universitat Politècnica de Catalunya,
Barcelona, Spain
and
Centre de Recerca Matemática, CRM
email: eva.miranda@upc.edu

Arnold Mathematical Journal
Volume 11, Issue 4, 2025

Discrete Painlevé equations from pencils of quadrics in $\mathbb{P}^3$ with branching generators

Jaume Alonso Yuri B. Suris

Received 02 Jun 2025; Accepted 07 Jan 2026

Abstract: In this paper we extend the novel approach to discrete Painlevé equations initiated in our previous work [2]. A classification scheme for discrete Painlevé equations proposed by Sakai interprets them as birational isomorphisms between generalized Halphen surfaces (surfaces obtained from $\mathbb{P}^1 \times \mathbb{P}^1$ by blowing up at eight points). Sakai's classification is thus based on the classification of generalized Halphen surfaces. In our scheme, the family of generalized Halphen surfaces is replaced by a pencil of quadrics in $\mathbb{P}^3$. A discrete Painlevé equation is viewed as an autonomous transformation of $\mathbb{P}^3$ that preserves the pencil and maps each quadric of the pencil to a different one. Thus, our scheme is based on the classification of pencils of quadrics in $\mathbb{P}^3$. Compared to our previous work, here we consider a technically more

DOI: 10.56994/ARMJ.011.004.008

demanding case where the characteristic polynomial $\Delta(\lambda)$ of the pencil of quadrics is not a complete square. As a consequence, traversing the pencil via a 3D Painlevé map corresponds to a translation on the universal cover of the Riemann surface of $\sqrt{\Delta(\lambda)}$, rather than to a Möbius transformation of the pencil parameter λ as in [2].

1 Introduction

This paper is the second contribution to our study devoted to a novel interpretation of discrete Painlevé equations, which builds up on [2]. Discrete Painlevé equations belong to the most intriguing objects in the theory of discrete integrable systems. After some examples sporadically appeared in various applications, their systematic study started when Grammaticos, Ramani and Papageorgiou proposed the notion of "singularity confinement" as an integrability detector, and found the first examples of second order nonlinear non-autonomous difference equations with this property, which they denoted as *discrete Painlevé equations* [9, 16]. The activity of their group was summarized in [8]. A general classification scheme of discrete Painlevé equations was proposed by Sakai [18] and it is given a detailed exposition in the review paper by Kajiwara, Noumi and Yamada [11]. In the framework of Sakai's scheme, discrete Painlevé equations are birational maps between *generalized Halphen surfaces* X. The latter can be realized as $\mathbb{P}^1 \times \mathbb{P}^1$ blown up at eight points. A monographic exposition of discrete Painlevé equations is given by Joshi [10].

Let us summarize the main ingredients and features of our alternative approach to discrete Painlevé equations, initiated in [2].

- A pencil of quadrics $\{Q_\lambda\}$ in $\mathbb{P}^3$ containing non-degenarate quadrics. Such pencils can be classified modulo projective transformations of $\mathbb{P}^3$, and they come in thirteen classes. The class of the pencil can be identified by the type of its *base curve* $Q_0 \cap$

Q_∞. This is a spatial curve of degree 4, whose type can vary from a generic one (irreducible smooth curve for a pencil of type (i)), through irreducible curves with a node (type (ii)) or with a cusp (type (iii)), to various types of reducible curves (from two non-coplanar conics intersecting at two points, type (iv), to a pair of intersecting double lines, type (xiii)).

- The second pencil of quadrics $\{P_\mu\}$ having one quadric in common with $\{Q_\lambda\}$, say $P_\infty = Q_\infty$. The base curves of both pencils intersect at eight points S_i, $i = 1, \dots, 8$.
- Given two pencils of quadrics, one can define a three-dimensional analog of a QRT map $F = i_1 \circ i_2$, where the 3D QRT involutions i_1, i_2 act along two families of generators of Q_λ, see [1]. Each involution puts into correspondence two intersection points of a generator with the quadric P_μ. By definition, such an involution, and therefore the 3D QRT map $F = i_1 \circ i_2$, leaves each quadric of two pencils invariant, and thus possesses two rational integrals of motion $\lambda = Q_0/Q_\infty$ and $\mu = P_0/P_\infty$.
- A *Painlevé deformation map* is the device which allows us to travel across the pencil $\{Q_\lambda\}$. More precisely, such a map L on $\mathbb{P}^3$ preserves the pencil, but not fiber-wise. Rather, it sends each quadric Q_λ to a different quadric $Q_{\widehat{\lambda}}$. Moreover, L preserves the base curve of the pencil $\{Q_\lambda\}$. In the cases considered in [2], the base curve is reducible and contains straight lines. In these cases, L does not necessarily fix these straight lines point-wise. In the cases considered in the present paper, L fixes the base curve $Q_0 \cap Q_\infty$ pointwise (in particular, it fixes all eight points S_i).
- A *3D Painlevé map* is obtained by composition $\widetilde{F} = L \circ i_1 \circ L \circ i_2$, provided it possesses the singularity confinement property. It is to be stressed that the pencil $\{Q_\lambda\}$ continues to play a fundamental role in the dynamics of $\widetilde{F}$: the maps $L \circ i_1$, $L \circ i_2$ preserve the pencil and map each quadric Q_λ to $Q_{\widehat{\lambda}}$. We do not have a straightforward description of the dynamical role of the pencil $\{P_\mu\}$, but anticipate its relation to the isomonodromic description of the discrete Painlevé equations.

One can say that in our approach the role of a family of generalized Halphen surfaces

is played by the quadrics of the pencil $\{Q_\lambda\}$ with eight distinguished points on the base curve of the pencil. The base curve itself plays the role of the unique anti-canonical divisor. Let us stress several features of our construction which are in a sharp contrast to the Sakai scheme.

- Neither the exceptional divisor nor the eight distinguished points evolve under the map $\widetilde{F}$. Their discrete time evolution is apparent and is due to their representation in the so-called *pencil-adapted coordinates*. These are coordinates $(x, y, \lambda) \in \mathbb{P}^1 \times \mathbb{P}^1 \times \mathbb{P}^1$ establishing an isomorphism between each quadric Q_λ of the pencil and $\mathbb{P}^1 \times \mathbb{P}^1$. The pencil-adapted coordinates of a point on the base curve do depend on λ, so traversing the pencil $\lambda \longmapsto \widehat{\lambda}$ under $\widetilde{F}$ induces an *apparent discrete time evolution* of the base curve and of the eight distinguished points.

- The shift parameter δ of discrete Painlevé equations (or its exponent $q = e^\delta$ for the q-difference equations among them) is not an intrinsic characteristic of the configuration of eight distinguished points, but is a free parameter of the construction.

One can say that our approach is a realization of the old-style idea of discrete Painlevé equations being non-autonomous versions (or modifications) of the QRT maps. This idea was instrumental in the discovery and early classification attempts of discrete Painlevé equations, summarized in [8]. A more geometric version of this procedure was proposed in the framework of the Sakai's scheme by Carstea, Dzhamay and Takenawa [5]. In their scheme, the de-autonomization of a given QRT map depends on the choice of one biquadratic curve of the pencil. In our approach, the choice of the base curve and eight distinguished point on it determines uniquely all the ingredients of the construction, starting with the two pencils of quadrics.

The structure of the paper is as follows. In Section 2, we describe the construction scheme of discrete Painlevé equations applicable to the present case and stress its distinctions from the previous paper [2]. The main distinction is that here we consider the pencils whose characteristic polynomial $\Delta(\lambda)$ is not a complete square. As a consequence,

the 3D QRT involutions i_1, i_2 and the 3D QRT map $F = i_1 \circ i_2$ are no more birational maps of $\mathbb{P}^3$. Rather, these maps become birational maps on $\mathcal{X}$, a branched double covering of $\mathbb{P}^3$, whose ramification locus is the union of the singular quadrics Q_{λ_i}, where λ_i are the branch points of the Riemann surface $\mathcal{R}$ of $\sqrt{\Delta(\lambda)}$.

In Section 3, we formulate a general recipe for the construction of the Painlevé deformation map L, responsible to the evolution $\lambda \longmapsto \widehat{\lambda}$ across the pencil of quadrics $\{Q_\lambda\}$. While in the first part [2] we had $\widehat{\lambda} = \sigma(\lambda)$, where $\sigma : \mathbb{P}^1 \to \mathbb{P}^1$ is a Möbius automorphism fixing the set $\mathrm{Sing}(Q) := \{\lambda \in \mathbb{P}^1 : \ Q_\lambda \text{ is degenerate}\}$, in the present paper the natural definition becomes $\widehat{\lambda} = \lambda(\widehat{\nu})$, where $\lambda = \lambda(\nu)$ is the holomorphic uniformization map for the Riemann surface $\mathcal{R}$, and $\widehat{\nu} = \nu + 2\delta$ is the translation on the universal cover $\mathbb{C}$. The recipe turns out to be applicable to all types of the pencil $\{Q_\lambda\}$ except for the generic type (i). The latter leads to the elliptic Painlevé equation, which will be treated in a separate publication.

In Section 4, we show that the so constructed L ensures the fundamental singularity confinement property for our 3D Painlevé maps.

There follow five Sections 5–9 containing a detailed elaboration of our scheme for all relevant types of the pencils except for the type (i). We recover, within our novel framework, all discrete Painlevé equations except for the elliptic one, which is left for a separate publication.

2 General scheme

We now describe the construction scheme of discrete Painlevé equations applicable to the present case and stress its distinctions from the previous paper [2]. The first steps are the same as there:

- Start with a pencil $\{C_\mu\}$ of biquadratic curves in $\mathbb{P}^1 \times \mathbb{P}^1$ and the corresponding QRT map. Let $s_1, \dots, s_8 \in \mathbb{P}^1 \times \mathbb{P}^1$ be the base points of this pencil. Lift $\{C_\mu\}$ to a pencil of quadrics $\{P_\mu\}$ in $\mathbb{P}^3$ using the *Segre embedding* of $\mathbb{P}^1 \times \mathbb{P}^1$ to $\mathbb{P}^3$. The base curve of this

pencil passes through the lifts $S_1, \dots, S_8$ of the base points $s_1, \dots, s_8$.

- Choose one distinguished biquadratic curve C_∞ of the pencil, along with its lift to a quadric P_∞.
- Based on these data, construct the pencil of quadrics $\{Q_\lambda = Q_0 - \lambda Q_\infty\}$ in $\mathbb{P}^3$ spanned by $Q_0 = \{X_1X_2 - X_3X_4 = 0\}$ and $Q_\infty := P_\infty$. Recall that Q_0 is nothing but the image of $\mathbb{P}^1 \times \mathbb{P}^1$ by the Segre embedding. The base curve of the pencil $\{Q_\lambda\}$ is, by definition, the curve $Q_0 \cap Q_\infty$, which is the image of C_∞ under the Segre embedding. The intersection of this curve with the base curve of the pencil $\{P_\mu\}$ consists exactly of the points $S_1, \dots, S_8$.

The characteristic polynomial of the pencil $\{Q_\lambda\}$ is

$$\Delta(\lambda) = \det(M_\lambda) = \det(M_0 - \lambda M_\infty), \tag{1}$$

where $M_0, M_\infty \in \mathrm{Sym}_{4\times 4}(\mathbb{C})$ are symmetric matrices of the quadratic forms Q_0, Q_∞. In the present paper, we are dealing with the cases where this polynomial is *not a complete square*. According to the projective classification of pencils of quadrics, discussed in [2], these are the following six cases:

(i) *Pencil of quadrics through a non-singular spatial quartic curve.*
Segre symbol $[1,1,1,1]$; $\Delta(\lambda) = (\lambda-\lambda_1)(\lambda-\lambda_2)(\lambda-\lambda_3)(\lambda-\lambda_4)$.

(ii) *Pencil of quadrics through a nodal spatial quartic curve.*
Segre symbol $[2,1,1]$; $\Delta(\lambda) = (\lambda-\lambda_1)^2(\lambda-\lambda_2)(\lambda-\lambda_3)$.

(iii) *Pencil of quadrics through a cuspidal spatial quartic curve.*
Segre symbol $[3,1]$; $\Delta(\lambda) = (\lambda-\lambda_1)^3(\lambda-\lambda_2)$.

(iv) *Pencil of quadrics through two non-coplanar conics sharing two points.*
Segre symbol $[(1,1),1,1]$; $\Delta(\lambda) = (\lambda-\lambda_1)^2(\lambda-\lambda_2)(\lambda-\lambda_3)$.

(v) *Pencil of quadrics through two non-coplanar conics touching at a point.*
Segre symbol $[(2,1),1]$; $\Delta(\lambda) = (\lambda-\lambda_1)^3(\lambda-\lambda_2)$.

(vi) *Pencil of quadrics tangent along a non-degenerate conic.*
Segre symbol $[(1,1,1),1]$; $\Delta(\lambda) = (\lambda-\lambda_1)^3(\lambda-\lambda_2)$.

As discussed in [2], for $X \in Q_\lambda$, the generators $\ell_1(X)$ and $\ell_2(X)$ are rational functions of X and of $\sqrt{\Delta(\lambda)}$. The dependence on λ can be expressed as a holomorphic dependence on the point of the Riemann surface $\mathcal{R}$ of $\sqrt{\Delta(\lambda)}$. This Riemann surface is a double cover of $\widehat{\mathbb{C}}$ branched at two or at four points. By the uniformization theorem, its universal cover is $\mathbb{C}$. We will denote the uniformizing variable $\nu \in \mathbb{C}$, so that the maps $\nu \longmapsto \lambda$ and $\nu \longmapsto \sqrt{\Delta(\lambda)}$ are holomorphic. The following three situations can be distinguished:

- case (i): four distinct branch points $\lambda_1, \lambda_2, \lambda_3, \lambda_4$, the Riemann surface $\mathcal{R}$ is a torus, whose conformal class is determined by the cross-ratio of the branch points. This case, corresponding to the elliptic Painlevé equations, will be treated in an upcoming work;

- cases (ii), (iv): two branch points λ_2, λ_3, one of the periods of the torus becomes infinite, so that $\mathcal{R}$ is a cylinder;

- cases (iii), (v), (vi): two branch points λ_1, λ_2, both periods of the torus become infinite, so that $\mathcal{R}$ is plane.

It becomes necessary to introduce modifications in the two major ingredients of the construction in [2].

- The generators ℓ_1, ℓ_2 are not rational functions on $\mathbb{P}^3$ anymore. Rather, they become well-defined rational maps on the variety $\mathcal{X}$ which is a branched double covering of $\mathbb{P}^3$, whose ramification locus is the union of the singular quadrics Q_{λ_i}, where λ_i are the branch points of $\mathcal{R}$. The same is true for a linear projective change of variables $X = A_\nu Y$ reducing the quadratic form $Q_{\lambda(\nu)}$ to the standard form Q_0, which we now write as

$$Q_{\lambda(\nu)}(A_\nu Y) = Q_0(Y), \quad \text{or} \quad A_\nu^{\mathrm{T}} M_{\lambda(\nu)} A_\nu = M_0, \tag{2}$$

and for the *pencil-adapted coordinates*

$$\begin{bmatrix} X_1 \\ X_2 \\ X_3 \\ X_4 \end{bmatrix} = A_\nu \begin{bmatrix} x \\ y \\ xy \\ 1 \end{bmatrix} =: \phi_\nu(x,y). \tag{3}$$

Thus, ϕ_ν gives a parametrization of $Q_{\lambda(\nu)}$ by $(x,y) \in \mathbb{P}^1 \times \mathbb{P}^1$, such that the generators ℓ_1, resp. ℓ_2 of Q_λ correspond to $x = \text{const}$, resp. to $y = \text{const}$. Interchanging two sheets of the covering corresponds to interchanging two families of generators ℓ_1, ℓ_2.

- Also the *3D QRT involutions* i_1, i_2 for the pencil $\{Q_\lambda\}$, defined by intersections of its generators ℓ_1, ℓ_2 with the quadrics P_μ (see [1]), are not birational maps of $\mathbb{P}^3$ anymore, and the same is true for the *3D QRT map* $F = i_1 \circ i_2$. Rather, these maps become birational maps on $\mathcal{X}$.

The next main deviation from the construction of [2] is that it becomes unnatural to consider Painlevé deformation maps L as birational maps $\mathbb{P}^3$ preserving the pencil $\{Q_\lambda\}$ and sending each Q_λ to $Q_{\sigma(\lambda)}$, where $\sigma : \mathbb{P}^1 \to \mathbb{P}^1$ is a Möbius automorphism fixing the set $\mathrm{Sing}(Q) := \{\lambda \in \mathbb{P}^1 : Q_\lambda \text{ is degenerate}\}$. Instead, in the present context we formulate the following requirement.

- A Painlevé deformation map L is a birational map on $\mathcal{X}$ preserving the pencil $\{Q_\lambda\}$ and sending $Q_{\lambda(\nu)}$ to $Q_{\lambda(\widehat{\nu})}$, where $\nu \longmapsto \widehat{\nu} = \nu + 2\delta$ is a translation on the universal cover of $\mathcal{R}$.

As compared with [2], our construction will involve some additional ingredients, required to establish the relation to the form of discrete Painlevé equations known from the literature. The Painlevé deformation map L is decomposed in two factors, each one depending only on one of the variables x, y, and shifting the variable ν by δ. This can be done in two ways:

$$L = L_1 \circ R_2, \quad \text{where} \quad L_1 : (x,y,\nu) \longmapsto (x,\widetilde{y},\nu+\delta), \quad R_2 : (x,y,\nu) \longmapsto (\widetilde{x},y,\nu+\delta), \tag{4}$$

resp.

$$L = L_2 \circ R_1, \quad \text{where} \quad L_2 : (x, y, \nu) \longmapsto (\widetilde{x}, y, \nu + \delta), \quad R_1 : (x, y, \nu) \longmapsto (x, \widetilde{y}, \nu + \delta). \tag{5}$$

(The indices 1, 2 refer to the variables which *do not* change under the map, like for i_1, i_2.) Each one of L_1, L_2, R_1, R_2 maps $Q_{\lambda(\nu)}$ to $Q_{\lambda(\nu+\delta)}$. We set

$$\nu_n = \nu_0 + 2n\delta \quad \text{for} \quad n \in \frac{1}{2}\mathbb{Z},$$

so that $\nu_{n+1/2} = \nu_n + \delta$. The variables associated to the discrete Painlevé equations known from the literature, parametrize in our formulation the quadrics with half-integer indices, namely

$$(x_n, y_n, \nu_{2n-1/2}) \in Q_{\lambda(\nu_{2n-1/2})}, \quad (x_{n+1}, y_n, \nu_{2n+1/2}) \in Q_{\lambda(\nu_{2n+1/2})}.$$

Definition 1. *A 3D Painlevé map is given by*

$$\widetilde{F} = \widetilde{i}_1 \circ \widetilde{i}_2, \quad \textit{where} \quad \widetilde{i}_1 = R_1 \circ i_1 \circ L_1, \quad \widetilde{i}_2 = R_2 \circ i_2 \circ L_2, \tag{6}$$

or, in coordinates,

$$(x_n, y_n, \nu_{2n-1/2}) \overset{L_2}{\to} (x, y_n, \nu_{2n}) \overset{i_2}{\to} (\widetilde{x}, y_n, \nu_{2n}) \overset{R_2}{\to} (x_{n+1}, y_n, \nu_{2n+1/2}) \tag{7}$$

$$\overset{L_1}{\to} (x_{n+1}, y, \nu_{2n+1}) \overset{i_1}{\to} (x_{n+1}, \widetilde{y}, \nu_{2n+1}) \overset{R_1}{\to} (x_{n+1}, y_{n+1}, \nu_{2n+3/2}). \tag{8}$$

The map $\widetilde{F}$ is conjugate to $L \circ i_1 \circ L \circ i_2$; note that the latter map acts between the quadrics with integer indices.

Our last requirement repeats the one in [2]:

- The singularity confinement properties of $\tilde{i}_1, \tilde{i}_2$ are the same as that of i_1, i_2.

Reduction to the symmetric case. If the eight points s_i are symmetric with respect to the symmetry switch $\sigma : (x, y) \longmapsto (y, x)$, we can define a 2D QRT root $f = i_1 \circ \sigma = \sigma \circ i_2$ such that $F = f \circ f$. In this case, the map L in the pencil-adapted coordinates satisfies $L = \sigma \circ L \circ \sigma$, and therefore its decomposition factors satisfy

$$L_2 = \sigma \circ L_1 \circ \sigma, \quad R_2 = \sigma \circ R_1 \circ \sigma.$$

The 3D Painlevé map F can be written as

$$\begin{aligned}\widetilde{F} &= R_1\circ i_1\circ L_1\circ R_2\circ i_2\circ L_2 = R_1\circ i_1\circ L_1\circ\sigma\circ R_1\circ\sigma\circ i_2\circ\sigma\circ L_1\\ &= R_1\circ i_1\circ\sigma\circ L_2\circ R_1\circ\sigma\circ i_2\circ L_2\\ &= (R_1\circ f\circ L_2)^2.\end{aligned}$$

Therefore, one can define the Painlevé deformed QRT root as $\widetilde{f} = R_1\circ f\circ L_2$, then the discrete Painlevé map decomposes as $\widetilde{F} = \widetilde{f}\circ\widetilde{f}$.

3 Construction of the Painlevé deformation map

The desired properties of the Painlevé deformation map L are ensured by the following construction.

Theorem 1. *If the polynomial Q_∞ does not depend on X_3, define the map $L : [X_1 : X_2 : X_3 : X_4] \longmapsto [\widehat{X}_1 : \widehat{X}_2 : \widehat{X}_3 : \widehat{X}_4]$ by requiring that, for $X \in Q_{\lambda(\nu)}$, there holds*

$$\begin{cases}\widehat{X}_1 = X_1X_4,\\ \widehat{X}_2 = X_2X_4,\\ \widehat{X}_3 = X_3X_4 - \big(\lambda(\widehat{\nu}) - \lambda(\nu)\big)Q_\infty(X),\\ \widehat{X}_4 = X_4^2,\end{cases} \tag{9}$$

where $\widehat{\nu} = \nu + 2\delta$. If Q_∞ does not depend on X_1, define

$$\begin{cases}\widehat{X}_1 = X_1X_2 + \big(\lambda(\widehat{\nu}) - \lambda(\nu)\big)Q_\infty(X),\\ \widehat{X}_2 = X_2^2,\\ \widehat{X}_3 = X_2X_3,\\ \widehat{X}_4 = X_2X_4.\end{cases} \tag{10}$$

Then L sends each $Q_{\lambda(\nu)}$ to $Q_{\lambda(\widehat{\nu})}$ and fixes all points of the base curve of the pencil $\{Q_\lambda\}$ not belonging to $\{X_4 = 0\}$ (resp. to $\{X_2 = 0\}$), including all eight base points S_i, $i = 1, \dots, 8$.

Proof. It follows by a simple computation. For instance, for the case (9):

$$\widehat{X}_1\widehat{X}_2 - \widehat{X}_3\widehat{X}_4 - \lambda(\widehat{\nu})Q_\infty(\widehat{X}) = X_4^2\Big(X_1X_2 - X_3X_4 - \lambda(\nu)Q_\infty(X)\Big).$$

Futher, if $Q_\infty(X) = 0$ and $X_4 \neq 0$, then $[\widehat{X}_1 : \widehat{X}_2 : \widehat{X}_3 : \widehat{X}_4] = [X_1 : X_2 : X_3 : X_4]$. ■

The recipe of Theorem 1 covers all cases treated in the present paper (pencils of the types (ii)-(vi)). In retrospect, we notice that, with a natural modification (replace $\widehat{\lambda} - \lambda = \lambda(\widehat{\nu}) - \lambda(\nu)$ by $\sigma(\lambda) - \lambda$), this recipe covers also the cases considered in the first part of this study [2]. For pencils of the type (i) the quadric Q_∞ is non-degenerate, so a modification of the recipe is required.

4 Singularity confinement

Our case-by-case computations reveal the following observation. In all examples of the present paper, the eight points $s_1, \dots, s_8$ in $\mathbb{P}^1 \times \mathbb{P}^1$ serve as the indeterminacy set for the 2D QRT involutions i_1, i_2. The singularity confinement structure can be summarised as:

$$\{x = a_i\} \xrightarrow{i_1} s_i \xrightarrow{i_2} \{y = b_i\}, \quad i = 1, \dots, 8. \tag{11}$$

In the pencil-adapted coordinates, the 3D QRT involutions restricted to $Q_{\lambda(\nu)}$ are given by the same formulas as the original 2D QRT involutions, with the points s_i replaced by their deformations $s_i(\nu)$. The latter still support a pencil of biquadratic curves, which are the pre-images under ϕ_ν of the intersection curves $Q_{\lambda(\nu)} \cap P_\mu$. Therefore, for the 3D QRT involutions i_1 and i_2, we have

$$\{x = a_i(\nu)\} \xrightarrow{i_1} s_i(\nu) \xrightarrow{i_2} \{y = b_i(\nu)\}. \tag{12}$$

Let $\Phi_i \subset \mathbb{P}^3$ be the ruled surface comprised of the lines on $Q_{\lambda(\nu)}$ given, in the pencil-adapted coordinates ϕ_ν, by the equations $\{x = a_i(\nu)\}$. Likewise, let $\Psi_i \subset \mathbb{P}^3$ be the ruled surface comprised of the lines on $Q_{\lambda(\nu)}$ given in the coordinates ϕ_ν by the equations $\{y = b_i(\nu)\}$. Then, in view of (12), we obtain the following singularity confinement patterns for i_1, i_2:

$$\Phi_i \xrightarrow{i_1} S_i \xrightarrow{i_2} \Psi_i. \tag{13}$$

We emphasize that the surfaces Φ_i are blown down to points (rather than curves), and these points are blown up to surfaces Ψ_i again.

Theorem 2. *Suppose that the involutions $i_1, i_2 : \mathbb{P}^3 \dashrightarrow \mathbb{P}^3$ have a singularity confinement pattern of the type* (13)*, and L satisfies*

$$L(S_i) = S_i. \tag{14}$$

Then for the deformed maps $\widetilde{i}_1 = R_1 \circ i_1 \circ L_1$, $\widetilde{i}_2 = R_2 \circ i_2 \circ L_2$ we have:

$$L_1^{-1}(\Phi_i) \overset{\widetilde{i}_1}{\to} R_1(S_i) \overset{\widetilde{i}_2}{\to} R_2(\Psi_i), \tag{15}$$

which implies for $\widetilde{F} = \widetilde{i}_1 \circ \widetilde{i}_2$ the singularity confinement pattern

$$(L_1 \circ \widetilde{i}_2)^{-1}(\Phi_i) \overset{\widetilde{F}}{\to} R_1(S_i) \overset{\widetilde{F}}{\to} (\widetilde{i}_1 \circ R_2)(\Psi_i). \tag{16}$$

An important observation is that the eight points $R_1(S_i)$ participating in these singularity confinement patterns do not support a net of quadrics.

5 From a pencil of type (v) to the *d*-Painlevé equation of the surface type $A_1^{(1)}$

2D QRT map. We consider the QRT map corresponding to the pencil of biquadratic curves $\{C_\mu\}$ through eight points $s_i = (a_i, b_i)$, $i = 1, \dots, 8$, where

$$b_i = -a_i, \quad i = 1, \dots, 4, \quad \text{and} \quad b_i = 1 - a_i, \quad i = 5, \dots, 8. \tag{17}$$

These eight points support a pencil of biquadratic curves if they satisfy the condition

$$a_1 + a_2 + a_3 + a_4 - a_5 - a_6 - a_7 - a_8 = -2. \tag{18}$$

This pencil contains a reducible curve, consisting of two (1,1)-curves:

$$C_\infty = \{(x + y)(x + y - 1) = 0\}. \tag{19}$$

The vertical involution i_1 for this pencil can be described by the following equation:

$$i_1(x, y) = (x, \widetilde{y}), \quad \frac{(\widetilde{y} + x)(x + y)}{(\widetilde{y} + x - 1)(x + y - 1)} = \frac{\prod_{i=1}^{4}(x - a_i)}{\prod_{i=5}^{8}(x - a_i)}. \tag{20}$$

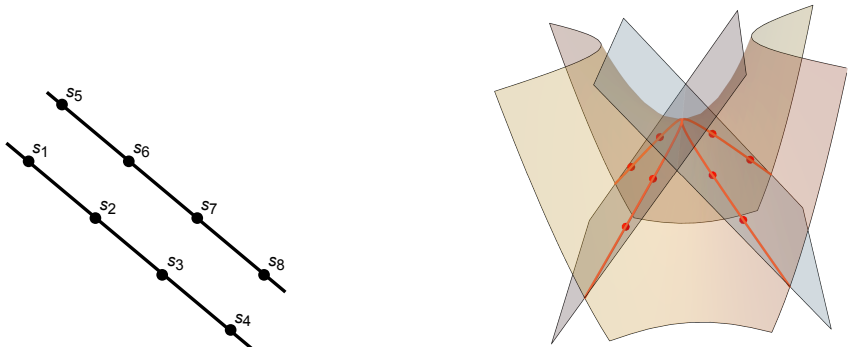

(a) (b)

Figure 1: (a) Base set of the surface type $A_1^{(1)}$: two quadruples of points on two touching (1,1)-curves in $\mathbb{P}^1 \times \mathbb{P}^1$. (b) Pencil of quadrics through two touching non-coplanar conics

Similarly, the horizontal involution i_2 can be described by the following equation:

$$i_2(x,y) = (\widetilde{x}, y), \quad \frac{(\widetilde{x}+y)(x+y)}{(\widetilde{x}+y-1)(x+y-1)} = \frac{\prod_{i=1}^{4}(y+a_i)}{\prod_{i=5}^{8}(y+a_i-1)}. \tag{21}$$

The QRT map is the composition of these two involutions, $F = i_1 \circ i_2$. The singularity confinement structure of the involutions i_1, i_2 is as in (11). The symmetric case corresponds to

$$a_{2i} = -a_{2i-1},\ i = 1,2, \qquad a_{2i} = 1 - a_{2i-1},\ i = 3,4.$$

In this case, $F = f \circ f$, with $f = i_1 \circ \sigma = \sigma \circ i_2$ being the QRT root (here $\sigma(x,y) = (y,x)$).

3D Painlevé map. We consider the pencil of quadrics $\{P_\mu\}$ in $\mathbb{P}^3$, the Segre lift of the pencil of curves $\{C_\mu\}$. The pencil $\{Q_\lambda\}$ is spanned by $Q_0 = \{X_1X_2 - X_3X_4 = 0\}$ and $Q_\infty = P_\infty = \{(X_1+X_2)(X_1+X_2-X_4) = 0\}$:

$$Q_\lambda = \Big\{X_1X_2 - X_3X_4 - \lambda(X_1+X_2)(X_1+X_2-X_4) = 0\Big\}. \tag{22}$$

The base set of the pencil Q_λ consists of the two conics, $\{X_1X_2 - X_3X_4 = 0,\ X_1+X_2 = 0\}$ and $\{X_1X_2 - X_3X_4 = 0,\ X_1+X_2 = X_4\}$, which have one common (touching) point $[0:0:1:0]$.

This is a pencil of type (v). The intersection of this base set with the base set of the pencil $\{P_\mu\}$ consists of eight points

$$S_i = [a_i : b_i : a_i b_i : 1], \quad i = 1, \dots, 8,$$

which are nothing but the lifts of the points s_i under the Segre embedding.

The matrix M_λ of the quadratic form Q_λ:

$$M_\lambda = \begin{pmatrix} -2\lambda & 1-2\lambda & 0 & -\lambda \\ 1-2\lambda & -2\lambda & 0 & -\lambda \\ 0 & 0 & 0 & -1 \\ -\lambda & -\lambda & -1 & 0 \end{pmatrix}. \tag{23}$$

The characteristic polynomial of the pencil $\{Q_\lambda\}$ is: $\Delta(\lambda) = \det(M_\lambda) = 1 - 4\lambda$, which is not a complete square, and $\mathrm{Sing}(Q_\lambda) = \{\frac{1}{4}, \infty\}$. We uniformize the Riemann surface of $\sqrt{\Delta(\lambda)}$ via

$$\lambda = \frac{1-\nu^2}{4}, \quad \sqrt{\Delta(\lambda)} = \nu. \tag{24}$$

Thus, $\lambda(-\nu) = \lambda(\nu)$, while $\sqrt{\Delta(\lambda)}$ changes its sign as $\nu \to -\nu$. This gives us a double cover of the original pencil branched at $\lambda = 1/4$ (corresponding to $\nu = 0$), and at $\lambda = \infty$ (corresponding to $\nu = \infty$). The normalizing transformation of $Q_{\lambda(\nu)}$ to the canonical form Q_0 can be found as follows:

$$\begin{bmatrix} X_1 \\ X_2 \\ X_3 \\ X_4 \end{bmatrix} = A_\nu \begin{bmatrix} Y_1 \\ Y_2 \\ Y_3 \\ Y_4 \end{bmatrix}, \tag{25}$$

where

$$A_\nu = \begin{pmatrix} \frac{1}{2\nu}(1+\nu) & \frac{1}{2\nu}(1-\nu) & 0 & 0 \\ \frac{1}{2\nu}(1-\nu) & \frac{1}{2\nu}(1+\nu) & 0 & 0 \\ \frac{1}{4\nu}(1-\nu^2) & \frac{1}{4\nu}(1-\nu^2) & 1 & 0 \\ 0 & 0 & 0 & 1 \end{pmatrix}. \tag{26}$$

Indeed, one immediately verifies that

$$A_\nu^{\mathrm{T}} M_{\lambda(\nu)} A_\nu = M_0.$$

Now, we are in the position to derive a parametrization of the quadric Q_λ:

$$\begin{bmatrix} X_1 \\ X_2 \\ X_3 \\ X_4 \end{bmatrix} = A_\nu \begin{bmatrix} x \\ y \\ xy \\ 1 \end{bmatrix} = \begin{bmatrix} \frac{1}{2\nu}((1+\nu)x + (1-\nu)y) \\ \frac{1}{2\nu}((1-\nu)x + (1+\nu)y) \\ xy + \frac{1-\nu^2}{4\nu}(x+y) \\ 1 \end{bmatrix} =: \phi_\nu(x,y). \tag{27}$$

Observe that this parametrization is neither valid for $\nu = 0$ nor for $\nu = \infty$. The pencil-adapted coordinates (x, y, ν) on (the double cover of) $\mathbb{P}^3$ are:

$$x = \frac{(1+\nu)X_1 - (1-\nu)X_2}{2X_4}, \quad y = \frac{(1+\nu)X_2 - (1-\nu)X_1}{2X_4}, \tag{28}$$

which have to be supplemented with

$$\lambda = \frac{1-\nu^2}{4} = \frac{X_1X_2 - X_3X_4}{(X_1+X_2)(X_1+X_2-X_4)}. \tag{29}$$

Theorem 3. *For any $\delta \in \mathbb{C} \setminus \{0\}$, define the Painlevé deformation map corresponding to the translation $\nu \longmapsto \widehat{\nu} = \nu + 2\delta$ by*

$$L: \quad \begin{cases} \widehat{X}_1 &= X_1X_4, \\ \widehat{X}_2 &= X_2X_4, \\ \widehat{X}_3 &= X_3X_4 - \big(\lambda(\widehat{\nu}) - \lambda(\nu)\big)Q_\infty(X) \\ &= X_3X_4 + \delta(\nu+\delta)(X_1+X_2)(X_1+X_2-X_4), \\ \widehat{X}_4 &= X_4^2. \end{cases}$$

Then, in pencil-adapted coordinates, the map L acts as follows:

$$L: (x,y,\nu) \longmapsto (\widehat{x},\widehat{y},\widehat{\nu}), \quad \widehat{x} = x + \frac{\delta}{\nu}(x+y), \quad \widehat{y} = y + \frac{\delta}{\nu}(x+y), \quad \widehat{\nu} = \nu + 2\delta. \tag{30}$$

For the latter map, the factorizations (4), (5) are given by

$$L_1 = R_1 : (x,y,\nu) \longmapsto (x,\widetilde{y},\nu+\delta), \quad L_2 = R_2 : (x,y,\nu) \longmapsto (\widetilde{x},y,\nu+\delta),$$

where

$$\widetilde{y} = y + \frac{\delta}{\nu}(x+y) \quad \Leftrightarrow \quad \frac{\widetilde{y}+x}{\widetilde{y}+x-\nu-\delta} = \frac{y+x}{y+x-\nu}, \tag{31}$$

$$\widetilde{x} = x + \frac{\delta}{\nu}(x+y) \quad \Leftrightarrow \quad \frac{\widetilde{x}+y}{\widetilde{x}+y-\nu-\delta} = \frac{x+y}{x+y-\nu}. \tag{32}$$

Relation to the d-Painlevé equation of the surface type $A_1^{(1)}$. We now compute the 3D Painlevé map $\widetilde{F} = R_1 \circ i_1 \circ L_1 \circ R_2 \circ i_2 \circ L_2$ in the pencil-adapted coordinates (x, y, ν). For each fixed ν, the intersection curves $Q_{\lambda(\nu)} \cap P_\mu$ form a pencil through eight points

$$s_i(\nu) = (a_i, -a_i), \quad i = 1, \dots, 4, \tag{33}$$

$$s_i(\nu) = \Big(\frac{\nu-1}{2} + a_i, \frac{1+\nu}{2} - a_i\Big), \quad i = 5, \dots, 8, \tag{34}$$

which are just the points $S_1, \dots, S_8$ (which are, recall, independent of ν) expressed in the pencil-adapted coordinates on $Q_{\lambda(\nu)}$. The curve $C_\infty(\nu)$, which is the image of the base curve of the pencil $\{Q_\lambda\}$ in the pencil-adapted coordinates on $Q_{\lambda(\nu)}$, is given by the equation

$$C_\infty(\nu) = \{(x+y)(x+y-\nu) = 0\}. \tag{35}$$

The map L sends $C_\infty(\nu)$ to $C_\infty(\nu + 2\delta)$, while the maps $L_1 = R_1$ and $L_2 = R_2$ send $C_\infty(\nu)$ to $C_\infty(\nu + \delta)$. We observe that the map L fixes the (x, y) coordinates of the points of the component $\{x + y = 0\}$ of $C_\infty(\nu)$, and acts as $(x, y) \longmapsto (x + \delta, y + \delta)$ on the component $\{x + y = \nu\}$. This "shift" under the map L is, however, only apparent, as this map fixes the curve $\mathcal{Q}_0 \cap \mathcal{Q}_\infty$ pointwise. Similarly, the map $L_1 = R_1$ acts on the second component as $(x, y) \longmapsto (x, y + \delta)$, while $L_2 = R_2$ acts as $(x, y) \longmapsto (x + \delta, y)$. These actions are non-trivial in homogeneous coordinates X.

The formulas for the 3D QRT involutions i_1, i_2 restricted to $Q_{\lambda(\nu)}$ coincide, in the pencil-adapted coordinates, with the original QRT involutions (20) and (21), upon replacing s_i by $s_i(\nu)$:

$$i_1(x, y) = (x, \widetilde{y}), \quad \frac{(\widetilde{y}+x)(x+y)}{(\widetilde{y}+x-\nu)(x+y-\nu)} = \frac{\prod_{i=1}^4 (x - a_i)}{\prod_{i=5}^8 (x - a_i - \frac{\nu-1}{2})} =: \psi_1(x, \nu), \tag{36}$$

$$i_2(x,y)=(\widetilde{x},y),\qquad \frac{(\widetilde{x}+y)(x+y)}{(\widetilde{x}+y-\nu)(x+y-\nu)}=\frac{\prod_{i=1}^{4}(y+a_i)}{\prod_{i=5}^{8}(y+a_i-\frac{1+\nu}{2})}=:\psi_2(y,\nu). \tag{37}$$

In the notation of the equations (7), (8), we have:

$$\frac{(\widetilde{x}+y_n)(y_n+x)}{(\widetilde{x}+y_n-\nu_{2n})(y_n+x-\nu_{2n})}=\psi_2(y_n,\nu_{2n}), \tag{38}$$

$$\frac{(\widetilde{y}+x_{n+1})(x_{n+1}+y)}{(\widetilde{y}+x_{n+1}-\nu_{2n+1})(x_{n+1}+y-\nu_{2n+1})}=\psi_1(x_{n+1},\nu_{2n+1}). \tag{39}$$

It remains to express $x,y,\widetilde{x},\widetilde{y}$ in these formulas in terms of x_n,y_n. According to (7), we have:

$$L_2:(x_n,y_n,\nu_{2n-1/2})\longmapsto(x,y_n,\nu_{2n})\quad\text{and}\quad R_2:(\widetilde{x},y_n,\nu_{2n})\longmapsto(x_{n+1},y_n,\nu_{2n+1/2}),$$

and with expressions (32) for the maps L_2, R_2, we find:

$$\frac{x+y_n}{x+y_n-\nu_{2n}}=\frac{x_n+y_n}{x_n+y_n-\nu_{2n-1/2}}, \tag{40}$$

$$\frac{\widetilde{x}+y_n}{\widetilde{x}+y_n-\nu_{2n}}=\frac{x_{n+1}+y_n}{x_{n+1}+y_n-\nu_{2n+1/2}}. \tag{41}$$

Similarly, according to (8), we have:

$$L_1:(x_{n+1},y_n,\nu_{2n+1/2})\longmapsto(x_{n+1},y,\nu_{2n+1})\quad\text{and}\quad R_1:(x_{n+1},\widetilde{y},\nu_{2n+1})\longmapsto(x_{n+1},y_{n+1},\nu_{2n+3/2}),$$

and with expressions (31) for the maps L_1, R_1, we find:

$$\frac{y+x_{n+1}}{y+x_{n+1}-\nu_{2n+1}}=\frac{x_{n+1}+y_n}{x_{n+1}+y_n-\nu_{2n+1/2}}, \tag{42}$$

$$\frac{x_{n+1}+\widetilde{y}}{x_{n+1}+\widetilde{y}-\nu_{2n+1}}=\frac{x_{n+1}+y_{n+1}}{x_{n+1}+y_{n+1}-\nu_{2n+3/2}}. \tag{43}$$

Combining equations (38), (39) with (40)–(43) results in the following non-autonomous system:

$$\frac{(x_{n+1}+y_n)(x_n+y_n)}{(x_{n+1}+y_n-\nu_{2n+1/2})(x_n+y_n-\nu_{2n-1/2})}=\psi_2(y_n,\nu_{2n}), \tag{44}$$

$$\frac{(x_{n+1}+y_{n+1})(x_{n+1}+y_n)}{(x_{n+1}+y_{n+1}-\nu_{2n+3/2})(x_{n+1}+y_n-\nu_{2n+1/2})}=\psi_1(x_{n+1},\nu_{2n+1}). \tag{45}$$

This is nothing but the d-Painlevé equation of the surface type $A_1^{(1)}$, as given in [11].

Remark. The symmetric case can be characterized by $\psi_1(x,\nu) = \psi_2(x,\nu)$. In this case the latter equations become two instances of

$$\frac{(u_{n+1}+u_n)(u_n+u_{n-1})}{(u_{n+1}+u_n-\nu_{n+1/2})(u_n+u_{n-1}-\nu_{n-1/2})} = \psi_1(u_n,\nu_n), \tag{46}$$

if we set $u_{2n-1} = x_n$, $u_{2n} := y_n$.

6 From a pencil of type (vi) to the d-Painlevé equation of the surface type $D_4^{(1)}$

By a simple limiting procedure, the results of the previous section lead to similar results for the d-Painlevé equation of the surface type $D_4^{(1)}$. We refrain from giving complete details here, and restrict ourselves only to the main results.

2D QRT map. We consider the QRT map corresponding to the pencil of biquadratic curves $\{C_\mu\}$ through eight points

$$s_i = (a_i, -a_i), \quad s_{i+4} = (a_i+\epsilon, -a_i+\epsilon), \quad i = 1,\dots,4, \tag{47}$$

where the points $s_5,\dots,s_8$ are infinitely near to $s_1,\dots,s_4$, respectively. This pencil contains a reducible curve:

$$C_\infty = \{(x+y)^2 = 0\}. \tag{48}$$

The vertical involution i_1 and the horizontal involution i_2 for this pencil can be described by the following equations:

$$i_1(x,y) = (x,\widetilde{y}), \quad \frac{1}{\widetilde{y}+x} + \frac{1}{x+y} = \frac{1}{2}\sum_{i=1}^{4}\frac{1}{x-a_i}, \tag{49}$$

$$i_2(x,y) = (\widetilde{x},y), \quad \frac{1}{\widetilde{x}+y} + \frac{1}{x+y} = \frac{1}{2}\sum_{i=1}^{4}\frac{1}{y+a_i}. \tag{50}$$

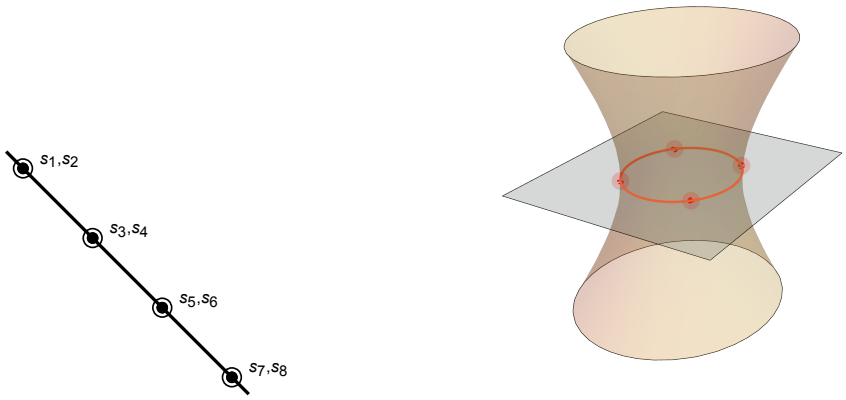

(a) (b)

Figure 2: (a) Base set of the surface type $D_4^{(1)}$: four double points on a double (1,1)-curve in $\mathbb{P}^1 \times \mathbb{P}^1$. (b) Pencil of quadrics touching along a conic

3D Painlevé map. We consider the pencil of quadrics $\{P_\mu\}$ in $\mathbb{P}^3$ obtained as the Segre lift of the pencil of curves $\{C_\mu\}$. The pencil $\{Q_\lambda\}$ is spanned by $Q_0 = \{X_1X_2 - X_3X_4 = 0\}$ and $Q_\infty = P_\infty = \{(X_1 + X_2)^2 = 0\}$:

$$Q_\lambda = \Big\{X_1X_2 - X_3X_4 - \lambda(X_1 + X_2)^2 = 0\Big\}. \tag{51}$$

The base set of the pencil Q_λ is the double conic $\{X_1X_2 - X_3X_4 = 0,\ X_1 + X_2 = 0\}$. This is a pencil of type (vi). The matrix M_λ of the quadratic form Q_λ is:

$$M_\lambda = \begin{pmatrix} -2\lambda & 1-2\lambda & 0 & 0 \\ 1-2\lambda & -2\lambda & 0 & 0 \\ 0 & 0 & 0 & -1 \\ 0 & 0 & -1 & 0 \end{pmatrix}. \tag{52}$$

The characteristic polynomial of the pencil $\{Q_\lambda\}$ is: $\Delta(\lambda) = \det(M_\lambda) = 1 - 4\lambda$, the same as in Section 5. The normalizing transformation of $Q_{\lambda(\nu)}$ to the canonical form Q_0 reads:

$$\begin{bmatrix} X_1 \\ X_2 \\ X_3 \\ X_4 \end{bmatrix} = A_\nu \begin{bmatrix} Y_1 \\ Y_2 \\ Y_3 \\ Y_4 \end{bmatrix}, \tag{53}$$

where

$$A_\nu = \begin{pmatrix} \frac{1}{2\nu}(1+\nu) & \frac{1}{2\nu}(1-\nu) & 0 & 0 \\ \frac{1}{2\nu}(1-\nu) & \frac{1}{2\nu}(1+\nu) & 0 & 0 \\ 0 & 0 & 1 & 0 \\ 0 & 0 & 0 & 1 \end{pmatrix}. \tag{54}$$

A parametrization of the quadric $Q_{\lambda(\nu)}$ is given by:

$$\begin{bmatrix} X_1 \\ X_2 \\ X_3 \\ X_4 \end{bmatrix} = A_\nu \begin{bmatrix} x \\ y \\ xy \\ 1 \end{bmatrix} = \begin{bmatrix} \frac{1}{2\nu}((1+\nu)x + (1-\nu)y) \\ \frac{1}{2\nu}((1-\nu)x + (1+\nu)y) \\ xy \\ 1 \end{bmatrix} =: \phi_\nu(x, y). \tag{55}$$

The pencil-adapted coordinates (x, y, ν) on (the double cover of) $\mathbb{P}^3$ are:

$$x = \frac{(1+\nu)X_1 - (1-\nu)X_2}{2X_4}, \quad y = \frac{(1+\nu)X_2 - (1-\nu)X_1}{2X_4}, \tag{56}$$

which have to be supplemented with

$$\lambda = \frac{1-\nu^2}{4} = \frac{X_1X_2 - X_3X_4}{(X_1+X_2)^2}. \tag{57}$$

Theorem 4. *For any $\delta \in \mathbb{C} \setminus \{0\}$, define the Painlevé deformation map corresponding to the*

translation $\nu \longmapsto \widehat{\nu} = \nu + 2\delta$ *by*

$$L : \begin{cases} \widehat{X}_1 &= X_1X_4, \\ \widehat{X}_2 &= X_2X_4, \\ \widehat{X}_3 &= X_3X_4 - \big(\lambda(\widehat{\nu}) - \lambda(\nu)\big)Q_\infty(X) \\ &= X_3X_4 + \delta(\nu+\delta)(X_1+X_2)^2, \\ \widehat{X}_4 &= X_4^2. \end{cases}$$

Then, in pencil-adapted coordinates, the map L *acts as follows:*

$$L : (x,y,\nu) \longmapsto (\widehat{x},\widehat{y},\widehat{\nu}), \quad \widehat{x} = x + \frac{\delta}{\nu}(x+y), \quad \widehat{y} = y + \frac{\delta}{\nu}(x+y), \quad \widehat{\nu} = \nu + 2\delta. \tag{58}$$

For the latter map, the factorizations (4), (5) *are given by*

$$L_1 = R_1 : (x,y,\nu) \longmapsto (x,\widetilde{y},\nu+\delta), \quad L_2 = R_2 : (x,y,\nu) \longmapsto (\widetilde{x},y,\nu+\delta),$$

where

$$\widetilde{y} = y + \frac{\delta}{\nu}(x+y) \quad \Leftrightarrow \quad \frac{\nu+\delta}{\widetilde{y}+x} = \frac{\nu}{y+x}, \tag{59}$$

$$\widetilde{x} = x + \frac{\delta}{\nu}(x+y) \quad \Leftrightarrow \quad \frac{\nu+\delta}{\widetilde{x}+y} = \frac{\nu}{x+y}. \tag{60}$$

Computing the 3D Painlevé map $\widetilde{F} = R_1 \circ i_1 \circ L_1 \circ R_2 \circ i_2 \circ L_2$ in the pencil-adapted coordinates (x,y,ν), we come to the following non-autonomous system:

$$\frac{\nu_{2n+1/2}}{x_{n+1}+y_n} + \frac{\nu_{2n-1/2}}{x_n+y_n} = \frac{\nu_{2n}}{2}\sum_{i=1}^{4}\frac{1}{y_n+a_i}, \tag{61}$$

$$\frac{\nu_{2n+3/2}}{x_{n+1}+y_{n+1}} + \frac{\nu_{2n+1/2}}{x_{n+1}+y_n} = \frac{\nu_{2n+1}}{2}\sum_{i=1}^{4}\frac{1}{x_{n+1}-a_i}. \tag{62}$$

This can be considered as a d-Painlevé equation of the surface type $D_4^{(1)}$, in a realization different from that in [11]. We remark here that the latter equation was put into our scheme in [2, sect. 9], however in the framework of pencils of quadrics with rational (non-branching) generators. There is no obvious relation between these two systems, and it would be desirable to clarify this point.

The symmetric case is characterised by $a_{2i} = -a_{2i-1}$, $i = 1, 2$. In this case the latter equations become two instances of

$$\frac{v_{n+1/2}}{u_{n+1} + u_n} + \frac{v_{n-1/2}}{u_n + u_{n-1}} = v_n\Big(\frac{u_n}{u_n^2 - a_1^2} + \frac{u_n}{u_n^2 - a_3^2}\Big), \tag{63}$$

if we set $u_{2n-1} = x_n$, $u_{2n} := y_n$.

7 From a pencil of type (iv) to the q-Painlevé equation of the surface type $A_1^{(1)}$

2D QRT map. Consider the QRT map corresponding to the pencil of biquadratic curves through eight points

$$s_i = (a_i, b_i) = \big(\kappa c_i, \kappa c_i^{-1}\big), \quad i = 1, \dots, 4, \tag{64}$$

$$s_i = (a_i, b_i) = \big(c_i, c_i^{-1}\big), \quad i = 5, \dots, 8, \tag{65}$$

with $\kappa \neq 0, 1$. These eight points support a pencil of biquadratic curves if they satisfy the condition

$$\frac{\prod_{i=1}^4 c_i}{\prod_{i=5}^8 c_i} = 1 \quad \Leftrightarrow \quad \frac{\prod_{i=1}^4 a_i}{\prod_{i=5}^8 a_i} = \kappa^4 \quad \Leftrightarrow \quad \frac{\prod_{i=1}^4 b_i}{\prod_{i=5}^8 b_i} = \kappa^4. \tag{66}$$

They are symmetric with respect to $\sigma(x, y) = (y, x)$ if $c_{2i} = c_{2i-1}^{-1}$, $i = 1, \dots, 4$. See Fig. 3 (a).

This pencil contains a reducible curve consisting of two (1,1)-curves:

$$C_\infty = \big\{(xy - 1)(xy - \kappa^2) = 0\big\}. \tag{67}$$

The vertical involution i_1 can be described by the following equation:

$$i_1(x, y) = (x, \widetilde{y}), \quad \frac{(x\widetilde{y} - \kappa^2)(xy - \kappa^2)}{(x\widetilde{y} - 1)(xy - 1)} = \frac{\prod_{i=1}^4 (x - \kappa c_i)}{\prod_{i=5}^8 (x - c_i)}. \tag{68}$$

Similarly, the horizontal involution i_2 can be described by the following equation:

$$i_2(x, y) = (\widetilde{x}, y), \quad \frac{(\widetilde{x}y - \kappa^2)(xy - \kappa^2)}{(\widetilde{x}y - 1)(xy - 1)} = \frac{\prod_{i=1}^4 (y - \kappa c_i^{-1})}{\prod_{i=5}^8 (y - c_i^{-1})}. \tag{69}$$

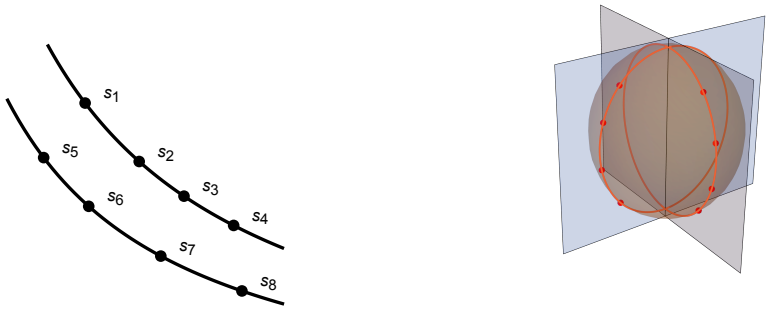

(a) (b)

Figure 3: (a) Base set of the surface type $A_1^{(1)}$: two quadruples of points on two (1,1)-curves (hyperbolas) in $\mathbb{P}^1 \times \mathbb{P}^1$ intersecting at two points $(\infty, 0)$ and $(0, \infty)$. (b) Pencil of quadrics through two non-coplanar conics intersecting at two points

The QRT map F is the composition of these two involutions, $F = i_1 \circ i_2$. The singularity confinement structure of the QRT involutions is as in (11). In the symmetric case we have $F = f^2$, with $f = i_1 \circ \sigma = \sigma \circ i_2$ being the QRT root.

3D Painlevé map. As usual, we identify $\mathbb{P}^1 \times \mathbb{P}^1$ with the quadric

$$Q_0 = \{X_1X_2 - X_3X_4 = 0\} \subset \mathbb{P}^3,$$

via $[X_1 : X_2 : X_3 : X_4] = [x : y : xy : 1]$. The points s_i are lifted to

$$S_i = [a_i : b_i : a_ib_i : 1] = \begin{cases} \left[\kappa c_i : \kappa c_i^{-1} : \kappa^2 : 1\right], \ i = 1, \dots, 4, \\ \left[c_i : c_i^{-1} : 1 : 1\right], \ i = 5, \dots, 8. \end{cases} \tag{70}$$

We declare Q_λ to be spanned by Q_0 and $Q_\infty = P_\infty = (X_3 - \kappa^2 X_4)(X_3 - X_4)$:

$$Q_\lambda = \Big\{X_1X_2 - X_3X_4 - \lambda(X_3 - \kappa^2 X_4)(X_3 - X_4) = 0\Big\}. \tag{71}$$

The base set of the pencil Q_λ consists of two conics, $\{X_1X_2 - X_3X_4 = 0,\ X_3 - \kappa^2 X_4 = 0\}$ and $\{X_1X_2 - X_3X_4 = 0,\ X_3 - X_4 = 0\}$, which intersect at two points $[0 : 1 : 0 : 0]$ and $[1 : 0 : 0 : 0]$. This is a pencil of type (iv).

The matrix M_λ of the quadratic form Q_λ:

$$M_\lambda = \begin{pmatrix} 0 & 1 & 0 & 0 \\ 1 & 0 & 0 & 0 \\ 0 & 0 & -2\lambda & -1+(1+\kappa^2)\lambda \\ 0 & 0 & -1+(1+\kappa^2)\lambda & -2\kappa^2\lambda \end{pmatrix} \tag{72}$$

The characteristic polynomial of the pencil $\{Q_\lambda\}$ is:

$$\Delta(\lambda) = \det(M_\lambda) = \big(1-(1+\kappa^2)\lambda\big)^2 - 4\kappa^2\lambda^2 = \big(1-(1+\kappa)^2\lambda\big)\big(1-(1-\kappa)^2\lambda\big),$$

so that $\mathrm{Sing}(Q_\lambda) = \{(1+\kappa)^{-2}, (1-\kappa)^{-2}, \infty\}$. This polynomial is not a complete square, and we have to uniformize $\sqrt{\Delta(\lambda)}$. The uniformizing variable is $\nu \in \mathbb{C}$. However, in the present situation it will be convenient to use $w = e^\nu$ instead, with $w \in \mathbb{C} \setminus \{0\}$. The shift $\nu \longmapsto \nu + \delta$ will be replaced by $w \longmapsto qw$ with $q = e^\delta$. We set

$$\lambda = \lambda(w) = -\frac{(\kappa - w)(1-\kappa w)}{(1-\kappa^2)^2 w}. \tag{73}$$

Then $\Delta(\lambda)$ becomes a square:

$$\Delta(\lambda) = \frac{\kappa^2(1-w^2)^2}{w^2(1-\kappa^2)^2} \quad \Rightarrow \quad \sqrt{\Delta(\lambda)} = \frac{\kappa(1-w^2)}{w(1-\kappa^2)}.$$

Observe that $\lambda(w) = \lambda(w^{-1})$, while $\sqrt{\Delta(\lambda)}$ changes its sign under $w \longmapsto w^{-1}$. This gives us a double cover of the original pencil branched at $\lambda = (1+\kappa)^{-2}$ (corresponding to $w = 1$), and at $\lambda = (1-\kappa)^{-2}$ (corresponding to $w = -1$). The point $\lambda = \infty$ (corresponding to $w = 0, \infty$) is not a branch point. The normalizing transformation of $Q_\lambda(X)$ to the canonical form $Q_0(Y) = Y_1Y_2 - Y_3Y_4$ is achieved by the transformation

$$\begin{bmatrix} X_1 \\ X_2 \\ X_3 \\ X_4 \end{bmatrix} = A_w \begin{bmatrix} Y_1 \\ Y_2 \\ Y_3 \\ Y_4 \end{bmatrix}, \tag{74}$$

where one can take

$$A_w = \begin{pmatrix} 1 & 0 & 0 & 0 \\ 0 & 1 & 0 & 0 \\ 0 & 0 & \dfrac{1-\kappa w}{1-w^2} & \dfrac{w(\kappa-w)}{1-w^2} \\ 0 & 0 & \dfrac{\kappa-w}{\kappa(1-w^2)} & \dfrac{w(1-\kappa w)}{\kappa(1-w^2)} \end{pmatrix}. \tag{75}$$

Indeed, one immediately verifies that

$$A_w^{\mathrm{T}} M_{\lambda(w)} A_w = M_0.$$

Now, we are in the position to derive a parametrization of the quadric Q_λ:

$$\begin{bmatrix} X_1 \\ X_2 \\ X_3 \\ X_4 \end{bmatrix} = A_w \begin{bmatrix} x \\ y \\ xy \\ 1 \end{bmatrix} =: \phi_w(x,y). \tag{76}$$

Observe that this parametrization is neither valid for $w = 0$ nor for $w = \infty$. The pencil-adapted coordinates (x, y, w) on (the double cover of) $\mathbb{P}^3$ are:

$$x = \frac{(1-\kappa w)X_3 - \kappa(\kappa-w)X_4}{(1-\kappa^2)X_2} = \frac{w(1-\kappa^2)X_1}{\kappa(1-\kappa w)X_4 - (\kappa-w)X_3}, \tag{77}$$

$$y = \frac{(1-\kappa w)X_3 - \kappa(\kappa-w)X_4}{(1-\kappa^2)X_1} = \frac{w(1-\kappa^2)X_2}{\kappa(1-\kappa w)X_4 - (\kappa-w)X_4}, \tag{78}$$

which have to be supplemented with

$$\lambda = -\frac{(\kappa-w)(1-\kappa w)}{(\kappa^2-1)^2 w} = \frac{X_1X_2 - X_3X_4}{(X_3-\kappa^2X_4)(X_3-X_4)}. \tag{79}$$

Theorem 5. *For any $q \neq \pm 1$, define the Painlevé deformation map corresponding to the translation $w \longmapsto \widehat{w} = q^2 w$ by*

$$L: \quad \begin{cases} \widehat{X}_1 = X_1X_2 + \big(\lambda(\widehat{w}) - \lambda(w)\big)(X_3-X_4)(X_3-\kappa^2X_4), \\ \widehat{X}_2 = X_2^2, \\ \widehat{X}_3 = X_2X_3, \\ \widehat{X}_4 = X_2X_4, \end{cases} \tag{80}$$

where $\lambda = \lambda(w)$ is given by (73). Then, in pencil-adapted coordinates, the map L acts as follows:

$$L: \quad \widehat{x} = \frac{q^2w^2-1}{w^2-1}x - \frac{(q^2-1)w^2}{w^2-1}y^{-1}, \quad \widehat{y}^{\,-1} = \frac{q^2w^2-1}{q^2(w^2-1)}y^{-1} - \frac{(q^2-1)}{q^2(w^2-1)}x, \quad \widehat{w} = q^2w. \tag{81}$$

For the latter map, the factorizations (4), (5) are given by

$$L_1 = R_1 : (x,y,w) \longmapsto (x,\widetilde{y},qw), \quad L_2 = R_2 : (x,y,w) \longmapsto (\widetilde{x},y,qw)$$

where

$$\widetilde{y}^{\,-1} = \frac{q^2w^2-1}{q^2(w^2-1)}y^{-1} - \frac{(q^2-1)}{q^2(w^2-1)}x \quad \Leftrightarrow \quad \frac{\widetilde{y}x - q^2w^2}{\widetilde{y}x-1} = q^2\,\frac{yx-w^2}{yx-1}, \tag{82}$$

and

$$\widetilde{x} = \frac{q^2w^2-1}{w^2-1}x - \frac{(q^2-1)w^2}{w^2-1}y^{-1} \quad \Leftrightarrow \quad \frac{\widetilde{x}y - q^2w^2}{\widetilde{x}y-1} = \frac{xy-w^2}{xy-1}. \tag{83}$$

Relation to the q-Painlevé equation of the surface type $A_1^{(1)}$. We now compute the 3D Painlevé map $\widetilde{F} = R_1 \circ i_1 \circ L_1 \circ R_2 \circ i_2 \circ L_2$ in the pencil-adapted coordinates (x,y,w). For each fixed w, the intersection curves $Q_{\lambda(w)} \cap P_\mu$ form a pencil through eight points

$$s_i(w) = \left(wc_i, wc_i^{-1}\right), \quad i = 1,\dots,4, \tag{84}$$

$$s_i(w) = \left(c_i, c_i^{-1}\right), \quad i = 5,\dots,8, \tag{85}$$

which are just the points $S_1,\dots,S_8$ expressed in the pencil-adapted coordinates on $Q_{\lambda(w)}$. The formulas for the 3D QRT involutions i_1, i_2 restricted to $Q_{\lambda(w)}$ coincide, in the pencil-adapted coordinates, with the original QRT involutions (68) and (69), upon replacing κ by w, and s_i by $s_i(w)$:

$$i_1(x,y) = (x,\widetilde{y}), \quad \frac{(x\widetilde{y}-w^2)(xy-w^2)}{(x\widetilde{y}-1)(xy-1)} = \frac{\prod_{i=1}^4 (x-wc_i)}{\prod_{i=5}^8 (x-c_i)}, \tag{86}$$

$$i_2(x,y) = (\widetilde{x},y), \quad \frac{(\widetilde{x}y-w^2)(xy-w^2)}{(\widetilde{x}y-1)(xy-1)} = \frac{\prod_{i=1}^4 (y-wc_i^{-1})}{\prod_{i=5}^8 (y-c_i^{-1})}. \tag{87}$$

In the notation of the equations (7), (8), the latter two equations read:

$$\frac{(\widetilde{x}y_n - w_{2n}^2)(xy_n - w_{2n}^2)}{(\widetilde{x}y_n - 1)(xy_n - 1)} = \frac{\prod_{i=1}^{4}(y_n - w_{2n}c_i^{-1})}{\prod_{i=5}^{8}(y_n - c_i^{-1})}, \tag{88}$$

$$\frac{(\widetilde{y}x_{n+1} - w_{2n+1}^2)(yx_{n+1} - w_{2n+1}^2)}{(\widetilde{y}x_{n+1} - 1)(yx_{n+1} - 1)} = \frac{\prod_{i=1}^{4}(x_{n+1} - w_{2n+1}c_i)}{\prod_{i=5}^{8}(x_{n+1} - c_i)}, \tag{89}$$

where

$$w_{2n-1/2} = q^{-1}w_{2n}, \quad w_{2n+1/2} = qw_{2n}. \tag{90}$$

According to (7), we have:

$$L_2 : (x_n, y_n, w_{2n-1/2}) \longmapsto (x, y_n, w_{2n}) \quad \text{and} \quad R_2 : (\widetilde{x}, y_n, w_{2n}) \longmapsto (x_{n+1}, y_n, w_{2n+1/2}).$$

With expressions (83) for the maps L_2, R_2, we find:

$$\frac{xy_n - w_{2n}^2}{xy_n - 1} = \frac{x_n y_n - w_{2n}w_{2n-1}}{x_n y_n - 1}, \tag{91}$$

$$\frac{\widetilde{x}y_n - w_{2n}^2}{\widetilde{x}y_n - 1} = \frac{x_{n+1}y_n - w_{2n+1}w_{2n}}{x_{n+1}y_n - 1}. \tag{92}$$

Similarly, according to (8), we have:

$$L_1 : (x_{n+1}, y_n, w_{2n+1/2}) \longmapsto (x_{n+1}, y, w_{2n+1}) \quad \text{and} \quad R_1 : (x_{n+1}, \widetilde{y}, w_{2n+1}) \longmapsto (x_{n+1}, y_{n+1}, w_{2n+3/2}),$$

and with expressions (82) for the maps L_1, R_1, we find:

$$q^{-2}\frac{x_{n+1}y - w_{2n+1}^2}{x_{n+1}y - 1} = \frac{x_{n+1}y_n - w_{2n+1}w_{2n}}{x_{n+1}y_n - 1}, \tag{93}$$

$$q^{2}\frac{\widetilde{y}x_{n+1} - w_{2n+1}^2}{\widetilde{y}x_{n+1} - 1} = \frac{x_{n+1}y_{n+1} - w_{2n+2}w_{2n+1}}{x_{n+1}y_{n+1} - 1}. \tag{94}$$

Combining equations (88), (89) with (91)–(94) results in the following non-autonomous system:

$$\frac{(x_{n+1}y_n - w_{2n+1}w_{2n})(x_n y_n - w_{2n}w_{2n-1})}{(x_{n+1}y_n - 1)(x_n y_n - 1)} = \frac{\prod_{i=1}^{4}(y_n - w_{2n}c_i^{-1})}{\prod_{i=5}^{8}(y_n - c_i^{-1})}, \tag{95}$$

$$\frac{(y_{n+1}x_{n+1}-w_{2n+2}w_{2n+1})(y_nx_{n+1}-w_{2n+1}w_{2n})}{(y_{n+1}x_{n+1}-1)(y_nx_{n+1}-1)}=\frac{\prod_{i=1}^{4}(x_{n+1}-w_{2n+1}c_i)}{\prod_{i=5}^{8}(x_{n+1}-c_i)}. \tag{96}$$

This is the q-Painlevé equation of the surface type $A_1^{(1)}$, as given in [11]. In the symmetric case, if $c_{2i}=c_{2i-1}^{-1}$, $i=1,\dots,4$, these equations become two instances of

$$\frac{(u_{n+1}u_n-w_{n+1}w_n)(u_nu_{n-1}-w_nw_{n-1})}{(u_{n+1}u_n-1)(u_nu_{n-1}-1)}=\frac{\prod_{i=1}^{4}(u_n-w_nc_i)}{\prod_{i=5}^{8}(u_n-c_i)}. \tag{97}$$

8 From a pencil of type (iii) to the d-Painlevé equation of the surface type $A_0^{(1)}$

2D QRT map. We consider the QRT map corresponding to the pencil of biquadratic curves through eight points $s_i=(a_i,b_i)$, $i=1,\dots,8$, where

$$a_i=z_i(z_i-\kappa_1),\quad b_i=z_i(z_i-\kappa_2).$$

These eight points support a pencil of biquadratic curves if they satisfy the condition

$$\sum_{i=1}^{8}z_i=2(\kappa_1+\kappa_2).$$

They belong to the curve with the equation

$$(x-y)^2=(\kappa_2-\kappa_1)(\kappa_2x-\kappa_1y).$$

This is a biquadratic curve in $\mathbb{P}^1\times\mathbb{P}^1$ with a cusp point at (∞,∞), see Fig. 4 (a).

The vertical involution i_1 can be described by the following equation:

$$i_1(x,y)=(x,\widetilde{y}),$$
$$\frac{\big(\widetilde{y}-\xi(\xi-\kappa_2)\big)\big(y-\xi(\xi-\kappa_2)\big)}{\big(\widetilde{y}-(\xi-\kappa_1)(\xi-\kappa_1+\kappa_2)\big)\big(y-(\xi-\kappa_1)(\xi-\kappa_1+\kappa_2)\big)}=\frac{U(\xi)}{U(\kappa_1-\xi)},\quad x=\xi(\xi-\kappa_1). \tag{98}$$

Here we use the abbreviation

$$U(z)=\prod_{i=1}^{8}(z-z_i). \tag{99}$$

(a) (b)

Figure 4: (a) Base set of the surface type $A_0^{(1)}$: eight points on a cuspidal (2,2)-curve in $\mathbb{P}^1 \times \mathbb{P}^1$. (b) Pencil of quadrics through cuspidal spatial quartic in $\mathbb{P}^3$

Formula (98) is understood as follows. Written as a polynomial in ξ, it is anti-symmetric with respect to $\xi \leftrightarrow \kappa_1 - \xi$. Upon division by $\xi - 2\kappa_1$, the resulting polynomial is symmetric and therefore it can be actually expressed as a polynomial in $x = \xi(\xi - \kappa_1)$. This defines i_1 as a birational involution (its symmetry w.r.t. $y \leftrightarrow \widetilde{y}$ is obvious).

Similarly, the horizontal involution i_2 can be described by the following equation:

$$i_2(x, y) = (\widetilde{x}, y),$$
$$\frac{\big(\widetilde{x} - \eta(\eta - \kappa_1)\big)\big(x - \eta(\eta - \kappa_1)\big)}{\big(\widetilde{x} - (\eta - \kappa_2)(\eta - \kappa_2 + \kappa_1)\big)\big(x - (\eta - \kappa_2)(\eta - \kappa_2 + \kappa_1)\big)} = \frac{U(\eta)}{U(\kappa_2 - \eta)}, \quad y = \eta(\eta - \kappa_2). \tag{100}$$

The QRT map F is the composition of these two involutions, $F = i_1 \circ i_2$. The eight points $s_1, \dots, s_8$ in $\mathbb{P}^1 \times \mathbb{P}^1$ serve as the indeterminacy set for i_1 and for i_2. The singularity confinement structure is as in (11).

Remark. In what follows, we restrict ourselves to the case $\kappa_1 + \kappa_2 = 0$. This restriction is not essential, but will allow us to shorten some of the formulas. Thus, from now on we set

$$\kappa_1 = -\kappa, \quad \kappa_2 = \kappa. \tag{101}$$

If, additionally, the points z_i satisfy the condition

$$z_{i+4} = -z_i, \quad i = 1, \dots, 4, \tag{102}$$

then the QRT involutions admits a symmetry $i_1 = \sigma \circ i_2 \circ \sigma$, where $\sigma(x, y) = (y, x)$, so that one can introduce the QRT root $f = i_1 \circ \sigma = \sigma \circ i_2$, such that $F = f \circ f$.

3D Painlevé map. As usual, we identify $\mathbb{P}^1 \times \mathbb{P}^1$ with the quadric $Q_0 = \{X_1X_2 - X_3X_4 = 0\} \subset \mathbb{P}^3$ via $[X_1 : X_2 : X_3 : X_4] = [x : y : xy : 1]$. The points s_i are lifted to

$$S_i = [a_i : b_i : a_ib_i : 1].$$

We declare Q_λ to be spanned by Q_0 and $Q_\infty = P_\infty = (X_1 - X_2)^2 - 2\kappa^2(X_1 + X_2)X_4$:

$$Q_\lambda = \Big\{X_1X_2 - X_3X_4 - \lambda\big((X_1 - X_2)^2 - 2\kappa^2(X_1 + X_2)X_4\big) = 0\Big\}. \tag{103}$$

The base set of the pencil Q_λ is a cuspidal space curve of degree 4, $\{X_1X_2 - X_3X_4 = 0,\ (X_1 - X_2)^2 - 2\kappa^2(X_1 + X_2)X_4 = 0\}$, with the cusp at $[0 : 0 : 1 : 0]$. This is a pencil of type (iii).

The matrix M_λ of the quadratic form Q_λ:

$$M_\lambda = \begin{pmatrix} -2\lambda & 1 + 2\lambda & 0 & 2\lambda\kappa^2 \\ 1 + 2\lambda & -2\lambda & 0 & 2\lambda\kappa^2 \\ 0 & 0 & 0 & -1 \\ 2\lambda\kappa^2 & 2\lambda\kappa^2 & -1 & 0 \end{pmatrix} \tag{104}$$

The characteristic polynomial of the pencil $\{Q_\lambda\}$ is: $\Delta(\lambda) = \det(M_\lambda) = 1 + 4\lambda$, so that $\mathrm{Sing}(Q_\lambda) = \{-\frac{1}{4}, \infty\}$. We set

$$\lambda = \frac{\nu^2 - 1}{4}, \quad \sqrt{\Delta(\lambda)} = \nu. \tag{105}$$

Thus, $\lambda(\nu) = \lambda(-\nu)$, while $\sqrt{\Delta(\lambda)}$ changes its sign as $\nu \longmapsto -\nu$. This gives us a double cover of the original pencil branched at $\nu = 0$, corresponding to $\lambda = -1/4$, and at $\nu = \infty$, corresponding to $\lambda = \infty$. The normalizing transformation of Q_λ to the canonical form Q_0

can be found as follows:

$$\begin{bmatrix} X_1 \\ X_2 \\ X_3 \\ X_4 \end{bmatrix} = A_\nu \begin{bmatrix} Y_1 \\ Y_2 \\ Y_3 \\ Y_4 \end{bmatrix}, \tag{106}$$

where

$$A_\nu = \begin{pmatrix} \frac{1}{2\nu}(\nu+1) & \frac{1}{2\nu}(\nu-1) & 0 & 0 \\ \frac{1}{2\nu}(\nu-1) & \frac{1}{2\nu}(\nu+1) & 0 & 0 \\ \frac{\kappa^2}{2}(\nu^2-1) & \frac{\kappa^2}{2}(\nu^2-1) & 1 & 0 \\ 0 & 0 & 0 & 1 \end{pmatrix}. \tag{107}$$

Indeed, one immediately verifies that

$$A_\nu^{\mathrm{T}} M_{\lambda(\nu)} A_\nu = M_0.$$

Now, we are in the position to derive a parametrization of the quadric $Q_{\lambda(\nu)}$:

$$\begin{bmatrix} X_1 \\ X_2 \\ X_3 \\ X_4 \end{bmatrix} = A_\nu \begin{bmatrix} x \\ y \\ xy \\ 1 \end{bmatrix} = \begin{bmatrix} \frac{1}{2\nu}((\nu+1)x + (\nu-1)y) \\ \frac{1}{2\nu}((\nu-1)x + (\nu+1)y) \\ xy + \frac{\kappa^2}{2}(\nu^2-1)(x+y) \\ 1 \end{bmatrix} =: \phi_\nu(x,y). \tag{108}$$

Observe that this parametrization is neither valid for $\nu = 0$ nor for $\nu = \infty$. The pencil-adapted coordinates (x, y, ν) on (the double cover of) $\mathbb{P}^3$ are:

$$x = \frac{(\nu+1)X_1 - (\nu-1)X_2}{2X_4}, \quad y = \frac{(\nu+1)X_2 - (\nu-1)X_1}{2X_4}, \tag{109}$$

which have to be supplemented with

$$\lambda = \frac{\nu^2-1}{4} = \frac{X_1X_2 - X_3X_4}{(X_1-X_2)^2 - 2\kappa^2(X_1+X_2)X_4}. \tag{110}$$

The degenerate quadrics for $\nu = \infty$ and for $\nu = 0$ are cones.

Theorem 6. *For any $\delta \in \mathbb{C} \setminus \{0\}$, define the Painlevé deformation map corresponding to the translation $\nu \longmapsto \widehat{\nu} = \nu + 2\delta$ by*

$$L : \begin{cases} \widehat{X}_1 &= X_1 X_4, \\ \widehat{X}_2 &= X_2 X_4, \\ \widehat{X}_3 &= X_3 X_4 - \big(\lambda(\widehat{\nu}) - \lambda(\nu)\big) Q_\infty(X) \\ &= X_3 X_4 - \beta(\nu+\beta)(X_1 - X_2)^2 + 2\kappa^2 \beta(\nu+\beta)(X_1 + X_2) X_4, \\ \widehat{X}_4 &= X_4^2. \end{cases}$$

Then, in pencil-adapted coordinates, the map L acts as follows:

$$L : (x, y, \nu) \longmapsto (\widehat{x}, \widehat{y}, \widehat{\nu}), \quad \widehat{x} = x + \frac{\delta(x-y)}{\nu}, \quad \widehat{y} = y + \frac{\delta(y-x)}{\nu}, \quad \widehat{\nu} = \nu + 2\delta. \tag{111}$$

For the latter map, the factorizations (4), (5) *are given by*

$$L_1 = R_1 : (x, y, \nu) \longmapsto (x, \widetilde{y}, \nu + \delta), \quad \widetilde{y} = y + \frac{\delta}{\nu}(y - x), \tag{112}$$

$$L_2 = R_2 : (x, y, \nu) \longmapsto (\widetilde{x}, y, \nu + \delta), \quad \widetilde{x} = x + \frac{\delta}{\nu}(x - y). \tag{113}$$

Relation to the d-Painlevé equation of the surface type $A_0^{(1)}$. In the pencil-adapted coordinates (x, y, ν), for each fixed ν, the intersection curves $Q_{\lambda(\nu)} \cup P_\mu$ form the pencil through the points

$$s_i(\nu) = (a_i(\nu), b_i(\nu)) = \big(z_i(z_i + \kappa\nu), z_i(z_i - \kappa\nu)\big), \quad i = 1, \dots, 8, \tag{114}$$

which are just the points S_i expressed in the pencil-adapted coordinates on $Q_{\lambda(\nu)}$. Thus, the 3D QRT involutions i_1, i_2 act on each quadric $Q_{\lambda(\nu)}$ in the pencil-adapted coordinates via formulas which are obtained from the corresponding 2D formulas by replacing κ by $\kappa\nu$:

$$i_1(x, y) = (x, \widetilde{y}),$$
$$\frac{\big(\widetilde{y} - \xi(\xi - \kappa\nu)\big)\big(y - \xi(\xi - \kappa\nu)\big)}{\big(\widetilde{y} - (\xi + \kappa\nu)(\xi + 2\kappa\nu)\big)\big(y - (\xi + \kappa\nu)(\xi + 2\kappa\nu)\big)} = \frac{U(\xi)}{U(-\kappa\nu - \xi)}, \quad x = \xi(\xi + \kappa\nu), \tag{115}$$

$i_2(x,y)=(\widetilde{x},y)$,

$$\frac{\big(\widetilde{x}-\eta(\eta+\kappa\nu)\big)\big(x-\eta(\eta+\kappa\nu)\big)}{\big(\widetilde{x}-(\eta-\kappa\nu)(\eta-2\kappa\nu)\big)\big(x-(\eta-\kappa\nu)(\eta-2\kappa\nu)\big)}=\frac{U(\eta)}{U(\kappa\nu-\eta)},\quad y=\eta(\eta-\kappa\nu). \tag{116}$$

In notations of (7), (8), the latter two equations take the following form:

$$\frac{\big(\widetilde{x}-\eta(\eta+\kappa\nu_{2n})\big)\big(x-\eta(\eta+\kappa\nu_{2n})\big)}{\big(\widetilde{x}-(\eta-\kappa\nu_{2n})(\eta-2\kappa\nu_{2n})\big)\big(x-(\eta-\kappa\nu_{2n})(\eta-2\kappa\nu_{2n})\big)}=\frac{U(\eta)}{U(\kappa\nu_{2n}-\eta)},$$
$$y_n=\eta(\eta-\kappa\nu_{2n}), \tag{117}$$

$$\frac{\big(\widetilde{y}-\xi(\xi-\kappa\nu_{2n+1})\big)\big(y-\xi(\xi-\kappa\nu_{2n+1})\big)}{\big(\widetilde{y}-(\xi+\kappa\nu_{2n+1})(\xi+2\kappa\nu_{2n+1})\big)\big(y-(\xi+\kappa\nu_{2n+1})(\xi+2\kappa\nu_{2n+1})\big)}=\frac{U(\xi)}{U(-\kappa\nu_{2n+1}-\xi)},$$
$$x_{n+1}=\xi(\xi+\kappa\nu_{2n+1}). \tag{118}$$

Recall that here

$$\nu_{2n+1}=\nu_{2n+1/2}+\delta=\nu_{2n}+2\delta.$$

To express in (117) the variables x, $\widetilde{x}$ through x_n, y_n, we observe that

$$L_2:(x_n,y_n,\nu_{2n-1/2})\longmapsto(x,y_n,\nu_{2n}),\quad R_2:(\widetilde{x},y_n,\nu_{2n})\longmapsto(x_{n+1},y_n,\nu_{2n+1/2})$$

can be written, according to (113), as follows:

$$x=x_n+\frac{\delta}{\nu_{2n-1/2}}(x_n-y_n),\quad \text{resp.}\quad x_{n+1}=\widetilde{x}+\frac{\delta}{\nu_{2n}}(\widetilde{x}-y_n).$$

A simple computation confirms that these relations are equivalent to

$$\frac{x-\eta(\eta+\kappa\nu_{2n})}{x-(\eta-\kappa\nu_{2n})(\eta-2\kappa\nu_{2n})}=\frac{x_n-\eta(\eta+\kappa\nu_{2n-1})}{x_n-(\eta-\kappa\nu_{2n})(\eta-\kappa\nu_{2n}-\kappa\nu_{2n-1})},\quad y_n=\eta(\eta-\kappa\nu_{2n}), \tag{119}$$

$$\frac{\widetilde{x}-\eta(\eta+\kappa\nu_{2n})}{\widetilde{x}-(\eta-\kappa\nu_{2n})(\eta-2\kappa\nu_{2n})}=\frac{x_{n+1}-\eta(\eta+\kappa\nu_{2n+1})}{x_{n+1}-(\eta-\kappa\nu_{2n})(\eta-\kappa\nu_{2n+1}-\kappa\nu_{2n})},\quad y_n=\eta(\eta-\kappa\nu_{2n}). \tag{120}$$

Similarly, to express in (118) the variables y, $\widetilde{y}$ through x_{n+1}, y_n, we observe that

$$L_1:(x_{n+1},y_n,\nu_{2n+1/2})\longmapsto(x_{n+1},y,\nu_{2n+1}),\quad R_1:(x_{n+1},\widetilde{y},\nu_{2n+1})\longmapsto(x_{n+1},y_{n+1},\nu_{2n+3/2}),$$

which, according to (112), can be put as follows:

$$y=y_n+\frac{\delta}{\nu_{2n+1/2}}(y_n-x_{n+1}),\quad y_{n+1}=\widetilde{y}+\frac{\delta}{\nu_{2n+1}}(\widetilde{y}-x_{n+1}).$$

Again, these relations are equivalent to

$$\frac{y-\xi(\xi-\kappa\nu_{2n+1})}{y-(\xi+\kappa\nu_{2n+1})(\xi+2\kappa\nu_{2n+1})}=\frac{y_n-\xi(\xi-\kappa\nu_{2n})}{y_n-(\xi+\kappa\nu_{2n+1})(\xi+\kappa\nu_{2n+1}+\kappa\nu_{2n})},\\ x_{n+1}=\xi(\xi+\kappa\nu_{2n+1}) \tag{121}$$

$$\frac{\widetilde{y}-\xi(\xi-\kappa\nu_{2n+1})}{\widetilde{y}-(\xi+\kappa\nu_{2n+1})(\xi+2\kappa\nu_{2n+1})}=\frac{y_{n+1}-\xi(\xi-\kappa\nu_{2n+2})}{y_{n+1}-(\xi+\kappa\nu_{2n+1})(\xi+\kappa\nu_{2n+2}+\kappa\nu_{2n+1})},\\ x_{n+1}=\xi(\xi+\kappa\nu_{2n+1}). \tag{122}$$

Substituting (119)–(122) into (117), (118), we arrive at the following system of non-autonomous difference equations for the variables x_n, y_n :

$$\frac{\big(x_{n+1}-\eta(\eta+\kappa\nu_{2n+1})\big)\big(x_n-\eta(\eta+\kappa\nu_{2n-1})\big)}{\big(x_{n+1}-(\eta-\kappa\nu_{2n})(\eta-\kappa\nu_{2n+1}-\kappa\nu_{2n})\big)\big(x_n-(\eta-\kappa\nu_{2n})(\eta-\kappa\nu_{2n}-\kappa\nu_{2n-1})\big)}\\ =\frac{U(\eta)}{U(\kappa\nu_{2n}-\eta)},\quad y_n=\eta(\eta-\kappa\nu_{2n}), \tag{123}$$

$$\frac{\big(y_{n+1}-\xi(\xi-\kappa\nu_{2n+2})\big)\big(y_n-\xi(\xi-\kappa\nu_{2n})\big)}{\big(y_{n+1}-(\xi+\kappa\nu_{2n+1})(\xi+\kappa\nu_{2n+2}+\kappa\nu_{2n+1})\big)\big(y_n-(\xi+\kappa\nu_{2n+1})(\xi+\kappa\nu_{2n+1}+\kappa\nu_{2n})\big)}\\ =\frac{U(\xi)}{U(-\kappa\nu_{2n+1}-\xi)},\quad x_{n+1}=\xi(\xi+\kappa\nu_{2n+1}). \tag{124}$$

This is the d-Painlevé equation of the surface type $A_0^{(1)}$, as given in [20], [11].

Remark. In the symmetric situation, when $U(z)=U(-z)$, the system (123), (124) can be interpreted as a one-field second order difference equation, with $x_n=u_{2n-1}$ and $y_n=u_{2n}$. To see this, one should make the change $\xi\longmapsto-\xi$ in equation (124), after which it matches (123).

9 From a pencil of type (ii) to the q-Painlevé equation of the surface type $A_0^{(1)}$

2D QRT map. We consider the QRT map corresponding to the pencil of biquadratic curves through eight points $s_i=(a_i,b_i)$, where

$$a_i=z_i+\frac{\kappa_1}{z_i},\quad b_i=\frac{1}{z_i}+\frac{z_i}{\kappa_2},\quad i=1,\dots,8.$$

These eight points support a pencil of biquadratic curves if they satisfy the condition

$$\prod_{i=1}^{8} z_i = \kappa_1^2 \kappa_2^2.$$

They belong to the curve with the equation

$$(x - \kappa_2 y)(y - \kappa_1^{-1} x) = (\kappa_1 \kappa_2)^{-1} (\kappa_1 - \kappa_2)^2.$$

This is a biquadratic curve in $\mathbb{P}^1 \times \mathbb{P}^1$ with a simple node at (∞, ∞), see Fig. 5 (a).

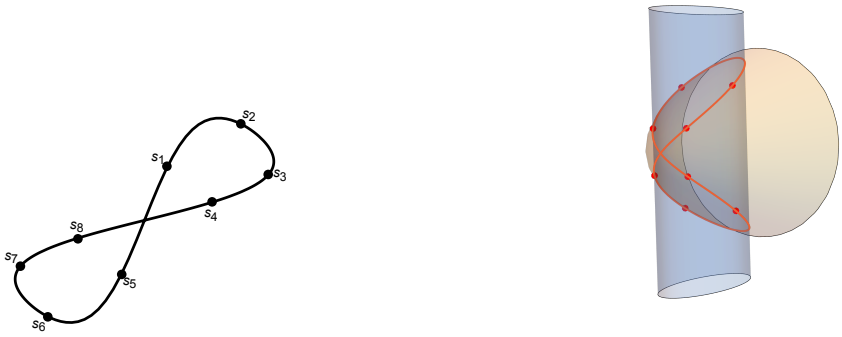

(a) (b)

Figure 5: (a) Base set of the surface type $A_0^{(1)}$: eight points on a nodal (2,2)-curve in $\mathbb{P}^1 \times \mathbb{P}^1$. (b) Pencil of quadrics through a nodal spatial quartic in $\mathbb{P}^3$

The vertical involution i_1 can be described by the following equation:

$$i_1(x, y) = (x, \widetilde{y}), \quad \frac{\left(\widetilde{y} - \frac{1}{\xi} - \frac{\xi}{\kappa_2}\right)\left(y - \frac{1}{\xi} - \frac{\xi}{\kappa_2}\right)}{\left(\widetilde{y} - \frac{\xi}{\kappa_1} - \frac{\kappa_1}{\kappa_2 \xi}\right)\left(y - \frac{\xi}{\kappa_1} - \frac{\kappa_1}{\kappa_2 \xi}\right)} = \frac{U(\xi)}{U\left(\frac{\kappa_1}{\xi}\right)}, \quad x = \xi + \frac{\kappa_1}{\xi}. \tag{125}$$

Here we use the abbreviation

$$U(z) = z^{-4} \prod_{i=1}^{8} (z - z_i). \tag{126}$$

Formula (125) is understood as follows. Written as a Laurent polynomial in ξ, it is anti-symmetric with respect to $\xi \leftrightarrow \kappa_1/\xi$. Upon division by $\xi - \kappa_1/\xi$, the resulting Laurent

polynomial is symmetric and therefore it can be actually expressed as a polynomial in $x = \xi + \kappa_1/\xi$. This defines i_1 as a birational involution (its symmetry w.r.t. $y \leftrightarrow \widetilde{y}$ is obvious).

Similarly, the horizontal involution i_2 can be described by the following equation:

$$i_2(x,y) = (\widetilde{x}, y), \quad \frac{\left(\widetilde{x} - \eta - \frac{\kappa_1}{\eta}\right)\left(x - \eta - \frac{\kappa_1}{\eta}\right)}{\left(\widetilde{x} - \frac{\kappa_2}{\eta} - \frac{\kappa_1\eta}{\kappa_2}\right)\left(x - \frac{\kappa_2}{\eta} - \frac{\kappa_1\eta}{\kappa_2}\right)} = \frac{U(\eta)}{U\left(\frac{\kappa_2}{\eta}\right)}, \quad y = \frac{1}{\eta} + \frac{\eta}{\kappa_2}. \tag{127}$$

The eight points $s_1, \dots, s_8$ in $\mathbb{P}^1 \times \mathbb{P}^1$ serve as the indeterminacy set for i_1 and for i_2. The singularity confinement structure is as in (11). The QRT map F is the composition of these two involutions, $F = i_1 \circ i_2$.

Remark. In what follows, we restrict ourselves to the case $\kappa_1\kappa_2 = 1$. This restriction is not essential, but will allow us to shorten some of the formulas. Thus, from now on we set in this section

$$\kappa_1 = \frac{1}{\kappa}, \quad \kappa_2 = \kappa. \tag{128}$$

If, additionally, the points z_i satisfy the condition

$$z_{i+4} = z_i^{-1}, \quad i = 1, \dots, 4, \tag{129}$$

then the QRT involutions admits a symmetry $i_1 = \sigma \circ i_2 \circ \sigma$, where $\sigma(x,y) = (y,x)$, so that one can introduce the QRT root $f = i_1 \circ \sigma = \sigma \circ i_2$, such that $F = f \circ f$.

3D Painlevé map. As usual, we identify $\mathbb{P}^1 \times \mathbb{P}^1$ with the quadric $Q_0 = \{X_1X_2 - X_3X_4 = 0\} \subset \mathbb{P}^3$ via $[X_1 : X_2 : X_3 : X_4] = [x : y : xy : 1]$. The points s_i are lifted to

$$S_i = [a_i : b_i : a_ib_i : 1].$$

We declare Q_λ to be spanned by Q_0 and

$$Q_\infty = P_\infty = \kappa(X_1^2 + X_2^2) - (1 + \kappa^2)X_1X_2 + (\kappa - \kappa^{-1})^2X_4^2. \tag{130}$$

The base set of the pencil Q_λ is a nodal space curve $\{Q_0 = 0,\, P_\infty = 0\}$ of degree 4, with the node at $[0 : 0 : 1 : 0]$. This is a pencil of type (ii).

The matrix M_λ of the quadratic form Q_λ:

$$M_\lambda = \begin{pmatrix} -2\kappa\lambda & 1+(1+\kappa^2)\lambda & 0 & 0 \\ 1+(1+\kappa^2)\lambda & -2\kappa\lambda & 0 & 0 \\ 0 & 0 & 0 & -1 \\ 0 & 0 & -1 & -2(\kappa-\kappa^{-1})^2\lambda \end{pmatrix}. \tag{131}$$

The characteristic polynomial of the pencil $\{Q_\lambda\}$ is:

$$\Delta(\lambda) = \det(M_\lambda) = \big(1+(1+\kappa^2)\lambda\big)^2 - 4\kappa^2\lambda^2 = \big(1+(1+\kappa)^2\lambda\big)\big(1+(1-\kappa)^2\lambda\big),$$

so that $\mathrm{Sing}(Q_\lambda) = \{-(1+\kappa)^{-2}, -(1-\kappa)^{-2}, \infty\}$. This polynomial is not a complete square, and we have to uniformize $\sqrt{\Delta(\lambda)}$. The uniformizing variable is $\nu \in \mathbb{C}$. As in Sect. 7, it will be convenient to use $w = e^\nu$ instead, with $w \in \mathbb{C} \setminus \{0\}$. We set

$$\lambda = \lambda(w) = \frac{(\kappa - w)(1-\kappa w)}{(1-\kappa^2)^2 w}. \tag{132}$$

Then $\Delta(\lambda)$ becomes a square:

$$\Delta(\lambda) = \frac{\kappa^2(1-w^2)^2}{w^2(1-\kappa^2)^2} \quad \Rightarrow \quad \sqrt{\Delta(\lambda)} = \frac{\kappa(1-w^2)}{w(1-\kappa^2)}.$$

Observe that $\lambda(w) = \lambda(w^{-1})$, while $\sqrt{\Delta(\lambda)}$ changes its sign under $w \longmapsto w^{-1}$. This gives us a double cover of the original pencil branched at $\lambda = -(1+\kappa)^{-2}$ (corresponding to $w = 1$), and at $\lambda = -(1-\kappa)^{-2}$ (corresponding to $w = -1$). The point $\lambda = \infty$ is not a branch point (it corresponds to $w = 0, \infty$). The normalizing transformation of $Q_\lambda(X)$ to the canonical form $Q_0(Y) = Y_1Y_2 - Y_3Y_4$ is achieved by the transformation

$$\begin{bmatrix} X_1 \\ X_2 \\ X_3 \\ X_4 \end{bmatrix} = A_w \begin{bmatrix} Y_1 \\ Y_2 \\ Y_3 \\ Y_4 \end{bmatrix}, \tag{133}$$

where one can take

$$A_w = \begin{pmatrix} \frac{w(1-\kappa w)}{\kappa(1-w^2)} & \frac{w(\kappa-w)}{\kappa(1-w^2)} & 0 & 0 \\ \frac{w(\kappa-w)}{\kappa(1-w^2)} & \frac{w(1-\kappa w)}{\kappa(1-w^2)} & 0 & 0 \\ 0 & 0 & \frac{w}{\kappa} & -\frac{(1-\kappa w)(\kappa-w)}{\kappa^2 w} \\ 0 & 0 & 0 & 1 \end{pmatrix}. \tag{134}$$

Indeed, one immediately verifies that

$$A_w^{\mathrm{T}} M_{\lambda(w)} A_w = \frac{w}{\kappa} M_0.$$

There follows a parametrization of the quadric $Q_{\lambda(w)}$:

$$\begin{bmatrix} X_1 \\ X_2 \\ X_3 \\ X_4 \end{bmatrix} = A_w \begin{bmatrix} x \\ y \\ xy \\ 1 \end{bmatrix} =: \phi_w(x,y). \tag{135}$$

This parametrization is neither valid for $w = 0$ nor for $w = \infty$. The pencil-adapted coordinates (x, y, w) on (the double cover of) $\mathbb{P}^3$ are:

$$x = \frac{\kappa}{w} \cdot \frac{(1-\kappa w)X_1 - (\kappa - w)X_2}{(1-\kappa^2)X_4}, \quad y = \frac{\kappa}{w} \cdot \frac{(1-\kappa w)X_2 - (\kappa - w)X_1}{(1-\kappa^2)X_4}, \tag{136}$$

which have to be supplemented with

$$\lambda = \frac{(\kappa - w)(1-\kappa w)}{(\kappa^2-1)^2 w} = \frac{X_1X_2 - X_3X_4}{\kappa X_1^2 + \kappa X_2^2 - (1+\kappa^2)X_1X_2 + (\kappa - \kappa^{-1})^2 X_4^2}. \tag{137}$$

Theorem 7. *For any $q \neq \pm 1$, define the Painlevé deformation map corresponding to the translation $w \longmapsto \widehat{w} = q^2 w$ by*

$$L: \quad \begin{cases} \widehat{X}_1 = X_1X_4, \\ \widehat{X}_2 = X_2X_4, \\ \widehat{X}_3 = X_3X_4 - \big(\lambda(\widehat{w}) - \lambda(w)\big)Q_\infty(X), \\ \widehat{X}_4 = X_4^2, \end{cases} \tag{138}$$

where $\lambda = \lambda(w)$ is given by (132), and $Q_\infty(X)$ is given in (130). Then, in pencil-adapted coordinates, the map L acts as follows:

$$L: \quad \widehat{x} = x + \frac{1-q^{-2}}{w^2-1}(x-wy), \quad \widehat{y} = y + \frac{1-q^{-2}}{w^2-1}(y-wx), \quad \widehat{w} = q^2 w. \tag{139}$$

For the latter map, the factorizations (4), (5) are given by

$$L_1 : (x,y,w) \longmapsto (x,\widetilde{y},qw), \quad \widetilde{y} = y + \frac{1-q^{-2}}{w^2-1}(y-qwx), \tag{140}$$

$$R_1 : (x,y,w) \longmapsto (x,\widetilde{y},qw), \quad \widetilde{y} = y + \frac{1-q^{-2}}{w^2-1}(y-wx), \tag{141}$$

$$L_2 : (x,y,w) \longmapsto (\widetilde{x},y,qw), \quad \widetilde{x} = x + \frac{1-q^{-2}}{w^2-1}(x-qwy), \tag{142}$$

$$R_2 : (x,y,w) \longmapsto (\widetilde{x},y,qw), \quad \widetilde{x} = x + \frac{1-q^{-2}}{w^2-1}(x-wy). \tag{143}$$

Relation to the q-Painlevé equation of the surface type $A_0^{(1)}$. In the pencil-adapted coordinates (x,y,w), for each fixed w, the intersection curves $Q_{\lambda(w)} \cup P_\mu$ form the pencil through the points

$$s_i(w) = (a_i(w), b_i(w)) = \Big(z_i + \frac{1}{wz_i}, \frac{1}{z_i} + \frac{z_i}{w}\Big), \quad i = 1, \dots, 8, \tag{144}$$

which are just the points S_i expressed in the pencil-adapted coordinates on $Q_{\lambda(w)}$. Thus, the 3D QRT involutions i_1, i_2 act on each quadric $Q_{\lambda(w)}$ in the pencil-adapted coordinates via formulas which are obtained from the corresponding 2D formulas by replacing κ by w:

$$i_1(x,y) = (x,\widetilde{y}), \quad \frac{\Big(\widetilde{y} - \frac{1}{\xi} - \frac{\xi}{w}\Big)\Big(y - \frac{1}{\xi} - \frac{\xi}{w}\Big)}{\Big(\widetilde{y} - w\xi - \frac{1}{w^2\xi}\Big)\Big(y - w\xi - \frac{1}{w^2\xi}\Big)} = \frac{U(\xi)}{U\Big(\frac{1}{w\xi}\Big)}, \quad x = \xi + \frac{1}{w\xi}, \tag{145}$$

$$i_2(x,y) = (\widetilde{x},y), \quad \frac{\Big(\widetilde{x} - \eta - \frac{1}{w\eta}\Big)\Big(x - \eta - \frac{1}{w\eta}\Big)}{\Big(\widetilde{x} - \frac{w}{\eta} - \frac{\eta}{w^2}\Big)\Big(x - \frac{w}{\eta} - \frac{\eta}{w^2}\Big)} = \frac{U(\eta)}{U\Big(\frac{w}{\eta}\Big)}, \quad y = \frac{1}{\eta} + \frac{\eta}{w}. \tag{146}$$

In notations of (7), (8), this takes the form

$$\frac{\left(\widetilde{x}-\eta-\frac{1}{w_{2n}\eta}\right)\left(x-\eta-\frac{1}{w_{2n}\eta}\right)}{\left(\widetilde{x}-\frac{w_{2n}}{\eta}-\frac{\eta}{w_{2n}^2}\right)\left(x-\frac{w_{2n}}{\eta}-\frac{\eta}{w_{2n}^2}\right)}=\frac{U(\eta)}{U\left(\frac{w_{2n}}{\eta}\right)},\quad y_n=\frac{1}{\eta}+\frac{\eta}{w_{2n}},\tag{147}$$

$$\frac{\left(\widetilde{y}-\frac{1}{\xi}-\frac{\xi}{w_{2n+1}}\right)\left(y-\frac{1}{\xi}-\frac{\xi}{w_{2n+1}}\right)}{\left(\widetilde{y}-w_{2n+1}\xi-\frac{1}{w_{2n+1}^2\xi}\right)\left(y-w_{2n+1}\xi-\frac{1}{w_{2n+1}^2\xi}\right)}=\frac{U(\xi)}{U\left(\frac{1}{w_{2n+1}\xi}\right)},\quad x_{n+1}=\xi+\frac{1}{w_{2n+1}\xi}.\tag{148}$$

Here, recall,

$$w_{2n+1}=qw_{2n+1/2}=q^2w_{2n}.\tag{149}$$

To express in (147) the variables x, $\widetilde{x}$ through x_n, y_n, we observe that

$$L_2:(x_n,y_n,w_{2n-1/2})\longmapsto(x,y_n,w_{2n}),\quad R_2:(\widetilde{x},y_n,w_{2n})\longmapsto(x_{n+1},y_n,w_{2n+1/2}).$$

According to (142), (143), we find:

$$x=x_n+\frac{1-q^{-2}}{w_{2n-1/2}^2-1}(x_n-qw_{2n-1/2}y_n),\quad x_{n+1}=\widetilde{x}+\frac{1-q^{-2}}{w_{2n}^2-1}(\widetilde{x}-w_{2n}y_n).$$

A straightforward computation confirms that these equations are equivalent to

$$\frac{x-\eta-\frac{1}{w_{2n}\eta}}{x-\frac{w_{2n}}{\eta}-\frac{\eta}{w_{2n}^2}}=\frac{x_n-\eta-\frac{1}{w_{2n-1}\eta}}{x_n-\frac{w_{2n}}{\eta}-\frac{\eta}{w_{2n}w_{2n-1}}},\quad y_n=\frac{1}{\eta}+\frac{\eta}{w_{2n}},\tag{150}$$

$$\frac{\widetilde{x}-\eta-\frac{1}{w_{2n}\eta}}{\widetilde{x}-\frac{w_{2n}}{\eta}-\frac{\eta}{w_{2n}^2}}=\frac{x_{n+1}-\eta-\frac{1}{w_{2n+1}\eta}}{x_{n+1}-\frac{w_{2n}}{\eta}-\frac{\eta}{w_{2n}w_{2n+1}}},\quad y_n=\frac{1}{\eta}+\frac{\eta}{w_{2n}}.\tag{151}$$

Similarly, to express in (148) the variables y, $\widetilde{y}$ through x_{n+1}, y_n, we observe that

$$L_1:(x_{n+1},y_n,w_{2n+1/2})\longmapsto(x_{n+1},y,w_{2n+1}),\quad R_1:(x_{n+1},\widetilde{y},w_{2n+1})\longmapsto(x_{n+1},y_{n+1},w_{2n+3/2}).$$

According to (140), (141), we find:

$$y=y_n+\frac{1-q^{-2}}{w_{2n+1/2}^2-1}(y_n-qw_{2n+1/2}x_{n+1}),\quad y_{n+1}=\widetilde{y}+\frac{1-q^{-2}}{w_{2n+1}^2-1}(\widetilde{y}-w_{2n+1}x_{n+1}).$$

These equations are equivalent to

$$\frac{y-\frac{1}{\xi}-\frac{\xi}{w_{2n+1}}}{y-w_{2n+1}\xi-\frac{1}{w_{2n+1}^2\xi}}=\frac{y_n-\frac{1}{\xi}-\frac{\xi}{w_{2n}}}{y_n-w_{2n+1}\xi-\frac{1}{w_{2n+1}w_{2n}\xi}},\quad x_{n+1}=\xi+\frac{1}{w_{2n+1}\xi}, \tag{152}$$

$$\frac{\widetilde{y}-\frac{1}{\xi}-\frac{\xi}{w_{2n+1}}}{\widetilde{y}-w_{2n+1}\xi-\frac{1}{w_{2n+1}^2\xi}}=\frac{y_{n+1}-\frac{1}{\xi}-\frac{\xi}{w_{2n+2}}}{y_{n+1}-w_{2n+1}\xi-\frac{1}{w_{2n+2}w_{2n+1}\xi}},\quad x_{n+1}=\xi+\frac{1}{w_{2n+1}\xi}. \tag{153}$$

Substitute (150)–(153) into (147), (148). This results in the following system of non-autonomous difference equations for the variables x_n, y_n:

$$\frac{\left(x_{n+1}-\eta-\frac{1}{w_{2n+1}\eta}\right)\left(x_n-\eta-\frac{1}{w_{2n-1}\eta}\right)}{\left(x_{n+1}-\frac{w_{2n}}{\eta}-\frac{\eta}{w_{2n}w_{2n+1}}\right)\left(x_n-\frac{w_{2n}}{\eta}-\frac{\eta}{w_{2n}w_{2n-1}}\right)}=\frac{U(\eta)}{U\left(\frac{w_{2n}}{\eta}\right)},\quad y_n=\frac{1}{\eta}+\frac{\eta}{w_{2n}}, \tag{154}$$

$$\frac{\left(y_{n+1}-\frac{1}{\xi}-\frac{\xi}{w_{2n+2}}\right)\left(y_n-\frac{1}{\xi}-\frac{\xi}{w_{2n}}\right)}{\left(y_{n+1}-w_{2n+1}\xi-\frac{1}{w_{2n+2}w_{2n+1}\xi}\right)\left(y_n-w_{2n+1}\xi-\frac{1}{w_{2n+1}w_{2n}\xi}\right)}=\frac{U(\xi)}{U\left(\frac{1}{w_{2n+1}\xi}\right)},$$
$$x_{n+1}=\xi+\frac{1}{w_{2n+1}\xi}. \tag{155}$$

This is the q-Painlevé equation of the surface type $A_0^{(1)}$, as given in [20], [11].

Remark. In the symmetric situation, when $U(z)=U(z^{-1})$, the system (154), (155) can be interpreted as a one-field second order difference equation, with $x_n=u_{2n-1}$ and $y_n=u_{2n}$. To see this, one should make in equation (155) the change $\xi\longmapsto\xi^{-1}$, after which it matches (154).

10 Conclusions

In this paper, we carried out the largest part of the task left open in [2], namely extended our novel approach to the pencils for which the generators through a point $X\in\mathbb{P}^3$

depend on X in a non-rational (branching) way. The only case left open for a further investigation is the pencil of the generic type (i), associated (in our scheme) with the elliptic Painlevé equation. Also the problem of an interpretation of the isomonodromic property of discrete Painlevé equations within our scheme remains open and is left for the future research. Finally, it will be important to extend the scheme of the present paper to discrete Painlevé equations corresponding to further translations in the corresponding affine Weyl symmetry groups. A path to this goal (via additional geometric involutions related to pencils and nets of quadrics) was sketched in the concluding remarks of [2]. The first step towards this goal (in the two-dimensional framework) has been performed in [3].

Acknowledgments

This research was supported (till June 2024) by the DFG Collaborative Research Center TRR 109 “Discretization in Geometry and Dynamics”.

References

[1] J. Alonso, Yu. B. Suris, K. Wei. *A three-dimensional generalization of QRT maps.* J. Nonlinear Sci. **33** (2023), 117. 199, 204

[2] J. Alonso, Yu. B. Suris, K. Wei. *Discrete Painlevé equations and pencils of quadrics in* $\mathbb{P}^3$. `arXiv:2403.11349 [nlin.SI]` 197, 198, 199, 200, 201, 202, 203, 204, 205, 207, 217, 237, 238

[3] J. Alonso, Yu.B. Suris. *Geometry of autonomous discrete Painlevé equations related to the Weyl group* $W(E_8^{(1)})$. `arXiv:2512.18288 [nlin.SI]`. 238

[4] M. P. Bellon, C.-M. Viallet. *Algebraic entropy*. Commun. Math. Phys. **204** (1999), 425–437.

[5] A.S. Carstea, A. Dzhamay, T. Takenawa. *Fiber-dependent deautonomization of integrable 2D mappings and discrete Painlevé equations.* J. Phys. A. Math. Theor. **50** (2017), 405202. 200

[6] E. Casas-Alvero. *Analytic projective geometry.* EMS Textbooks in Mathematics. Zürich: European Mathematical Society (2014).

[7] J.J. Duistermaat. *Discrete Integrable Systems. QRT Maps and Elliptic Surfaces.* Springer Monographs in Mathematics. Springer, New York (2010).

[8] B. Grammaticos, A. Ramani. *Discrete Painlevé equations: a review*. In: Grammaticos, B. et al. (eds.), *Discrete integrable systems*, Proceedings of the international CIMPA school, Pondicherry, India, February 2–14, 2003. Lecture Notes in Physics **644** (2004), 245–321. 198, 200

[9] B. Grammaticos, A. Ramani, V. Papageorgiou. *Do integrable mappings have the Painlevé property?* Phys. Rev. Lett. **67**, No. 14 (1991) 1825–1828. 198

[10] N. Joshi. *Discrete Painlevé equations*. CBMS Regional Conference Series in Mathematics 131. Providence, RI: American Mathematical Society (2019). 198

[11] K. Kajiwara, M. Noumi, Y. Yamada. *Geometric aspects of Painlevé equations*. J. Phys. A. Math. Theor. **50** (2017), 073001. 198, 214, 217, 224, 230, 237

[12] T. Mase, R. Willox, A. Ramani, and B. Grammaticos. *Singularity confinement as an integrability criterion*, J. Phys. A **52** (2019), 205201.

[13] M. Noumi, S. Tsujimoto, Y. Yamada. *Padé interpolation for elliptic Painlevé equation*. In: *Symmetries, Integrable Systems and Representations*, Ed. K. Iohara et al, Springer Proceedings in Mathematics and Statistics **40** (2013), pp. 463–482.

[14] G.R.W. Quispel, J.A.G. Roberts, C.J.Thompson. *Integrable mappings and soliton equations.* Phys. Lett. A **126**, no. 7 (1988) 419–421.

[15] G.R.W. Quispel, J.A.G. Roberts, C.J.Thompson. *Integrable mappings and soliton equations II.* Phys. D **34**, no. 1–2 (1989) 183–192.

[16] A. Ramani, B. Grammaticos, J. Hietarinta. *Discrete versions of the Painlevé equations*. Phys. Rev. Lett. **67**, No. 14 (1991) 1829–1832. 198

[17] M. Reid. *The complete intersection of two or more quadrics*. Thesis, Cambridge, 1972. `http://homepages.warwick.ac.uk/~masda/3folds/qu.pdf`

[18] H. Sakai. *Rational surfaces associated with affine root systems and geometry of the Painlevé equations*. Commun. Math. Phys. **220** (2001), 165–229. 198

[19] T. Takenawa. *Discrete dynamical systems associated with the configuration space of 8 points in* $\mathbb{P}^3(\mathbb{C})$. Commun. Math. Phys. **246**, No. 1 (2004) 19–42.

[20] Y. Yamada. *A simple expression for discrete Painlevé equations.* RIMS Kôkyûroku Bessatsu **B47** (2014), pp. 87–95 . 230, 237

[21] Y. Yamada. *Theory and applications of the elliptic Painlevé equation*. In: *Partition Functions and Automorphic Forms*, Eds. V.A. Gritsenko and V.P. Spiridonov, Moscow Lectures **5** (2020) pp. 369–415.

AUTHORS

Jaume Alonso
Institut für Mathematik, MA 7-1
Technische Universität Berlin,
Str. des 17. Juni, 10623 Berlin, Germany
email: alonso@math.tu-berlin.de

Discrete Painlevé equations

Yuri B. Suris
Institut für Mathematik, MA 7-1
Technische Universität Berlin,
Str. des 17. Juni, 10623 Berlin, Germany
email: suris@math.tu-berlin.de